THE UNIVERSITY *of* EDINBURGH

Investigation of a low-energy thermal energy recovery system for passive ventilation applications

Submitted in accordance with the requirements for the degree of Doctor of Philosophy

By

Alastair Harry Mahon

The University of Edinburgh

School of Engineering

2023

The candidate confirms that the work submitted is their own, except where work which has formed part of jointly-authored publications has been included. The work herein has not been submitted for any other degree or qualification except where specified. The contribution of the candidate and the other authors to this work has been explicitly indicated. The candidate confirms that appropriate credit has been given within the thesis where reference has been made to the work of others.

Acknowledgements

Firstly, I would like to thank the University of Edinburgh, Free Running Buildings, and the Scottish Research Partnership in Engineering for providing the opportunity, facilities, and funding to carry out this research.

Thank you to my supervisors, Professors Ben Hughes and Daniel Friedrich, for their guidance and support throughout this process and to everyone I have worked alongside at Free Running Buildings in my time there.

Finally, I would like to thank my family. Being able to rely on their unconditional encouragement and support has eased this journey immensely.

Abstract

Passive ventilation systems such as wind towers can provide fresh air to buildings with no energy demand, however, are often closed throughout the winter of cooler climates due to the introduction of untreated fresh air into the indoor environment which can result in increased building energy demand. Wind towers were originally used throughout The Middle East for centuries to provide passive cooling in hot, arid climates. They have since been modified for European climates, altering the shape of the external envelope, the number of sides, and the use of louvres to channel the flow of air through the system. Various forms of heat recovery have been explored within passive ventilation, however their performance is limited by the small temperature differences between the exhaust and inlet air channels and the allowable pressure drop over the heat recovery device. Therefore, it is desirable to introduce a heat recovery system capable of providing a greater degree of heating and cooling than existing systems, with greater control afforded to the user, whilst incurring a low pressure drop to maintain ventilation rates through the system. As such, this research aimed to combine heat recovery within a passive ventilation system to create a low-energy heating, cooling, and thermal energy recovery system.

The study followed an iterative design approach, using two separate physical tests and corresponding numerical models. First, the impact of an increasing number of horizontal pipe layers through a multi-sided wind tower was explored, measuring the volumetric flow rate into the room below as well as the potential direct heat recovery from the exhaust to inlet air channels. A full-scale wind tunnel test was conducted in an environmental chamber at the Building Research Establishment site in the UK, with the results used to validate a corresponding numerical model developed through ANSYS Fluent under steady state conditions. Once validated, simulations were

conducted under increasing wind speeds and under differing inlet and outlet air temperatures to understand system performance.

The results of the wind tunnel test and numerical modelling were used to guide design decisions for the integration of a water-based thermal loop to extract and deliver thermal energy from and to the system. Once the design of the system was settled, a field trial of the proposed system was conducted at an office site in Sheffield, UK. The ability of the system to cool fresh air was recorded over several days, with the results used to validate a second numerical model through a transient simulation, again developed through ANSYS Fluent. Once validated simulations further steady state simulations were conducted, varying the wind speed, air temperatures, water temperatures, and water velocities, measuring the ability of the system to provide heating and cooling to fresh air whilst recovering waste thermal energy.

For the wind tunnel test, heat pipes were installed within a wind tower to facilitate the direct recovery of waste heat from the exhaust to inlet air channels. The wind tower and heat pipe system maintained a volumetric flow rate of 0.1 m^3/s at an inlet velocity of 1 m/s. The fresh air temperature was raised by up to 2.8 °C, with the amount of heating increasing as the inlet velocity fell and the temperature difference between the exhaust and inlet channels rose.

For the field trial, a run-around heat exchanger was integrated into a wind tower to recover waste thermal energy and eventually link the system with seasonal thermal energy storage. Validating the numerical model using experimental data, simulations revealed the potential of the system to provide fresh air at 0.09 m^3/s when the inlet velocity was 1 m/s, marginally lower than the wind tunnel test owing to the increased wind tower height. A maximum pressure drop over the heat exchanger of 2.07 Pa was

recorded at a wind speed of 5 m/s. The fresh air temperature was decreased and increased by up to 4.36 and 4.14 °C respectively due to cooling and heating provided through the heat exchanger, with the amount of heating or cooling again increasing with decreasing wind speed. Under the same boundary conditions, an increase or decrease of 6.15 °C in water temperature through the heat exchanger was reported, when providing heating and cooling. The change in water temperature remained the same under heating and cooling conditions due to the variations in inlet and exhaust air temperature through the wind tower inlet and outlets. Considering the system was intended to recover thermal energy for storage through a form of seasonal thermal storage, a maximum of 2 kW of sensible energy was transferred between the fluids.

Adding fins to the heat exchanger reduced the volumetric flow rate into the room but improved the heat transfer between the fluids. The performance of the standard heat exchanger was evaluated through the efficiency and overall heat transfer coefficient, achieving a maximum efficiency of 30% and a heat transfer coefficient of 5.1 W/m^2 – K.

Contents

List of tables

List of Figures

Nomenclature

ρ	Density, (kg/m3)
t	Time, (s)
$\vec{v}$	Fluid velocity (m/s)
p	Static pressure, (Pa)
μ	Molecular viscosity, (Pa s)
U	Overall heat transfer coefficient (W/m^2·K)
D_o	Pipe outer diameter (m)
D_i	Pipe inner diameter (m)
λ_{pipe}	Thermal conductivity pipe material (W/m·K)
h_w	Water heat transfer coefficient (W/m^2·K)
h_a	Air heat transfer coefficient (W/m^2·K)
λ_a	Air thermal conductivity
Nu	Nusselt number
Re	Reynolds number
Pr	Prandtl number
ς_L	Dimensionless longitudinal pitch
ς_T	Dimensionless transversal pitch
ς_T	Dimensionless diagonal pitch
S_L	Longitudinal pitch (m)
S_T	Transversal pitch (m)
S_D	Diagonal pitch (m)
U_{max}	Max velocity through tube banks (m/s)
U_{app}	Approach velocity (m/s)
η	Efficiency (%)

ΔT_{LMTD} Log mean temperature difference (°C)

T_{supp} Fluid supply temperature (°C)

T_{out} Fluid outlet temperature (°C)

Abbreviations

Air Changes per Hour (ACH)

Anti-Short-Circuit Device (ASCD)

Aquifer Thermal Energy Storage (ATES)

Bodies Of Influence (BOI)

Borehole Heat Exchanger (BHE)

Borehole Thermal Energy Storage (BTES)

Building Research Establishment

Computational Fluid Dynamics (CFD)

Computer Aided Design (CAD)

Grid Convergence Index (GCI)

Ground Source Heat Exchanger (GSHE)

Heat Transfer Fluid (HTF)

Heating, Ventilation, and Air conditioning (HVAC)

High-Temperature Aquifer Thermal Energy Storage (HT-ATES)

High-Temperature Borehole Thermal Energy Storage (HT-BTES)

Indoor Air Quality (IAQ)

Latent Heat Storage (LHS)

Log Mean Temperature Difference (LMTD)

Night Ventilation (NV)

Number of Transfer Units (NTU)

Phase Change Material (PCM)

Pit Thermal Energy Storage (PTES)

Predicted Mean Vote (PMV)

Pulsating Heat Pipe (PHP)

Reynolds-Averaged Navier-Stokes (RANS)

Run-around Heat Exchanger (RAHE)

Seasonal Thermal Energy Storage (STES)

Semi-Implicit Method For Pressure-Linked Equations (SIMPLE)

Sensible Heat Storage (SHS)

Sick Building Syndrome (SBS)

Tank Thermal Energy Storage (TTES)

Thermal Energy Storage (TES)

Thermochemical Heat Storage (THS)

Thermosyphon Heat Pipe (TSHP)

Transient Simulation System (TRNSYS)

Underground Thermal Energy Storage (UTES)

Volume Of Fluids (VOF)

Preface

The work presented in this document has been carried out between February 2020 and October 2023 at Free Running Buildings, Sheffield. It is supported by the University of Edinburgh, the University of Hull, and the Scottish Research Partnership in engineering (SRPe).

List of publications

Journal papers

1. Mahon, H, O'Connor, D., Friedrich, D., and Hughes, B. (2022) A review of thermal energy storage technologies for seasonal loops, Energy, Volume 239, Part C, Article #122207
2. Mahon, H, Friedrich, D, and Hughes, B. (2022) Wind tunnel test and numerical study of a multi-sided wind tower with horizontal heat pipes, Energy, Volume 260, Article #125118

Conference paper

1. Mahon, H, Friedrich, D, and Hughes, B. (2023) Experimental and numerical analysis of a wind tower with run-around heat exchanger, Sustainable Energy Technologies (SET) conference, 2023

1 Introduction

This chapter presents an overview of the motivations behind this study, introducing the concepts of passive ventilation, heat recovery, and seasonal thermal energy storage, before the methodology and structure of the thesis are presented.

1.1 Motivation

Buildings account for approximately 40% of energy consumption in the U.S and Europe (Pérez-Lombard et al., 2008; Amasyali and El-Gohary, 2018), with Heating, Ventilation, and Air Conditioning (HVAC) systems in commercial buildings responsible for up to 50% of this total (Figure 1-1) (Vakiloroaya et al., 2014; Maasoumy and Sangiovanni-Vincentelli, 2016; Qian et al., 2020). Climate change will profoundly impact building energy demand, with the need for space heating and cooling set to change drastically over the coming decades (Zhai and Helman, 2019). In response, the EU-wide 2030 climate and energy framework aims to reduce greenhouse gas emissions by at least 40% from 1990 levels while improving energy efficiency to 32.5% (European Council, 2014; European Commission, 2020). On a national level, the UK government aims to reduce emissions by 78% relative to 1990 levels (Jing et al., 2022). As such, buildings have been identified as one area where significant reductions in energy consumption can be achieved, contributing to creating a sustainable energy network and forming an essential part of a carbon-neutral society. Although achieving emissions reduction targets for the built environment is crucial to reducing total energy demand, the thermal comfort and health of the building occupants must be considered throughout.

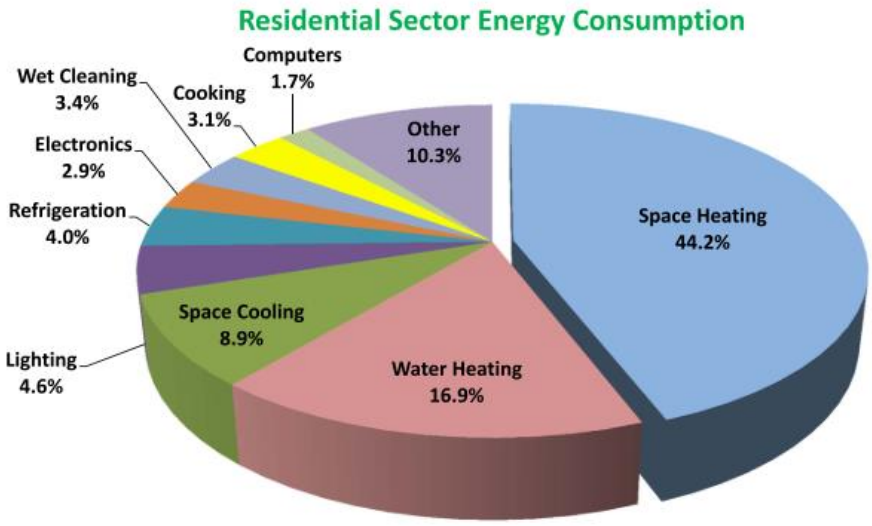

Figure 1-1 - Breakdown of energy consumption in a typical building in the US (Maasoumy and Sangiovanni-Vincentelli, 2016)

Indoor air pollutants arise from both human activity and building materials, the buildup of which can impact occupant well-being, performance, and productivity, and in the worst cases, cause the onset of Sick Building Syndrome (SBS) (De Dear et al., 2013; Baloch et al., 2020). Stale air must be constantly expelled and replaced with fresh air to prevent the buildup of pollutants, with ventilation rates legislated according to building type and primary use (CIBSE Guide A, 2015).

To replace stale air with fresh air, active or passive ventilation systems can be used, whereby active ventilation uses mechanically powered fans to move air throughout buildings, and passive ventilation uses naturally occurring driving forces to generate airflow. Mechanical ventilation such as HVAC systems are often also used to remove airborne particulates through filtering, as well as control indoor temperature and humidity through heat exchangers, with ventilation rates of up to 10 L/s required to account for the removal of contaminants such as those produced by building materials and furnishings (Jones and Molina, 2017).

Passive ventilation systems such as wind towers, openable windows, and solar thermal chimneys offer an alternative to active ventilation systems by harnessing areas of relative positive and negative pressure as well as the stack effect to create a flow of air into and out of buildings (Walker and Wilson, 1993). As a static body in a fluid flow, wind towers generate an area of positive pressure on the windward face of the wind tower and a corresponding area of relative negative pressure on the leeward side. This creates a combined driving and suction force through the ventilation system, with stale air exiting towards the low-pressure region and fresh air flowing to replace it (Figure 1-2). The stack effect is generated through room temperature differences, creating a buoyancy-driven flow. Warm stale air rises, exiting through the passive ventilation system, reducing the internal air pressure and enabling cool air to flow in to replace it.

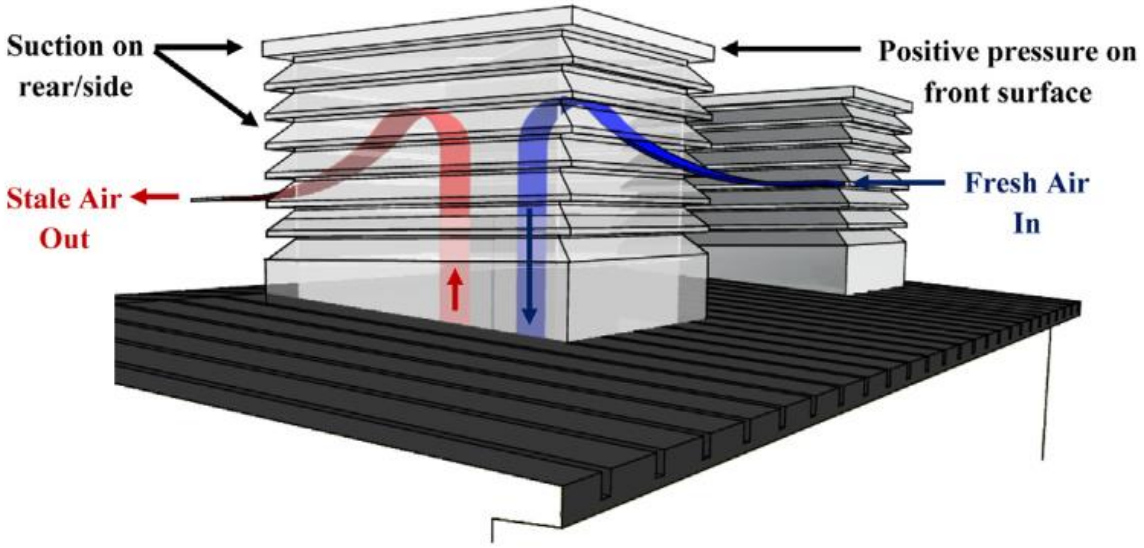

Figure 1-2 - Ventilation flow process through a commercial wind tower (Calautit and Hughes, 2014b)

Although passive ventilation systems consume no energy by nature, they are subject to several limitations. The stack effect is only apparent at low air velocities. It diminishes throughout the summer as the temperature difference between indoors and

outdoors decreases (Wu *et al.*, 2021) meaning that passive ventilation systems primarily depend on wind speed to generate meaningful airflow and ventilation. In addition, as a standalone system, they fail to provide any heating or cooling to fresh air, which can result in an increase in building energy demand as untreated fresh air enters the indoor environment. To prevent this, passive ventilation systems are often closed throughout the winter months of cold climates as ambient temperatures decline. In response, studies have explored using heat recovery devices within passive ventilation systems to increase their viable operational window and decrease the reliance on conventional HVAC systems.

Heat recovery devices can be used to recover and transfer waste heat between fluid streams in both industrial and residential systems (Figure 1-3), where waste heat can be defined as heat rejected from commercial or industrial activities because its temperature is too low for direct use (Lagoeiro et al., 2022). Examples of heat recovery devices include heat pipes, plate heat exchangers, rotary thermal wheels, and run-arounds, with reviews regarding the integration of heat recovery within passive ventilation systems focusing on heat transfer rates, ease of integration, and incurred pressure drop (O'Connor et al., 2016; Xu et al., 2019).

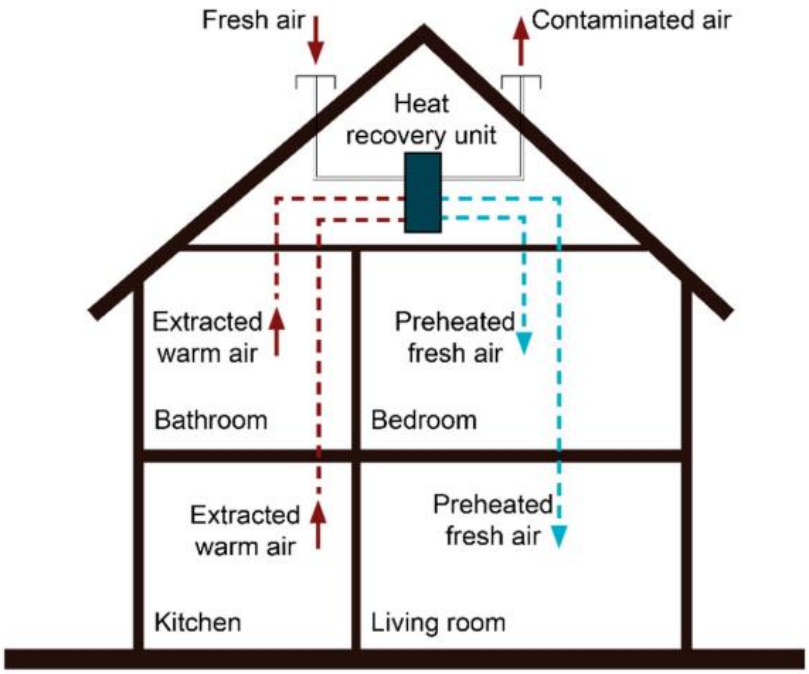

Figure 1-3 - Heat recovery system for a residential building (Mardiana-Idayu and Riffat, 2012)

Individual studies regarding heat recovery within passive ventilation tended to focus on the potential for heat recovery from the exhaust to inlet air to raise supply temperatures. Due to the lack of fans used within passive ventilation systems, the driving pressure through the inlets is often low, therefore making the allowable pressure drop over the heat recovery device crucial to consider (Shao et al., 1998; Hviid and Svendsen, 2011; O'Connor et al., 2015; Calautit et al., 2016). Overly impeding the airflow can result in ventilation rates falling below expected levels, impacting the ventilation system's primary function of providing fresh air. Although described as heat recovery devices, these technologies can also effectively recover cold by using a cool fluid stream as a heat sink during an energy exchange to lower the temperature of another fluid stream.

Of the heat recovery methods listed, heat pipes and plate heat exchangers are static, requiring no energy input, and are therefore considered passive. In contrast, run-

arounds and rotary thermal wheels are considered active as they incur some energy demand to operate the pump and motor respectively. Heat recovery devices are limited by the necessity for a constant supply of waste heat and the limited temperature difference between the inlet and exhaust air streams; however, supply does not necessarily coincide with demand. For example, ambient temperatures and thermal gains in occupied buildings are high during summer when there is little demand for space heating.

Thermal Energy Storage (TES) can address the mismatch between supply and demand of waste thermal energy. TES can be categorised according to how thermal energy is stored. Sensible Heat Storage (SHS) is considered the simplest of the three, using a material to directly keep heat within the body by raising its temperature (Zhao et al., 2022); Latent Heat Storage (LHS) uses thermal energy to induce a phase change within a material that then releases the thermal energy upon returning to its original state (Cabeza et al., 2015; Nithyanandam et al., 2017; Umair et al., 2019); Thermochemical Heat Storage (THS) uses reversible chemical reactions to separate chemical compounds that when recombined generate heat (Pardo et al., 2014; Carrillo et al., 2019).

Seasonal Thermal Energy Storage (STES) is a form of SHS capable of storing thermal energy for up to 6 months, helping to address the seasonal mismatch between the supply of waste heat in the summer and the demand for space heating in the winter. Aquifers, pits, tanks, and boreholes are all used as forms of STES, differentiated by the way they store thermal energy but also according to their storage volumes, temperatures, and durations (Mahon et al., 2022). Large storage volumes help reduce thermal energy loss to the environment, enabling STES systems to store thermal

energy for several months without incurring prohibitive losses before the redistribution of heat into the system. The ability to store heat and cold is not universal to all forms of STES. Still, it is particularly beneficial in mild-cold climates that incur seasonal demand for both heating and cooling.

Designing a system that could effectively combine passive ventilation and heat recovery to capture waste thermal energy for storage using STES would present an opportunity to significantly reduce the energy required to provide heating, cooling, and ventilation for buildings compared to mechanical HVAC systems. Although STES is not directly explored within this research, the system design and temperature ranges are consistent with the requirements and temperature ranges such that it would be feasible to integrate a form of STES to enhance the performance of the passive ventilation and heat recovery system. The proposed system is intended to provide heating and cooling in the winter and summer by using waste heat and cold recovered and stored in the opposing seasons. To do this, a heat recovery device must be effectively integrated within a passive ventilation system, ensuring that the pressure drop over the heat recovery device remains sufficiently low to maintain ventilation rates above stipulated levels. The recovery of waste thermal energy must also be maximised for storage through STES, limiting the energy demand within the system through heat pumps or chillers to provide heating and cooling.

1.2 Aims and Objectives

The overarching aim of this study was to develop a system capable of combining passive ventilation and heat recovery to provide heating and cooling to fresh air whilst recovering waste thermal energy. In doing so, the pressure drop over the heat exchanger must remain low so that the ventilation rate through the passive ventilation system is sufficient to comply with building standards seeking to maintain indoor air

quality. The integration of a heat recovery system will enable the treatment of fresh air prior to mixing throughout the room, reducing building energy demand by reducing or eliminating the need for mechanical systems to bring fresh air temperature to a comfortable range. The system will make use of waste heat and cold available in the summer and winter respectively to provide heating and cooling in the opposing seasons.

1. Conduct a literature review to establish the key performance indicators of passive ventilation systems, heat recovery devices, and seasonal thermal energy storage systems. Evaluate individual elements as well as instances where several technologies have been combined. Use the literature review to identify gaps in the existing body of research and clarify this thesis's aims.
2. Use wind tunnel testing and numerical modelling to investigate the impact of installing an increasing number of staggered heat pipe layers through the base of a wind tower on the volumetric flow rate into the room below as wind speed increases.
3. Use wind tunnel testing and numerical modelling to explore the potential for heat pipes to recover heat directly from the exhaust to inlet air channels of a passive ventilation system. Measure the heat pipes performance when varying the inlet and exhaust air temperatures to determine how the temperature difference between the inlet and exhaust air channels affects the change in fresh air temperature before it enters the room. Determine how an increasing number of pipe layers impacts the heat recovery between the air channels.
4. Using the results of the wind tunnel test to guide design decisions, integrate a water-based heat exchanger into a passive ventilation system to provide heating, cooling, and thermal energy recovery on a seasonal basis.

5. Using a field trial and numerical modelling, determine the potential of the water-based system to pre-heat and cool fresh air using heat exchanger water temperatures that could be reasonably expected to be delivered from a form of STES.
6. Using a field trial and numerical modelling, quantify the sensible energy recovered through the heat exchanger when the fresh air temperature, wind speed, water temperature, and water velocity are varied to evaluate its performance.

1.3 Methodology

Upon establishing the research gap this study will employ an iterative approach to combining the passive ventilation, heat recovery, and water-based thermal loop elements. The research gap will be attained through a comprehensive literature review of the fields of interest. Computational Fluid Dynamics (CFD) modelling will be used alongside experimental methods to determine the viability of the proposed system. System performance will be evaluated under a range of boundary conditions, varying wind velocity, direction, and temperature, water velocity and temperature, and room temperature.

The primary parameters of interest regarding the proposed system are the ventilation rates, pressure drop over the heat recovery device, pre-heating and cooling of fresh air, and recovery of waste thermal energy. Figure 1-4 indicates the intended flow of work conducted throughout the project.

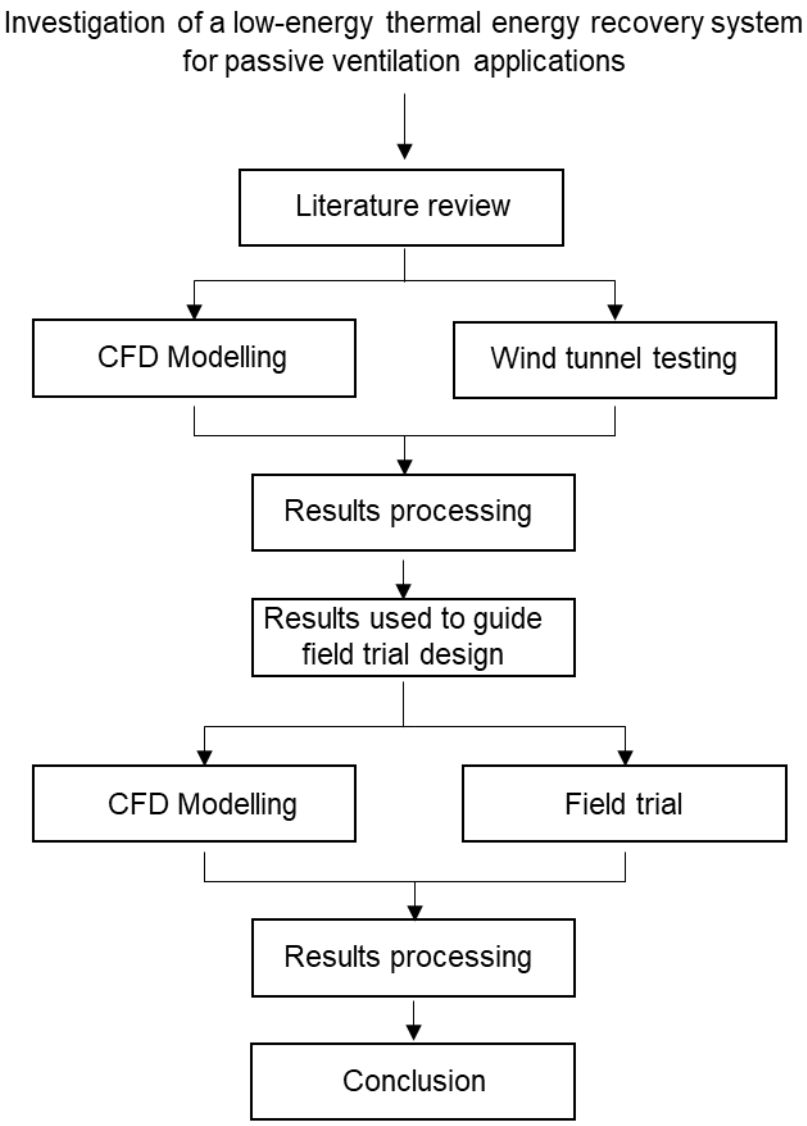

Figure 1-4 - Project methodology flow chart

Wind tunnel testing was used to evaluate the performance of a wind tower and heat pipe heat recovery system, measuring the volumetric flow rate through the wind tower and heat recovery from the exhaust to inlet channels. The experimental results validated a numerical model developed using the CFD program ANSYS 21. For the validation, the simulation's boundary conditions matched those experienced in physical testing. After validation, a wider range of boundary conditions were applied as the number of heat pipes varied to maximise the increase in fresh air temperature through the wind tower.

The results of the wind tunnel test and CFD simulations were used to inform design decisions when integrating a water-based thermal loop into the system to extract and deliver waste thermal energy. Following the same process, a field trial of the proposed wind tower and heat recovery system was conducted at a test site in Sheffield, UK. The boundary conditions and results recorded during physical testing were used to validate a second numerical model designed to replicate the field trial. Further simulations sought to maximise the pre-heating and cooling of fresh air through the wind tower whilst also maximising the sensible energy recovery through the heat exchanger. The compliance of the volumetric flow rate through the wind tower with British building standards for ventilation was also evaluated.

1.4 Thesis Structure

The remainder of the thesis is divided into five chapters, relaying the flow of work carried out that together result in the drawn conclusions in the final chapter. The structure of the thesis and the contents of each chapter are as follows:

Chapter 2 presents a review of existing literature covering passive ventilation, heat recovery, and seasonal thermal energy storage as individual elements before instances where they have been combined. The literature review is used to identify gaps in the existing research and suitable experimental and numerical methods that can be used to achieve the established research objectives.

Chapter 3 establishes the methods and theory followed for developing the numerical models. It then runs through the calculations used to find the heat exchanger's efficiency and overall heat transfer coefficient.

Chapter 4 details the experimental design of the full-scale wind tunnel test and subsequent development, validation, and simulation of the corresponding numerical model, the results of which are also presented.

Chapter 5 presents the experimental design of the field trial conducted to explore the performance of a wind tower and run-around heat exchanger. The numerical model's development, validation, and simulation are detailed before evaluating the results.

Chapter 6 presents the conclusions drawn from the preceding chapters and identifies future work to continue the development of the system proposed herein.

2 Literature Review

The following chapter presents a review of research in the fields of passive ventilation, heat recovery, and STES. The literature review will first compare natural and mechanical ventilation with regards to indoor air quality and thermal comfort. Forms of passive ventilation will then be explored, including the development of commercial wind towers from traditional designs, followed by comparisons of available heat recovery and STES technologies to identify the most suitable method for integration within passive ventilation. To gain understanding each element is first evaluated individually before reviewing instances where technologies have been combined. Finally, a summary of the reviewed literature is provided alongside the identified research gap.

2.1 Air Quality

Indoor Air Quality (IAQ) can have a significant impact on human health (Sundell, 2004), particularly as people in the current time spend up to 90% of their time indoors (Huo et al., 2020). Many standards for domestic and non-domestic buildings are used during the design phase to ensure IAQ is maintained (Ahmed Abdul–Wahab et al.,

2015), where IAQ is evaluated according to the concentration of pollutants in the air within the room. IAQ depends upon various factors, including ambient temperature, wind velocity, humidity, ceiling height, surface temperature, air density, contaminant generation/deposition/removal rate, and number of occupants (Ma et al., 2021).

Poor IAQ can lead to short-term health problems such as fatigue, nausea, and chronic respiratory diseases in the worst cases (Abraham and Li, 2014). Sick Building Syndrome (SBS) has been described as “Situations in which building occupants experience acute health and comfort effects that appear to be linked to time spent in a building, but no specific illness or cause can be identified” (EPA, 1991). Common symptoms of SBS include headaches, fatigue, difficulty concentrating, and mucosal symptoms that are relieved after leaving the building (Sarkhosh et al., 2021). Improving the quality of the indoor environment has been found to reduce the occurrence of SBS symptoms relative to conventional office spaces (MacNaughton et al., 2016).

Mechanical and natural ventilation systems replace stale air with fresh air, where mechanical ventilation uses fans to move air and natural ventilation relies on naturally occurring forces. Ben-David and Waring (2016) simulated the impacts of mechanical versus natural ventilation in offices on the concentration of critical indoor pollutants. Hourly ventilation rates, recirculation, and infiltration rates were used in models replicating typical office buildings in fourteen US cities, monitoring concentrations of carbon monoxide, carbon dioxide, formaldehyde, nitrogen dioxide, ozone, and fine particles. Comparing mechanical and natural ventilation strategies with similar ventilation rates, the indoor concentration of the measured pollutants was largely independent of the ventilation strategy, bar fine particle concentration which increased

in the passive ventilation case due to the lack of filtration. Filters are often installed within mechanical ventilation systems to remove fine particulates within the air, however due to the increased pressure required to generate sufficient flow through the filter they are neglected within passive ventilation systems.

A review of the effectiveness of natural ventilation methods such as single-sided ventilation, cross-ventilation, wind towers, and solar chimneys was conducted in hot climates (Ahmed et al., 2021). It found that natural ventilation was effective at removing pollutants produced indoors by generating high ventilation rates, reporting up to 7.6 ACH in single-sided or cross ventilation, up to 75 ACH in wind towers, and up to 18 ACH in solar chimneys. Despite this, there was often an associated increase in the indoor concentration of pollutants produced outdoors, again due to the lack of filtration. Seppanen and Fisk (2001) reviewed ventilation systems and their association with SBS symptoms, discussing potential explanations. They found that despite the lack of filtering through natural ventilation, mechanically air-conditioned buildings were associated with 30 – 200% higher instances of one or more SBS symptoms. The relative increase in SBS symptoms was attributed to deficiencies within the HVAC system design, construction, and operation that may have led to pollutant emissions from the HVAC system, however there was no more clearly defined reasoning supplied.

Although the need for the control of IAQ to maintain occupant health is clear, the preference for a ventilation method to facilitate it is less so. The lack of filtration in natural ventilation systems can lead to the introduction of outdoor pollutants into the indoor environment, yet this is also dependent upon the infrastructure surrounding the building. Similarly, mechanical elements such as cooling coils and dehumidifiers can create environments suitable for microbial growth. The air exchange necessary

between indoors and outdoors to maintain IAQ subsequently affects the thermal conditions of the interior. As a result, an additional system or systems are required to maintain a comfortable indoor temperature for the occupants, measured through thermal comfort.

2.2 Thermal Comfort

Thermal comfort is defined as the condition of mind that expresses satisfaction with the thermal environment, assessed through subjective evaluation (Mansi et al., 2021). In general, thermal comfort occurs when body temperatures remain within a narrow range, skin moisture is low, and the physiological effort of temperature regulation is minimised (Djongyang et al., 2010).

Attempts have been made to compare the abilities of mechanical and natural ventilation methods to provide thermal comfort to building occupants. Shifts in design practices are looking to move away from mechanical HVAC systems towards natural ventilation, saving energy by reducing or eliminating the need for fans and increasing the tolerable temperature range in which occupants achieve thermal comfort (De Dear and Brager, 2002). People who spend large amounts of time in air-conditioned spaces come to expect temperatures that fall within the centre of the comfort zone of the building and so become less tolerable to deviation outside of this range. Conversely, people who occupy naturally ventilated buildings are more accustomed to thermal diversity reflecting local climatic conditions, so preferences and tolerances extend over a wider temperature range (De Dear and Brager, 2002).

Ben-David and Waring (2016) demonstrated that for naturally ventilated buildings occupants are comfortable in a broader range of temperatures than those that use mechanical ventilation. As a result, the natural ventilation strategies were found to

decrease the amount of energy required for heating and cooling due to the broader setpoint bands afforded. The energy saved due to reduced fan use was also found to be an order of magnitude lower than the energy savings for heating and cooling. It, therefore, should not be considered a driving factor in decision-making.

Wang and Greenberg (2015) explored the potential for openable windows used alongside HVAC systems to reduce building energy consumption. Simulating various control strategies for natural and mixed-mode ventilation which employed mechanical and passive ventilation strategies, they found that energy savings between 17 – 47% could be achieved with mixed-mode ventilation versus HVAC only depending on the local climate. Leaving windows open constantly however resulted in an increase in energy consumption between 3.5 – 15.2%, indicating the need for management strategies of passive ventilation and its limitations in some climatic conditions.

Natarajan et al. (2015) conducted a field study of indoor thermal comfort in Bogota, Colombia. The study included buildings with mechanical, natural, and mixed-mode ventilation systems. Thermal comfort data gathered during the trial was compared against the predictions made by several international standards for thermal comfort. Although the models generally predicted the thermal comfort of the mechanically ventilated buildings well, they all underestimated the level of discomfort of the occupants in those with natural ventilation. This was likely due to factors such as high thermal expectations of the occupants and the lack of personal control over the passive ventilation system.

Natural ventilation has been shown to actively reduce building energy consumption when applied with a considered operating schedule. Occupants in buildings with natural ventilation achieve thermal comfort at a broader range of temperatures,

reducing the energy demand for space heating and cooling. As was shown by Natarajan et al. (2015), evaluating thermal comfort must be done with consideration for the expectations of the occupants relative to their experiences with mechanical systems which allow for a greater degree of control over the indoor environment. Natural ventilation has also been shown to be effective in a range of climates, primarily for cooling purposes, however, the mode of natural ventilation is highly impactful on the effectiveness (Omrani et al., 2017).

2.3 Natural Ventilation Systems

Natural ventilation has been established as an effective alternative to mechanical ventilation systems. Several approaches to natural ventilation have been developed relative to differing climates, however all work under the principles of either wind-driven flow, the stack effect, or both.

2.3.1 Solar Chimneys

Solar chimneys have been widely researched due to their relative affordability, reliable operation, and ease of construction (Maghrabie et al., 2022), with studies mainly focusing on the potential for buoyancy-driven ventilation through passive thermal gains. Solar chimneys have three main elements: the ventilation shaft, a solar collector area, and openings for stale and fresh air to flow out of and in through respectively. The solar collector area can comprise part or all of the chimney shaft (Figure 2-1) and is used to warm the air within. As the air is heated its density is reduced, causing it to rise out through the chimney lowering the internal room pressure, drawing fresh air in through the inlet to replace it (Kasaeian et al., 2017). The airflow rate through the chimney is influenced by the pressure difference between the outlet and inlet created by the thermal gradient and wind velocity (Maghrabie *et al.*, 2022).

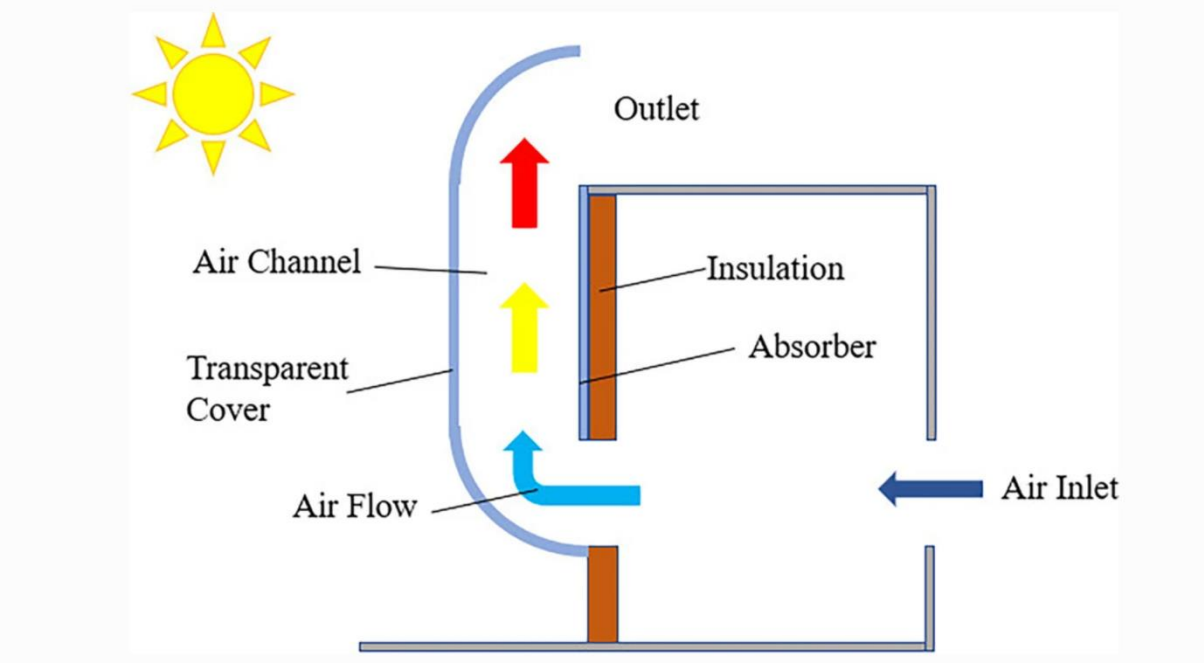

Figure 2-1 - Mechanism for solar chimney ventilation (Kassaei et al., 2022)

Ventilation rate increases linearly with increasing solar intensity (Maghrabie et al., 2022), with ventilation rates between 2 – 9 Air Changes per Hour (ACH) reported (Khosravi et al., 2019; He et al., 2021) and reaching 27.11 ACH in one laboratory case (Villar-Ramos et al., 2020). The large increase in ventilation rate was attributed to the angling of the solar chimney to increase the absorption of solar radiation and by varying the size of the air gap through which the space was ventilated. Parameters such as the solar intensity, cavity gap size, chimney height, chimney inclination angle, area of the inlets and outlet, external wind speed, and the solar collector material have all been shown to impact the ventilation rate (Maghrabie et al., 2022). Generating ventilation through the stack effect means solar chimneys can provide ventilation even on windless days. Thick walls also act as short-term thermal storage, continuing to provide heat even as solar irradiance falls ensuring ventilation rates are maintained until later in the day. However, reliance on solar insolation to increase air temperature means solar chimneys are constrained mainly to hotter climates.

Cooling methods have been explored within solar chimneys to reduce inlet air temperatures. Serageldin et al. (2020) combined a solar chimney with an earth-to-air heat exchanger. Using a small wooden room with a solar chimney attached, air entering the inlet was drawn through an underground heat exchanger, allowing the ground to cool the air before entering the test room. Before installation, the temperature within the test room was 5 – 6 °C higher than the ambient while after the indoor temperature was between 5 – 9 °C below the ambient, saving 42.9 kWh/m^2/year.

Moosavi et al. (2020) integrated a wind tower into a solar chimney and water spray system to further improve space cooling and ventilation for a two-story office building in a warm and arid climate. The wind catcher was used to guide fresh air into the room and the solar chimney is used to exhaust stale air, with a scale model and numerical modelling used to compare configurations with and without the wind tower and water spray. When combined, the wind tower, solar chimney produced, and water spray system achieved ventilation rates up to 9 ACH whilst reducing the indoor temperature by an average of 5.2 °C. This resulted in a 75% reduction in cooling energy demand and a 90% reduction in ventilation energy demand during peak summer relative to the case with no cooling.

2.3.2 Night Ventilation

Night ventilation (NV) is a passive cooling strategy relying solely on buoyancy or wind-driven ventilation (Hughes et al., 2011). By opening ventilation systems overnight structural materials can release heat gained throughout the day to the environment, cooling the fabric of the building and effectively using it as cold thermal storage. The building materials then absorb heat as temperatures increase into the day, delaying

the point at which the peak indoor temperature is reached and lowering cooling energy demand (Geros et al., 1999). This strategy is beneficial for buildings which experience high internal heat gains (Becker and Paciuk, 2002). The daily ambient temperature amplitude dictates the effectiveness of NV, the difference between the indoor and outdoor temperature, the ventilation rate, the thermal capacity of the building, the duration of the nighttime ventilation, and the coupling of the airflow and thermal mass (Becker and Paciuk, 2002).

Bakhtiari et al. (2020) simulated the effect of NV on a historic office building in Sweden. Using a ventilation rate of 1.66 ACH between 20:00 – 06:00, the number of hours in which office rooms exceeded 26 °C throughout the day was reduced by up to 33%, and electricity use for cooling decreased by up to 40%. Leaving doors open overnight to allow more expansive infiltration of cold throughout the building also served to increase the effectiveness of NV. Doubling designed ventilation rates throughout the day was found to reduce the number of hours in which comfortable indoor temperatures are exceeded by up to 27.1%.

Mehmood et al. (2022) explored the potential for several passive cooling methods to improve the heat resilience of buildings in extremely hot countries. TRNSYS (Transient System Simulation Tool) characterises climate zones and calculates building cooling energy demand and discomfort hours. Night ventilation reduced energy demand by up to 13.1 kWh/m^2 and the number of hours of indoor discomfort by up to 320 over a year.

Phase Change Materials (PCMs) can be used to improve the effectiveness of NV further. PCMs are a form of LHS that harden overnight as they are cooled through NV and then melt throughout the day, absorbing heat and delaying the indoor temperature peak. An increasing thickness of PCM increased the energy savings for cooling

demand, with the energy savings also linked to the climate conditions and the thermal insulation used throughout the building (Solgi et al., 2019).

2.3.3 Wind Towers

Developed in hot climates for passive cooling, wind catchers, also known as wind towers, have been used for centuries throughout the Middle East (Figure 2-2). Although beneficial for indoor cooling, they also provide ventilation, reducing the concentration of indoor pollutants and helping to decrease instances of SBS (Alwetaishi and Gadi, 2020).

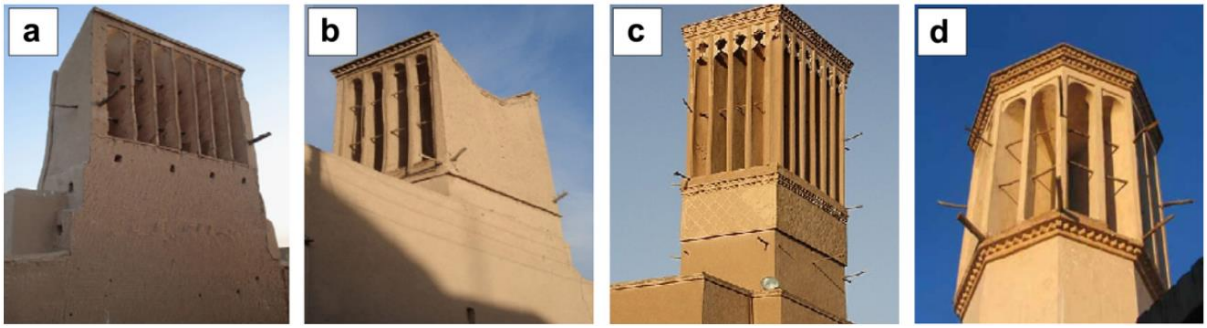

Figure 2-2 - Traditional wind towers with different numbers of openings a) one-sided, b) two-sided, c) four-sided, d) eight-sided (Hughes et al., 2012)

Varying designs have since been employed, operating under the same basic principles of wind-driven flow and the stack effect to generate airflow through buildings (Walker and Wilson, 1993). Research has concentrated mainly on the impact of the number of sides and shape of the wind tower on ventilation rates, improving the pressure gradient between the windward and leeward sides through louvre design, reducing or eliminating short-circuiting between the incoming and outgoing air channels, and ease of incorporation with heat recovery methods (Hughes et al., 2012; Saadatian et al., 2012).

Figure 2-3 - Modern square-based wind tower with an integrated solar panel (Hughes and Ghani, 2011)

2.3.3.1 Wind Tower Operating Principles

Wind towers generate ventilation primarily by exploiting regions of relative positive and negative pressure around themselves and the adjoining building (Figure 2-4), where these regions of high and low pressure are created by wind-driven flow and the passive stack effect (Walker and Wilson, 1993).

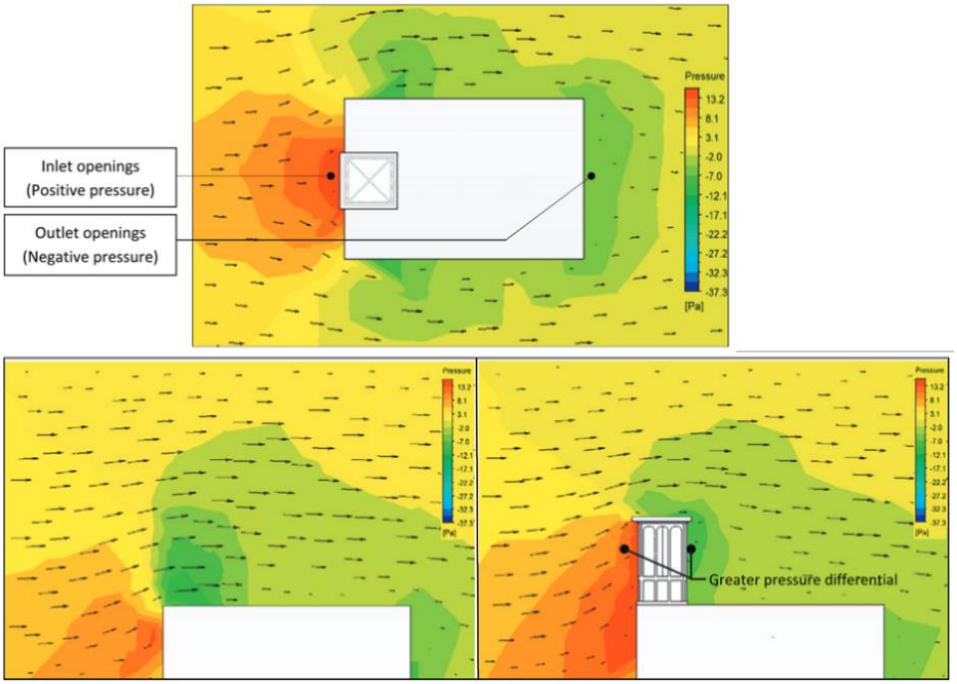

Figure 2-4 - CFD analysis showing positive pressure on the windward building façade and negative pressure on the leeward side (Hughes et al., 2012)

The internal volume of the wind tower is divided into two or more channels, each of which can perform as an inlet or outlet depending upon the wind direction. The inlet or inlets guide the air down into the building where it is distributed throughout the room, providing cooling through convective and evaporative heat transfer (Al-Sallal and Al-Rais, 2012). Stale indoor air flows out of the wind tower outlet towards the negative pressure region on the wind tower's leeward side, creating a combined suction and driving force (Figure 1-2).

Ventilation is also provided through the stack effect which is created by the temperature differences between the indoor and outdoor air. Thermal gains within the building increase the internal air temperature above the ambient. As with solar chimneys, warm air rises exiting through the wind tower's exhaust channel, at which point cooler fresh air flows in to replace it (Khan et al., 2008).

Montazeri (2011) determined that the wind tower should be designed to create the maximum pressure difference possible to improve ventilation efficiency. The factors affecting the wind tower’s ability to harness these pressure differences include the wind tower dimensions, incident air angle, pressure coefficient at the opening, and the design of the opening itself (Alwetaishi and Gadi, 2020). The research explored how the external shape of the wind catcher impacted the air velocity within the building, using lab-based experimental work to validate a numerical model. They found that curving the body of the wind catcher served to increase the internal air velocity by 0.5 m/s relative to a wind catcher with a straight bodies as they produced greater dynamic movement at the flow at the outlet

2.3.3.2 Wind Tower Design Features

Traditional wind towers are raised above the building to capture air at a higher velocity in urban environments whereas commercial wind towers adapted for Western climates are often attached directly to the structure roof (Ghadiri, 2011).

The optimum incident angle for wind flows onto a wind tower is the angle at which the most effective area is exposed to the stream (Montazeri, 2011). Elmualim and Awbi (2002) compared the performance of square and circular wind tower geometries at wind angles from 0° to 45° and speeds from 0.5 – 6 m/s. The square wind tower was shown to outperform the circular version, generating greater ventilation rates under the same conditions. This results from the sharp edges of the square creating a large region of flow separation around the wind tower, creating a greater pressure difference between the inlet and outlet faces of the wind tower.

Generally, increasing the number of openings decreases the air velocity through the wind tower, however fewer openings make the wind tower more susceptible to changes in wind direction (Saadatian et al., 2012), with single-sided wind towers capable of capturing a much narrower range of wind angles than a multi-sided wind tower (Montazeri, 2011; Hughes et al., 2012). Calautit and Hughes (2014) found that an incident angle of 45 degrees was optimum for a four-sided wind tower, creating a volumetric flow rate of 0.47 m^3/s at a wind speed of 3 m/s, 32% higher than the case of a wind angle of 0 degrees.

A series of stacked louvres compose the outer faces of the wind tower, angled to encourage air flow through the wind tower to the building below and assist in limiting the impact of adverse weather by keeping out rain and snow. Liu et al. (2011) used CFD models validated against experimental data to determine the optimum number

and length of the louvres. An increasing number of louvre layers served to increase the flow rate into the wind tower, showing that from 2 to 3 louvre layers the airflow rate increases by 12.7%, whereas past six layers the relative improvement was below 1.5% (Figure 2-5).

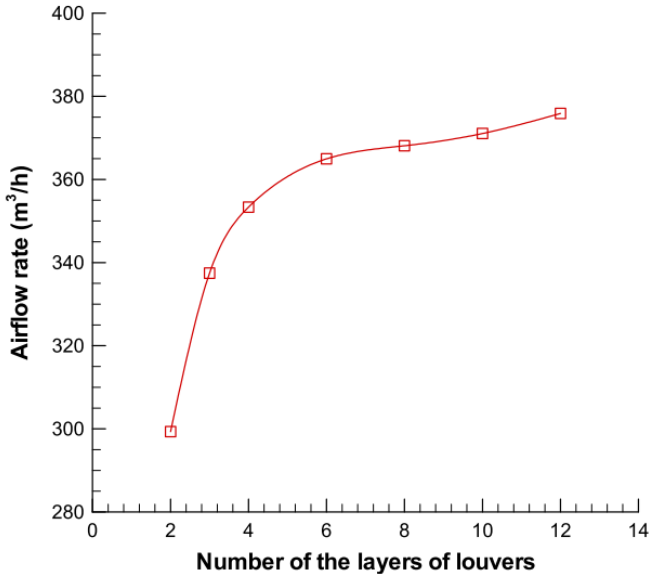

Figure 2-5 - Variation of airflow rate with the number of louvre layers (Liu et al., 2011)

Hughes et al. (2012) presented a comprehensive review of wind-driven and passive ventilation systems, detailing the features and limitations of both traditional and modern designs whilst comparing the achievable flow rates. At the time, the commercial Windvent device generated the highest air flow rates, supplying up to 650 l/s at a wind speed of 5 m/s.

Wind towers are often used in urban settings where the airflow is disrupted by nearby buildings meaning open windows alone do not provide sufficient ventilation. Using wind towers in conjunction with other forms of natural ventilation such as windows can improve ventilation rates (Drach, 2009). For a room with a wind tower and internal heat source, adding a window to the leeward wall of the room was found to increase the

effects of buoyancy-driven ventilation by 47% (Hughes and Mak, 2011). Elmualim (2006) showed that wind towers could induce a substantially greater ventilation rate than an open window of an equivalent area, however the greatest day and nighttime cooling was achieved by using the wind tower in conjunction with an openable window, enabling the indoor temperature peak to remain the same or below the peak outdoor temperature.

Flow separation at the leading edge of the roof impacts the flow profile into the wind tower inlet (Ozmen et al., 2016). A large portion of the studies conducted around wind towers only include the wind tower in the boundary layer as this replicates the conditions of the wind tunnel test that is often employed within the studies. This however is not an accurate reflection of the real world conditions, where the building and wind tower together are subjected to the airflow. By removing the building from the boundary layer, the flow rate measured through the wind tower may be larger than in reality as the impact of the flow separation at the leading edge of the building is not accounted for. Wu et al. (2021) conducted a CFD study of a multi-sided wind tower attached to a low-rise house with additional single-sided ventilation. The wind tower and building geometry were simulated under two boundary layer conditions, the first with just the wind tower exposed to the wind and then the wind tower and building together (Figure 2-6).

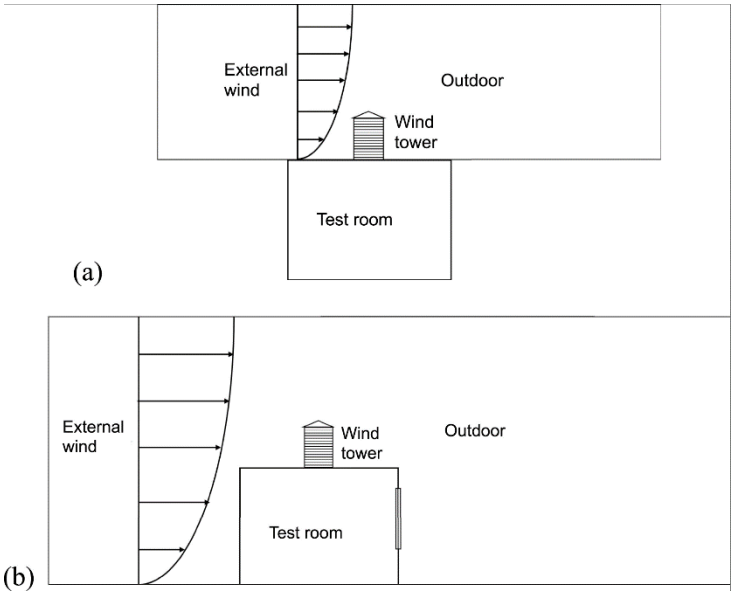

Figure 2-6 - Physical models of underground and low-rise house applications (Wu et al., 2021)

They found that under the same boundary conditions, the wind tower with the building included had an average supply velocity approximately 40% lower than the wind tower only application due to the flow separation experienced at the leading edge of the building.

Short-circuiting occurs when the incoming air leaves straight through the exhaust channel without mixing with the air in the room, reducing the effectiveness of the ventilation system (Figure 2-7). Nejat et al. (2016) investigated the impact of an Anti-Short-Circuit Device (ASCD) to help reduce short-circuiting by angling the airflow away from the exhaust channel of the windcatcher. An ASCD device with an angle between 20 – 80 degrees was sufficient to prevent fresh air from entering the exhaust region, however smaller angles between 20 – 40° negatively impacted the average air inflow velocity as they blocked large areas of the diffuser. In addition to eliminating short-circuiting, the ASCD device also served to direct air away from the centre of the room towards the corners where ventilation rates are generally lower, further improving the characteristics of the wind tower for the removal of pollutants.

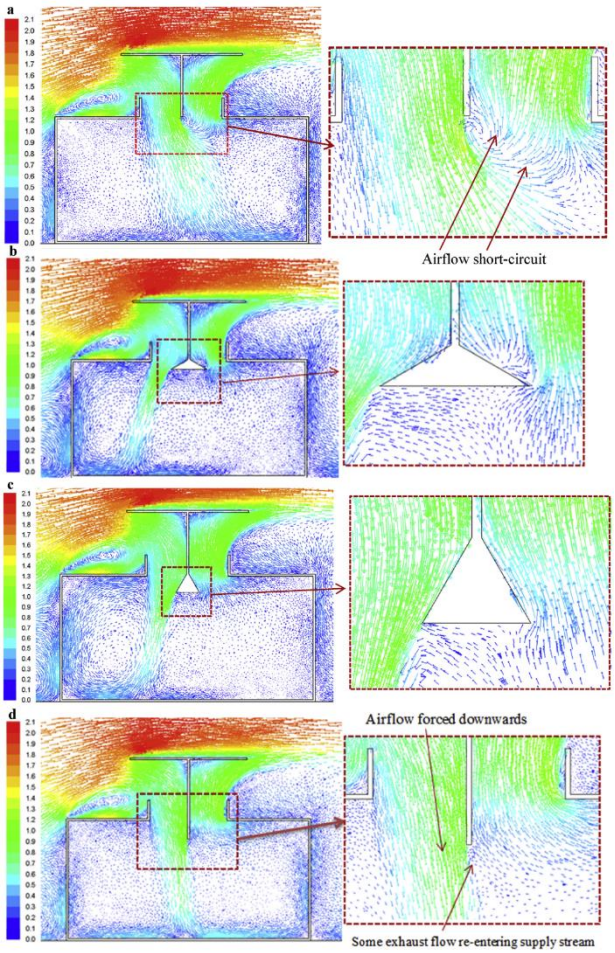

Figure 2-7 – Velocity vectors through (a) reference windcatcher, (b) windcatcher with ASCD at 30 °, (c) windcatcher with ASCD at 60 °, (d) windcatcher with ASCD at 90 ° (Nejat et al., 2016)

2.3.4 Numerical Studies of Wind Towers using CFD

Much of the research surrounding wind towers uses CFD modelling as it is a quick and efficient way of making incremental changes to a design without spending time building and testing each new element while generating more complete data. Turbulence models and wall functions are used within CFD to predict the turbulent nature of the flow throughout the computational domain and in near-wall regions. The selection of each can significantly affect the results produced through simulation.

Perén et al. (2015) conducted a sensitivity analysis for several computational parameters affecting the results of a CFD study of an isolated building with asymmetric

openings for crossflow ventilation. The impact of changing parameters such as the turbulence model, wall functions, and grid refinement on the velocity through the building was measured, with each parameter changed one at a time and compared against a reference case. The parameters were selected as they have been found in related studies to have a significant impact on the final results produced through CFD modelling. Six turbulence models were tested, including the standard, RNG, and realisable k-epsilon models, and the standard and SST k-omega models. Using the k-omega SST as the reference case, the standard and RNG k-epsilon models were found to best agree with the volumetric flow rate produced through the experimental results, although the variation in volumetric flow rate for the other models was only between -0.05% and 3.67%. However, the difference in local indoor air velocity was much more significant, up to 300% in some areas owing to the slight differences in the direction of the incoming flow.

Hughes and Ghani (2010) explored the impact of altering the external louvre angle on a commercial wind tower against internal pressure and wind velocity. The commercial CFD software ANSYS Fluent was used to model a commercial wind tower with ten louvre layers spaced 50 mm apart. The standard k-epsilon model was used to model the turbulent elements of the flow throughout the domain. The maximum induced internal air velocity was achieved with a louvre angle of 35 °, increasing occupant comfort by 45% and reducing trailing-edge stall pressure by 42% relative to the benchmark model with louvres at 45 °.

Calautit and Hughes (2014) used wind tunnel testing to validate a CFD model evaluating the performance of a multi-sided wind tower. The wind tunnel test used a 1:10 scale model of a commercial wind tower design with four sides, investigating the

velocity and pressure patterns within a test room below. Results indicated that the wind tower could supply fresh air for a classroom of 15 people (10 L/s per person) at wind speeds as low as 2 m/s and that the room was generally under negative pressure at wind speeds greater than 0.5 m/s, indicating more air was expelled from the room than was supplied.

Hosseinnia et al. (2013) measured the impact of an increasing number of partitions within a wind tower on inlet velocity and the potential of evaporative cooling using a numerical model to predict performance (Figure 2-8). The entire wind tower and building were modelled within the boundary layer, applying wet surfaces to the wind tower partitions to replicate evaporative cooling. Applying the standard k-epsilon turbulence model they found that increasing the number of partitions increased the air velocity into the room from 1 to a maximum of 1.53 m/s whilst maintaining other geometrical parameters constant.

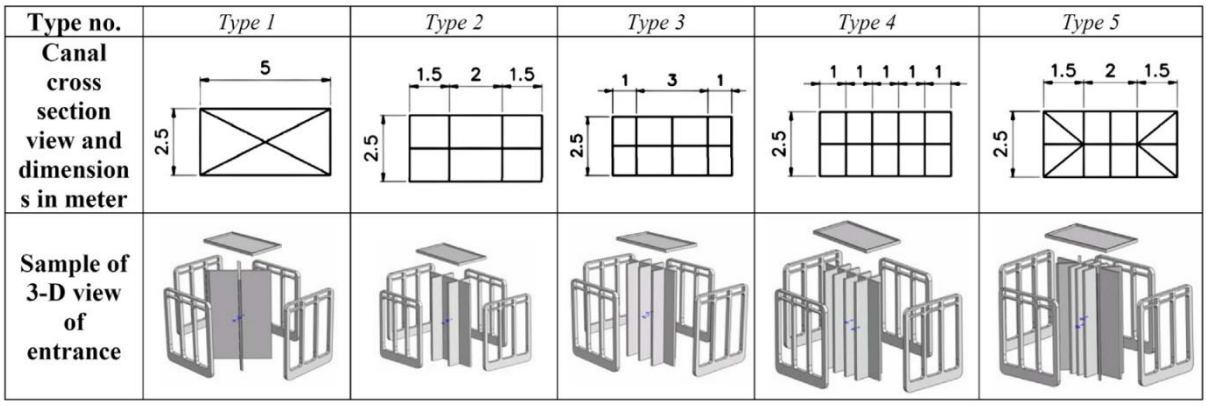

Figure 2-8 - Five types of partitions for a traditional wind tower (Hosseinnia et al., 2013)

Calautit et al. (2014) investigated the impact of wind tower arrangement and spacing on ventilation rates and internal CO_2 concentration when considering the application of multiple wind towers to the same roof in a parallel or staggered arrangement. CFD analysis shows that the wake of the windward wind tower negatively impacts the wind

tower behind, with increased spacing between wind towers increasing inlet velocity on the leeward wind tower (Figure 2-9). Moving the leeward wind tower out of the wake of the windward wind tower was also shown to prevent the re-entry of CO_2 expunged from the building.

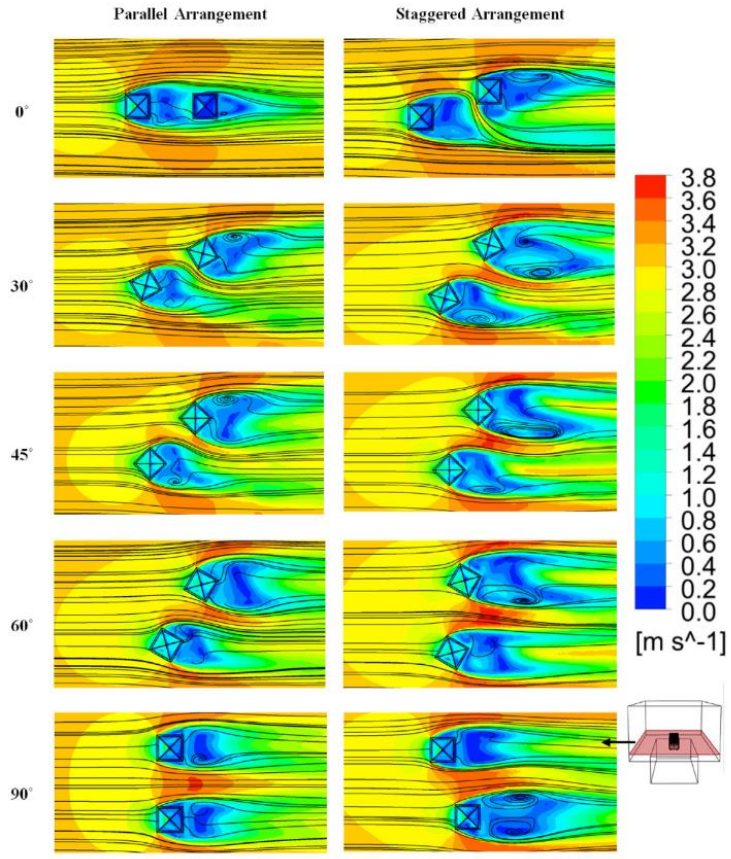

Figure 2-9 - Effect of wind angle on the airflow in and around the windward and leeward wind towers (Calautit et al., 2014)

Several viable turbulence models can be applied to review CFD studies related to wind towers. Identifying the most suitable model can be done on a case-by-case basis and may require some trial and error to find the best fit for each numerical model. CFD models are validated against experimental or previous numerical data that can be used to indicate the accuracy of each turbulence model. It has also been shown that the ventilation rates achievable through wind towers are sufficient to satisfy designed air change rates.

2.3.5 Design Criteria

After reviewing literature relevant to the development of wind towers, several design aspects were identified as crucial to dictating the performance of the wind tower system. To maximise the flow rate through the wind tower, it is generally desirable to create the greatest pressure difference between the windward and leeward faces of the wind tower. Square wind towers were shown to outperform circular wind towers, generating greater ventilation rates at the same wind speed due to the flow separation that occurs at the sharp edges of the corners of the wind tower (Elmualim & Awbi, 2002). The flow separation created a greater pressure difference between the windward and leeward faces of the wind tower, inducing a greater flow rate between the inlet and exhaust channels. This is beneficial when high ventilation rates are desired, however internal air velocity has been shown to impact the thermal comfort of the occupants and therefore must be controlled using volume control dampers to limit ventilation rates under high wind speeds.

Wind towers generate the greatest flow rates when the internal frame is perpendicular to the airflow as this exposes the greatest surface area to the wind. An increasing number of sides reduces the susceptibility of the wind tower to changing wind direction, as a greater number of channels can capture the flow at a greater range of wind angles (Montazeri, 2011; Hughes et al., 2012) . However, increasing the number of sides also reduces the flow rate through the wind tower (Saadatian et al., 2012).

Louvres were introduced into modern wind tower designs to channel the airflow through the opening. An increasing number of louvre layers served to increase the flow rate through the wind tower, although limited benefit was seen beyond six louvre layers due to the short circuiting of air entering through the upper layers exiting through the lower layers (Liu et al., 2011). The impact of louvre angle on ventilation rate has

also been explored, with an angle of 35 ° found to be preferable as this limited the flow separation that occurred at the leading edge of the of the louvre (Hughes & Ghani, 2010).

Similarly, the angle of the roof also impacts the flow rate through the wind tower. A flat roof created a thicker boundary layer over the wind tower relative to an angled roof. When the wind tower was placed within this boundary layer, ventilation rates through the wind tower fell by between 15 –40 % relative to the wind tower subject to a uniform flow (Wu et al., 2021). It is therefore important to consider the positioning of the wind tower within the roof, considering the average local wind speed, direction, and roof angle. Placing the wind tower at the edge of the building would negate some of the impact of the flow separation at the leading edge of the building. Alternatively raising the wind tower higher above the roof level to place it outside of the boundary layer would achieve the same effect.

Finally, anti-short-circuiting devices should be considered to direct the flow of air away from the exhaust channels as it enters the room, reducing the amount of short-circuiting that occurs between the channels. This also serves to increase mixing throughout the room as the fresh air is directed towards the corners of the room, helping to remove indoor pollutants (Nejat et al., 2016).

2.4 Heat Recovery

Air-to-air heat exchangers are used in three areas of application: process-to-process, process-to-comfort, and comfort-to-comfort energy exchange (Sauer and Howell, 1981). Comfort-to-comfort heat recovery is a method of extracting waste heat or cold from exhaust air streams to heat or cool incoming air streams, reducing building energy demand by lowering the reliance on mechanical heating and cooling systems.

This process requires a steady stream of air to pass over the heat exchange interface in both the hot and cold channels with little or no direct mixing between the air streams.

As the behaviour of building occupants' changes, technology must continue to adapt with them. Many countries have experienced an increase in the use of heating and cooling, with HVAC systems now more affordable for much of the world's population. The increase in thermally regulated indoor environments presents an opportunity to exploit the warm or cool air leaving the building through heat recovery. Compared with traditional HVAC systems, heat recovery systems have been proven to significantly reduce overall building energy demand (Kalbasi et al., 2020).

The thermal energy within air streams can be separated into sensible and latent heat. The amount of sensible heat in the air is related directly to the temperature of the exhaust stream. In contrast, the latent energy relates to both the temperature and the energy contained within the moisture in the air. Heat recovery methods can extract sensible or both sensible and latent heat, with methods that exploit both (enthalpy exchangers) capable of generating higher overall recovery efficiencies (Choi et al., 2018) at the expense of higher initial and maintenance costs (Mardiana-Idayu and Riffat, 2011).

There are four leading heat recovery technologies: Heat pipes, run-arounds, rotary thermal wheels, and fixed plate heat exchangers, with the application of each dictated by the wider system design. Although it has been predicted that 70 – 90% of the energy needed for the conditioning of incoming air could be saved (Zhang, 2012), heat recovery methods are often absent from passive ventilation due to the incurred pressure drop over the heat exchanger limiting the air flow rate into the room (Shao et al., 1998). A pressure drop of 1 – 5 Pa is typical in passive ventilation systems, with

anything greater often considered too substantial. As there is no fan driving the airflow into the room through passive systems only small pressure losses over the heat exchanger are acceptable.

2.4.1 Rotary Thermal Wheel

Rotary thermal wheels are mechanically powered porous metallic wheels that transfer heat from one air stream to another by circulating through both air streams periodically (Figure 2-10). The porous medium acts as a temporary thermal store, holding thermal energy gained from the exhaust air stream within the matrix before transferring it to the inlet stream (Herath et al., 2020). They are often characterised by high effectiveness values and low installation and operating costs but are limited in that both air streams must be near one another (Khanmohammadi and Shahsavar, 2018).

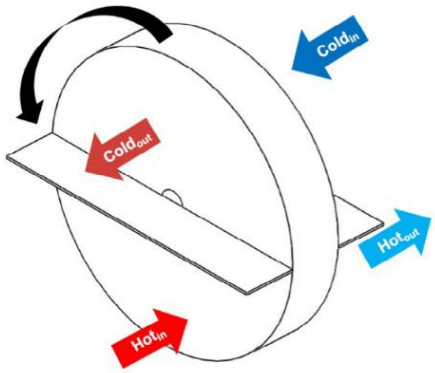

Figure 2-10 - Rotary thermal wheel operation (Seo et al., 2018)

Using a porous medium to construct the thermal wheel increases the effective area for heat transfer. Wheels with larger heat transfer surface areas achieve higher sensible effectiveness but incur a higher pressure drop over the system (Zmrhal et al., 2023). As the air velocity over the wheel increases so does the pressure drop experienced by the air stream. An increasing inlet velocity results in a greater build-up of pressure on the upper side of the rotary wheel, and therefore a greater pressure

drop over the wheel. Consequently, introducing thermal wheels into passive ventilation systems can be challenging (O'Connor et al., 2016).

Rotary wheels can be divided into sensible wheels (heat wheels) and enthalpy wheels (energy wheels), where sensible wheels only exchange the sensible heat between air streams. In contrast, enthalpy wheels transfer sensible and latent heat (Herath et al., 2020). Each wheel is constructed the same, however, enthalpy wheels use desiccant material to transfer sensible and latent heat (Khanmohammadi and Shahsavar, 2018). Enthalpy wheels within mechanical ventilation systems can achieve heat recovery efficiencies as high as 80% (Herath et al., 2020).

De Antonellis et al. (2014) performed an optimisation study of an enthalpy wheel, exploring the impact of wheel length, channel base, height, thickness, air velocity, and revolution speed on the effectiveness of heat recovery. The airflow rate varied between 1000 and 3000 m^3/h and the pressure drop was measured. The results indicated that a greater wheel length increases the effectiveness but also the pressure drop. A balance that satisfies both parameters is found at a thickness of around 0.2 m. An increase from 1.5 to 4 m/s corresponds to a rise in pressure drop from 75 to approximately 200 Pa.

O'Connor et al. (2015) explored the impact of rotary wheel rotation speed up to 500 rpm on the ventilation supply rate when installed within a passive ventilation system. To maintain the recommended air supply rate of 8 L/s per person a rotation speed of up to 50 rpm was manageable but beyond this proved overly detrimental to the air supply rate. The maximum temperature recovery of 1.77 °C is realised at 20 rpm, and therefore an operating range of 5 – 20 rpm was suggested.

O’Connor et al. (2016) presented a novel design of a desiccant rotary wheel, replacing the traditional porous matrix with radial blades coated in silica gel particles. Through experimental and CFD studies the design achieved a pressure drop of just over 2 Pa at an air velocity of 0.8 m/s and a reduction in relative humidity up to 55%. Lowering the pressure drop over the system significantly improves the thermal wheel's viability for installation within a passive ventilation system. It would however be expected to see the pressure drop rise with an increase in air velocity as reported in other studies.

2.4.2 Fixed Plate Heat Exchanger

Fixed plate heat exchangers are composed of thin metal plates layered with a small gap between each to allow air to flow between them. The plates separate the incoming and outgoing air flows while providing a surface for indirect heat transfer between them. As the warm air stream heats the plate on one side, the heat is conducted through the plate to the cold air stream as it passes over and gains some of the available heat (Figure 2-11). Fixed plate exchangers can transfer sensible and latent heat depending on the available temperature and moisture gradient (Liu et al., 2016) and can achieve efficiencies of up to 90% (Nielsen et al., 2009). The passage of air through the heat exchanger can be arranged as concurrent, counter-flow, or cross-flow, where counter-flow is preferred due to its higher heat transfer performance (Borjigin et al., 2020).

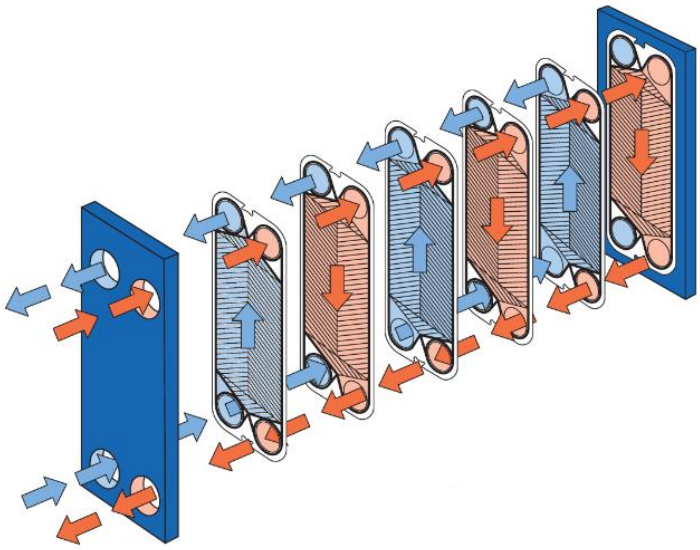

Figure 2-11 - Counter-flow plate heat exchanger (Walraven, 2014)

Fernandez-Seara et al. (2011) reported on the performance of an air-to-air plate heat exchanger under increasing flow rates. Raising the inlet flow rate from 50 to 175 m^3/hr reduced the heat transfer rate but improved the heat exchange efficiency from 30 to 70%. The pressure drop over the length of the exchanger increased almost linearly with increasing flow rate to a maximum of 275 Pa at 175 m^3/hr.

2.4.3 Membrane Fixed Plate Exchanger

More recently, plate heat exchangers have been modified by introducing a thin, semi-permeable membrane instead of metallic plates that can recover both sensible and latent heat. For total heat recovery these membranes should ideally be highly permeable, selecting for water vapour over other gases and particulates that may be present in the exhaust air. Water vapour transport through the membrane is determined by the membrane thickness, thermal conductivity, mass diffusivity, and porosity (Engarnevis et al., 2018).

Siegele and Ochs (2019) compared the effectiveness of plate and enthalpy heat exchangers. Both were counterflow heat exchangers made of unspecified polymers.

The plate exchanger had a nominal efficiency of 92% at a flow rate of 100 m^3/h, while the enthalpy exchanger had an efficiency of 88% at 100 m^3/h. Both designs incurred a pressure drop of approximately 12 Pa at a flow rate of 100 m^3/h. For the plate exchanger the energy transfer was found to be independent of the relative humidity if condensation did not occur, whilst the enthalpy exchanger was highly dependent upon the humidity of the exhaust air, even under conditions where condensation did not occur. Furthermore, even with a reduced surface area the energy transfer of the enthalpy exchanger was comparable to that of the heat exchanger, with higher relative humidity values resulting in improved energy transfer between air streams.

Sabek et al. (2016) explored the use of a membrane for total heat exchange. They found that an increase in air velocity from 0.125 m/s to 0.25 m/s increased heat and mass transfer, reducing the temperature within a controlled climate from 19.5 to 17.6°C and the relative humidity from 78.3 to 75.2%. The efficiency of the heat exchanger decreased with increasing inlet velocity, with an efficiency of approximately 80 and 55% reported at 0.125 and 0.25 m/s respectively. The surface area was also shown to significantly impact the temperature and humidity profiles, highlighting the need for a large membrane surface area to ensure higher sensible and latent efficiencies. Membrane clogging was also observed, whereby the accumulation of particles, colloids, and bacteria reduced the membrane's permeability over time.

2.4.4 Heat Pipes

Heat pipes transfer thermal energy between hot and cold fluid streams, transferring heat along their length through a repeating evaporation-condensation cycle within themselves enabled by the thermal energy in the respective hot and cold streams. They are created by evacuating the air from a wicked pipe and then filling it with a

small amount of liquid. The wick is made from porous or grooved metal on the inside surface of the pipe and is used to draw the liquid from the condenser back to the evaporator through capillary forces. The internal fluid undergoes constant phase changes between gas and liquid as it is heated and cooled at each end. Via this process heat is absorbed at one end causing the internal fluid to evaporate and travel to the other end of the pipe where the vapour condenses, releasing the heat back to the alternate fluid stream through the pipe wall (Figure 2-12). Heat pipes are designed to operate within specific temperature ranges, with the ideal operating temperature dictated by the working fluid, fill ratio, and internal pressure (Jouhara et al., 2017).

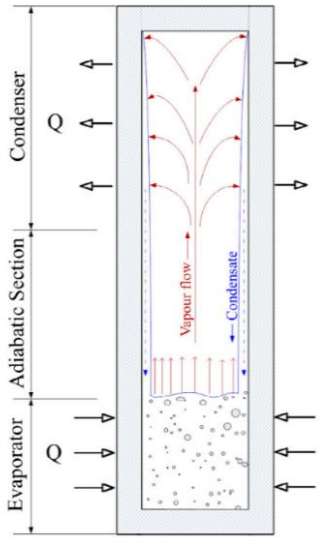

Fig. 2. Schematic of a working heat pipe.

Figure 2-12 - Schematic of a working heat pipe (Ramos et al., 2016a)

Heat pipes are compact, have a high rate of heat recovery and heat transfer, have no moving parts, require little to no maintenance, incur a small pressure drop for the fluid flowing across them, and can operate in a wide range of temperatures depending on the material choice and internal heat transfer fluid (Srimuang and Amatachaya, 2012; Shabgard et al., 2015). They cannot however recover latent heat and are limited by the boiling point or capillary limit, with the latter exhibited through an overheating of the evaporator section due to a lack of cooling fluid (Yang et al., 2008).

Wickless heat pipes are also known as two-phase closed loop thermosyphons or Thermosyphon Heat Pipes (THPs) (Srimuang and Amatachaya, 2012). THPs are often orientated vertically with the evaporator at the bottom and the condenser above. The working fluid evaporates, and the resulting vapour rises up the pipe. The vapour condenses at the top of the pipe and is transported back to the evaporator section under the influence of gravity. Where possible, THPs are preferred to standard heat pipes as wicks can resist the condensate's flow. Chaudhry et al. (2012) reviewed several other types of heat pipe, including tubular, pulsating, and micro, comparing the basic features and limitations and highlighting some of the roles played in heat recovery and energy conservation.

Heat pipes subject to a flow with a low Reynolds number can be arranged in a staggered tube arrangement to improve heat transfer from the fluid stream to the heat pipe and vice versa. A staggered configuration is preferred as a greater portion of the surface area of the downstream tube remains in the path of the main flow (Hviid and Svendsen, 2011). Khan et al. (2006) compared linear and banked tube arrangements, finding that the average heat transfer coefficient was dependent on the longitudinal and transversal pitches and the Reynolds and Prandtl numbers. Compact banks, both inline and staggered, gave higher heat transfer rates than those that were widely spaced, however due to the arrangement this is likely to incur a pressure drop higher than is suitable for passive ventilation applications.

Yang et al. (2019) tested the ability of Pulsating Heat Pipes (PHPs) (Figure 2-13) to recover cool from exhaust air in an air-to-air heat exchanger. The heat exchanger consisted of 40 PHPs, each with a length of 21.6 m, 40 turns, and an inner diameter of 2 mm. It was concluded that the optimum installation angle of the PHP was at 60°,

with 90° producing a slightly lower effectiveness. Increasing outdoor air temperature improved the system's effectiveness from 37% to 48% between 30 – 40 °C. Cooling recovery capacity increased almost linearly with wind speed, rising from 440 W to 821 W with an increase in wind speed from 1.3 to 3.3 m/s, however, this negatively impacts the effectiveness as the decrease in fresh air temperature and increase in exhaust air temperature were both lower. Increasing wind speed also causes a rapid rise in pressure drop over the PHP, from around 15 Pa at 1.25 m/s to above 45 Pa at 3.25 m/s.

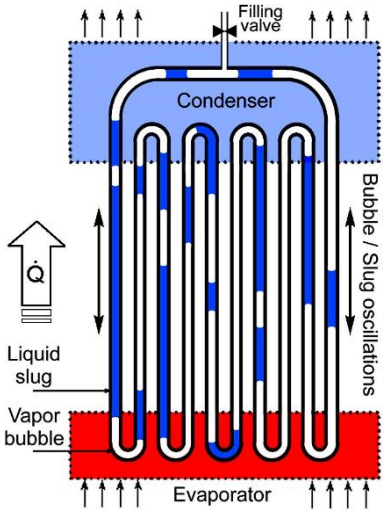

Figure 2-13 - Pulsating heat pipe operation (Baradol et al., 2019)

El-Baky and Mohamed (2007) tested wicked heat pipes installed in a staggered arrangement through ductwork to transfer heat from exhaust to fresh air in a mechanical ventilation system (Figure 2-14). The fresh air inlet temperature varied between 32 - 40 °C while the exhaust air temperature remained constant at 26 °C. The heat pipes used R-11 as the internal working fluid at a pressure of 0.127 MPa corresponding to a saturation temperature of 30 °C. The effectiveness of the evaporator and condenser section increased with the fresh air inlet temperature. Doubling the mass flow rate through the exhaust channel increased the temperature reduction to the fresh air by 20% and the effectiveness of the heat exchanger by 26%.

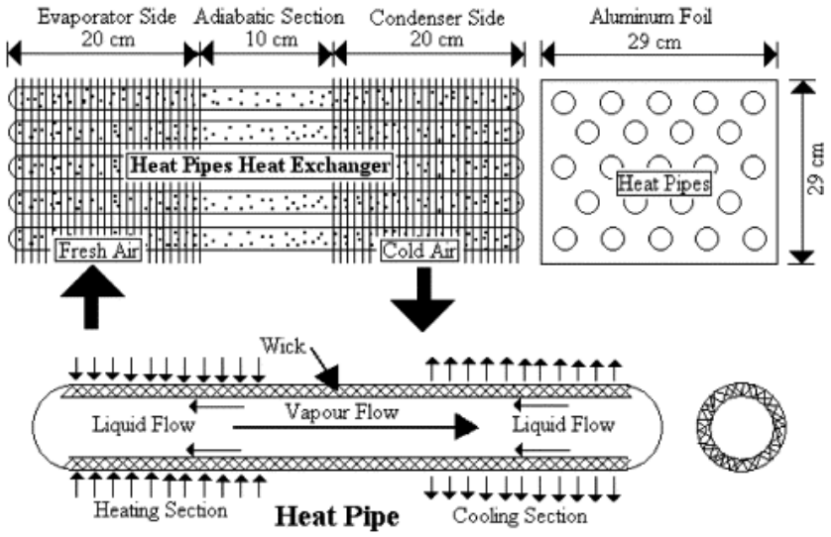

Figure 2-14 - Heat pipe heat exchanger and heat pipe design (Abd et al., 2007)

The longitudinal and transversal pitches between the pipe centres of the heat pipes in the array has a significant impact on the velocity and pressure loss, as well as the heat transfer occurs between the inbound fluid and the heat pipe surface. Chaudhry et al (2017) used wind tunnel testing and CFD modelling to determine the optimum spacing between pipe centres to minimise pressure loss whilst maximising heat transfer three banks of staggered heat pipes. Each pipe had an outer diameter of 16 mm and were oriented perpendicular to the direction of the flow through the wind tunnel test section. The transversal pitch remained constant at 50 mm whilst the longitudinal pitch was increased from 20 to 40 mm in increments of 5 mm (Figure 2-15).

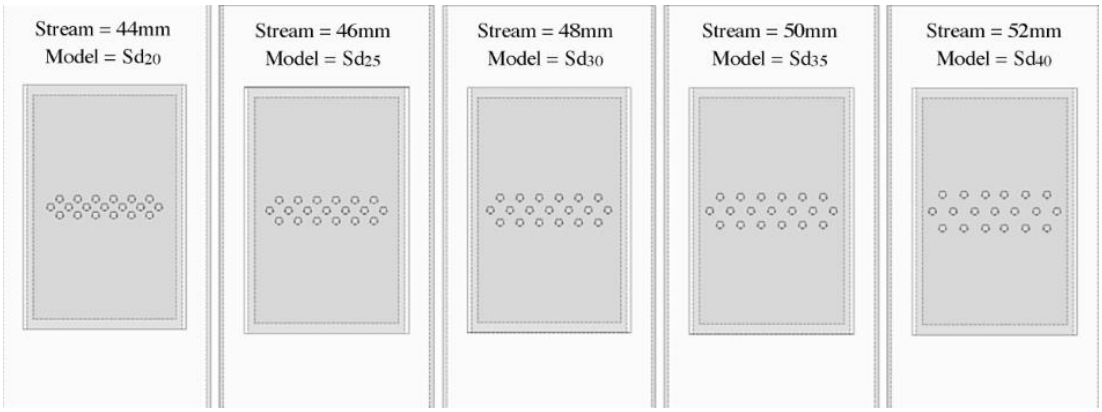

Figure 2-15 - Pipe arrays with increasing longitudinal pitch (Chaudhry et al., 2017)

They found that the greatest decrease in average velocity and the greatest temperature difference to the air passing over the heat pipe array occurred at the smallest spacing, with velocity decrease and change in temperature decreasing with increasing spacing as would be expected. The average velocity through the channel decreased by 45% when the spacing was 20 mm, and by 40% when the spacing was 40 mm. The cooling capacity of the heat pipe array decreased by approximately 11% when the streamwise spacing was increased from 20 to 40 mm.

In a similar study Hughes et al. (2014) used wind tunnel testing and CFD modelling to measure the outlet velocity after three layers of staggered heat pipes when they increased the longitudinal pitch from 20 to 45 mm in increments of 5 mm. The outlet velocity was found to decrease by a maximum of 26.4% and a minimum of 19.8% when the longitudinal pitch was 20 and 35 mm respectively. Increasing the pitch beyond 35 mm resulted in a greater reduction in the outlet velocity.

2.4.4.1 Heat Pipe CFD Modelling

Due to the repeating phase change cycle of the heat transfer fluid within heat pipes, modelling the heat transfer process using CFD can be challenging. As a result, several differing approaches have been developed.

Alizadehdakhel et al. (2010) used a Volume Of Fluids (VOF) approach to model the gas-liquid interface within a single 2D thermosyphon heat pipe and predict the heat transfer along its length. The VOF method follows the interface between fluids during simulation, where the phase interface is represented by the liquid volume fraction within each cell (Sun and Zhang, 2020). A range of heat flux values recorded during the experimental work were applied as a boundary condition to the evaporator section of the heat pipe in the numerical model. Comparison between experimental and

numerical results indicated a reasonable agreement between the data except through the adiabatic section of the heat pipe. This results from the numerical model ignoring heat losses in this section entirely. Although this method is perhaps the most accurate at modelling the phase change cycle within the heat pipe, the simulation is conducted at tiny time steps (< 10^{-3} s) in only two dimensions and therefore is not considered suitable for this case.

Calautit et al. (2013) created a three-dimensional model of thirteen heat pipes to compare the cooling effectiveness versus evaporative cooling through a wind tower. Each pipe had an outer diameter of 20 mm and a wall thickness of 2.5 mm with a mass flow inlet at one end and a pressure outlet at the other, creating a flow through the centre of the pipe to replicate the transfer of heat along the length of the pipe [Figure 2-16]. Boundary conditions applied to the pipes included a constant surface temperature of 323.15 K and inlet mass flow rates of 0.0104 and 0.169 kg/s for water and ethanol, respectively. The Euler-Euler approach was utilised whereby differing phases are treated as mathematically interacting, with the sum of all phasic volumes being equal to one. The model is validated using experimental results for velocity and evaporative cooling, and therefore there is no comparison for the accuracy of the heat pipe modelling approach.

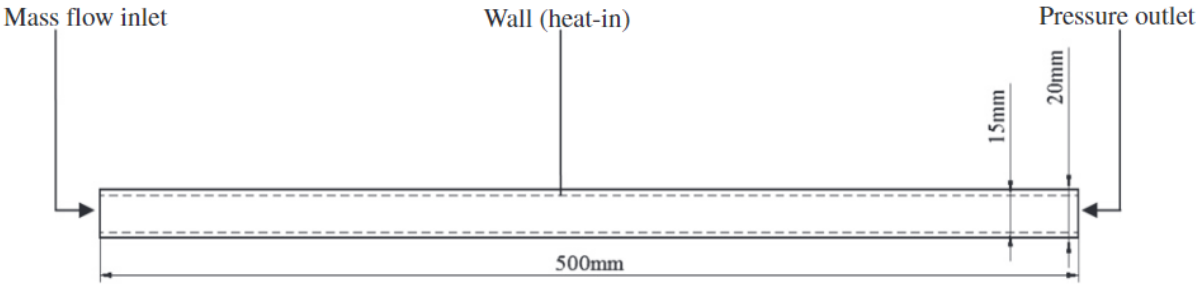

Figure 2-16 - Heat pipe sectional specifications and boundary conditions (Calautit et al., 2013)

Mroue et al. (2015) and Ramos et al. (2016b) both approximated wickless thermosyphon heat pipes as superconducting solid bodies by deriving the total thermal resistance of a THP during heat transfer (Figure 2-17). The numerical models applied a constant thermal conductivity to the bodies of the heat pipes with the standard k-epsilon turbulence model. The heat pipe is split into three parts for calculating the thermal resistance: the evaporator section, an adiabatic section, and the condenser section. The total thermal resistance is the sum of the resistances from conduction and convection at the evaporator and condenser and the resistances from the boiling, pressure change, and condensation of the heat transfer fluid. Mroue et al. (2015) tested a heat exchanger with two air and two water passes linked by six thermosyphon heat pipes. In testing the inlet air temperature and mass flow rate were increased from 100 – 250 °C and 0.05 – 0.14 kg/s respectively. The water in the condenser was kept constant at 14 °C and 0.08 kg/s. This method found an average temperature difference of 3% in the evaporator section and 5% in the condenser between the experimental and numerical results. The translation of this modelling approach to lower temperature applications has however not been tested, where the limited temperature difference between the evaporator and condenser sections of the heat pipe may impact the effectiveness of approximating the heat pipe as a superconductor.

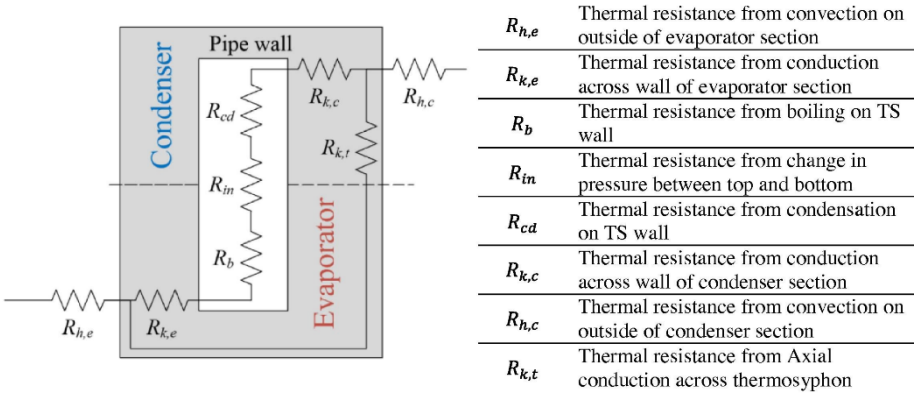

Figure 2-17 - Schematic of the thermal resistances within a thermosyphon (Ramos et al., 2016b)

Calautit et al. (2016) explored vertically arranged thermosyphon heat pipes within a wind tower to heat fresh air. They developed a three-dimensional numerical model of a roof-mounted wind tower and heat sink to transfer heat between the heat pipes through the wind tower outlets and inlet. To model the heat pipes' cooling effect, a constant surface temperature of 293 K was applied, equal to the standard operating temperature of heat pipes. The numerical model was validated using a wind tower with no heat pipes, comparing supply airflow, the airflow pattern around the wind tower, and indoor air temperature against results from a scale model wind tunnel test. As a result, the accuracy of the heat pipe modelling approach is not compared against any experimental data and therefore the accuracy is unknown. Nevertheless, applying a constant surface temperature as a boundary condition is an approach that has been used in several studies (Calautit and Hughes, 2016; Calautit et al., 2020).

Using CFD to model heat pipes can be a complex process that has resulted in the development of several approaches with differing degrees of complexity. Due to the repeating evaporation-condensation cycle within the heat pipe, accurately capturing the heat transfer along the length of the pipe is difficult to reproduce, especially in three dimensions. Although the VOF approach is the most accurate, it is only conducted in

2D at incredibly small timesteps and is therefore only applicable to isolated heat pipe studies. Approximating the heat pipe as a superconductor by summing the thermal resistances along its length was shown to be effective at reproducing experimental results, however these experiments were conducted at high temperatures and so its application at low ambient temperatures is untested. Despite its obvious limitations, applying a surface temperature to the wall of the heat pipe is the most common approach found in literature, however there is a lack of validated studies to show that the replication is accurate.

2.4.5 Run-around Heat Exchangers

Run-around heat exchangers incorporate other types of recuperative heat exchange within a thermal loop using a working fluid to link two individual heat exchangers. A run-around is often implemented when the respective fluid streams are far from one another or when cross-contamination between the two flows needs to be prevented (Jouhara et al., 2018).

The thermal loop requires a pump to drive the heat transfer fluid between the two heat exchange points (Figure 2-18). The fluid is often water mixed with an anti-freezing agent and transfers heat from one fluid stream to another as it is pumped through the system, although cooling energy can also be recovered on warm days (Wallin et al., 2012). The flow rate to the heat exchangers is often controlled by a three-way valve or by controlling the speed of the pump, hence the temperature of the supply air can be controlled also (Wallin et al., 2012). Run-arounds have been found to achieve efficiencies between 45 – 65% (Mardiana-Idayu and Riffat, 2012), where the effectiveness of the heat exchangers primarily influences the efficiency however the

pump power, flow rate, and concentration of anti-freeze within the working fluid should also be considered (Wallin et al., 2009; Lu et al., 2016).

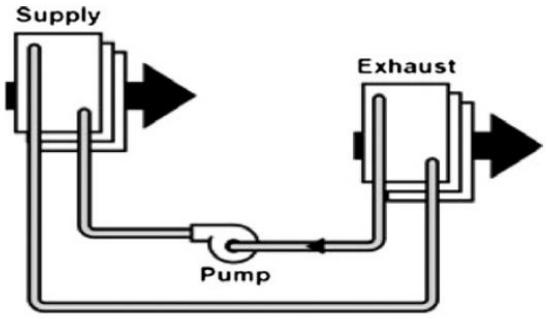

Figure 2-18 - Run-around heat recovery system (Wallin et al., 2012)

Run-arounds are often integrated through pipe-based heat exchangers as the working fluid can easily be pumped through the heat exchanger without changing the design. Davidsson et al. (2013) designed a run-around water-to-air heat exchanger using copper pipes running through an air channel. Fins were soldered to the surface of the copper pipes to increase the surface area for heat transfer. The system was designed for use with a passive ventilation system relying only on the natural wind speed and stack effects to generate ventilation. Although there were discrepancies between the modelled and tested results, a heat recovery efficiency of around 70% was achievable for a pressure drop of 1 Pa. This low-pressure drop was contingent on perfectly parallel fins, as the introduction of waves along their length forces contact with the air stream, increasing heat transfer and the pressure drop as it inhibits the flow.

Figure 2-19 - Fins soldered to copper pipe surface in the heat exchanger (Davidsson et al., 2013)

Vali et al. (2009) developed a two-dimensional steady-state numerical model to study the heat transfer in a run-around heat recovery system. The run-around connected two exchangers that featured a combination of counter and cross-flow between parallel plates or membranes. The numerical model determined that the overall effectiveness was a function of the Number of Transfer Units (NTU), the heat capacity ratio of the fluids, the aspect ratio of the exchangers, and the entrance ratio of the exchangers. The highest sensible effectiveness was achieved with exchangers with a small exchanger aspect ratio and relatively small solution flow inlet and outlet lengths.

Wallin et al. (2012) presented a comparative study of three run-around systems using TRNSYS. The base system was a traditional run-around coil heat recovery system to which a three-stage on/off controlled heat pump and a variable capacity heat pump were added. A constant source temperature is delivered by adding a heat pump to the system, making the system less susceptible to changes in ambient temperature. From the base case, a 3-stage heat pump increased the annual heat recovery rate from 47% to 65%, and a variable capacity heat pump increased the heat recovery rate from 47% to 66% with payback periods of 5.7 and 6.2 years, respectively. Given the

improvement in heat recovery and the payback period, it is concluded that adding a heat pump to a run-around system justifies the initial cost.

2.4.5.1 Fins

Fins can be used to improve the effectiveness of heat exchangers by increasing the surface area available for heat transfer. Owing to the variety of uses for heat exchangers numerous designs have been tested, where the impact on the pressure drop through a passive ventilation system must be considered when determining the optimal design.

Calautit et al. (2020) used extended surfaces through the inlet of a single-sided wind tower to determine the impact on inlet velocity relative to a system with no fins. The fin designs were extended rows of metal over the surface of heat pipes traversing the entire inlet. As a result of fin addition, the internal air velocity fell by 18 – 25% for inlet velocities of 0.5 and 5 m/s. No consideration was given to the impact of the fins on the inlet temperature through the wind tower.

Banu et al. (2022) used CFD to analyse the properties of a fin and tube heat exchanger for use within mechanical HVAC systems. They found that under the simulated conditions, an increase in fin spacing up to a spacing of 5 mm reduced the heat transfer coefficient, however beyond 5 mm it remained essentially unchanged.

Sparrow and Kang (1985) used longitudinal fins on cross-flow tube banks, measuring the difference in heat transfer and pressure drop across them. They compared differing designs where the fins were placed on the front of the tube, at the rear, and the front and rear (Figure 2-20).

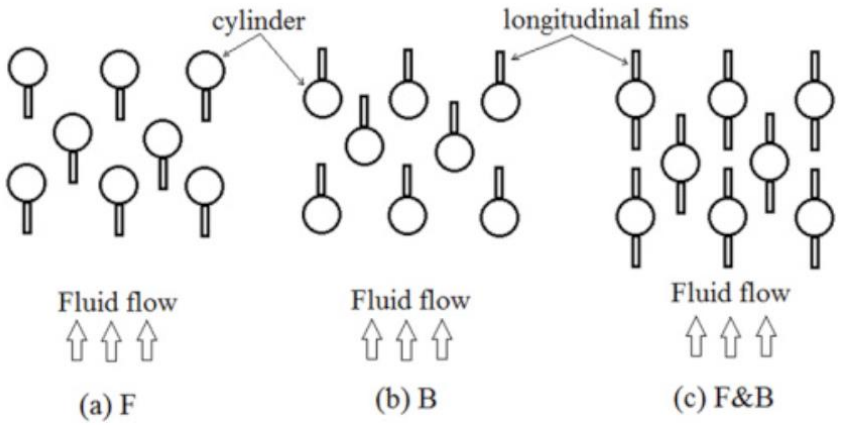

Figure 2-20 - Longitudinal fin design showing a) front side, b) back side, and c) front and back side (Sparrow and Kang, 1985)

Compared to standard tube banks the pressure drop was 80% and 33% greater for front and back side fins respectively, with the increased pressure drop for front-facing fins arising from the flow separation at the tip of the fin. The design with front and back side fins incurred a lower pressure drop than the tubes with just front side fins due to the channelling of the flow. All three designs improved heat transfer from the tubes to the air, with the back side only fins performing better than the front side.

Liu and Calautit (2023) explored the effect of fin wall angle on pressure drop and heat transfer using back-side longitudinal fins. Increased fin angle resulted in a much more significant pressure drop and improved heat transfer rate given the larger surface area available for heat transfer and increased flow separation and reattachment.

2.4.6 Heat Recovery within Passive Ventilation

Heat recovery devices have been integrated within passive ventilation systems to pre-heat and cool fresh air. O'Connor et al. (2014) installed a rotary thermal wheel at the base of a wind tower to recover waste heat from the exhaust to inlet air channels. A 1:10 scale wind tower was 3D printed and subjected to a range of inlet velocities in a closed-loop subsonic wind tunnel, with the results used to validate a CFD model of the

wind tunnel test section, wind tower, rotary wheel, and attached test room (Figure 2-21).

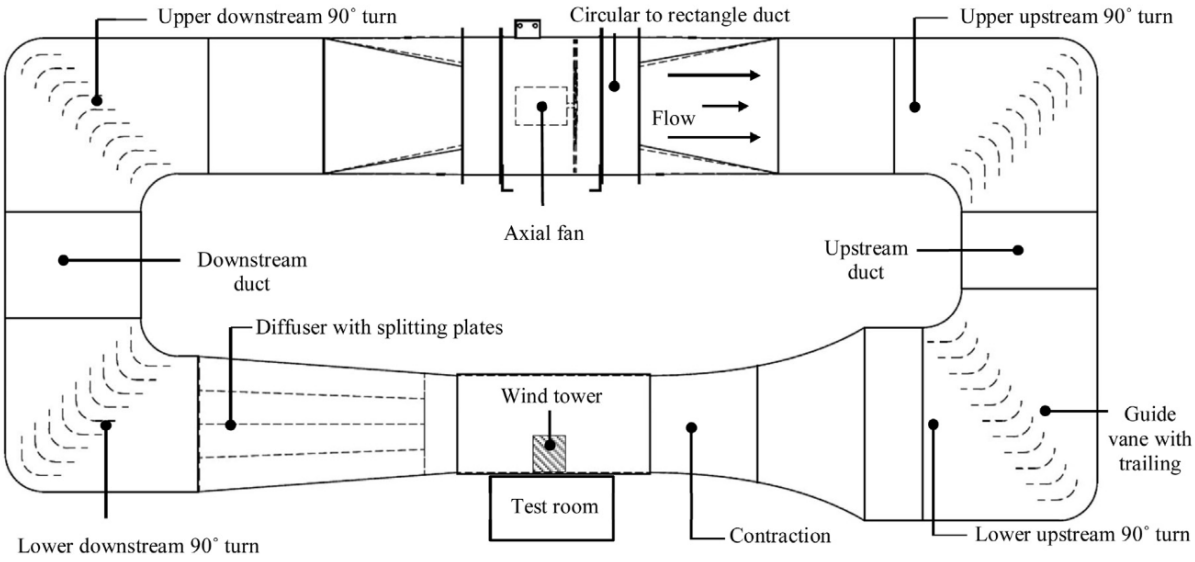

Figure 2-21 - Cross section of closed-loop subsonic wind tunnel and test section (O'Connor et al., 2014)

When comparing the CFD and experimental results the average error was 36%, however the same trend for the air velocity within the building model was established in both sets of results and therefore is deemed sufficient to validate the model. This feature has been established in several studies featuring passive ventilation, with errors up to 100% accepted, providing positive trends between the two data sets are observed (Chen and Srebric, 2002; Hughes and Mak, 2011; Connor et al., 2019). The maximum pressure drop through the inlet quadrant across the heat exchanger was 45.4 Pa at 10 m/s inlet velocity, falling to 30 Pa when the inlet velocity was 3.1 m/s. The air supply rate through the wind tower and thermal wheel achieved minimum guideline ventilation rates of 8 L/s per person at an inlet velocity of 3 m/s when the occupancy density was 1.8 m^2 per person.

Adamu and Price (2015) describe a concept for a natural ventilation and heat recovery system with a plate heat exchanger. Stack effects cause hot air within the room to rise

and exit the space from a high-level return vent attached to a U-shaped channel. Cool air is drawn into a low-level vent to replace the exhaust air, passing through the heat exchanger in a counter-current and co-current flow arrangement where a thin plate of copper or aluminium separates the hot and cold channels. Assuming indoor passive thermal gains from occupants, electronic devices, and lighting, a mean ventilation rate of 0.9 ACH was produced. Compared with a room ventilated via a window with no heat exchanger the heating energy demand was between 65.7% and 72.1% lower.

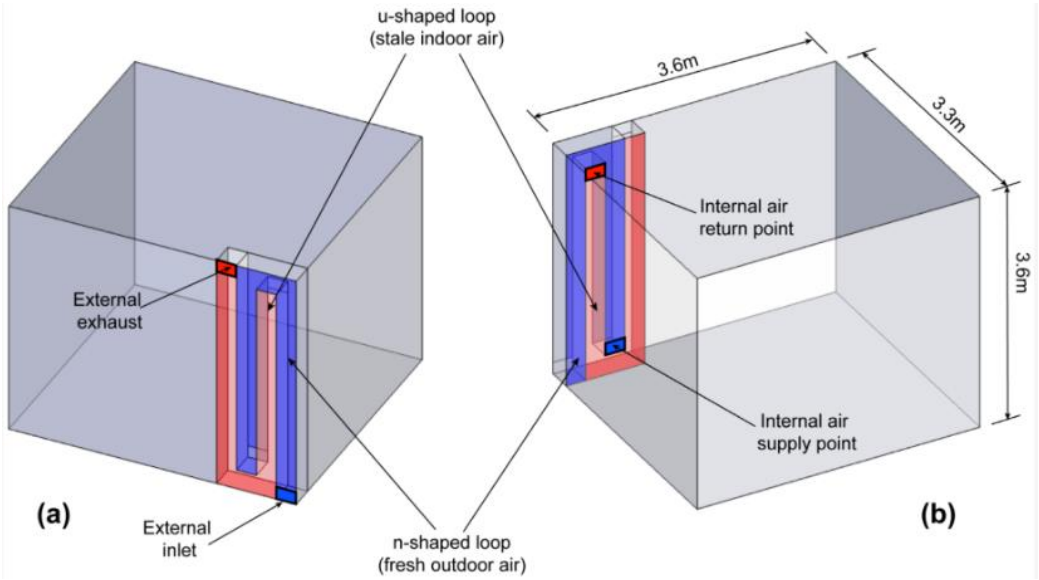

Figure 2-22 – Position of a plate heat exchanger within a room from (a) external view and (b) internal view (Adamu and Price, 2015)

A study by Riffat and Gan (1998) compared the performance of three types of heat pipes for heat recovery for a naturally ventilated building (Figure 2-23). The first featured an inline bank of seven heat pipes with external fins, the second used three pipes with cylindrical spines made of copper wire, and the third used two staggered rows each with three finned pipes. During operation air enters the lower zone of the test chamber via the supply duct as return air is extracted from the upper zone through the exhaust duct. The heat pipes connect the two ducts to transfer heat between the air flowing through them.

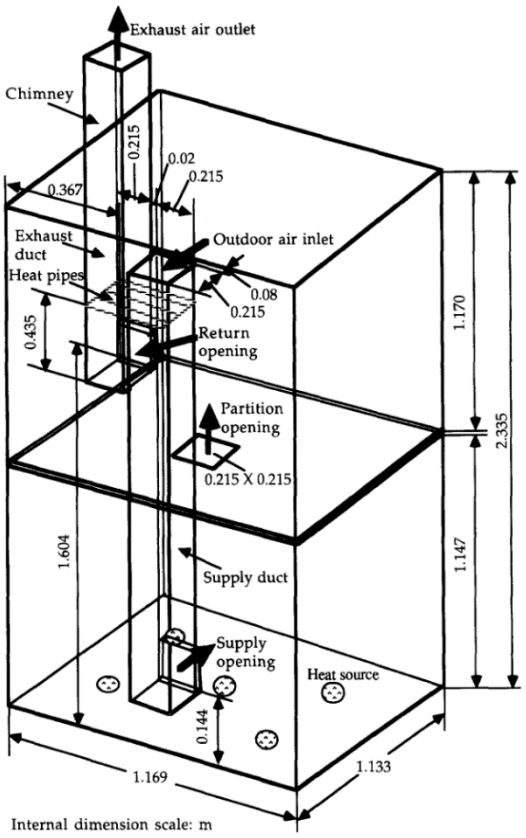

Figure 2-23 – Schematic of a two-zone test chamber for heat pipes (Riffat and Gan, 1998)

Tests were performed with average inlet velocities between 0.3 – 5.2 m/s. As expected, the resistance to flow increases when the number of pipe banks increases from one to two but also increases the heat recovery efficiency by 16 – 17%. Increasing inlet velocity reduced the effectiveness of the pipe banks. The spine fins exhibited a much lower effectiveness than the plain fin configuration, primarily due to the poor thermal contact between the fins and pipes. Finally, the design velocity should be less than 1 m/s for the heat recovery system to function correctly in naturally ventilated low-rise buildings without the wind effect or solar energy. Despite the improvement in heat recovery efficiency when using fins, more recent studies often neglect to include them on the surface of the heat pipe, presumably due to the incurred pressure drop. Many of the solutions are calculated analytically compared with the

CFD studies that are preferred in more recent studies which may generate some differences between studies of similar geometries.

Calautit et al. (2020) conducted a field test, scale-model wind tunnel test, and CFD study of a single-sided wind tower with heat pipes and a cold sink to cool fresh air in the UAE. As hot air passes over the heat pipes through the wind tower the working fluid inside the heat pipes evaporates effectively removing heat from the fresh air and lowering its temperature. The water in the cold sink condenses the vapour, absorbing the released heat and repeating the cycle.

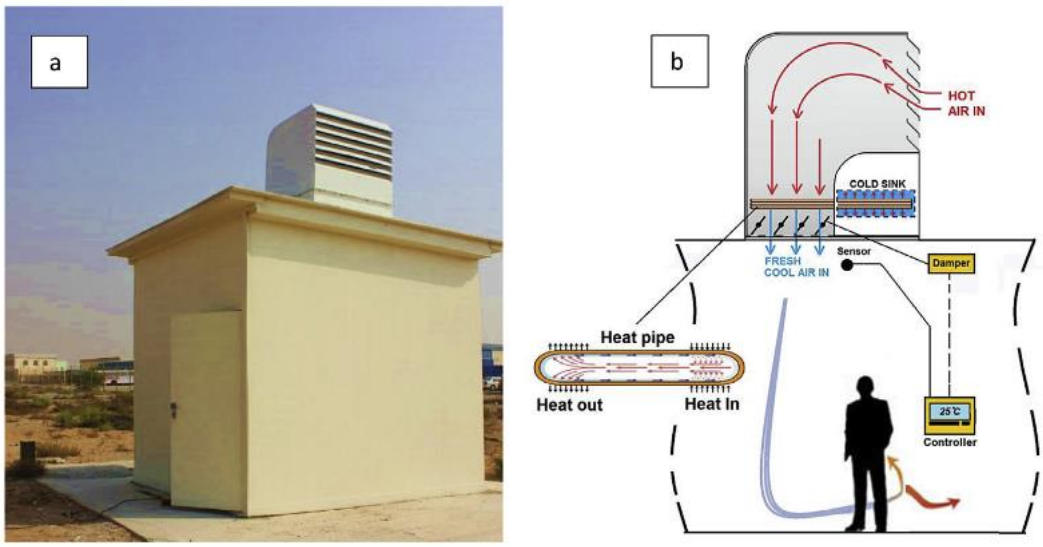

Figure 2-24 - (a) Roof-mounted wind tower with heat transfer devices; and (b) schematic diagram of the wind tower operation (Calautit et al., 2020)

The system provided between 79 – 445 L/s of air at inlet velocities of 1 – 5 m/s, with the heat pipe configuration reducing the velocity by up to 0.4 m/s across them. In peak summer a reduction in fresh air temperature of 10 °C is achieved, falling to 1 – 2 °C in the winter as the temperature difference between the cold sink and the ambient air falls. Adding extended surfaces to the heat pipes caused the internal air velocity within the room to be reduced by 18 – 25% versus the case without fins. No results for the impact of fin addition on pre-cooling were provided in this study.

A similar study explored vertical heat pipes within each quadrant of a four-sided wind tower with a top-mounted cold sink (Calautit et al., 2017). Results from a scaled-model wind tunnel test validated a CFD model created within ANSYS Fluent. The integration of the heat pipes caused an 8 to 17% reduction in the supply rate through the wind tower inlet but maintained a minimum of 10 L/s per person at inlet velocities as low as 2 m/s. The incoming air temperature was reduced by up to 12 K, with lower inlet velocities positively affecting the cooling ability of the system (Figure 2-25).

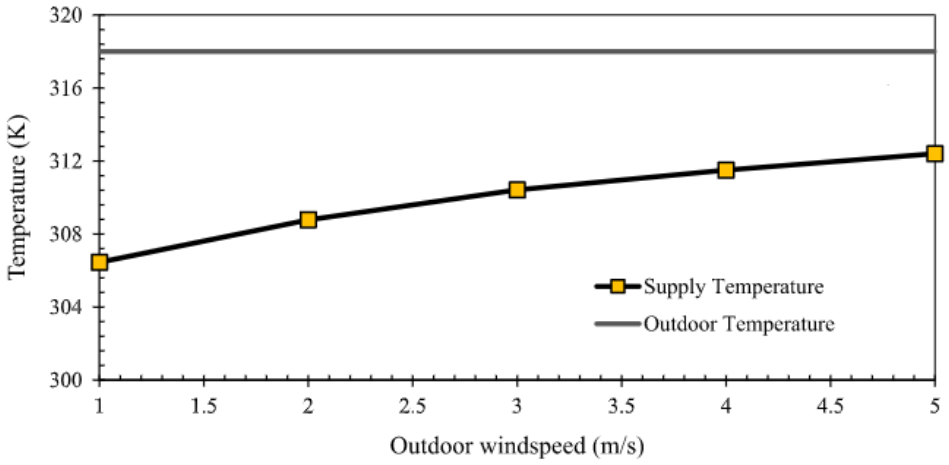

Figure 2-25 - Effect of outdoor wind speed on supply temperature (Calautit et al., 2017)

Employing the same system for pre-heating fresh air in the winter months of a cold climate the fresh air temperature was raised by up to 4.5 °C when the incoming fresh air was at 10 °C and the heat pipe surface at 20 °C (Calautit et al., 2016). Simulations also compared the impact of applying a uniform versus an atmospheric boundary layer to the building and wind tower, where the atmospheric boundary layer features an increasing wind velocity with height away from the ground due to reducing aerodynamic drag. Comparing the results, a wind tower under an atmospheric boundary layer supplied 20.45 – 22.92% less air than one subject to a uniform boundary layer.

In an early study, Hesdat et al. (1999) used a run-around to link two heat exchangers, recovering heat from exhaust to fresh air entering through a passive ventilation system. The heat recovery system increased supply air temperature by approximately 15 °C when the flow rate was approximately 133 L/s. The heat exchangers were designed to give a pressure drop of 6 Pa at a flow rate of 400 L/s, achieving an efficiency of 50 %.

Hviid and Svensen (2011) explored a run-around system connecting two air-to-liquid heat exchangers designed for use within passive ventilation systems. The heat exchanger consisted of parallel tubes crisscrossing the airflow with water flowing through them in a counter-flow arrangement. The tubes were made of polyethylene tubing with an outer diameter of 8 mm and a wall thickness of 1.1 mm. The longitudinal and transversal pitches were 11 and 12 mm respectively. For the design airflow rate of 560 L/s, the pressure loss was as low as 0.37 Pa with an efficiency of 75.6% for a single exchanger. This was however contingent on an inlet velocity on the air side of 0.06 m/s, far below likely the flow rates experienced through an actual passive ventilation system. The total heat recovery for the two coupled exchangers was 64.5 – 75.4% with a pressure drop of 0.74 Pa.

2.4.7 Comparison of Heat Recovery Methods

Owing to the level of interest in heat recovery, extensive reviews have been conducted into the mentioned technologies. Mardiana-Idayu and Riffat (2012) carried out a review of heat recovery methods for building applications, considering both mechanical and passive ventilation. They concluded that for passive ventilation methods, heat pipes were most suitable as they contain no moving parts, while for mechanical ventilation heat pumps were most prevalent. The achievable efficiencies of each method of heat

recovery were presented along with some advantages of each respective technology (Mardiana-Idayu and Riffat, 2012)

Table 2-1 - Heat recovery types, efficiencies, and advantages (Mardiana-Idayu and Riffat, 2012)

Types of heat recovery	Typical efficiency	Advantages
Fixed-plate	50–80%	Compact, highly efficient due to high heat transfer coefficient, no cross contamination, can be coupled with counter-current flow which enabling to produce close en-temperature differences
Heat pipe	45–55%	No moving parts, no external power requirements, high reliability, no cross contamination, compact, suitable for naturally ventilated building, fully reversible, easy cleaning
Rotary wheel	Above 80%	High efficiency, capability of recovering sensible and latent heat
Run-around	45–65%	Does not require the supply and exhaust air ducts to be located side by side, supply and exhaust duct can be physically separated, no cross contamination

O'Connor et al (2016) later conducted a review of the suitability of heat recovery methods specifically for passive ventilation. They concluded that heat pipes and rotary thermal wheels were most suitable for passive ventilation due to their high thermal efficiency and low-pressure drop-in comparison with the other reviewed technologies (O'connor et al., 2016). The reported achievable efficiencies differ slightly from those reported by Mardiana-Idayu and Riffat (2012), likely due to the presence of more recent research in the study.

Of the evaluated heat recovery devices, rotary thermal wheels, heat pipes, and run arounds have all been shown to be suitable for integration within passive ventilation systems. Although rotary wheels generate high heat recovery efficiencies and allow for humidity control, they also incur a larger pressure drop than heat pipes and run-arounds. In addition, the design of rotary thermal wheels makes it difficult to integrate within a water-based thermal loop capable of extracting and redelivering waste thermal energy to fresh air flowing through a wind tower.

Table 2-2 - Summary of heat recovery devices and their attributes (O'connor et al., 2016)

Type of HRV	Advantages	Disadvantages	Performance Parameters	Efficiency %	Pressure Drop (Pa)	Humidity Control
Rotary thermal wheel	High efficiency Sensible and latent heat recovery Compact design Frost control available	Cross contamination possible Requires adjacent airstreams Mechanically driven, requiring energy input	Rotation speed Air velocity Wheel Porosity	80+	4–45	Yes
Fixed plate	No moving parts hence high reliability High heat transfer coefficient No cross contamination Compact design Frost control possible Sensible and latent heat recovery	High pressure loss across exchanger Limited to two separate airstreams Condensation build up Frost build up in cold climates	Material type Operating pressure Temperature Flow arrangement	70–90	7–30	Yes
Heat pipes	No moving parts, high reliability No cross contamination Low pressure loss Compact design Heat recovery in two directions possible	Requires close airstreams Internal fluid should match local climate conditions	Fluid type Contact time Arrangement/configuration Structure	80	1–5	No
Run-around	Airstreams can be separate No cross contamination Low pressure loss Multiple sources of heat recovery	Multiple pumps required to move fluid Difficult to integrate into existing structures Low efficiency Cost	Exchanger type Fluid type Heat source	50–80	~1	No
Phase change materials	Easy incorporation into building materials Offset peak energy demands No pressure loss No cross contamination No moving parts Long life cycle	Thermal storage as opposed to instantaneous transfer Expensive Not proven technology Difficulty in selecting appropriate material	Material type Impregnation method	~	0	No

Heat pipes appear to provide the best opportunity for high heat recovery efficiency and low pressure drop, however are limited in that some designs rely on gravity to return the condensate to the evaporator section of the heat pipe. The reported heat recovery efficiency of run-arounds is lower than the other heat recovery methods, however as the fluid-loop is integrated into the design it lends itself to use alongside seasonal thermal storage. The design of the heat exchanger within the run-around system will however play a critical role in determining the overall effectiveness of the system in addition the energy demand of the pump to circulate the fluid through the system.

2.5 Seasonal Thermal Energy Storage

TES addresses the mismatch in supply and demand between renewable resources and energy demand, storing energy when there is a surplus and redelivering it as required, generally over hours or days. Seasonal Thermal Energy Storage (STES) applies this same concept over months. Waste or excess heat generally produced in the summer when heating demand is low can be stored for up to 6 months. The stored heat can then be re-introduced to heating systems throughout the winter as demand

increases, negating some of the requirements to generate new heat and lowering total energy consumption.

Of the three forms of heat storage, SHS is currently the most developed and widely utilised form of TES with storage materials chosen according to their heat capacity, space availability, and cost, with water the most popular choice. Tiskatine et al. (2017) present a comprehensive list of materials used for SHS and their associated material properties.

Underground Thermal Energy Storage (UTES) makes use of favourable geological conditions directly as a thermal store or as an insulator for the storage of heat. UTES can be divided into open and closed loop systems, with Tank Thermal Energy Storage (TTES), Pit Thermal Energy Storage (PTES), and Aquifer Thermal Energy Storage (ATES) classified as open loop systems, and Borehole Thermal Energy Storage (BTES) as a closed loop. Other methods of UTES such as cavern and mine TES exist but are seldom employed commercially. UTES can be used for both space cooling and heating, with or without heat pumps, although cooling is less common in BTES, TTES, and PTES systems whereas ATES actively benefits from a balanced heating and cooling load.

Industrial excess heat is the heat exiting any industrial process at any given moment, divided into usable, internally usable, externally usable, and non-usable streams (Anastasovski et al., 2020). Waste heat can be recovered directly through recirculation or indirectly through heat exchangers. It can be classified according to temperature as low grade (< 100 °C), medium grade (100 – 400 °C), or high grade (>400 °C) (Anastasovski et al., 2020), with low grade being the most abundant but also most difficult to recover (Xu et al., 2019). It is estimated that the total waste heat potential in

the EU is approximately 300 TWh/year, with one-third of this at temperatures below 200 °C (Papapetrou et al., 2018). STES can harness and store low-grade heat, with the receiving temperature range determined by storage type and eventual redistribution target. Storing heat at higher temperatures incurs higher thermal losses yet enables heating provision without requiring heat pumps to raise fluid temperatures.

Seasonal SHS faces several challenges that fail to impact shorter-term thermal storage. Longer storage times make it necessary to use larger storage volumes to reduce thermal losses. As a result, capital expenditure is higher, generating accurate models is more complex, and limitations through geographical and legal requirements can be restrictive.

2.5.1 Aquifer Thermal Energy Storage

An aquifer is a subsurface layer of water-bearing permeable rock that can be exploited to extract and store groundwater. While aquifers are geographically limited, they are often found underneath large population centres (Schmidt *et al.*, 2018), making them helpful in co-locating considerable storage potential with areas already likely to generate a sizeable thermal energy demand. ATES has received renewed interest in recent years owing to its large storage capacities, low environmental impact, versatility of application, and improving economic viability (Schmidt *et al.*, 2018; Matos et al., 2019).

Two differing well designs are used to facilitate thermal storage in aquifers. Multi-well systems use one or more sets of well doublets within the aquifer to store thermal energy at spaced lateral points separating hot and cold (Babaei and Nick, 2019). Mono-well systems separate hot and cold storage vertically through a single well resulting in reduced drilling costs and space requirements (Zeghici *et al.*, 2015),

however they require an aquifer with a greater thickness or that is in two layers separated by a cap rock to effectively separate the hot and cold regions and avoid thermal interaction. Figure 2-26 below indicates the difference between the two arrangements.

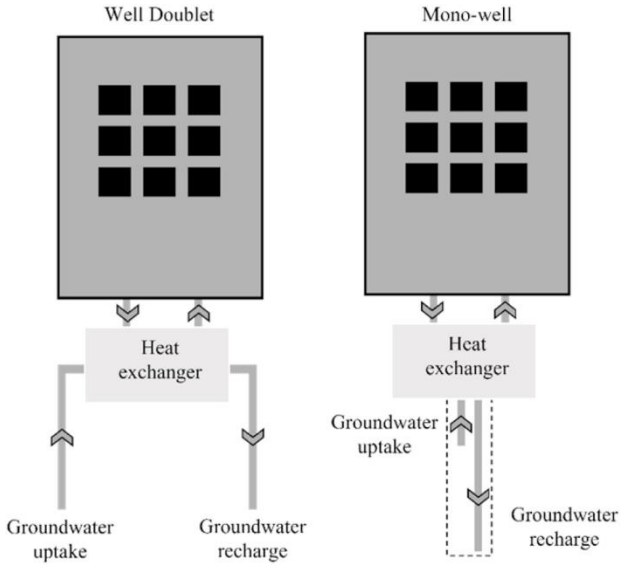

Figure 2-26 - Well doublets (left) vs. mono well (right)

ATES passes extracted groundwater through heat exchangers, providing heating and cooling as the groundwater acts as a heat sink and heat source in the summer and winter, respectively, before being re-injected to the aquifer (Figure 2-27). Warm well injection temperatures of reviewed systems varied between 13 - 25 °C and cold injection temperatures were between 3 - 17°C (Gao *et al.*, 2017; Fleuchaus *et al.*, 2018; Bozkaya and Zeiler, 2019), with higher cooling temperatures used in hotter countries. In most ATES systems, groundwater is re-injected with an upper limit approaching 25 °C to preserve the quality of the water within the aquifer (Bonte, 2013) however systems with reinjection temperatures above 50 °C have also been tested (Wesselink *et al.*, 2018).

The extraction temperature is dependent on the injection temperature, injection volumes, and the hydraulic behaviour of the aquifer (Schout *et al.*, 2014). Abuasbeh et al. (2021) found that for an undisturbed ground temperature of 9.5 °C, the average injection and extraction temperatures in the warm well were 13.3 and 12.2 °C, while for the cold well the average injection and extraction temperatures were 7.6 and 10.5 °C. The cold well extraction temperature was higher than the injection temperature due to a greater volume of warm water being injected to the aquifer as a result of an imbalanced heating and cooling load.

Storage efficiencies are typically high for ATES systems, recovering between 67.5 – 87 % of stored heat and cold, with increasing storage volume serving to improve storage efficiencies (Zeghici *et al.*, 2015; Schout et al., 2016; Bloemendal and Hartog, 2018). ATES is commonly installed in universities, hospitals, large commercial buildings, and airports (Bozkaya and Zeiler, 2019), with ventilation cooling during summer often providing the heat to be stored and subsequently used for heating throughout the winter.

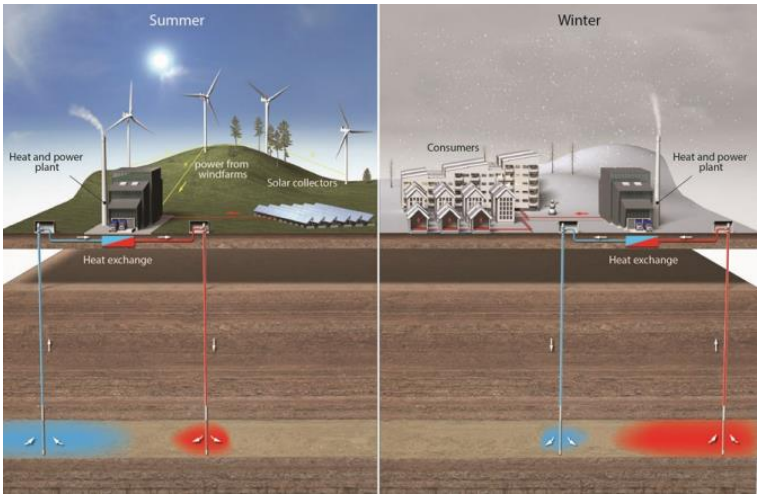

Figure 2-27 - Principle of ATES for district heating network (Kallesøe et al.*, 2021)*

Although ATES has been proven to be both energy and cost-efficient the adoption rate has been slow, primarily due to technical barriers such as unfamiliarity with the subsurface, presumed limited compatibility with existing energy systems, energy imbalances, and groundwater contamination, but also through a lack of tailored legal frameworks (Lu et al., 2019; Pellegrini *et al.*, 2019).

Lu et al. (2019) evaluated global ATES potential to predict highly suited areas. The evaluation builds on previous work carried out such as that by Bloemendal et al. (2015) and Fleuchaus et al. (2018), but accounts for a broader range of factors including groundwater, geo-hydrological, climatic, and socio-economic conditions, therefore improving the reliability of the results (Figure 2-28).

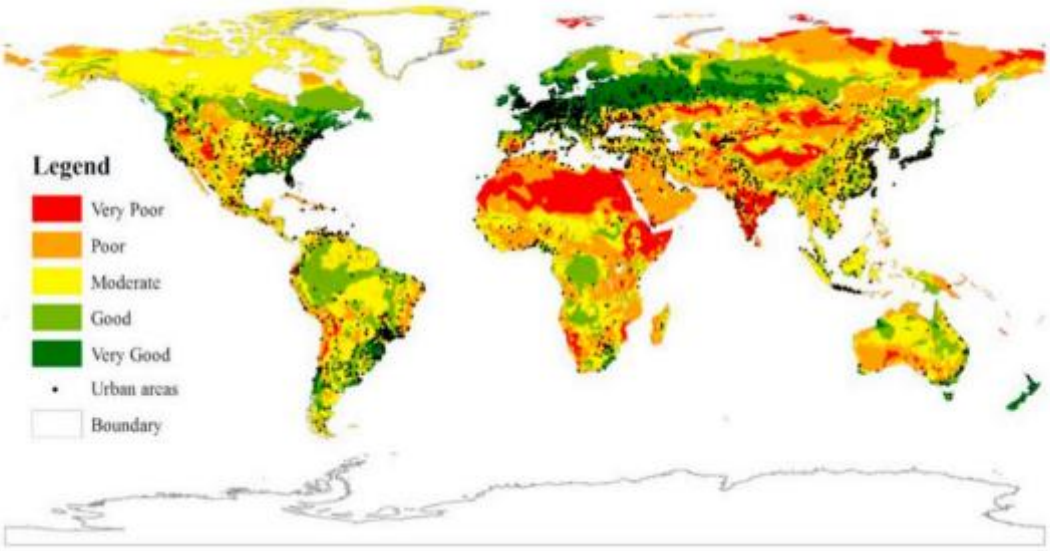

Figure 2-28 - Prediction of worldwide aquifer thermal storage potential with urban centres (Lu et al., 2019)

The results indicate predicted suitability for ATES in combination with existing urban areas, with the authors expecting findings to provide policy recommendations for governments and stimulate ATES applications. Areas with a high potential are predominantly spread throughout Europe, although coastal regions of North and South

America and Japan also present substantial opportunities. Although global analysis helps predict total potential, local characterisation is also required.

2.5.1.1 High-temperature ATES

High temperature (HT) ATES is considered a potential development to enable the use of waste heat from a wider range of sources. While most ATES systems operate in the range of 5 – 25 °C, HT-ATES is characterised by an injection temperature of at least 50 °C, using heat sources such as CHP plants or incinerators (Wesselink *et al.*, 2018). The heat stored may also be used directly for heating without the need for heat pumps making it suitable for a wider range of heating applications and reducing energy consumption (Collignon *et al.*, 2020). The extraction temperature from the warm well increases over successive storage cycles as the heat losses from the previous cycle result in higher ambient groundwater temperatures (Drijver et al., 2012).

These systems are unlikely to achieve a long-term energy balance due to the increased operating temperature, and as a result are typically located in deeper aquifers to reduce the environmental impact and likelihood of interfering with drinking water sources (Wesselink *et al.*, 2018). To facilitate the deeper drilling depths, mono-well systems are generally used to help minimise the initial costs (Zeghici *et al.*, 2015).

Although there are benefits, high storage temperatures exacerbate the issues felt in lower temperature systems such as clogging of wells due to mineral precipitation, increased mineral and CO2 solubility, and promoting algae growth (Hähnlein *et al.*, 2013). This makes extraction increasingly difficult without preventative measures, increasing the relative storage cost and reducing the system's viability. In addition, losses experienced through density-driven flow were found to increase non-linearly with increasing injection temperature (Bonte, 2013), with typical recovery efficiency for

low temperatures (< 30 °C) between 70 – 90% and between 40 – 70% for high temperatures (> 60 °C) (Schout et al., 2016).

2.5.2 Borehole Thermal Energy Storage

BTES uses a closed-loop ground heat exchange system to store sensible thermal energy in soil or rock below ground. This is made possible by the relatively stable ground temperatures observed below the surface beyond a depth of around 10 metres (Cheruy *et al.*, 2017), creating favourable conditions for storing and extracting heat either for direct use or through ground source heat pumps (GSHPs).

The BTES system consists of a heat source, borehole heat exchangers (BHEs) that make up the thermal storage, and often a buffering tank due to the slow charge and discharge rate (Lim *et al.*, 2020). A BHE is commonly composed of a borehole, thermal grout, and a U-tube arrangement encased within the grout to circulate the Heat Transfer Fluid (HTF) along the vertical length of the borehole. Boreholes are drilled to depths of between 30 - 200 m (Ann et al., 2016), however boreholes of much greater depths have been explored in attempts to reduce the number of boreholes required to generate a larger storage capacity (Morchio and Fossa, 2020). The charging temperature of the BTES is dictated by the heat source, with solar thermal collectors commonly used to provide heat at temperatures around 85 - 90 °C (Pavlov and Olesen, 2011; Sarkar and Bhattacharyya, 2012). Alternatively, waste heat from industrial processes and heat and power cogeneration can also be used, with low-grade heat becoming more applicable with lower distribution temperatures in district heating schemes. Outlet temperatures during extraction range between approximately 25 – 45 °C (Li *et al.*, 2017; Wang *et al.*, 2017; Deng *et al.*, 2019), with heat pumps

used to raise further the temperature of the HTF circulating through the borehole after extraction if necessary.

The storage efficiency of the BTES system is determined by the design and arrangement of the BHEs, material properties, ground properties and operating parameters (Wołoszyn, 2020). Recovery efficiencies typically start very low in the first year of operation however by the fourth or fifth year can reach between 40 – 60 % (Reuss, 2015; Renaldi and Friedrich, 2019), with BTES commonly used to distribute heat throughout district heating schemes (Pavlov and Olesen, 2011; Schmidt, 2016; Wong and Mesquita, 2020). Design parameters include the length, number, and spacing of the BHEs and must consider geological conditions such as ground thermal conductivity and quantity and movement of groundwater. Operating parameters include inlet and outlet temperatures of the HTF, HTF velocity, and the charging/extraction operation (intermittent or continuous).

The performance of a BHE is dependent upon the thermal resistance of the borehole as well as the thermal properties of the ground. Total borehole resistance was defined by Beier and Ewbank (2012) as the resistance between the circulating fluid in the BHE and the undisturbed ground temperature. Zero borehole resistance infers instantaneous heat transfer from the HTF to the ground and vice versa (Sanner, 2017). With increasing thermal conductivity of the soil, thermal resistance decreases, resulting in an overall decrease of the borehole resistance. It is desirable to reduce the thermal resistance of the borehole as this helps to reduce the number and depth of the BHEs.

Although established through several large and smaller-scale projects (Mesquita *et al.*, 2017; Zhu and Chen, 2019), BTES still faces several barriers to further

development. These are primarily the high construction costs due to borehole drilling, the time taken to reach operational efficiency, and accurately predicting the interaction between numerous BHEs and the ground over several years (Zhu and Chen, 2019). Both design parameters (i.e. BHE depth) and operational parameters (i.e. fluid flow velocity) have been proven to have a significant impact on BHE performance (Han and Yu, 2016).

2.5.2.1 Borehole charging

Borehole fields can take up to 5 years to reach their maximum operating efficiency, with much of the injected heat lost throughout the charging season before reaching a steady state of operation (Figure 2-29) (Skarphagen *et al.*, 2019). With each year of operation, lateral heat transfer away from the borehole field to the ground reduces as the thermal gradient between borehole temperature and ground temperature decreases (Başer and McCartney, 2020). The low thermal efficiency encountered in the initial years of operation encourages improvements to charging methods to help the BTES system reach operating efficiency in a shorter timeframe.

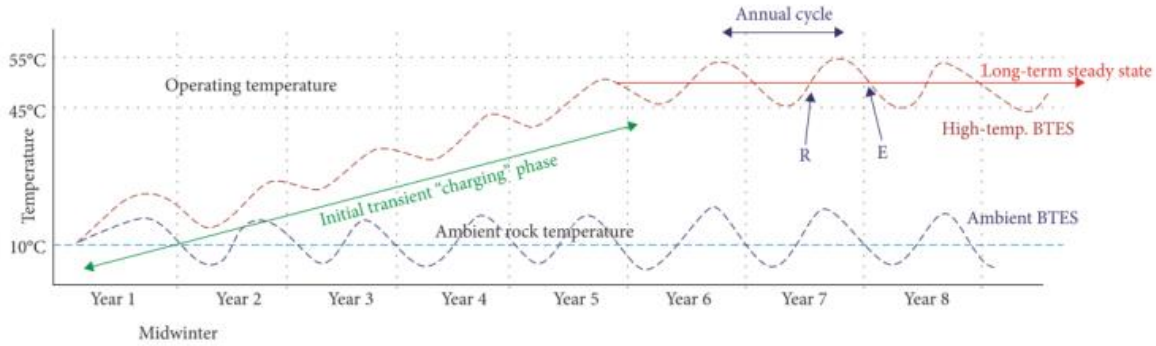

Figure 2-29 - Example BTES system operating temperature over time (Skarphagen *et al.*, 2019)

2.5.3 Medium-deep boreholes

In further efforts to reduce costs, increasingly deeper boreholes are being explored. Deeper boreholes have less impact on shallow aquifers, require fewer boreholes, and

are predicted to achieve efficiencies of up to 83% (Sarkar and Bhattacharyya, 2012). At greater depths ground permeability tends to decrease, limiting the transfer of heat away from the storage volume by groundwater flow. The thermal gradient between the storage area and surrounding rock is also reduced, enabling higher extraction temperatures as stored heat does not dissipate away from the BHE (Schulte *et al.*, 2016). Co-axial borehole arrangements are used for deep borehole systems (Figure 2-30) to reduce pressure losses for the circulating fluid, allowing for more significant mass flow rates and improved thermal extraction. The inner piper is also insulated to prevent thermal interaction between the down and up flow (Beier, 2020).

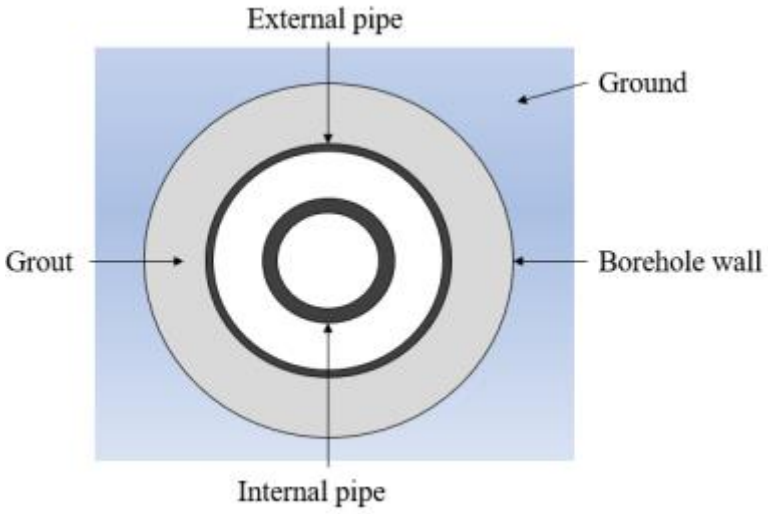

Figure 2-30 - Co-axial borehole arrangement

Medium-deep boreholes exist up to depths of 2 - 3 km, allowing for much fewer boreholes to provide the same storage capacity, enable much higher storage temperatures without impacting shallow aquifers, and benefit increasingly from geothermal heat (Deng *et al.*, 2019). The boreholes in question delivered a heat transfer rate of 61 – 144 W/m, a significant increase compared to the 40 W/m generally achieved through standard depth boreholes. Consequently, the heat extraction

through one deep BHE can be equivalent to 30 – 70 standard depth BHEs, with the average outlet temperature over 5 test sites reaching 33 °C.

An HT-BTES at Emmaboda, Sweden (Nordell *et al.*, 2015), stores waste heat from a foundry in an array of 140, 150 m deep boreholes. Heat is stored at between 40 – 45 °C, with the highest efficiency achieved to date at 19% in its sixth year of operation. Below-expected extraction levels are owed to lower than anticipated quantity and quality of excess heat, hindering the storage from reaching the required temperatures for extraction. Despite this, the amount of bought district heating was reduced by approximately 4 GWH/year. This experience highlights the importance of adequately quantifying waste heat and subsequent system design. By using heat pumps heat can be extracted at lower temperatures with minimal energy demand therefore making the stored heat more viable.

2.5.4 Pit/Tank Thermal Energy Storage

Although often employed as buffer storage, TTES is also used seasonally. The storage tank is made of reinforced concrete, steel, or fibre-reinforced plastics (Schmidt *et al.*, 2018), using water as a storage material with internal liners to create a watertight layer. As the tank is purpose-built the storage can be located anywhere, independent of the local geological conditions that dictate the suitability of borehole and aquifer systems. The tank is either fully or partially buried in the ground to insulate against the ambient temperature, reducing the level of thermal insulation required (Languri and Cunningham, 2019).

PTES uses excavated ground to create a sunken storage area. The excavated soil can be used to raise the banks at the sides of the storage, increasing the overall volume of the storage. The lid is either supported by the sidewalls of the pit or floats

on the surface and is often the most expensive part of the PTES construction (Kallesøe and Vangkilde-Pedersen, 2019). PTES generally uses water as a storage material but sometimes employs a mixture of water and gravel. Due to the water-gravel mix having a lower thermal capacity than the just water case, the volume of the basin needs to be approximately 50% higher (Novo *et al.*, 2010) but is often applied to avoid the costs of disposing of the excavated ground material. The cost of building PTES is around a quarter of that of building TTES (Kubiński and Szabłowski, 2020). Insulation is commonly installed along the top and sides of the storage, with the thickness determined by the storage temperature and local ambient and geological conditions.

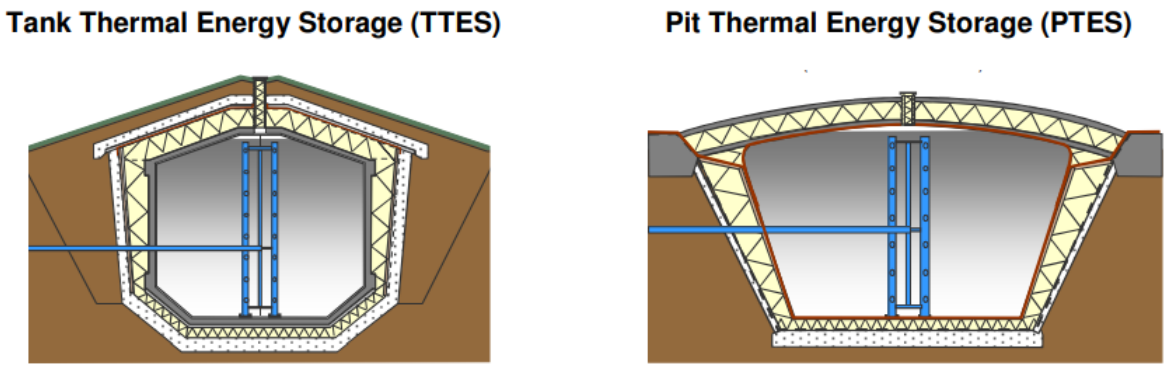

Figure 2-31 - Geometrical differences between tank and pit STES (Schmidt and Miedaner, 2012)

TTES and PTES operate under the same principles through their relative structures. Heat is charged and discharged into and out of the container by directly pumping water into the store or through a heat exchanger with another thermal system. Hot and cold regions naturally develop within the storage due to the differences in density between the hot and cold water, enabling hot water to be extracted from the top of the tank and cold water to be re-injected at the bottom of the tank without overly disturbing either region. Maintaining these thermal regions with as little mixing as possible is desirable to prevent heat losses throughout the storage.

Tanks and pits are designed to store water up to temperatures of around 90 – 95 °C (Pavlov and Olesen, 2011). Inlet temperatures depend on the heat sources used in conjunction with the thermal storage and the application of heat pumps. Solar collectors, bio-mass boilers, and industrial waste heat are often employed as heat sources, generating charging temperatures between 70 - 95 °C (Schmidt, 2016; Hakkarainen et al., 2019; Ahrens *et al.*, 2021). As a result of the high storage temperatures the stored heat is commonly utilised through district heating schemes (Pavlov and Olesen, 2011; Schmidt, 2016; Hakkarainen et al., 2019). Storage efficiencies between 45 – 65% are common (Chang, Wu *et al.*, 2017; Bai *et al.*, 2020; Meister and Beausoleil-Morrison, 2021), with instances of up to 90% reported (Schmidt, 2016).

2.5.5 Seasonal Thermal Storage Summary

Derived from the reviewed studies, Table 2-3 summarises the common heat sources, storage temperatures, storage efficiencies, and uses for stored thermal energy.

Table 2-3 - Typical heat sources, storage temperatures, efficiencies, and applications of STES technologies

Type of TES	Heat source	Storage temperature	Storage efficiency	Common applications
Aquifer	Heat recovery within ventilation, geothermal wells	13 - 25 °C in low temperature storage, >50 °C in high temperature storage	67.5 - 90%	Universities, hospitals, large commercial buildings, and airports for both heating and cooling
Borehole	Solar collectors, industrial waste heat, heat and power co-generation	40 - 90 °C	40 - 60% once at operational efficiency	District heating schemes, internal heating system
Tank/pit	Solar collectors, bio-mass boilers, industrial waste heat	70 - 95 °C	45 - 90%	District heating schemes

Whilst considering the intended heat source, storage temperature, and target destination for any stored thermal energy, the relative benefits and drawbacks of each technology must also be accounted for when determining which type of STES to include (Table 2-4).

Table 2-4 - Advantages, disadvantages, and factors influencing performance of different types of seasonal thermal energy storage.

Type of TES	Advantages	Disadvantages	Factors influencing performance
Aquifer	Large storage volumes	Only applicable where aquifers are present	Groundwater flow rate
	Benefits from balanced heating and cooling load	Potential negative impact to drinking water	Groundwater quantity
	Low cost	Storage temperatures limited by law	Groundwater recharge
	Aquifers often located under large population centres	Requires accurate subsurface characterisation	Heating and cooling demand
	Nearby doublets of similar temperature can improve performance	Nearby doublets of similar temperature can decrease performance	Local legislation
		Prone to clogging	
Borehole	Storage efficiency increases with increasing storage volume	Takes approx. 5 years to reach operating conditions	Design and arrangement of borehole heat exchanger
	Relatively low cost	Drilling costs	Ground and construction material thermal properties
	Modular storage approach that can be expanded	Thermal losses to surroundings when surface area to volume ratio is high	Groundwater flow
	Benefits from stable temperatures below surface		Charging and discharging operation
	Deep boreholes (>1 km) will significantly improve performance		
Tank/Pit	Independent of hydrogeological conditions	Expensive	Atmospheric conditions
	Partially/fully burying below ground reduces space and insulation requirements	Tank size restricted with construction limits	Application of insulation Tank geometry
		Losses within the storage if stratification isn't preserved	
	Storage volume made to suit demand		Material choices
	High storage efficiencies		Preservation of stratification
	High storage temperatures		

TTES and PTES are more independent of the local geological and hydrogeological conditions whereas ATES and BTES suitability is heavily dependent on local conditions, therefore making accurate characterisation of sub-surface highly important. Increasing storage temperatures in high-temperature ATES and mid-deep boreholes would create more opportunities for easier to recover waste heat, however, is inhibited by limitations on storage temperatures within aquifers and expensive drilling costs with increasing depths. Issues with maintaining water quality can be limited by closely monitoring injection temperatures in lower temperature systems, as well as requiring heating and cooling loads to be approximately balanced over the course of the year. Thermal losses throughout the aquifer can be improved by better mapping of hydrogeological conditions to improve the placement of extraction wells

relative to injection wells. Although deeper drilling depths are costly, the increased rate of heat transfer along the length of the borehole can reduce the number of boreholes required to store and recover the same quantity of thermal energy. Issues with long times to reach operational efficiency and low storage efficiencies are being addressed through material improvements, charging operations, and borehole spacing to create a more stable temperature distribution throughout the borehole field.

The geometry of tanks and pits has been shown to affect the thermal performance of the storage. By considering the angle of the walls and the height to diameter ratio losses through the side walls can be reduced. Tanks are limited in the size to which they can be built, and therefore the storage size is restricted. In comparison pits can be dug to almost any size, with the lid the only limiting factor. Further improvements to inlet and extraction devices to maintain stratification would help improve storage efficiencies and in turn help to lower costs by reducing material demands.

Although solar thermal collectors are widely used to provide heat for STES they are not as effective in many climates, and therefore waste heat is often used as an alternate or supplementary source. Bio-mass boilers and CHP units are also employed, with STES enabling the operation of electricity production independently of heating demand for CHP.

The development of CFD and other methods of computational modelling has made predicting system performance somewhat easier and is helping to envisage systems in a variety of scenarios. There are still however physical engineering issues within each storage type that when addressed result in improved storage efficiencies, higher outlet temperatures, and lower costs.

2.6 Passive Ventilation with Thermal Energy Storage

As evidenced through the literature review there are numerous real-world examples of STES application alongside waste heat sources, however there are limited examples of integration with passive ventilation systems.

The integration of TES into ventilation systems is limited mainly to using PCMs. For the majority this involves locating the PCM within the air duct and using night ventilation, allowing the PCM to harden overnight when outdoor temperatures are cooler then slowly melting as the daytime temperature increases helping to keep indoor temperatures lower by absorbing heat. Although PCMs are effective for short-to-medium-term TES, they are limited in assisting with heating or cooling but not both.

In contrast, external thermal storage systems can provide much larger storage capacities, capable of storing and releasing thermal energy over longer periods and storing heat and cold when required. Seyed-Ahmadi et al. (2009a, 2009b) developed a numerical model and completed a sensitivity analysis for a system comprised of two cross-flow liquid-to-air membrane energy exchangers and two intermediary storage tanks containing a salt solution that is used as the heat transfer fluid throughout the system (Figure 2-32). At lower air mass flow rates fewer circulations of the liquid desiccant were required to reach steady state as there was more time for heat transfer between the desiccant and the air. The storage volume and concentration of the salt solution were found to be most impactful to the transient response time of the system, indicating that the storage tank size should be minimised. Larger storage tanks were

less reactive to sudden changes in ambient temperature and humidity resulting in longer times to reach steady state.

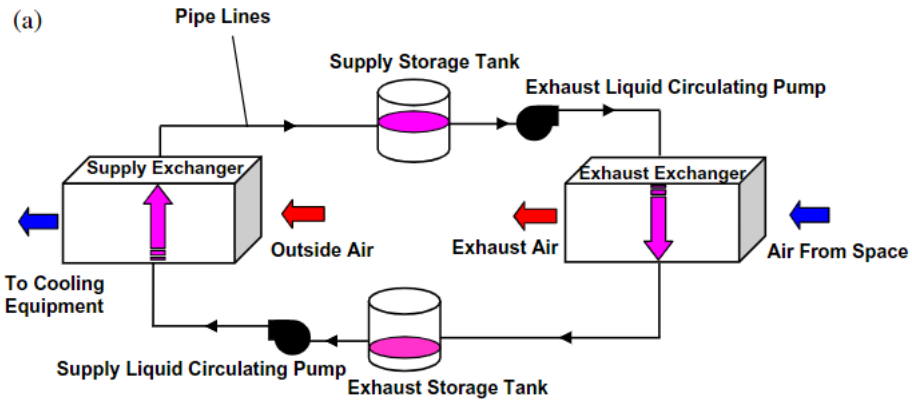

Figure 2-32 - Schematic of a run-around membrane energy exchanger system (*Seyed-Ahmadi et al.,* 2009a, 2009b)

Paksoy et al. (2004) integrated ATES with an HVAC system to reduce energy consumption in a supermarket building in Turkey with peak cooling and heating loads of 195 and 74 kW, respectively. Groundwater extracted from the aquifer at 18 °C was used to cool the condenser of the HVAC system, with the heat gained during the process stored underground and used in the following winter to provide heating. As a result, predicted total electrical energy use fell by 60%, increasing the average COP of the HVAC system from 2.67 to 4.18.

Ghoreishi-Madiseh et al. (2017) explored using a large-scale rock pit to provide heating and cooling via ventilation for a mine. The rock pit is a conic-shaped cavity 697 m in diameter and 330 m deep dug into the ground and filled with waste rock, creating a porous mass. Sensible heat is stored within the broken rock through natural seasonal temperature differences. Six trenches underneath the pit are connected to ventilation shafts through which fans continuously blow air. This generates airflow from the top to the bottom of the pit, allowing fresh air to be heated or cooled as it passes over the rock mass. Using a CFD model to predict the system's performance, they

were able to raise or lower the air temperature by between 15-20 °C relative to the ambient. This saved on average 10.9 GWh and 10.1 GWh per year for heating and cooling, respectively, saving approximately $437,000. It was concluded that to maximise the storage capacity of the rock pit, rocks with a higher heat capacity should be used.

2.7 Summary

The key findings of the literature review are presented below:

1. Passive ventilation has been shown to improve the comfortable temperature range for building occupants by increasing indoor air velocity and improving tolerance for thermal diversity, hence lowering energy demand for heating and cooling (De Dear and Brager, 2002) (Ben-David and Waring, 2016). Instances of sick building syndrome are reduced when using passive versus mechanical ventilation, however the lack of air filtration through passive ventilation systems can increase the concentration of outdoor pollutants (Seppanen and Fisk, 2001) (Ahmed et al., 2021). The use of passive ventilation can result in increased building energy demand if improperly managed (Wang and Greenberg, 2015).
2. Owing to the low driving pressure through passive ventilation systems, the blockage of any channels and incurred pressure drop must be considered when integrating heat recovery to maintain ventilation rates (Shao and Riffat, 1997; Shao et al., 1998; Davidsson et al., 2013; O'Connor et al., 2015).
3. Heat pipes and run-arounds were deemed the most suitable heat recovery devices for integration within a wind tower owing to their low-pressure drops, high efficiencies, and versatility of design. In addition, each lends itself to

removing recovered waste heat and cold for storage through STES using a water-based thermal loop.

4. Wind tunnel testing is used extensively to validate numerical models (Montazeri, 2011; Calautit and Hughes, 2014b; O'Connor et al., 2014; Perén *et al.*, 2015).
5. CFD studies are widely used to study the performance of passive ventilation and heat recovery systems. The most suitable turbulence model is dependent upon the simulation parameters, with a range of models found to be suitable under various boundary conditions (Calautit et al., 2014; O'Connor et al., 2014; Perén *et al.*, 2015; Hosseini *et al.*, 2016; Wu *et al.*, 2021).
6. The validation of CFD models regarding passive ventilation systems seeks to match trends in results, with errors between experimental and numerical datasets up to 100% accepted (Chen and Srebric, 2002; Hughes and Mak, 2011; Connor *et al.*, 2019).
7. Selecting a form of STES depends on parameters including delivery and storage temperature, storage volume requirement, storage time, location, and cost. ATES benefits from a balanced heating and cooling load to maintain a thermal balance within the aquifer.

2.8 Research Gap

After reviewing relevant literature, several research gaps were identified. Studies including wind towers were found to rely on scale model wind tunnel testing for evaluation primarily. As a result, CFD models are often validated through velocity and pressure measurements which assume heat recovery performance without comparable data. Therefore, testing heat recovery systems within a full-scale wind tower is desirable to understand their performance fully.

Heat pipes have been used horizontally within a single-sided wind tower (Calautit *et al.*, 2020) and vertically within a multi-sided wind tower (Calautit *et al.*, 2017), however, both systems employed a heat sink integrated within the wind tower design to remove heat from the heat pipes and provide cooling to fresh air. Consequently, there were no instances where heat pipes had been used for direct heat recovery between air streams within passive ventilation, using the respective inlet and exhaust flows as the heat sink and source without an intermediary system.

Examples of run-arounds within passive ventilation systems explored linking two individual air streams with air-to-water heat exchangers to transfer heat between them (Hestad et al., 1999; Hviid & Svendsen, 2011). In these laboratory-based studies, the water-based systems are designed to recover heat from exhaust air streams. Therefore, they rely on the building's internal temperature to increase fresh air temperature. No cases were found that suggested combining STES with a passive ventilation and heat recovery system to provide a more stable and predictable thermal energy source to pre-heat and cool fresh air on a seasonal basis. Given the context of the applied run-around systems in the literature, there were no attempts to quantify the potential sensible energy recovery through a run-around heat exchanger.

3 Numerical Modelling and Calculations

The following chapter details the underlying theory behind CFD modelling and aspects essential to consider when developing numerical models for simulation. It then details the calculations used to evaluate the performance of the heat exchanger used in the field trial.

3.1 CFD Modelling Approach

CFD is increasingly used alongside experimental work for research based upon fluid dynamics owing to its ability to rapidly solve complex equations related to fluid flow, simplifying the design process by enabling the simulation of a range of boundary conditions and geometries within validated models, lowering costs, and reducing time implications. CFD is beneficial when exploring flow properties involving complex geometries that result in flow regimes that can be difficult to define fully through wind tunnels and other types of physical testing. In addition, a more complete field of data is generated with the values of each variable available at the centre of every cell throughout the computational domain.

3.1.1 Theory

The commercial CFD software ANSYS Fluent simulates fluid flows through the numerical models. Fluent resolves the flow characteristics by solving the Reynolds-Averaged Navier-Stokes (RANS) equations throughout the computational domain.

The k-epsilon turbulence model with standard wall functions was employed in both cases, solving the governing equations for mass, momentum, and energy conservation, as well as the Reynolds-averaged Navier-Stokes and k-epsilon transport equations. The difference between available turbulence models and the reasoning for the selection of the standard k-epsilon model in this work is detailed in section 3.1.6. The governing equations can be found in the ANSYS Fluent Theory Guide (Ansys, 2020). The flow is assumed to be three-dimensional, fully turbulent, and incompressible to reach a solution.

3.1.2 Solution Algorithms

There are four segregated, pressure-based solvers available for selection by the user which are generally used to solve low-speed incompressible flows within ANSYS Fluent:

- Semi-Implicit Method for Pressure-Linked Equations (SIMPLE)
- SIMPLE-Consistent (SIMPLEC)
- Pressure-Implicit with Splitting of Operations (PISO)
- Fractional Step Method (FSM)

Segregated algorithms solve each governing equation sequentially as opposed to the coupled solver which solves the equations simultaneously. The SIMPLE algorithm is the default scheme presented by the program due to its robust and versatile nature. The algorithm uses a relationship between velocity and pressure corrections to enforce mass conservation and to obtain the pressure field. SIMPLEC generates a converged solution quicker for uncomplicated problems such as laminar flows as the under-relaxation factors are higher, a technique used to improve the stability of the solution. The PISO algorithm is suggested for transient simulations with large time steps as it can maintain stables calculations for both momentum and pressure. The FSM is only available for non-iterative time advancement. Given that most of the simulations carried out is under steady state with relatively complex flows, the SIMPLE algorithm was applied for calculation throughout the numerical work undertaken. (Ansys, 2020).

3.1.3 Computational Domain

Computer Aided Design (CAD) software is used to build the geometry of the computational models, with the elements and their measurements derived from the

experimental geometries. Each model geometry is a composition of several components or ‘bodies’ combined to represent the solid and fluid regions that make up the physical experiment. In this process some assumptions and simplifications may be made providing that the changes do not impact fluid flow and heat transfer in areas of interest within the domain. This is done to limit the size and complexity of the domain, lowering calculation times and ensuring a high-quality mesh is created whilst ensuring accurate results are still produced. The impact of these adjustments can be assessed when validating the numerical model and changes made where necessary.

The commercial CAD software Autodesk Inventor 21 was used to model the solid bodies of the wind tunnel test and field trial. The parts are combined in an assembly before being exported to Design Modeler within the ANSYS workbench where the fluid regions are extracted. The properties of the shared boundaries between the solid and fluid regions dictate the interaction between the connected bodies. Inlets and outlets are applied to the relevant faces of fluid bodies to generate a flow throughout the fluid volume. The thermal and physical properties of the relevant materials are applied after the meshing process.

3.1.4 Mesh Generation

Before simulation, the 3D geometry must be discretised to generate a mesh. The mesh is comprised of many smaller elements that together construct the model geometry shape and are the elements in which the flow properties are solved. Owing to the range of complexity in modelled geometries several approaches to mesh design have been developed.

Typically, simple geometries are broken down into a structured mesh that forms a regular pattern of hexahedral cells. The simplicity of this mesh type results in low

computational demand, allowing rapid mesh generation and solution convergence during simulations. An unstructured mesh is used for more complex geometries that cannot be modelled exclusively using hexahedral mesh elements. These meshes are typically formed of tetrahedral cells with no discernible pattern. Hybrid meshes use several cell types to discretise the model geometry (Figure 3-1). This allows complex areas to be modelled with tetrahedral cells while areas or bodies away from these regions can be modelled using the more straightforward hexahedral elements. With this mesh type the boundary between cell types must be considered as non-conformity along the boundaries may result in calculation errors. Local sizing functions allow the use of a greater number of smaller elements in areas of interest, where sizing's can be applied individually to each body but also to the individual edges and faces that comprise the body.

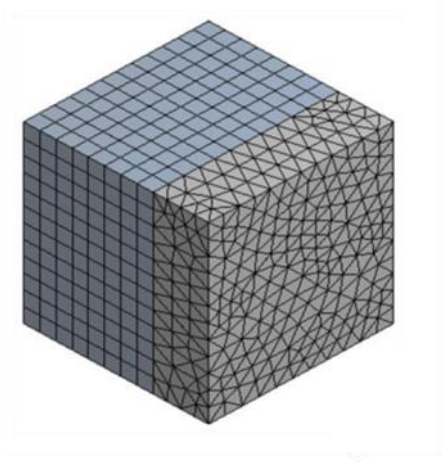

Figure 3-1 - Hybrid mesh formed of hexahedral and tetrahedral elements (Sofotasiou, 2017)

The tetrahedral elements can be converted to polyhedral based on the unstructured mesh framework. As the polyhedral elements have more sides, they have a higher number of neighbouring cells, improving accuracy as gradient values are less stiff and more accurate than other element types (Kim and Chung, 2015). Polyhedral meshes

also require fewer mesh elements than a corresponding tetrahedral mesh, reducing simulation times (Figure 3-2).

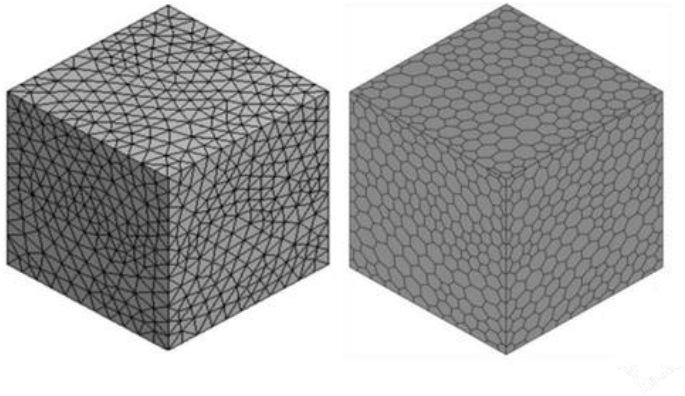

Figure 3-2 - Unstructured mesh with tetrahedral (left) and polyhedral (right) elements (Sofotasiou, 2017)

Mesh defeaturing allows the program to create a mesh that may differ slightly from the original geometry. When turned on, features smaller than or equal to the defeaturing tolerance are removed automatically (ANSYS Inc., 2015). Geometries with small radii or sharp corners with acute angles can be difficult to mesh with good-quality elements, and therefore allowing the program to alter the geometry in these areas slightly helps maintain a high-quality mesh throughout. The defeaturing tolerance is automatically set to 50% of the minimum cell size to limit the impact on the flow through the domain.

The sequence in which the mesh is generated can also impact the final mesh quality, particularly when developing a hybrid mesh with more than one element type. The preferred order of meshing can be controlled through the recording process, dictating the order in which bodies are meshed to assist the program in creating a good-quality mesh.

3.1.5 Evaluating Mesh Quality

The ANSYS Fluent Theory Guide states, "The quality of the mesh plays a significant role in the accuracy and stability of the numerical computation" (Ansys, 2020), where mesh quality is assessed through orthogonal quality, skewness, and aspect ratio.

Orthogonal quality is computed using several vectors: from the cell centroid to each of its faces, the corresponding face area vector, and the vector from the cell centroid to the centroids of each adjacent cell. Orthogonal quality is measured from zero to one, where zero indicates poor and one excellent quality. All cells should have values higher than 0.01, with a higher average value throughout the domain to ensure accurate results.

Skewness measures the difference between the cell shape and that of an equilateral cell of equivalent volume and shape (Figure 3-3). A skewness of zero indicates that the cell is equilateral, with a maximum recommended value of 0.95, although again, the average throughout the domain should be well below this.

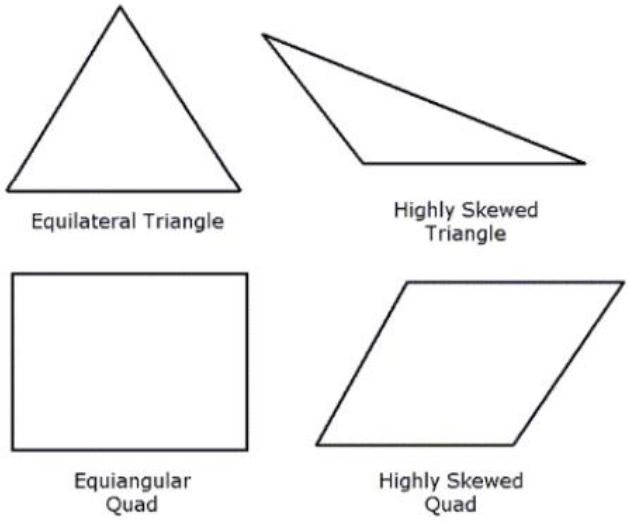

Figure 3-3 - Ideal and highly skewed cell shapes (ANSYS Inc., 2015)

The aspect ratio measures the stretching of the cell through the ratio of the maximum and minimum edge length. It is preferable to avoid significant changes in cell aspect ratio in areas where the flow field may exhibit significant changes or strong gradients (ANSYS Inc., 2015).

3.1.6 Turbulence models

Turbulence is an instability of laminar flow that occurs at higher Reynolds numbers, exhibited through chaotic variations in pressure and velocity within the flow. Turbulence models are used within CFD to capture the turbulent elements of the flow, with a range of turbulence models available for selection based upon the boundary conditions and design of the numerical model. Two equation turbulence models allow for the determination of both a turbulent length and time scale by solving two separate equations (Ansys, 2020).

Considered the simplest model, the standard k-epsilon model has been widely employed to calculate confined, recirculating flows, with relatively small pressure gradients (Ansys, 2020). It is well known for its robustness, economy, and reasonable accuracy for a wide range of turbulent flows. The Renormalisation Group (RNG) k-epsilon model differs in that it is better suited to solving rapidly strained flows and the effect of swirl on turbulence is included, making it applicable to a wider range of flows. Similarly, the Realisable k-epsilon model contains an alternative formula for calculating the turbulent viscosity and a modified transport equation for the dissipation rate, making it suitable for flows with separation and complex secondary flow features (Ansys, 2020).

The k-omega turbulence model is an alternative two-equation turbulence model that solves for kinetic energy (k) and specific dissipation rate (omega) which allows for a

more accurate calculation in the near wall region by switching between wall functions for high and low Reynolds numbers. Further adaptations have been made to the k-omega model such as the Baseline (BSL) and Shear-Stress Transport (SST) models, seeking to improve the accuracy of results by reducing the sensitivity of the model in the near wall regions to the free-stream conditions and improving the flow calculations under adverse pressure gradients respectively (Ansys, 2020).

Peren et al (2015) compared the accuracy of various turbulence models against experimental data for crossflow ventilation through a building. The turbulence models tested included the standard, RNG, and realisable k-epsilon models, as well as the standard and SST k-omega models. They found that for all the tested turbulence models, the maximum deviation in the volumetric flow rate through the openings was approximately 3.6%, indicating little difference between them. Evaluating local measurements, the differences were however as high as 300%, arising from differences in the direction of the jet flow through the inlet opening.

Evaluating CFD studies around wind towers and heat recovery, the standard k-epsilon model was found to be widely applied (Liu et al., 2011; Montazeri, 2011; Hosseinnia et al., 2013; Calautit and Hughes, 2014; Calautit et al., 2015). The widespread use the model was attributed to the relative strengths of the standard k-epsilon model in calculating bounded, recirculating flows, as well as its reliability and relatively low computational demand (Ansys, 2020). In addition, as there is a wide range of research using the model, it is shown to be consistent in predicting velocity, pressure, and temperature changes throughout the computational domain when compared against experimental data.

Given the flow properties likely to arise in the numerical models developed within this study, the k-epsilon turbulence model was selected. The main area of interest is the flow that occurs within the bounds of the wind tower, with relatively low Reynolds numbers throughout the domain due to the low wind speeds modelled. In addition, the areas of recirculation that occur within the wind tower are important to model accurately as they will have a significant impact on the ventilation rate through the wind tower. Finally, the nature of the numerical modelling is comparable with past studies around wind towers and heat recovery that have employed the standard k-epsilon model, allowing greater confidence in its suitability from the outset as they have shown good agreement between experimental and numerical results.

3.1.7 Wall Y+

Wall functions are used within ANSYS to model the laminar sublayer of the flow in the near-wall region. The dimensionless y^+ value can be used to find the appropriate thickness of near-wall elements to capture the flow properties through the wall functions accurately (Equation 3-1).

$$y^+ = \frac{\rho u_* y}{\mu}$$

Equation 3-1

Where ρ is the density of the fluid, u_* is the friction velocity, y is the distance normal to the wall, and μ is the dynamic viscosity. The y^+ value is measured as the distance from the wall to the centroid of the adjacent cell, with the y^+ value ideally falling between 30 and 300 when using standard wall functions (Salim and Cheah, 2009). The thickness of the first cell next to the wall can be dictated through inflation layer parameters within the meshing program, but the mesh can also be coarsened or

refined within ANSYS Fluent after the initial mesh is created to produce the y^+ desired by the user for the relevant wall functions.

Y^* can also measure the dimensionless distance from the wall to the first cell centroid, where y^+ and y^* are almost equivalent in equilibrium turbulent boundary layers (Ansys, 2020). Y^* is calculated through the following equation:

$$y^* = \frac{\rho y \left(\sqrt{C_\mu^{0.5} k_p}\right)}{\mu}$$

Equation 3-2

Where the bracketed term refers to the turbulent kinetic energy of the flow. Cellek (2020) used y^* to determine the impact of mesh structure on numerical results for standard wall functions, scalable wall functions, and enhanced wall treatment with the k-epsilon turbulence model. They found that although $y^* < 1$ was computationally more demanding, the difference in results versus the $30 < y^* < 500$ case was minimal. Calculating y^+ for the same meshes, the relative error between the experimental and numerical results was shown to decrease from 9.01% to 7.58% when the wall y^+ decreased from 30.5 to 0.11 for standard wall functions, indicating that producing y^+ values between 30 and 300 are not essential to accurately calculate the flow properties in the near wall region.

3.1.8 Atmospheric boundary layer

As established through the literature review, several approaches have been made when modelling wind tower and heat recovery systems using CFD, with one of the key points being the inclusion of the whole wind tower and building in the atmospheric boundary layer.

When modelling wind tower systems using CFD, numerous studies have included only the wind tower under a uniform inlet flow as this replicated the conditions experienced in wind tunnel testing that was used to validate the numerical models (Calautit et al., 2015; Calautit et al., 2016; Liu et al., 2022). Although this provides as estimation of the flow rate through the wind tower under the applied inlet velocity, this does not accurately reflect real world conditions where the entire building is subject to the airflow. When considered the impact of flow separation at the leading edge of the building, the inlet velocity into the wind tower inlet or inlets may be less than the free wind speed if the wind tower is placed with the boundary layer that occurs over the building roof.

In response, several studies compared the flow rate through wind towers when the wind tower alone was subjected to a uniform airflow, and with the wind tower and building subjected to an atmospheric boundary layer where velocity increases logarithmically with increasing height. Comparing the two scenarios, placing the wind tower and building together under an atmospheric boundary layer was shown to decrease the average supply ventilation rate through the wind tower by 40 % in one study when the wind speed was 3m/s (Figure 3-4)(Wu *et al.*, 2021), and by between 21 – 23% in another when the wind speed was increased from 1 –5 m/s (Calautit et al., 2016).

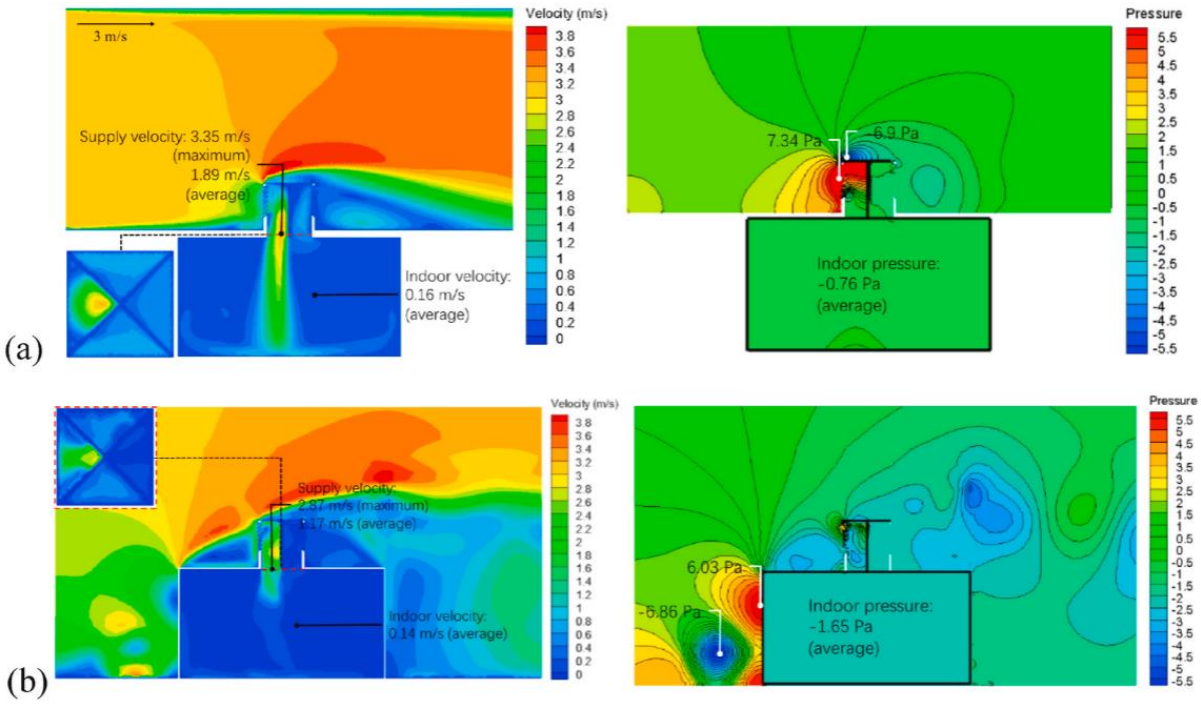

Figure 3-4 - Air velocity and pressure distribution of the two cases: (a) underground application; (b) low-rise house (Wu et al.*, 2021)*

Despite the similarities between the two studies there was a clear discrepancy between the predicted decreases in flow rate through the wind tower, highlighting the need for individual assessment in differing cases. The differences likely arose from differences in the wind tower geometry (wind tower height, number of louvre layers, volume of inlet channel), the placement of the wind tower within the roof, and the scale of the building relative to the wind tower.

Flow separation does however not always occur at the leading edge of a building. In a study of cross-ventilation through buildings with increasing roof angles, a greater roof inclination was shown to decrease the thickness of the boundary layer that occurred over the roof arising from flow separation at the leading edge (Perén *et al.*, 2015). A roof angle beyond 27 ° resulted in a thin boundary layer that followed that angle of the roof (Figure 3-5). In these cases, the wind speed onto the wind tower would be much closer to the free wind speed as the wind tower inlet is above the

boundary layer that occurs over the roof. Higher roof angles did however result in some decrease in velocity on the windward side of the roof due to the blockage of the flow in the direction of the airflow.

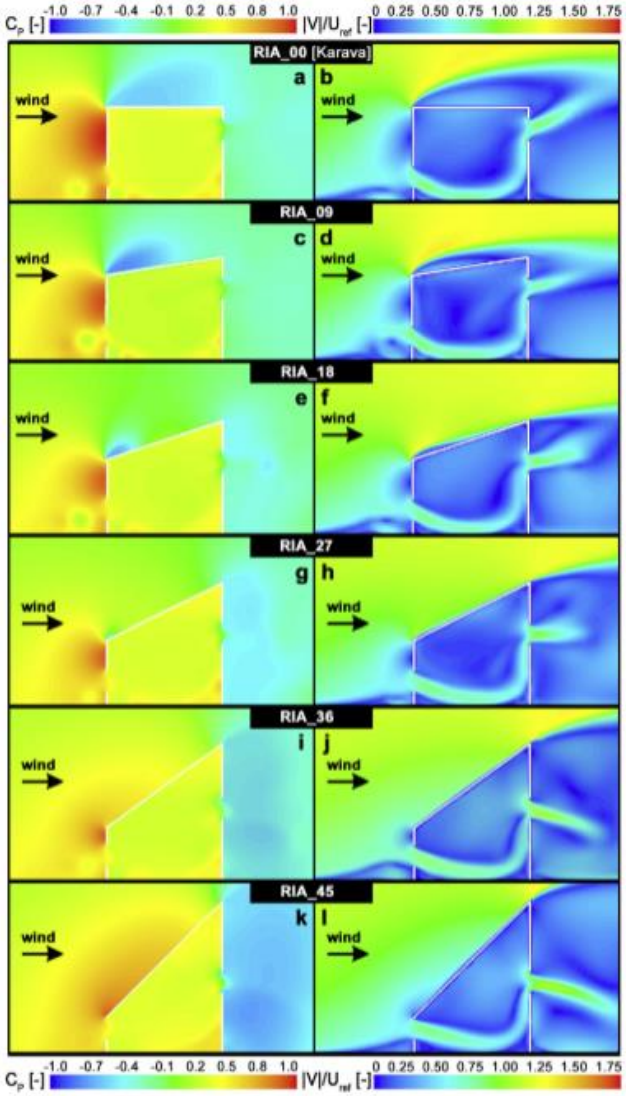

Figure 3-5 - The effect of roof angle on crossflow ventilation and flow separation at the leading edge (Perén et al., 2015)

Consequently, for buildings with inclined roofs it may be less critical to include the whole building within the airflow, providing the direction of the airflow aligns with the inclination of the building roof. For flat roofs, if the whole building is not included within the airflow, then the potential decrease in volumetric flow rate through the wind tower should be calculated. It should also be considered that the logarithmic boundary layers

applied to the numerical models may not accurately reflect the boundary layer onto a building in urban areas, where surrounding buildings have a significant impact on the airflow onto the building.

To negate the impact of the boundary layer on ventilation rates consideration should be given to the local wind speed, the proximity of the wind tower to the leading edge of the building, the roof angle, the roughness length of the surroundings, and the height of the wind tower above roof level.

3.1.9 Verification and Validation

The verification and validation of the numerical model is an exercise in proving that the equations are being solved correctly throughout the domain, with the verification dealing with numerical errors and uncertainties while validation is concerned with modelling errors and uncertainties (Eça and Hoekstra, 2014). It is crucial to quantify the error and uncertainty produced through numerical models to have confidence in the results produced through simulation, however accurately capturing this can be challenging (Paudel and Saenger, 2017).

Uncertainty can be roughly categorised as numerical and physical uncertainty, where numerical uncertainty includes discretisation errors, errors in numerical boundary conditions, solvers, or geometry descriptions. Physical uncertainty includes errors due to unknown boundary and initial conditions and insufficient knowledge of the flow geometry (Karniadakis, 2002).

Systematic grid refinements are most commonly used for assessing numerical uncertainty (Paudel and Saenger, 2017). Under consistent boundary conditions, increasing mesh cell density systematically should reduce the relative error between each mesh design, where among several methods Richardson extrapolation is often

used to estimate the numerical uncertainty throughout the domain (Stern *et al.*, 2001a).

3.1.9.1 Mesh Independence

A mesh independence study can be used to verify the numerical model. Meshing introduces discretisation errors because of the finite resolution of the grid and calculation time. Even when the results of the numerical model agree with the experiment, there are still discretisation errors in the solution (Schwer, 2008). To verify the results of the generated mesh, a mesh independence study is undertaken to assess the numerical error and uncertainty of the calculations. Sofotasiou (2017) laid out one method which is repeated below to determine the accuracy of the results using a minimum of three mesh sizes.

The Grid Convergence Index (GCI) was developed by Roache (1994), using Richardson Extrapolation to find the discretisation error based upon a series of meshes increasing in size with a constant grid refinement ratio and uniform order of accuracy in space and time (Sofotasiou, 2017). The GCI is calculated as an error percentage and represents a confidence band within which the numerical solution will likely lie (Schwer, 2008).

Equation 3-3 and Equation 3-4 can be used to determine the discretisation error in coarse and fine grids respectively:

$$E_2[coarsegrid] = r^p * \varepsilon_{32}/(r^p - 1)$$

Equation 3-3

$$E_1[finegrid] = \varepsilon_{21}/(r^p - 1)$$

Equation 3-4

Where $E_{1,2}$ are the coarse (E_2) and fine (E_1) grid Richardson error estimators, r is the grid refinement ratio, p is the order of accuracy equal to the order of the discretisation scheme, and ε indicates the difference in the numerical solution between progressively finer grids:

$$\varepsilon_{32} = (\phi_3 - \phi_2)/\phi_2$$

Equation 3-5

$$\varepsilon_{21} = (\phi_2 - \phi_1)/\phi_1$$

Equation 3-6

$\phi_{3,2,1}$ are numerical solutions generated at the same point in space in the coarse, medium, and fine grids respectively. While the grid refinement ratio is ideally equal to 2 and applied consistently over the entire mesh, this is not always practical. A three-dimensional model using a grid refinement ratio of 2 would require an 8x increase in the number of cells in the mesh. Therefore, for scenarios where r and p are not equal to 2, Roache (1997) later introduced a safety factor, using Equation 3-7 and Equation 3-8 to calculate the GCI index for coarse and fine grids respectively:

$$GCI_{32}^{coarse} = F_s|E_2|$$

Equation 3-7

$$GCI_{21}^{fine} = F_s|E_1|$$

Equation 3-8

Where F_s = 1.25 is commonly applied (Roache, 1998). In the case that the refinement ratio between the coarse-medium and medium-fine grids is equal, r is calculated according to Equation 3-9 and Equation 3-10:

$$r_{21} = (N_1/N_2)^{1/D}$$

Equation 3-9

$$r_{32} = (N_2/N_3)^{1/D}$$

Equation 3-10

Where N_3, N_2, and N_1 are the number of cells in the coarse, medium, and fine grids respectively, and D is the dimensionality of the model (D = 3 for a 3D model). The order of the solution can be calculated according to Equation 3-11 when r is constant or Equation 3-12 when not (Stern *et al.*, 2001b; Sofotasiou, 2017):

$$p = \frac{ln(\varepsilon_{32}/\varepsilon_{21})}{ln\,(r)}$$

Equation 3-11

$$p_k = \frac{ln(\varepsilon_{32}/\varepsilon_{21})}{ln\,(r_{21})} + \frac{1}{ln\,(r_{21})}\left[ln\left(r_{32}^{p_k} - 1\right) - ln\left(r_{21}^{p_k} - 1\right)\right]$$

Equation 3-12

p_k is calculated iteratively, with the first value equal to the best guess. The extrapolated values and resulting extrapolative error can then be found using Equation 3-13:

$$\phi_{21,ext} = \left(r_{21}^{p}\phi_1 - \phi_2\right)/\left(r_{21}^{p} - 1\right)$$

Equation 3-13

The observed order of accuracy is used to determine the reliability of the Richardson extrapolation error estimate (Phillips and Roy, 2014), with Eca and Hoekstra (2002) suggesting an acceptable range of $0 < p_k < 8$. The average observed order of accuracy is used to calculate the GCI (Celik *et al.*, 2008). The extrapolated values predict the solution at zero cell size and can be used alongside the extrapolative error to determine if it is necessary or not to further refine the grid.

3.1.10 Convergence

ANSYS Fluent uses the finite element method to iteratively solve partial differential equations throughout the discretised domain. Residuals indicate the error throughout the model, where a higher residual indicates a worse solution. The default convergence criteria deem the solution to have converged when the residual monitor falls below 10^{-6} for the energy equation and 10^{-3} for all other equations (Ansys, 2020). This however does not occur in all cases and therefore convergence can also be judged by the individual by monitoring residuals and values at specific points to evaluate if changes are still occurring throughout the model with each iteration of the simulation.

To do this monitor points are placed at areas of interest within the computational domain to monitor variables such as velocity and temperature with each iteration. Convergence was deemed to have been achieved once the value at each point remained unchanged for at least 500 iterations (Calautit et al., 2016).

3.2 Calculations

The performance of the heat exchanger installed in the field trial can be evaluated through the efficiency of heat recovery and the overall heat transfer coefficient at different inlet velocities, with the process for calculating each detailed below.

3.2.1 Efficiency

The efficiency of a heat exchanger is defined as the temperature change of one fluid divided by the temperature difference between the two inbound fluids and is calculated according to Equation 3-14 (Hviid and Svendsen, 2011):

$$\eta = \frac{T_{h,in} - T_{h,out}}{T_{h,in} - T_{c,in}}$$

Equation 3-14

Where $T_{h,in}$ and $T_{h,out}$ are the air temperatures and above and below the heat exchanger respectively, and $T_{c,in}$ is the inlet water temperature. When the heat exchanger features more than one row of pipes, the direction of flow passed the water through the lowest layer first to create the greatest temperature difference between the two fluids (Figure 3-6).

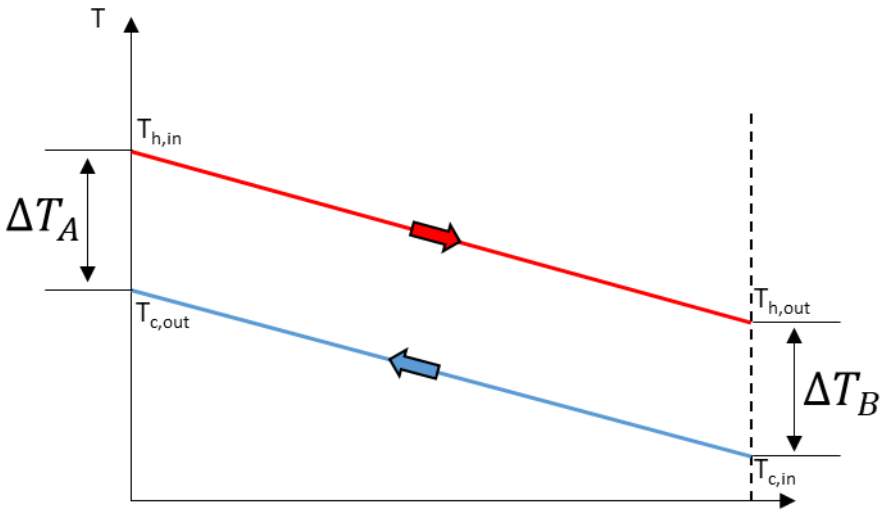

Figure 3-6 - Cross flow heat exchanger fluid temperatures

As the temperature difference between the two fluids changes over the heat exchanger, the average temperature difference between the two fluids is found through the Log Mean Temperature Difference (LMTD) (Equation 3-15):

$$\Delta T_{LMTD} = \frac{\Delta T_A - \Delta T_B}{ln\,(\Delta T_A / \Delta T_B)}$$

Equation 3-15

Where ΔT_A is the temperature difference between the two fluids at point A and ΔT_B is the temperature difference between the two fluids at point B. Substituting the LMTD into the lower half of the equation results in Equation 3-16:

$$\eta = \frac{T_{h,in} - T_{h,out}}{\Delta T_{LMTD}}$$

Equation 3-16

3.2.2 Heat Transfer Rate Calculations

The overall heat transfer coefficient was calculated to determine the heat transfer between the two fluid streams in W/m^2·K. The overall heat transfer coefficient, U, is found through the individual heat transfer coefficients for the water and air, and the resistance to heat transfer through the pipe wall. Correlations proposed by Khan et al. (2006) and applied by Hviid and Svenson (2011) for staggered banks of pipes in a cross-flow were used for the analytical calculations (Figure 3-7).

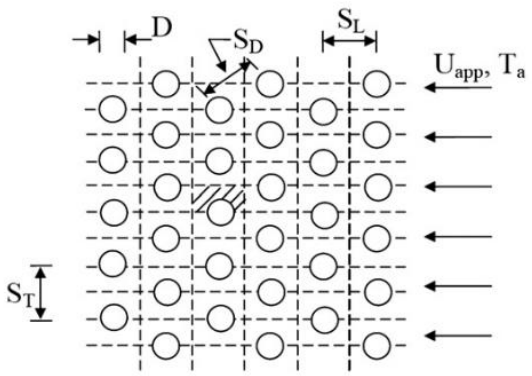

Figure 3-7 - Schematic of staggered pipe arrangement (Khan et al., 2006)

All fluid properties were evaluated at the mean temperature of the fluid (Equation 3-15). The overall heat transfer coefficient was calculated using Equation 3-17:

$$U = \frac{1}{\frac{1}{\pi D_o h_a} + \frac{ln\,(D_o/D_i)}{2\pi\lambda_{pipe}} + \frac{1}{D_i h_w}}$$

Equation 3-17

Where h_a is the heat transfer coefficient of the air, D_o and D_i are the outer and inner diameters of the pipe respectively, λ_{pipe} is the thermal conductivity of the pipe material, and h_w is the heat transfer coefficient of the water.

First, h_a was calculated using Equation 3-18:

$$h_a = \frac{Nu_a \lambda_a}{D_o}$$

Equation 3-18

Where λ_a is the thermal conductivity of air and Nu_a is the Nusselt number, the dimensionless ratio between convective and conductive heat transfer found through Equation 3-19 for cylinders in a cross-flow (Khan et al., 2006):

$$Nu_a = C_1 Re_{D_o}^{1/2} Pr_a^{1/3}$$

Equation 3-19

The coefficient C_1 is related to the pitch ratio of the staggered arrangement, R_{D_o} is the Reynolds number, and Pr_a is the Prandtl number evaluated at the LMTD. For staggered tube banks, C_1 is calculated through Equation 3-20:

$$C_1 = \frac{0.61 \varsigma_T^{0.091} \varsigma_L^{0.053}}{1 - 2\exp\,(-1.09\varsigma_L)}$$

Equation 3-20

Where ς_L, ς_T, and ς_D are the dimensionless longitudinal, transversal, and diagonal pitches found by dividing the longitudinal (S_L), transversal (S_T), and diagonal (S_D) pitches by the outer diameter of the pipe:

$$\varsigma_L = S_L/D_o$$

Equation 3-21

$$\varsigma_T = S_T/D_o$$

Equation 3-22

$$\varsigma_D = S_D/D_o$$

Equation 3-23

Equation 3-24 was used to find Re_{D_o}:

$$Re_{D_o} = \frac{\rho_a U_{max} D_o}{\mu_a}$$

Equation 3-24

Where ρ_a is the air density, μ_a is the dynamic viscosity, and U_{max} is the approximate maximum velocity through the tube banks (Equation 3-25):

$$U_{max} = max\left\{\begin{matrix} \frac{\varsigma_T}{\varsigma_T - 1} U_{app} \\ \frac{\varsigma_T}{2(\varsigma_D - 1)} U_{app} \end{matrix}\right\}$$

Equation 3-25

Where U_{app} is the approach velocity, taken as the inlet velocity in this instance. The heat transfer coefficient on the water side was then calculated (Equation 3-26):

$$h_w = \frac{Nu_w \lambda_w}{D_i}$$

Equation 3-26

Nu_w can be calculated by Equation 3-27, where n = 0.3 for heating and 0.4 for cooling (Taler and Taler, 2017)

$$Nu_w = 0.023 Re_{Di}^{0.8} Pr^n$$

Equation 3-27

The Reynolds number is then calculated to find the Nusselt number (Equation 3-28):

$$Re_{D_i} = \frac{\rho_w U_w D_i}{\mu_w}$$

Equation 3-28

Upon calculating the heat transfer coefficients for the air and water individually, the U value can be calculated (Equation 4-24), indicating the heat transfer rate from the air to the water through conductive and convective heat transfer.

As the U value is dependent on the thermal and physical properties of the water and air, the value is likely to differ between each quadrant of the wind tower. To find the U value through the wind tower inlet quadrant the properties of the air are taken from that quadrant. As it is impossible to separate the water flow into individual quadrants, the properties are taken from the changes in temperature through the whole heat exchanger.

3.3 Summary

The information compiled in the above chapter was used to develop the numerical models derived from the wind tunnel test and field trial of the wind tower and heat

recovery systems. Creating an accurate geometry is just a small part of the modelling process, with the dedication of time towards meshing often noted as one of the most time-consuming aspects of CFD modelling. The meshes must be generated with high-quality cells before verifying and validating the numerical model. Once these steps are complete further simulations can take place, applying a range of boundary conditions and making incremental changes to geometries to generate information regarding the performance of the proposed systems.

The calculations then detailed were used to evaluate the performance of the heat exchanger based upon the efficiency of heat exchange between the two fluids. The efficiency and overall heat transfer coefficient of the heat exchanger can be used to compare the performance to other systems and help determine where improvements can be made in future iterations.

4 Experimental Testing and Validation

The following chapter established the experimental and numerical methods used for the evaluation of a full-scale wind tower integrated with heat pipes for passive heat recovery. The design of a wind tunnel test conducted at the Building Research Establishment (BRE), UK, is first explored before introducing the measurement points and boundary conditions used throughout testing to indicate the performance of the system. The development of the numerical model is detailed, exploring the creation of the mesh, mesh independence study, and heat pipe modelling approach.

Results recorded during experimental testing were used to validate the model for both velocity and temperature measurements. Following validation, simulations were conducted with models featuring one to three rows of heat pipes, exploring the relationship between the heat pipe array, inlet velocity, supply ventilation rate, and

heat transfer. Finally, the potential heating energy demand reduction as a result of heat recovered from exhaust air was calculated.

4.1 System design

A wind tower with a square frame, four sides, and 6 louvre layers on each side was selected as the passive ventilation unit. Square wind towers have been shown to outperform circular wind towers due to the greater pressure difference between the windward and leeward faces that occurs due to the flow separation at the sharp corners of the frame. Although increasing the number of sides reduces the susceptibility of the wind tower to changing wind direction, it also reduces the flow rate through the wind tower and so a wind tower with four sides was selected to strike a balance between the two. Each side featured seven external louvres with six gaps between them for the air to pass through. Increasing the number of louvre layers beyond 6 has been shown to have a limited impact on the flow rate through the wind tower and therefore no additional layers were added.

4.1.1 Heat recovery

After reviewing the available literature, the available forms of heat recovery were compared according to their pressure drop, heat recovery efficiency, and the future ease of integration of a water-based thermal loop into the wind tower and heat recovery system.

Although rotary wheels are ideally placed to recover heat between the changing inlet and outlets of a wind tower, their geometry makes it difficult to remove or deliver thermal energy from the wheel itself via a water-based thermal loop. Plate heat exchangers achieve high efficiencies and could feasibly be integrated into a water-

based thermal loop, however, the pressure drop over them is too significant to consider for passive ventilation scenarios.

By contrast, heat pipes offer a low pressure drop, reported between 1 – 5 Pa in the literature, as well as a high heat recovery efficiency up to 80%. Although they don't offer any control over the humidity of the air passing through the ventilation system, their geometry lends itself to integration within a thermal loop. Run-around heat exchangers were reported to achieve lower heat recovery efficiency than heat pipes and lack the ability to actively control humidity, however they incur a low pressure drop over the geometry and have a fluid loop built into the design. Run-around systems however require heat exchangers to be built into the system, with the design of the heat exchanger having a significant impact on the performance of the system. Resulting from the available information, heat pipes were selected for testing within a full-scale wind tower.

Despite the decrease in cooling performance associated with a larger longitudinal pitch, a streamwise pitch of 35 mm was chosen for the heat pipe array installed through the base of the wind tower. This was done to preserve the primary function of the wind tower to provide fresh air to the room below whilst maintaining a reasonable heat exchange efficiency. The transversal pitch was 50 mm in line with the research conducted by Chaudry et al (2017) In cases where average wind speeds are high it may be possible to further decrease the spacing between the pipes to deliberately decrease the velocity of the inbound fresh air and to increase the heat exchange efficiency. Heat pipes with an outer diameter of 16 mm partially filled with water as the working fluid were used throughout testing.

4.2 System Description

As wind towers were traditionally used throughout the middle east to provide cooling only, generating large ventilation rates in climates that experience cold seasons results in increased building energy demand as warm air is exhausted from the room and fresh air temperature must be raised to create a thermally comfortable environment. As a result, heat recovery is used to transfer some of the available heat from the exhaust to inlet air stream to raise fresh air temperature and limit the increase in building energy demand. The experiment sought to determine the impact of installing banks of THPs horizontally through the base of a commercial wind tower on inlet volumetric flow rate and to quantify the potential pre-heating of fresh air using waste heat recovered from the wind tower exhaust channels.

To achieve this, a purpose-built wind tunnel test section was used to generate a flow of air through a four-sided wind tower and adjoining test room. Cold air enters through the wind tower inlet, flowing over the pipes and into the test room below. Inside the room the fresh air was drawn over heated coils before being discharged back into the room, eventually exiting through the wind tower exhaust channels. The heat addition of the coils is varied to generate the outlet temperatures desired. As hot air passes over the evaporator section of the THPs through the exhaust channels of the wind tower the working fluid inside them evaporates. The resulting vapour travels along the length of the pipe to the condenser section through the wind tower inlet, where fresh air simultaneously passing over the pipe surface causes the vapour to condense and release some of the available heat. In this way heat is transferred from the exhaust to inlet air streams and the incoming fresh air temperature is increased, reducing the energy required to raise the fresh air temperature to the room set point (Figure 4-1). The rate of heat transfer is a function of the temperature difference between the heat

pipe surface and the fresh air, the temperature of the air leaving through the wind tower exhaust channels, and the velocity of the air, with measurements taken with this in mind.

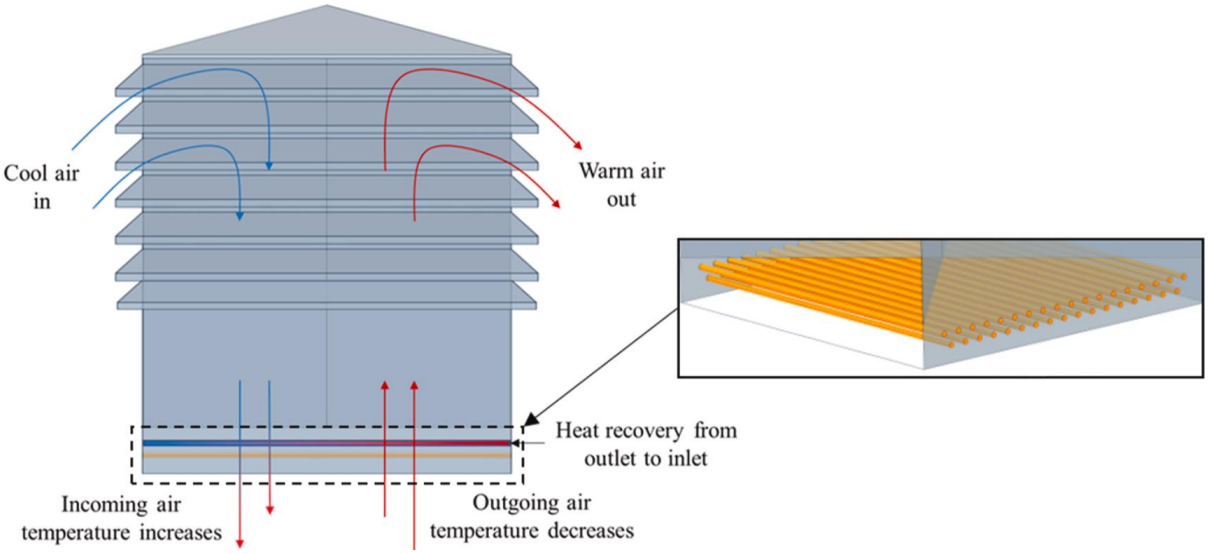

Figure 4-1 - Heat recovery between the inlet and outlet of a multi-sided wind tower

The same process can be used to recover cooling energy, with the thermal energy used to lower room temperature in summer months recovered through the THPs to cool fresh air, however, for the purpose of this experiment only pre-heating is explored.

4.3 Experiment Design

A commercial wind tower design was adapted to house two staggered layers of heat pipes through its base (Figure 4-2). The four-sided wind tower is constructed from 2 mm thick aluminium and measured 1 x 1 x 1.28 m with an internal x-frame that divided the volume into four equal quadrants. Each side has 7 external louvres with a gap of 100 mm between each to channel the flow of air through the wind tower. Each louvre has an angle of 45° and is 1.1 m long, extending out beyond the base of the wind tower.

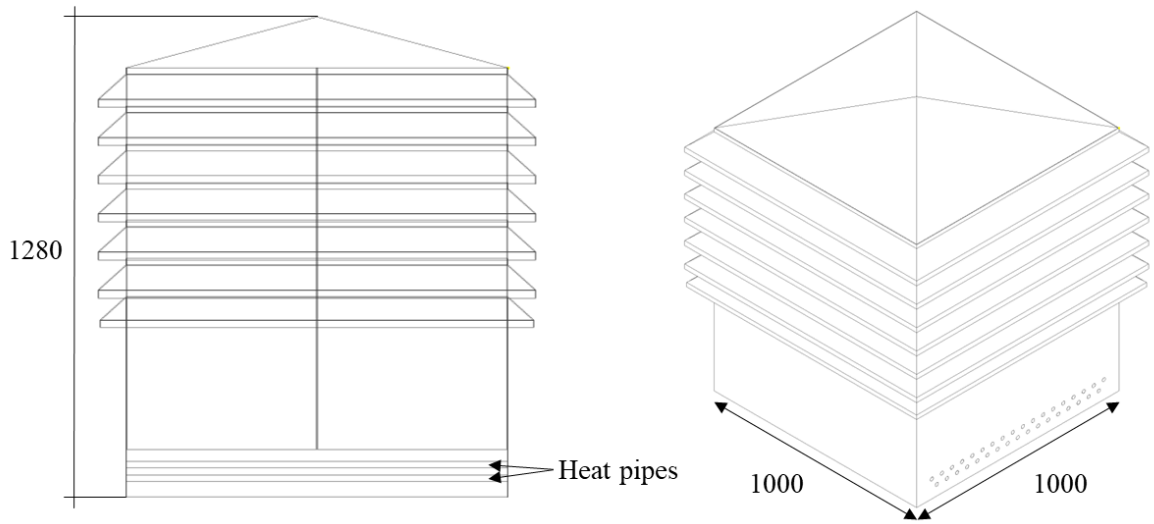

Figure 4-2 - Wind tower dimensions

The two staggered rows were comprised 35 THPs, split into a row of 18 above and a row of 17 below, which were installed through the base of the wind tower with the height of the x-frame shortened by 120 mm relative to the height of the wind tower to create space for the heat pipes to pass beneath traversing all four quadrants. Although staggering the pipes results in a greater velocity reduction than if they were in line with one another it serves to maximise the interaction of the pipe surface with the air passing through each quadrant. Figure 4-3 and Figure 4-4 show the arrangement of the pipes within the wind tower. The pipes were spaced sufficiently so that almost the entire inlet quadrant was covered whilst ensuring that each heat pipe traversed at least two quadrants.

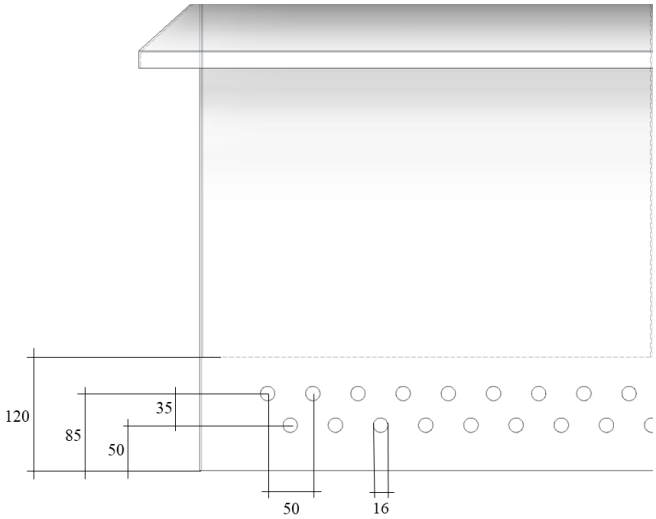

Figure 4-3 – Pipe spacing within the wind tower

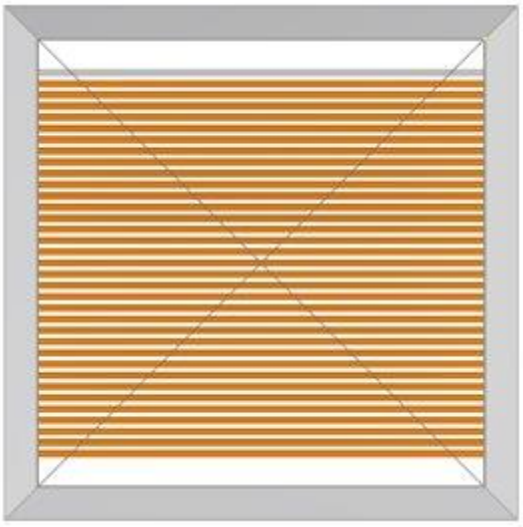

Figure 4-4 - Top down view of heat pipes traversing wind tower quadrants

An open loop wind tunnel test section was constructed inside an environmental chamber at the BRE. A test room with dimensions 3.5 x 2.3 x 2.2 m made of metal supports, plywood, and 50 mm thick insulation sheets was built in the chamber. A 1 x 1 m hole was cut in the centre of the roof and the wind tower placed over it, connecting the volume of air inside the test room with the wind tunnel test section (Figure 4-5).

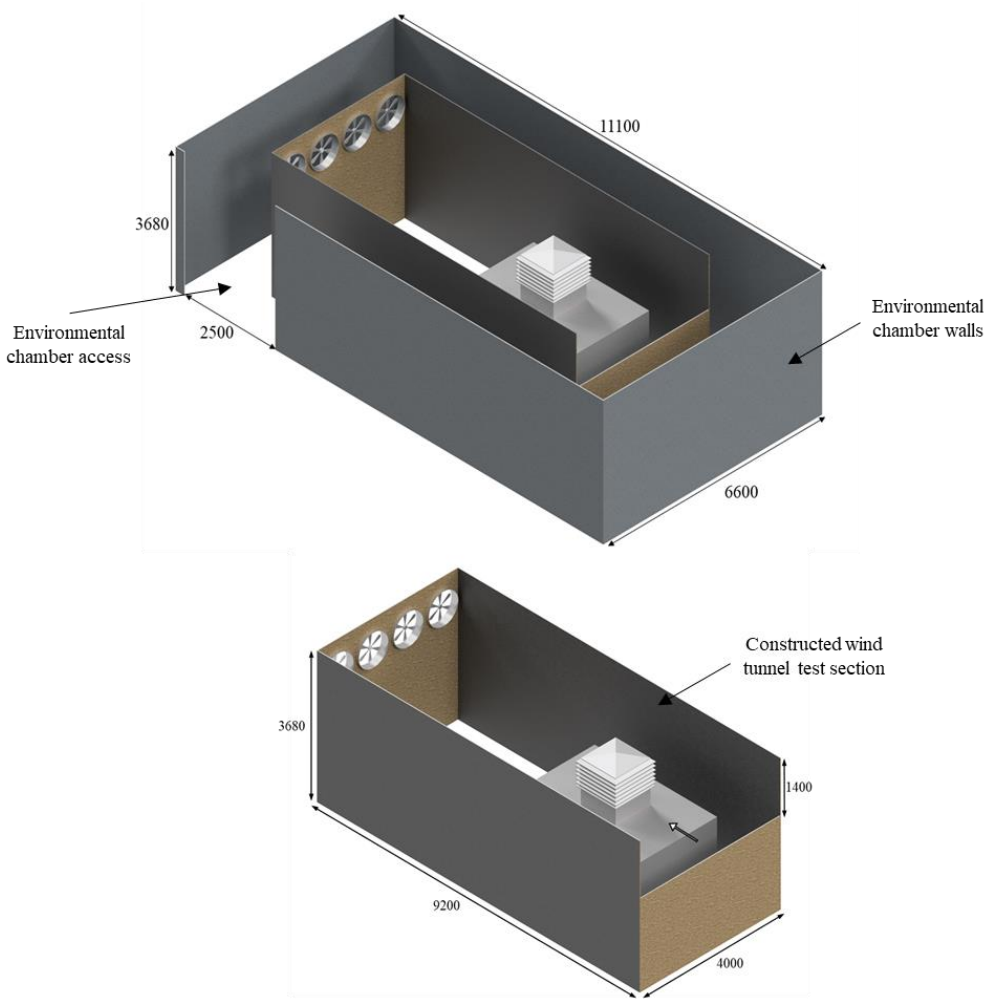

Figure 4-5 –Wind tunnel test section inside the environmental chamber (Top) and wind tunnel test section (Bottom) where the white arrow indicates the direction of flow

Four fans were installed to convert a section of the environmental chamber into a wind tunnel. Walls were erected either side of the test room in line with the outer edges of the fan array to constrain the flow of air around the wind tower. The fans draw air over the wind tower from the opposite end of the wind tunnel test section through a gap measuring 4 x 1.4 m. Given the scale of the system, the fans were only large enough to draw air over the wind tower rather than the entire test room (Figure 4-6). Drawing rather than blowing air has been shown to produce a more consistent flow profile which is easier to reproduce in numerical models (Calautit, O'Connor, *et al.*, 2020).

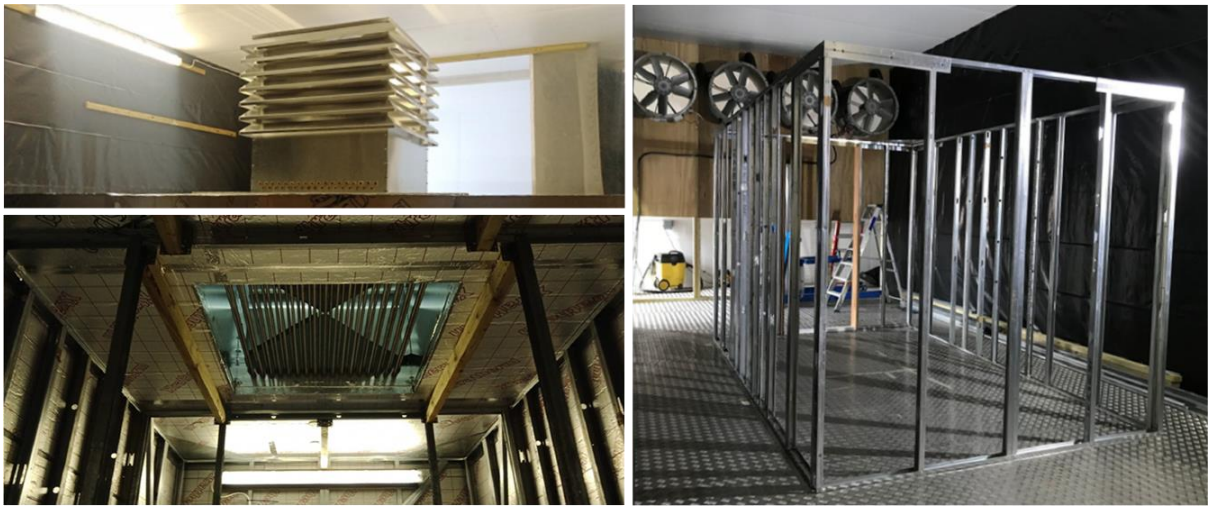

Figure 4-6 - Wind tunnel experimental set up showing wind tower on top of test room (top left), heat pipes through base of wind tower (bottom left), and test room frame inside the constructed wind tunnel test section (right)

A 12-kW gas boiler feeds the heated coils within the test room to generate heating in place of the passive and active thermal gains that would be experienced in an occupied building, equivalent to a maximum of 1.5 kW/m^2. The heating capacity of the gas boiler was varied to produce the desired outlet temperatures rather than matching the expected heat output in an occupied building.

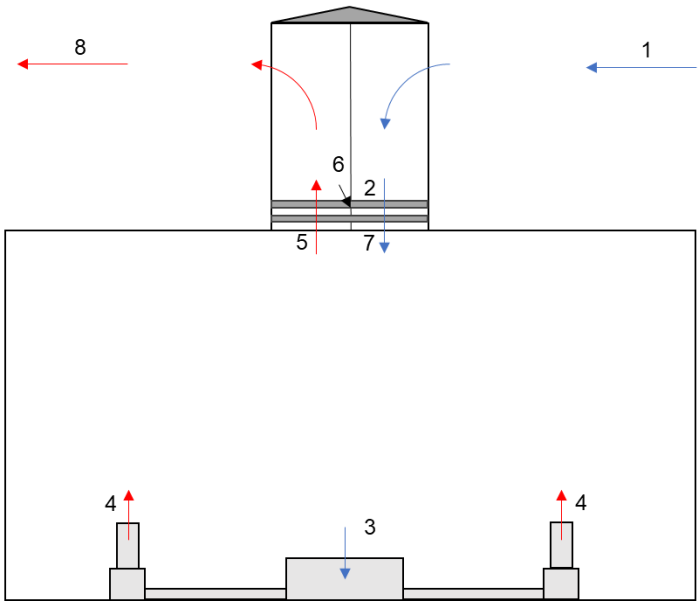

Figure 4-7 - Energy flow through wind tower, heat pipes, and test room

The wind tunnel test operated as follows; 1) Fresh air is drawn over the wind tower using the inline fans installed within the environmental chamber; 2) Fresh air flows in through the wind tower inlet, over the heat pipes, and into the room below where it is distributed throughout the room; 3) A fan is used to draw cool air over a series of heated coils fed via the gas boiler to increase air temperature; 4) Hot air is discharged back in to the room through supply plenums at the desired outlet temperature; 5) Hot air is exhausted through the wind tower outlets, passing over the evaporator section of the heat pipes; 6) The hot air passing over the heat pipes causes the internal fluid to evaporate. The resulting vapour travels along the length of the heat pipe to the condenser section which is located within the inlet quadrant of the wind tower; 7) Cool fresh air passing over the heat pipe causes the internal fluid to condense, releasing some of the available heat, increasing fresh air temperature; 8) Stale air is exhausted back to the ambient.

Fresh air entering the test room was drawn over the coils by two inline fans and then discharged back into the room via semi-rigid ducts and supply plenums. Discharging hot air back into the test room through the supply plenums forces a high degree of mixing between the fresh and stale air and was found to be necessary to generate an outlet temperature that was sufficiently higher than the inlet temperature. As a downside, the air velocity within the room is artificially increased, likely having some effect on the velocity of the air through the wind tower outlets and therefore the heat transfer along the length of the THPs.

4.3.1 Heat Pipes

The heat pipes used were water filled aluminium THPs, pressurised to saturation point with an operating temperature of 20 °C. Traditionally THPs are installed vertically with the evaporator section at the bottom and the condenser above, allowing gravity to

return the condensed internal fluid. Although more effective at inclination angles around 60°, studies have shown that at low or flat inclination angles THPs are still capable of transferring heat along their length, particularly when the heat input is low (Alammar et al., 2016; Reji *et al.*, 2021). Alammar et al. (2016) found that when increasing inclination angle from 10 to 90°, the thermal resistance of the heat pipe fell from 1.92 to 1.82 K/W when the heat input was 39 W. similarly when the heat input was 101 W, the thermal resistance fell from 0.92 to 0.82 K/W. Reji et al (2021) tested heat inputs from 40 to 200 W and inclination angles from 0 to 90°. Figure 4-8 shows the heat input to the evaporator section of the heat pipe versus the heat output at the condenser section with increasing inclination angle. The heat pipe at 60 degrees performs the best at any heat inputs greater than 120 W, however the flat heat pipe performs best at 80 W heat input and is comparable with other inclination angles at 40 W heat input.

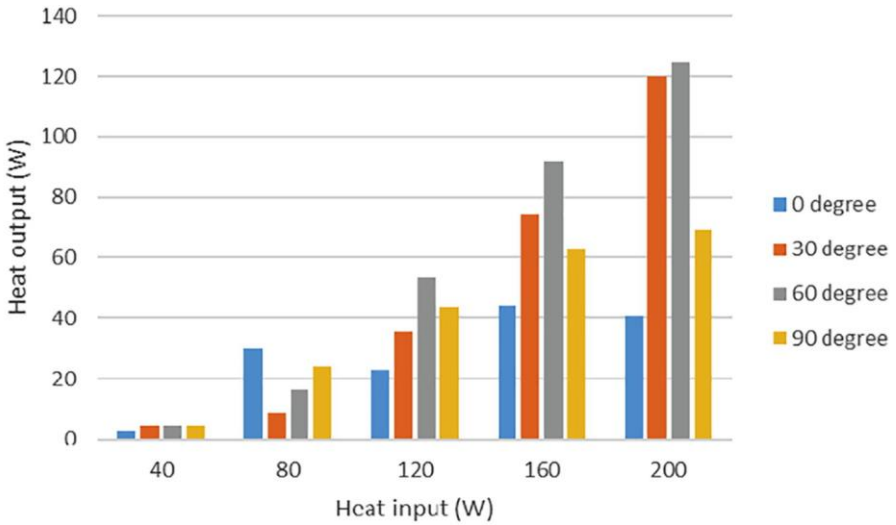

Figure 4-8 - Heat input vs output with increasing inclination angle for a single heat pipe (Reji et al., 2021)

A lack of inclination is also likely to affect the cooling of the evaporator section as the water inside the pipe will not flow in one direction consistently. In this case, as the

temperature difference between the outlet and the inlet is low it is highly unlikely that the THPs will reach the capillary limit, at which point all the fluid inside the THP is gaseous as not enough cooling is occurring.

4.3.2 Test Equipment

Hot wire or bead anemometers are widely used to measure flow velocity due to their fast response time and small size, limiting the disturbance of the flow. A current is passed through the device, causing its temperature to increase. As the fluid passes over the bead or wire it is cooled, with the rate of cooling used to determine the velocity.

A TSI 8475 omni-directional spherical hot bead anemometer was used to take velocity measurements, with a range of 0 – 60 °C and an uncertainty of ± 3% of the reading. The anemometer was mounted to a moveable stand to maintain the positioning of the probe throughout the recording window. Velocity readings were taken over 2 minutes periods and averaged at each point under a constant inlet velocity.

Temperatures were recorded using k-type thermocouple probes with a range of -75 – 250 °C and an uncertainty of ± 1% at 25 °C. Temperature readings were taken as the average reading over the course of an hour under steady state conditions (Figure 4-9).

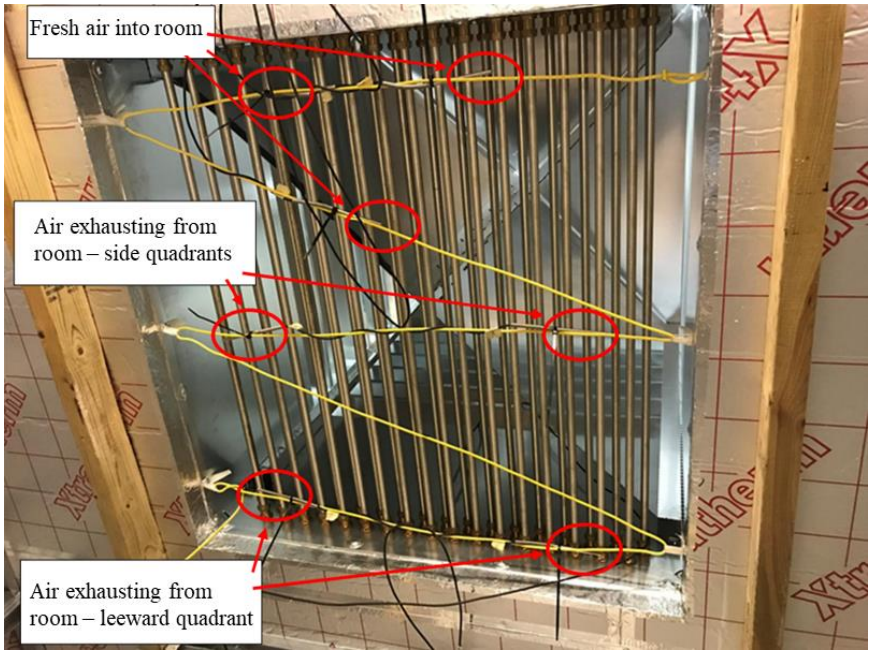

Figure 4-9 - Temperature sensor location

4.3.3 Measurement Points

Velocity and temperature measurements were taken at numerous points throughout the wind tunnel to accurately capture the changes to the flow that occur through the wind tower and heat pipe system.

4.3.3.1 Volumetric Flow Rate

The inlet quadrant of the wind tower was divided into six approximately equal areas and the wind speed measured at the centre of each (Figure 4-10). The total volumetric flow rate through the inlet was then calculated according to Equation 4-1:

$$Q_v = \sum_{i=1}^{n} A_i \times U_i$$

Equation 4-1

Where Q_v is the flow rate through the entire quadrant, A_i is the area of point *i*, and U_i is the velocity measured at the centre of point *i*. Figure 4-10 shows the position of points

A – F within the wind tower inlet quadrant and the division of the quadrant into six approximately equal areas.

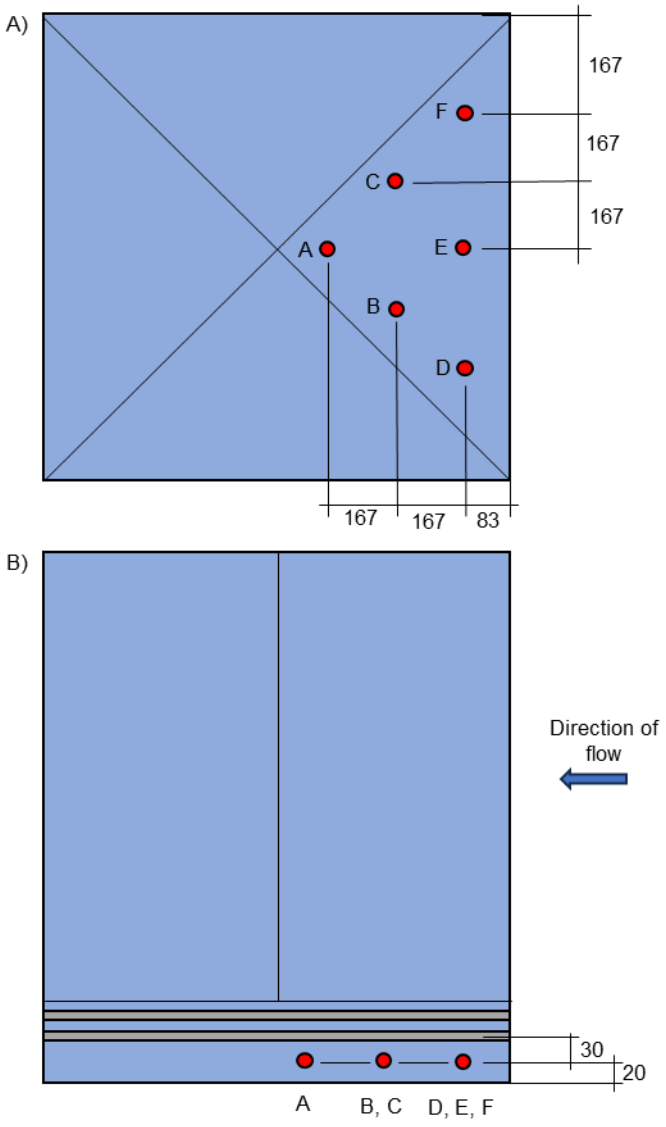

Figure 4-10 - Inlet quadrant area divisions and measurement points

When performing wind tunnel testing, the placement of a bluff body in the flow can result in increased wind speeds in areas where the flow is constricted due to the walls of the wind tunnel test section. The degree to which the results are affected is defined by the blockage ratio, found by dividing the frontal area of the test object by the cross-sectional area of the wind tunnel. Using the ratio of the frontal area of the wind tower

to that of the fans, the blockage ratio is calculated to be 23.3%. Although this is above the 10% recommended (Claudia Klein *et al.*, 2018), given the scale of the wind tower, increasing the size of the fans to reduce the blockage ratio below 10% was impractical. The inlet velocity through the wind tower was measured 0.8 m upwind of the inlet quadrant and this is the inlet velocity reported, approximating free wind speed, and therefore no corrections were made to the results.

4.3.3.2 Temperature

To evaluate heat pipe performance temperature measurements were taken at points upwind of the wind tower, in each of the wind tower quadrants below the heat pipes, and above the pipes through the downwind quadrant. Due to significant variations in air velocity across the inlet, temperature measurements were taken in two lateral regions of the upwind quadrant (Figure 4-11). The average of points 2 and 3 is averaged against the value at point 1 to find the average temperature increase of the air after it has passed over the heat pipes. A single sensor was placed in the two lateral quadrants (points 4 and 5) to measure the outlet temperature through them. Due to the direction of the flow, the majority of the stale air was exhausted through the far left quadrant and so two sensors were placed below the pipes and one above to measure the decrease in air temperature through the channel.

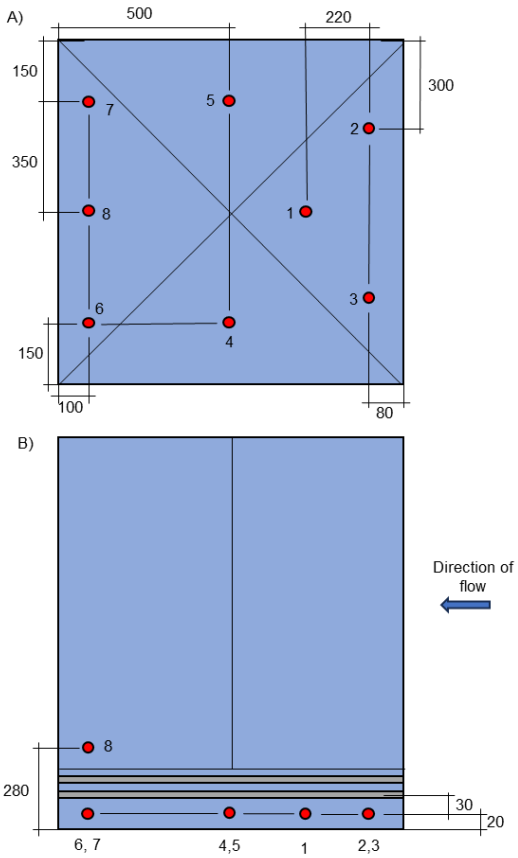

Figure 4-11 - a) top-down view of temperature sensor locations and b) side view of temperature sensor locations. The arrow indicates direction of flow.

Inlet air temperature is taken as the average of two points 800 mm upwind of the wind tower inlet (Figure 4-12).

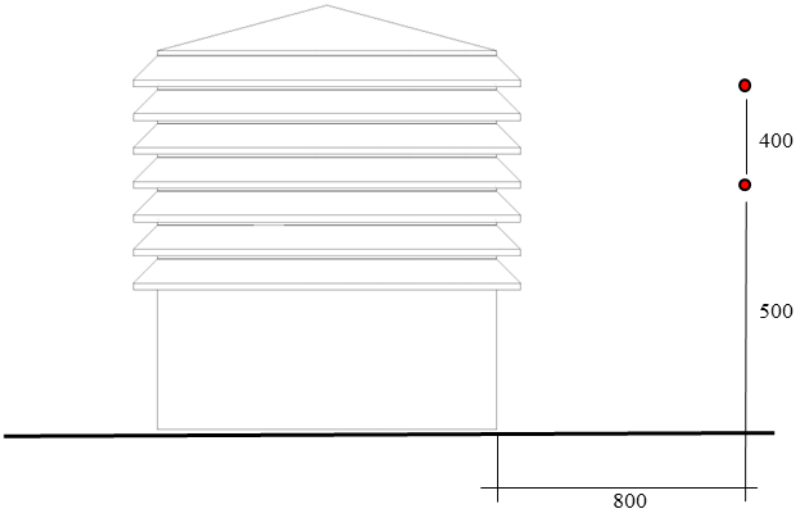

Figure 4-12 - Air temperature sensors upwind of wind tower

4.3.4 Boundary Conditions

Testing was initially conducted with the heating coils deactivated to measure the volumetric flow rate of air through the wind tower inlet into the test room. Four inlet velocities of 1.33, 2.02, 4.17, and 5.96 m/s were tested, and the corresponding velocities at points A – F recorded. For a flat roofed building, Peren et al (2015) indicated that the velocity onto the wind tower could be between 20 – 60% of the free wind speed due to the wind tower being located within the boundary layer that occurs at the leading edge of the building. This was however only conducted at a single inlet velocity and the effects would vary with differing free wind speed.

Subsequently the heating coils were turned on and the tests listed below in Table 4-1 were conducted, recording the temperature at the indicated points throughout the wind tunnel test section.

Table 4-1 – Boundary conditions applied during wind tunnel temperature testing.

Test #	Inlet temperature (°C)	Outlet temperature (°C)	Inlet velocity (m/s)	Duration of test at steady state (Hours)
1	5	24	2	1
2	5	27	2	1
3	5	30	2	1
4	5	24	4	1
5	5	27	4	1
6	5	30	4	1
7	10	24	2	1
8	10	27	2	1
9	10	30	2	1
10	10	24	4	1
11	10	27	4	1
12	10	30	4	1

4.3.5 Limitations

Owing to the scale of the system being tested, the experiment is constrained in several manners. Firstly, only the wind tower was exposed to the flow of the wind tunnel test section. As was discussed in Section 2.3.3.2, the leading edge of the building has been shown to affect the flow profile onto the wind tower inlet, and when included in

the boundary layer results in a decrease in air velocity through the ventilation system due to flow separation. Consequently, for the inlet speeds tested it may be anticipated that under real-world conditions the volumetric flow rate into the room may be lower than is reported in the results, but this is also dependent upon a variety of factors including the surrounding buildings and local topography.

Secondly, the use of supply plenums to mix hot air within the test room and increase exhaust temperature may artificially increase the velocity of the air through the wind tower outlets. Increased velocity serves to reduce the time available for heat transfer between the air and the surface of the heat pipes thereby reducing the amount of heat transferred to the THPs at the evaporator section. As producing the same outlet temperatures without the use of the supply plenums was not feasible, the impact of the increased velocity within the test room could not be quantified.

Finally, as several fans are used in tandem and there are no flow straighteners present in the wind tunnel the turbulence intensity and velocity distribution of the flow profile is unknown.

4.4 Numerical Model

The following sections detail the development of the numerical model replicating the wind tunnel test following the procedures as were described in Chapter 3.

4.4.1 Geometry

The three-dimensional CFD geometry was designed to replicate the wind tunnel test, simplifying where possible to reduce the computational demand of the subsequent simulations. A wind tower was created in Autodesk Inventor, modelled from the commercial wind tower design described in Section 4.3.

Thirty-five heat pipes were modelled as solid bodies through the base of the wind tower in two staggered rows with an external diameter of 16 mm, and transversal and longitudinal pitches of 50 and 35 mm respectively (Figure 4-13). Further wind tower models were created featuring 1 and 3 rows of pipes (18 and 52 pipes respectively) for simulation once the initial model has been validated to determine the impact of the number of pipe layers on the volumetric flow rate.

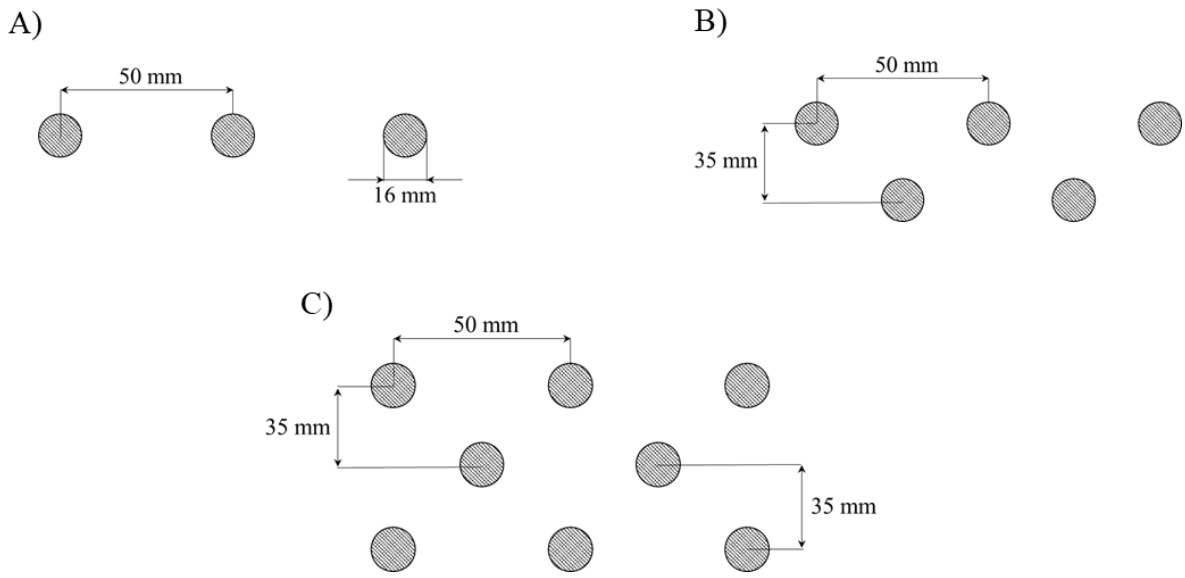

Figure 4-13 - Heat pipe array dimensions for 1, 2, and 3 rows of pipes

The combined wind tower and heat pipe CAD model were imported into Spaceclaim, a CAD program within the ANSYS workbench. Here the fluid volumes within the boundaries of the test room and wind tunnel test section were extracted to create two individual fluid regions coupled via a boundary through the base of the wind tower (Figure 4-14). The fluid body representing the wind tunnel test section measured 10.5 x 4 x 1.4 m while the volume extracted from the inside of the test room measured 3.5 x 2.3 x 2.1 m. The length of the downwind portion of the wind tunnel test fluid body was increased slightly beyond the experimental length to help remove issues with

reverse flow at the pressure outlet, however, is still shorter than the length of the environmental chamber through which the air is drawn and discharged.

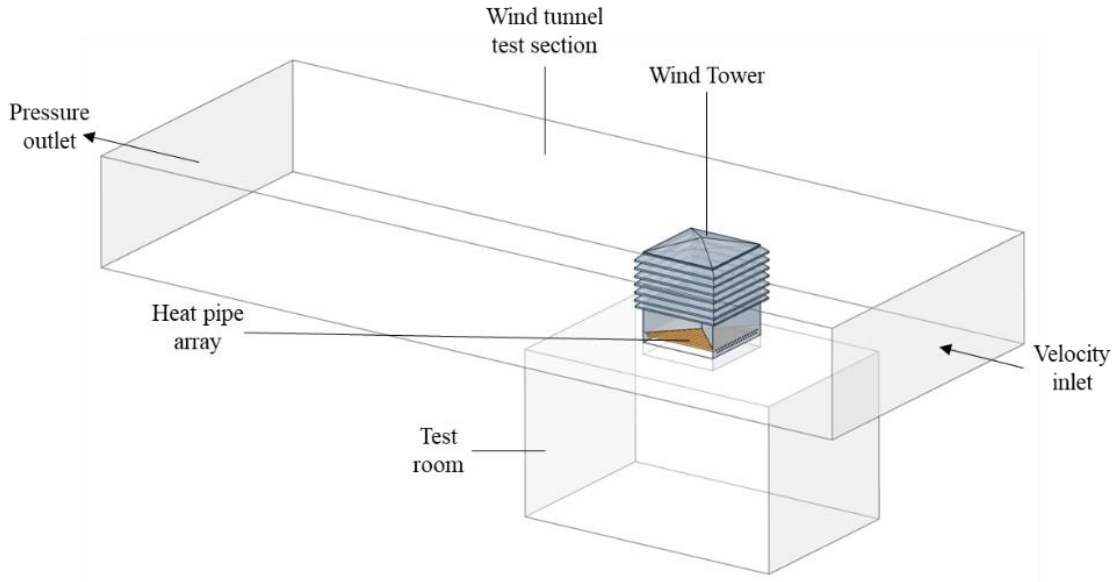

Figure 4-14 - CFD model geometry

To simplify the domain only the area directly subjected to the flow induced by the fans is modelled, ignoring the remaining volume of air around the test room that is constrained by the walls erected within the environmental chamber. As is seen in the resulting velocity contours in Section 5.5.1 the flow of air over the roof of the wind tower is restricted, however the prediction of the flow rate through the wind tower is consistent with the experimental results. As the computational model is at a 1:1 scale with the wind tunnel test, geometric and dynamic similarity was achieved and therefore no scaling of inlet velocity or temperature was required.

4.4.2 Mesh Generation

The CAD geometry had to be discretised prior to simulation, splitting the bodies into many smaller volumes that constitute the mesh. The automatic meshing algorithm will generate a mesh for the domain but often defaults to using tetrahedral mesh elements with little refinement and so providing the program with additional information through

size functions and mesh cell type helped to refine the mesh in areas of interest. Although tetrahedral elements are better suited to modelling complex geometries, where possible it is preferable to use hexahedral elements as unstructured meshes typically require 4 – 10 times the number of cells to achieve the same level of accuracy (Zubair et al 2013).

Given the contrast in complexity between the bodies of the wind tower and wind tunnel test section, a hybrid mesh of hexahedral-tetrahedral elements was selected. The wind tunnel test section and test room were first divided into several smaller bodies to allow for greater control in the element type and size throughout the computational domain while ensuring a consistent boundary between tetrahedral and hexahedral elements (Figure 4-15).

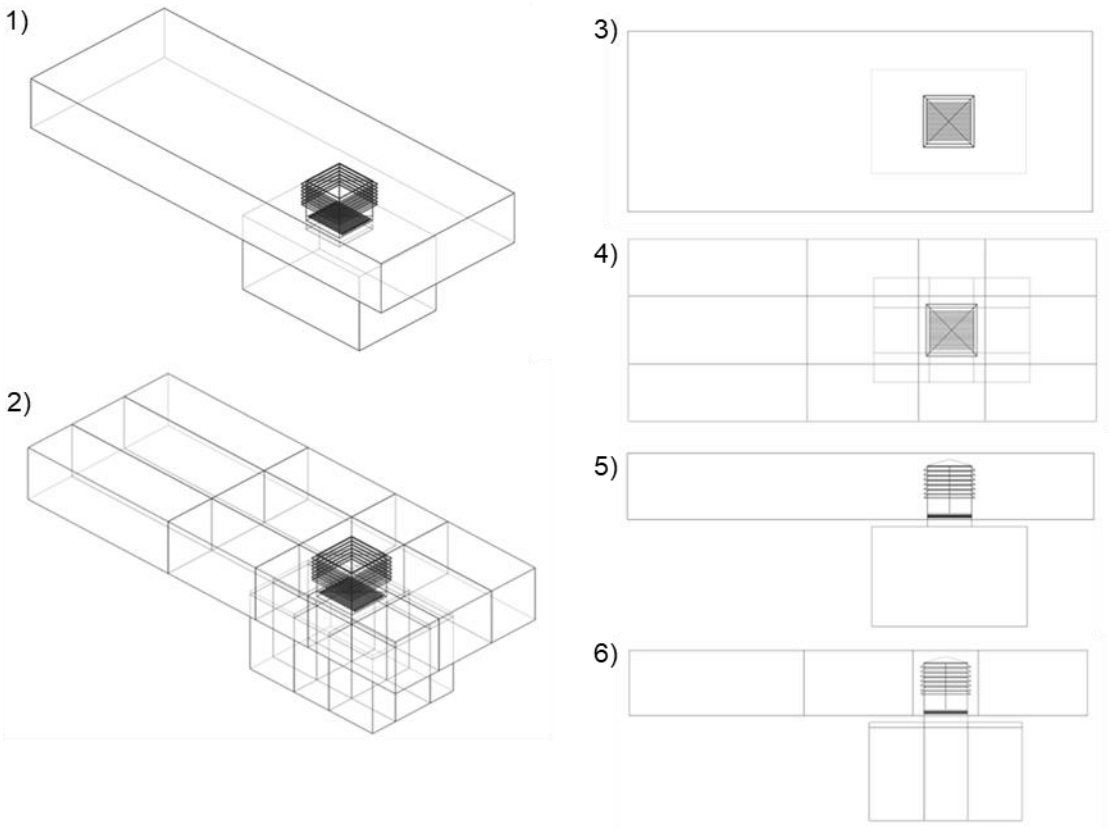

Figure 4-15 - CAD geometry before and after division of bodies for meshing. 1, 3, and 5 are pre-division, and 2, 4, and 6 are after division of the bodies

For the wind tower and immediate surrounding fluid body an unstructured tetrahedral mesh was used with size functions applied to the wind tower body, louvres, and x-frame faces to help resolve the flow in these regions. Away from the wind tower a structured mesh of hexahedral elements was developed. Size functions dictated the number of divisions along each edge of the bodies comprising the test section and test room with bias ratios used to increase the size of elements away from the wind tower in the streamwise direction as the resolution became less critical (Figure 4-16).

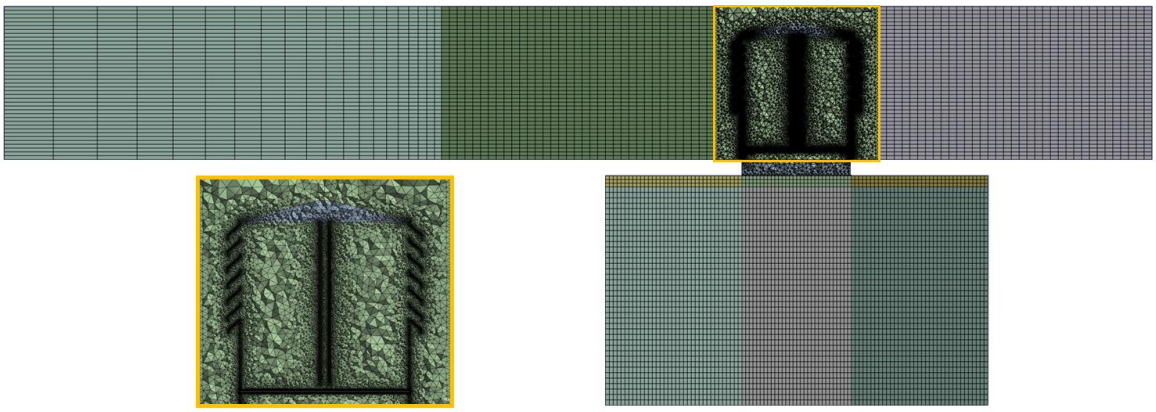

Figure 4-16 - Hybrid mesh of hexahedral and tetrahedral elements displayed over a plane through the centre of the model geometry

The heat pipes were modelled as solid bodies using the multizone method to decompose the volume into hexahedral elements. Inflation layers were applied to the faces of the louvres and the heat pipes to ensure the flow in these near wall regions is accurately captured. Inflation layers expand the two-dimensional faces of the surface into layers of three-dimensional prisms that progressively increase in thickness away from the wall (Rigas and Sklavounos, 2005). The first layer thickness at the wall of the heat pipes and louvres was 1 mm and 5 mm respectively with a growth rate of 1.2 applied for the thickness of the subsequent layers. Applying 5 total

inflation layers to each surface, the local cell size increased away from the wall, again using a growth rate of 1.2 to ensure a smooth transition.

The distance of the cell centroid from the wall determines the y^+ value and hence the ability of the wall functions to accurately calculate the flow properties in these regions. For the k-epsilon turbulence model with standard wall functions it is recommended to have a wall y^+ value between 30 and 300 to place the cell centroid in the log law region of the boundary layer. Evaluating the wall y^+ at the surface of the heat pipes, the y^+ was found to fall approximately between 0.13 and 22, with a higher y^+ in areas with higher velocities (Figure 4-17). Attempts to increase the y^+ through coarsening the mesh resulted in poor quality cells, whereas using alternative wall functions that are designed to work at lower y^+ values such as enhanced wall treatment produced results that were inconsistent with the experimental values. Cellek (2020) showed that the standard wall functions produced reasonable results when the y^+ was as low as 0.1 and therefore further simulations were conducted with the mesh without further refinement.

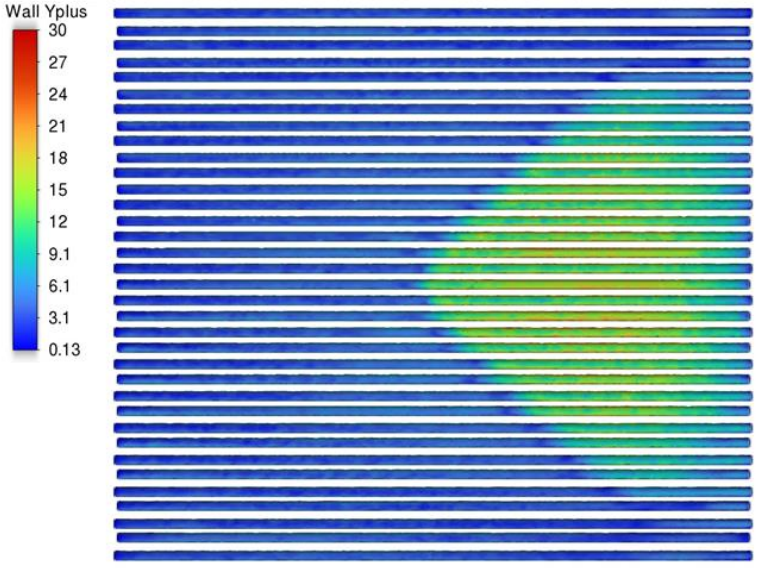

Figure 4-17 - y^+ at the heat pipe wall

4.4.2.1 Mesh Independence

A mesh independence study was undertaken to calculate the fine GCI according to the process established in Chapter 3 estimating the error throughout the domain as a result of discretisation relative to the actual solution at zero cell size.

Adaptive meshing techniques such as the h (mesh refinement) and p (mesh enrichment) methods are used to selectively refine mesh regions that require a high level of accuracy, where the h-method increases the number of cells in regions with poor quality and the p-method increases the polynomial order of the cells within the existing mesh (Figure 4-18)(Chung, 2002). In this case the h-method was applied using a consistent approach to increasing mesh cell density to create three meshes for the coarse, medium, and fine meshes, with 12,513,490, 22,487,165, and 39,029,483 cells respectively.

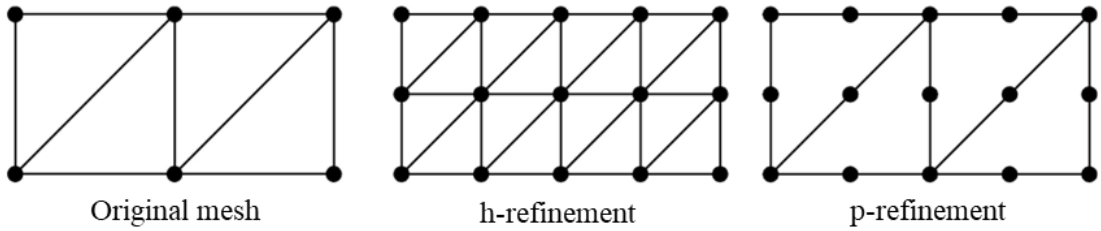

Figure 4-18 - h and p grid refinement

By reducing the cell size and number of divisions along edges dictated by the size functions within the meshing program the mesh is progressively refined. The cell density of the hexahedral mesh bodies was only marginally increased to maintain a smooth transition from the tetrahedral cells of the region around the wind tower as they have little bearing on the results throughout the domain (Figure 4-19).

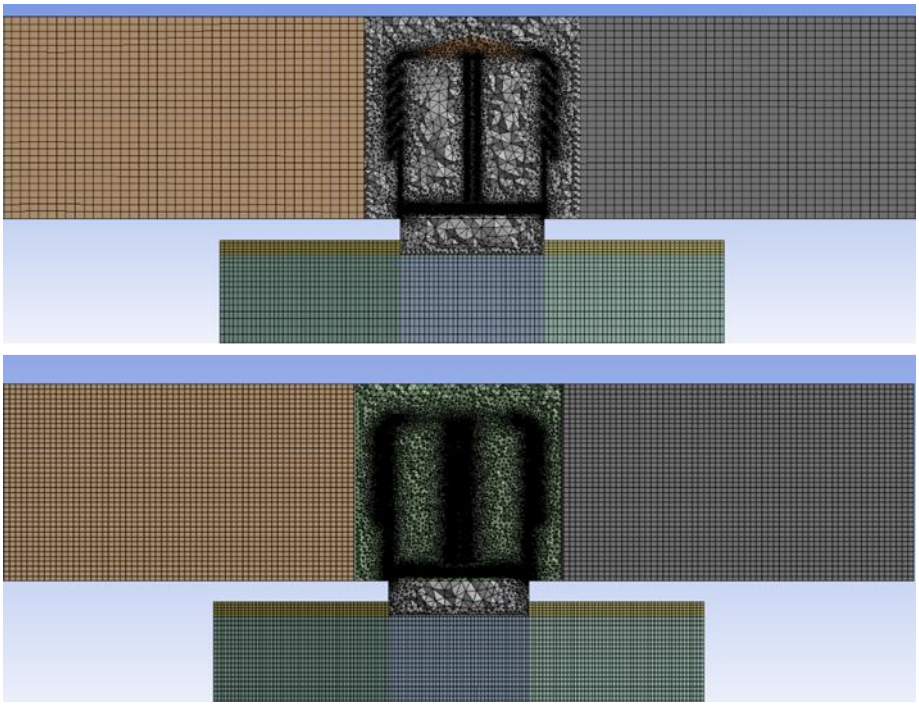

Figure 4-19 - Cross section of increasing mesh cell density from medium (Top) to fine (Bottom) mesh resolution

Velocity was selected as the most suitable parameter for evaluation and was measured in each grid at three points 0.15, 1.05, and 1.95 m below the base of the wind tower inlet quadrant, taking the base of the wind tower as 0 m (Figure 4-20).

Figure 4-20 - Mesh independence measurement points

Table 4-2 contains the results of the mesh independence study. The refinement ratios, r_{32} and r_{21} between the coarse and medium and medium and fine grids fall below the recommended value of 1.3 (Roache, 1997), however are within the range established

by studies that use similar processes for establishing mesh independence (Volk, Ghia and Stoltz, 2017; Pakari and Ghani, 2019; Carreto-Hernandez *et al.*, 2023).

Table 4-2 – Results of the mesh independence study for the wind tunnel test numerical model

	At height -0.15 m below inlet	At height -1.05 m below inlet	At height -1.95 m below inlet
N3	12,513,490	12,513,490	12,513,490
N2	22,487,165	22,487,165	22,487,165
N1	39,029,483	39,029,483	39,029,483
r_{21}	1.22	1.22	1.22
r_{32}	1.20	1.20	1.20
ϕ_3	1.38	1.12	0.34
ϕ_2	1.31	1.02	0.27
ϕ_1	1.27	0.97	0.26
pk	6.28	5.30	9.65
$\phi_{21,ext}$	1.23	0.93	0.25
$\phi_{21,ext}$ error	2.96%	4.21%	2.37%
e_{21}	2.98%	4.19%	2.41%
GCI_{coarse}	10.18%	18.63%	52.25%
GCI_{fine}	1.77%	2.52%	3.30%

The convergence conditions of a grid triplet can be classified as follows:

Monotonic convergence: 0 < R < 1

Oscillatory convergence: -1 < R < 0

Monotonic divergence: R >1

Oscillatory divergence: R < -1

Where the convergence ratio, R, is calculated by Equation 4-2 (Eça and Hoekstra, 2006):

$$R = \frac{\phi_2 - \phi_1}{\phi_3 - \phi_2}$$

Equation 4-2

Where $\phi_{3,2,1}$ are the coarse, medium, and fine grid solutions respectively. From the recorded values at each point in the three grids the R value is found to fall between 0.14 and 0.57 indicating monotonic convergence with increasing mesh resolution.

The extrapolated values ($\phi_{21,ext}$) at zero cell size were calculated from the values in the three developed grids, presenting errors ($\phi_{21,ext}error$) ranging from 2.4 to 4.2%

between the fine grid and extrapolated values. The relative error between the medium and fine grids (e_{21}) at each point also ranges between approximately 2.4 to 4.2%. The observed local order of accuracy p_k ranged between 3.9 and 9.8, with an average of 6.3. The average observed order of accuracy was used to calculate the GCI values. Figure 4-21 below illustrates the results of the mesh independence study, with the coarse and fine GCI indicated through the error bars for the medium and fine meshes respectively. Although the difference in the measured values between the medium and fine grids is relatively small, the coarse GCI for the medium mesh is as high as 52.3% indicating a low degree of confidence in the result and therefore the fine mesh is chosen for all further simulations.

The numerical uncertainty in the fine mesh represented by the fine Grid Convergence Index (GCI_{fine}) ranged between 1.8% and 3.3%, corresponding to a range of ± 0.024 m/s at the point 1.05 m below the wind tower inlet for the fine mesh.

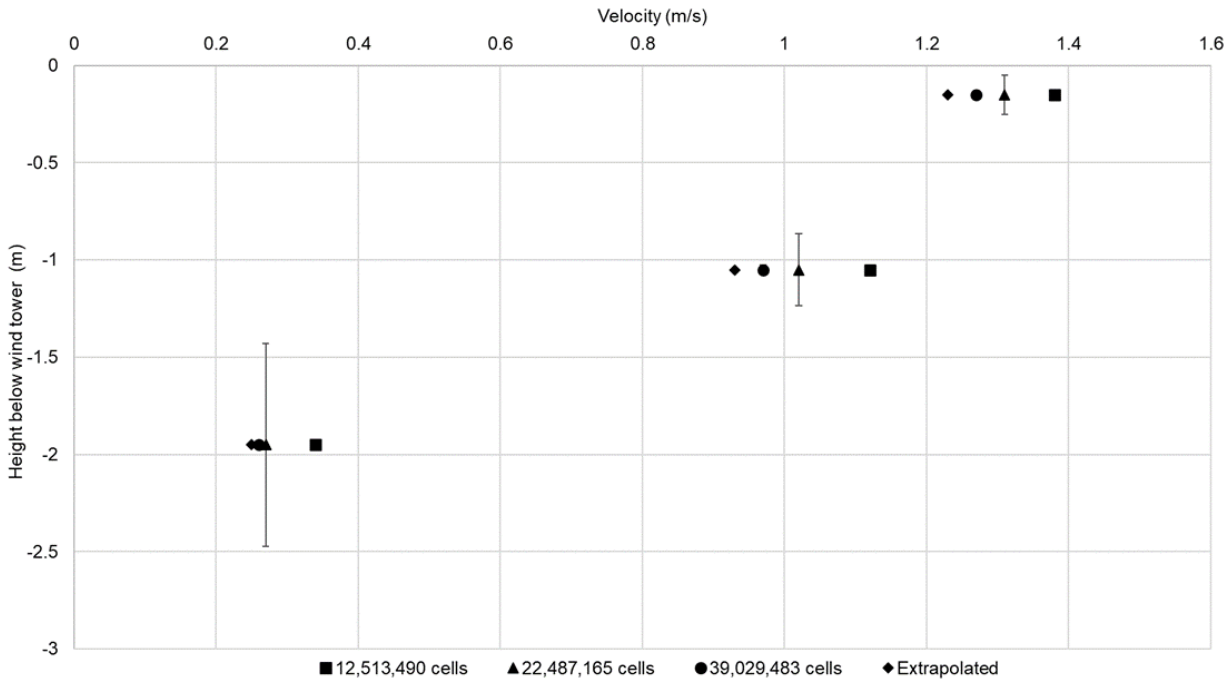

Figure 4-21 - Mesh independence values and errors

4.4.2.2 Mesh Quality

Upon selection of the fine mesh, the quality was evaluated according to the orthogonal quality, skewness, and aspect ratio with the average, maximum, and minimum values recorded (Table 4-3).

Table 4-3 - Mesh quality assessment through chosen parameters for wind tunnel test numerical model

Parameter	Statistics
Aspect ratio	(max, avg) = (32.4, 2.96)
Orthogonal quality	(min, avg) = (0.03, 0.69)
Skewness	(max, avg) = (0.97, 0.31)

Cells with low orthogonal quality were created within the walls of the wind tower due to the thin wall thickness and sharp edges at the corners of the louvres. The minimum allowable orthogonal quality for simulation is 0.01 and therefore the mesh is considered sufficient (Ansys, 2020).

4.4.3 Heat Pipe Modelling Approach

Using flow properties derived from the experimental velocity and temperature data, the overall heat transfer coefficient of the heat pipe was calculated according to the process laid out by Mroue et al (2015) and Ramos et al (2016b) in Section 2.4.4.1, modelling each heat pipe as a solid conducting body. In early simulations however, the pre-heating of the incoming air achieved through this was drastically lower than the results recorded during the wind tunnel test. This is potentially due to the relatively low temperature difference between the evaporator and condenser sections of the heat pipes when compared with other papers that have employed this method, resulting in a small temperature gradient between the evaporator and condenser

sections of the pipe and an inability of the heat pipe to transfer heat along its length fast enough to replace the heat removed by the fresh air.

As a result, the method as described by Calautit et al (2016) was employed, assuming a constant surface temperature along the length of the heat pipe and applying this as a boundary condition within the simulation to the heat pipe geometry. The average surface temperature of the heat pipe was assumed to be approximately equal to the average temperature of the heat source, which in this case is the warm outgoing air passing through the wind tower outlets. Although applying surface temperature as a boundary condition is an oversimplification of the heat transfer process along the length of the heat pipes, as is shown in section 4.5.2 the error between the CFD and experimental results indicate that this method can provide a reasonable estimation of the pre-heating of the fresh air achieved through heat recovery. As a drawback this method limits the useful information available through the numerical model to the change in temperature through the wind tower inlet as the change in air temperature over the pipes through the wind tower outlets will not be representative of real conditions.

4.4.4 Boundary Conditions

Boundary conditions are used to define the thermal and fluid properties throughout the domain. Boundaries within the model are defined as walls, internal face boundaries, and fluid inlets and outlets (Ansys, 2020).

Initial boundary conditions equivalent to those of the wind tunnel test were used to verify the accuracy of the numerical model in predicting velocity and temperature changes through the wind tower under steady state conditions. Inlet velocities of 1.33, 2.02, 4.17, and 5.96 m/s were simulated using a uniform inlet velocity profile. Inlet

temperatures provided through the environmental chamber of 5 and 10 °C were then applied at an inlet velocity of 2m/s, with heat pipe surface temperatures of 24, 27, and 30 °C, equal to the temperature of the exhaust air leaving the room. These air temperatures are higher than any exhaust temperatures from an occupied building in the UK but were used so that there was a sufficient temperature difference between the inlet and outlet. Given the linear relationship between the amount of pre-heating of the fresh air and the temperature difference between the inlet and exhaust channels, the results can be extrapolated to lower temperature differences if required.

Following the validation, the inlet velocity was varied between 1 - 5 m/s for wind tower models featuring 1 - 3 rows of heat pipes, investigating the impact of an increasing number of heat pipes on inlet mass flow rate. To evaluate the potential for pre-heating of fresh air constant surface temperatures of 24, 27, and 30 °C were applied to the walls of the heat pipes, equal to the outlet air temperatures reached during the wind tunnel test. Air inlet temperatures of 5 and 10 °C were applied.

The default Semi-Implicit Method for Pressure Linked Equations (SIMPLE) algorithm for velocity-pressure coupling with the k-epsilon turbulence model and standard wall functions. The boundary conditions are summarised below in Table 4-4:

Table 4-4 – Summary of boundary conditions for wind tunnel test numerical model

Discretisation scheme	Second order upwind
Algorithm	SIMPLE
Time Scheme	Steady state
Turbulence Model	k-epsilon
Wall functions	Standard
Inlet velocity (m/s)	1 - 6
Inlet Temperature (°C)	5 - 10
Outlet Temperature (°C)	24 - 30

4.5 Numerical Model Validation

Comparisons between the results of the wind tunnel test and CFD simulations were used to validate the numerical model, taking the velocity and temperature measurements below the heat pipes through the wind tower inlet. To deem the model validated the percentage error between the two datasets must fall into an acceptable range.

4.5.1 Velocity

Once the results at the monitor points throughout the simulation were no longer changing the velocity was measured at the six points below the heat pipes and the values recorded. Table 4-5 compares the results from the experiment and CFD model for four inlet velocities.

Table 4-5 - Experimental vs CFD velocity results used to validate the numerical model

Inlet Velocity	1.33 m/s			2.02 m/s		
Point	Experiment (m/s)	CFD (m/s)	% Error	Experiment (m/s)	CFD (m/s)	% Error
A	0.90	0.94	4.8	1.20	1.50	25.4
B	0.80	0.88	10.3	1.00	1.32	32.4
C	0.70	0.77	10.6	1.20	1.20	0.0
D	0.50	0.43	-13.8	0.70	0.65	-7.3
E	0.80	0.72	-9.5	1.10	1.12	1.8
F	0.50	0.41	-17.1	0.60	0.63	5.8
Normalised average error			11.0	Normalised average error		12.1

Inlet Velocity	4.17 m/s			5.96 m/s		
Point	Experiment (m/s)	CFD (m/s)	% Error	Experiment (m/s)	CFD (m/s)	% Error
A	2.60	3.19	22.8	3.90	4.59	17.7
B	1.80	2.79	55.2	3.00	4.02	33.9
C	2.20	2.55	16.0	3.40	3.64	7.1
D	0.90	1.35	49.5	1.40	1.95	39.3
E	2.00	2.36	18.2	1.70	3.40	100.0
F	0.80	1.32	65.4	1.60	1.90	18.8
Normalised average error			37.8	Normalised average error		36.1

The largest velocity is seen at point A and the lowest at points D and F consistently across both the experimental and numerical results. The lower velocities at points D and F result from areas of recirculation above the heat pipes. These are created as the air flows over the louvres into the inlet quadrant and makes contact with the x-frame towards the corners of the wind tower. The fast-moving air is naturally guided towards the centre of the wind tower by the angle of the x-frame, leaving pockets of slow-moving air in which recirculation occurs. This results in a slower velocity over the heat pipes in these regions, increasing short circuiting and lowering the recorded velocities at points D and F. Conversely, through the centre of the inlet in line with points A and E there are little disruptions to the flow and therefore the velocity above and below the heat pipes is much higher. The average error across the measurement points for each inlet velocity varies from 11.0 to 37.9%, however as both sets of results follow the same general trend the accuracy is considered sufficient to validate the numerical model as has been established in past works covering wind tunnel testing of passive ventilation (Chen and Srebric, 2002; Hughes and Mak, 2011; Connor *et al.*, 2019).

Comparing the experimental and numerical volumetric flow rates through the wind tower inlet (Table 4-6), there is a consistent over-estimation of the amount of fresh air delivered to the room. Overestimating the volumetric flow rate through the inlet is likely to lead to an underestimation of heat transfer to the fresh air, although as the velocities are low this will not be significant. The average error for the volumetric flow rates differs from the errors at the individual points due to the combination of over and underestimation of the individual velocities, as well as the impact of multiplying individual velocities by the area of each section that point was selected to represent to find the volumetric flow rate.

Table 4-6 - Comparison of the experimental and numerical mass flow rate through wind tower inlet

	Volumetric Flow Rate (m^3/s)		
Inlet Velocity (m/s)	Experimental	CFD	% Error
1.33	0.17	0.17	2.1
2.02	0.21	0.27	21.6
4.17	0.41	0.57	27.5
5.96	0.60	0.81	26.2

By dividing the velocity at each point by the inlet velocity (U_{ref}), the dimensionless velocity can be calculated. U/Uref represents the ratio between the inlet velocity and the velocity measured at each of the six points below the heat pipes. Calculating the dimensionless velocity enables an easier comparison between differing inlet velocities to determine if the behaviour of the airflow through the wind tower is consistent as inlet velocity increases. When comparing the dimensionless velocities at each point in relation to the inlet velocity, it is apparent that the behaviour of the velocity calculated through the CFD simulation is very predictable in comparison to the experimental results (Figure 4-22).

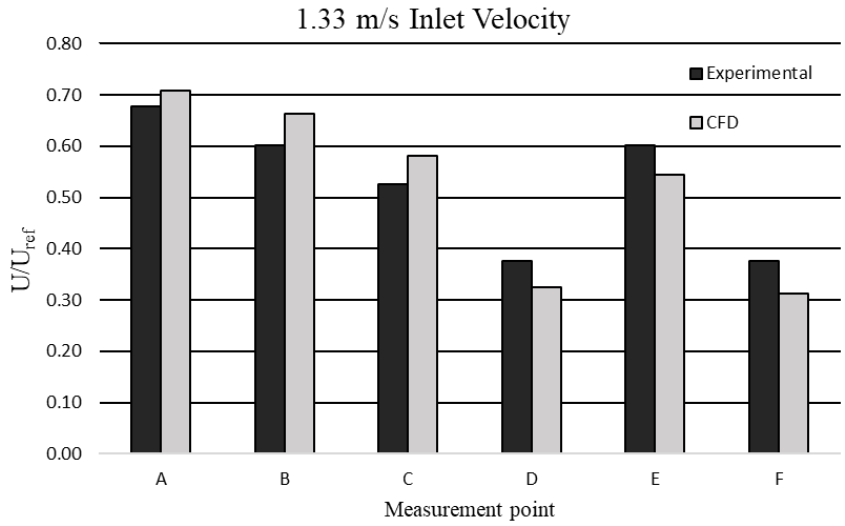
1.33 m/s Inlet Velocity
0.80
0.70
0.60
0.50
0.40
0.30
0.20
0.10
0.00
U/U_ref
Experimental
CFD
A
B
C
D
E
F
Measurement point

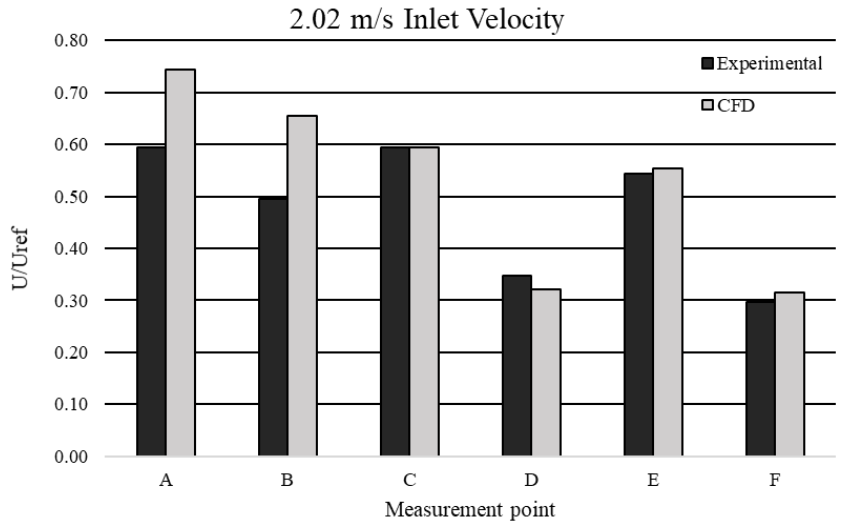
2.02 m/s Inlet Velocity
0.80
0.70
0.60
0.50
0.40
0.30
0.20
0.10
0.00
U/Uref
Experimental
CFD
A
B
C
D
E
F
Measurement point

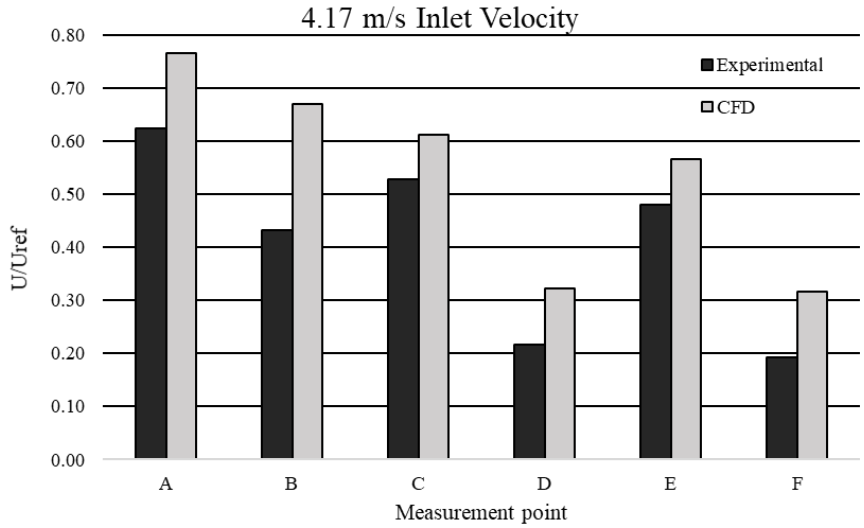
4.17 m/s Inlet Velocity
0.80
0.70
0.60
0.50
0.40
0.30
0.20
0.10
0.00
U/Uref
Experimental
CFD
A
B
C
D
E
F
Measurement point

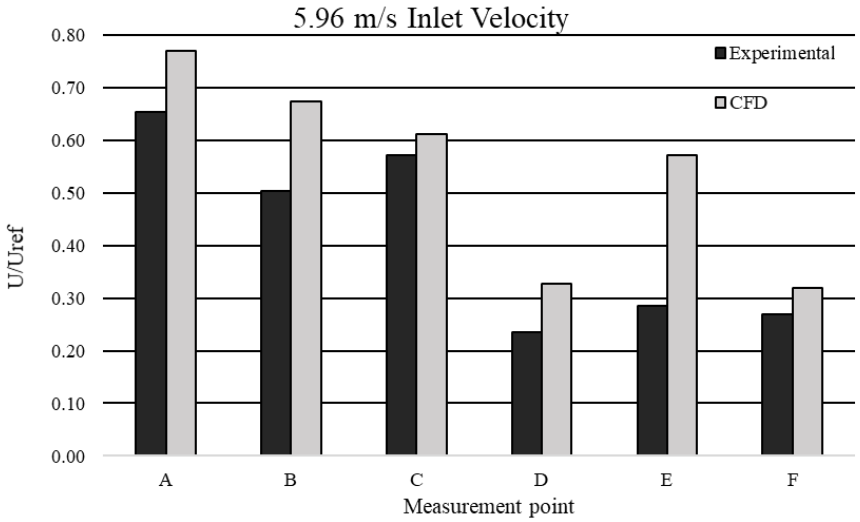

Figure 4-22 - U/Uref at velocity measurement points below heat pipes for experimental and CFD results

Observing where the largest differences are seen in the results at points D and F, these points are in the vicinity of areas recirculation for which the limitations of the k-epsilon wall function equation in modelling have been acknowledged (Cheng *et al.*, 2003; O'Connor et al., 2014). Looking at the measured experimental velocity at point E with an inlet velocity of 5.96 m/s, the value recorded is far below the expected value provided it was consistent with the other inlet velocities, and therefore the error is much higher. Considering the measured velocities at each of the other points are consistent with previous trends, it is deemed that this likely resulted from errors made during the measuring process. The U/U_{ref} value at each point remains stable as the inlet velocity increases for the CFD results, whilst the variation in the experimental results is much greater. This highlights the predictable nature of the flow through the CFD model, whereas the wind tunnel flow is much more variable resulting in differences in the recorded values.

4.5.2 Temperature

Figure 4-23 compares the pre-heating of fresh air during the wind tunnel test and CFD simulation against the difference in temperature between the fresh air and heat pipes.

When accounting for the measurement error and the error introduced through the fine GCI, the average relative error between the two datasets was a minimum of 4.7% and a maximum of 10.3%. The maximum difference between the experimental results was measured at a temperature difference of 22 °C, with a maximum error of 13.8%, equivalent to 0.26 °C. When plotting a line of best fit for the experimental results it is seen that the CFD results match up almost exactly along this trend. The error bars indicate the uncertainty due to discretisation in the CFD results as calculated by the fine GCI which was approximately 1.8% in the region closest to the heat pipes.

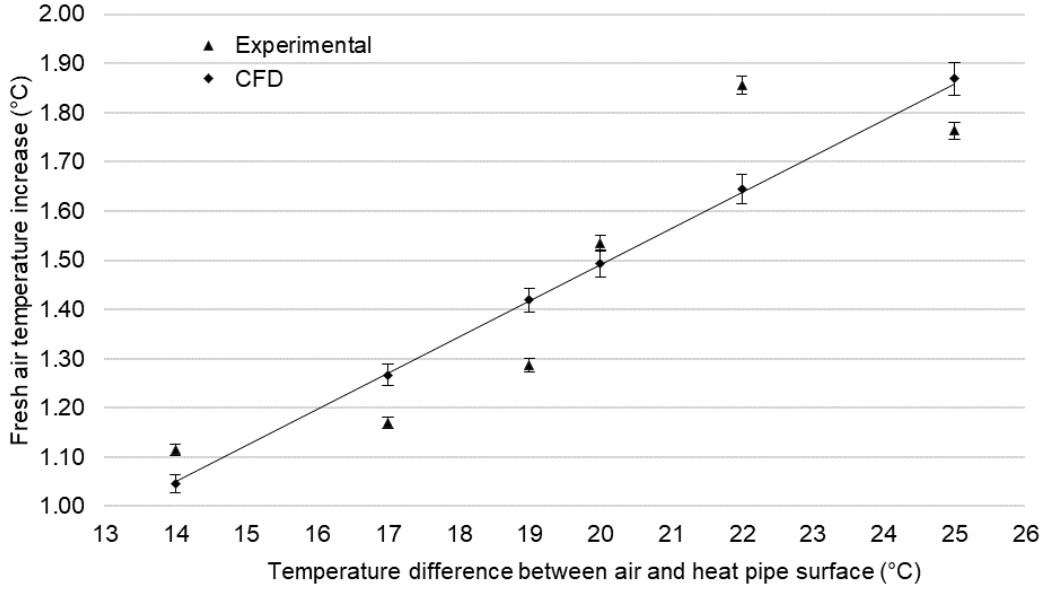

Figure 4-23 - Experimental vs CFD results for pre-heating of fresh air

4.6 Results and Discussions

Following the validation of the numerical model further simulations were conducted under steady state conditions, varying the inlet velocity, pipe surface temperature, and number of heat pipes.

4.6.1 Ventilation Rates

Figure 4-24 shows the effect of increasing the number of rows of heat pipes on the inlet mass flow rate through the wind tower.

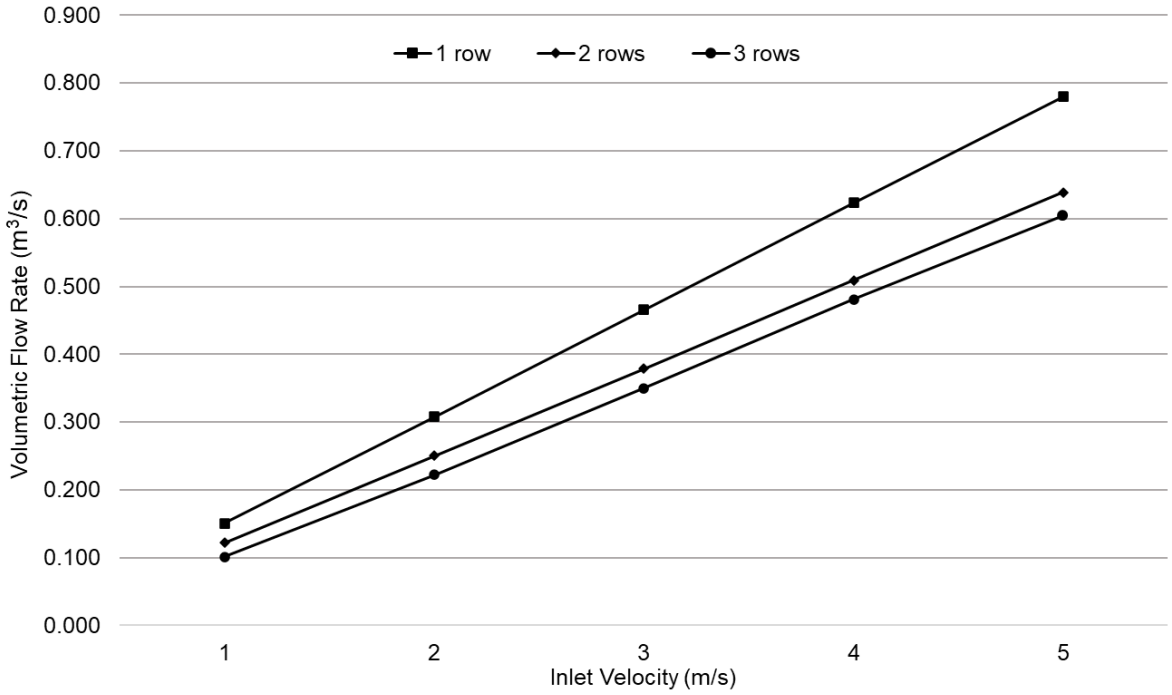

Figure 4-24 - Change in the inlet volumetric flow rate with increasing inlet velocity and number of heat pipes

An increasing number of heat pipes was found to be indirectly proportional to the volumetric flow rate, with an average decrease of 18.6% from 1 to 2 rows and 9.4% from 2 to 3. The reduced impact of an additional row of pipes between 2 and 3 rows is thought to be due to the staggered arrangement. When increasing the number of rows from 1 to 2, the blockage of the inlet channel increases proportionally by a much greater amount than from 2 to 3, considering that rows 1 and 3 are in line with one another. This insinuates that additional rows of heat pipes could be installed without a significant detrimental effect to the inlet mass flow rate. Slower velocities over the heat pipes also allow more time for heat transfer to take place from the surface of the heat pipe to the incoming air. A single wind tower with 3 rows of heat pipes at an average

inlet velocity of 4 m/s provides sufficient ventilation to achieve 6 ACH in a space with an approximate volume of 290 m^3.

Figure 4-25 shows the contours of velocity through the wind tower model. Here the increase in the velocity of the air due to the narrowing of the channel over the roof of the wind tower is apparent. As a result of the blockage of the channel the pressure at the windward face of the wind tower is increased, while the pressure at the leeward face of the wind tower is decreased by the fast-flowing air over the roof of the wind tower. This generates an increased suction force from the regions of high to low pressure, artificially increasing the flow rate of air through the wind tower exhaust.

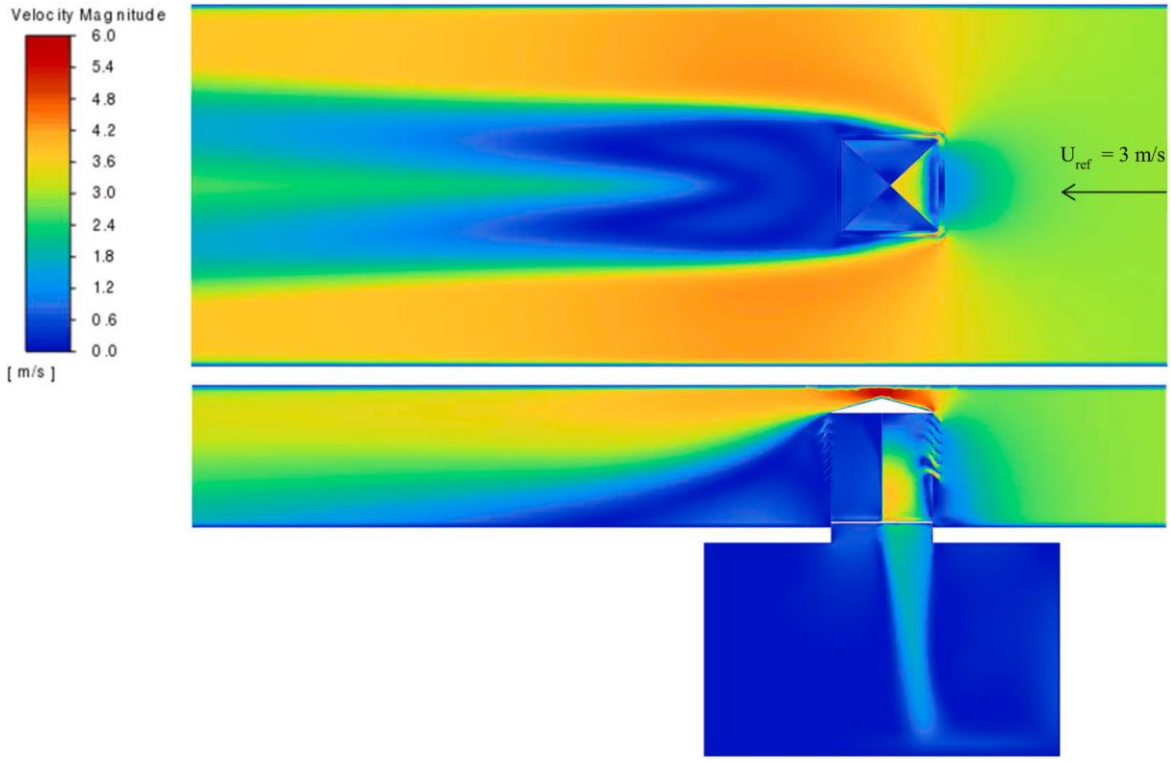

Figure 4-25 - Contours of velocity through the wind tunnel test section and test room with 2 rows of heat pipes

The air moving in through the inlet flows into the room below, hitting the floor and then distributing throughout the room. The use of a diffuser would further increase the distribution of fresh air and prevent a draught directly below the inlet of the wind tower. A small amount of short circuiting is observed between the inlet and the outlets. The

use of automated dampers would allow the flow of air to be cut off in the case that wind speeds or temperatures were outside of a pre-determined acceptable range.

4.6.2 Heat Recovery

Figure 4-26 indicates the average fresh air temperature increase for wind towers with 1 - 3 rows of heat pipes at inlet velocities of 2 and 4 m/s. Again, heat pipe temperatures of 24, 27, and 30 °C and inlet temperatures of 5 and 10 °C were applied, presented as the temperature difference between the two.

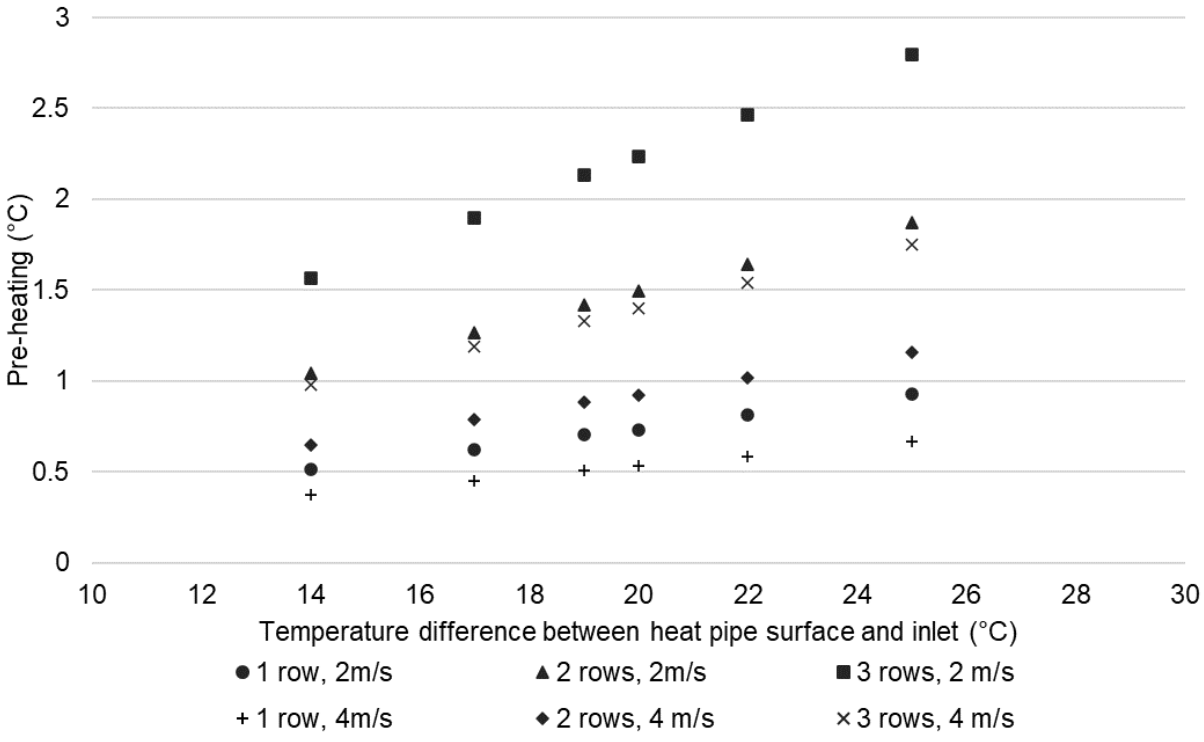

Figure 4-26 - Fresh air temperature increase compared to temperature difference between the fresh air and heat pipes

An increasing number of heat pipes served to increase the pre-heating of fresh air, with a greater impact seen when increasing from one to two rows than from two to three. As with the volumetric flow rate, adding the third layer has less of an impact due to the staggered arrangement of the heat pipes.

Using three pipe layers with a temperature difference of 25 °C between the fresh air and the heat pipes, the incoming air temperature was raised by 2.80 °C and 1.75 °C for inlet velocities of 2 and 4 m/s respectively. Both inlet velocity and the number of heat pipes have a significant impact on the level of pre-heating. Although increasing the number of heat pipes reduces the volumetric flow rate, as the velocity through the inlet is reduced the contact time between the fresh air and the heat pipes is increased, therefore increasing total heat transfer.

A temperature contour of the flow through the wind tower inlet is shown in Figure 4-27 featuring two rows of heat pipes with inlet conditions of 5 °C and 2 m/s. Pre-heating of the fresh air increases towards the outer edges of the heat pipe array where the velocity is lower, however the flow is subject to some short-circuiting between the inlet and outlets due to their proximity at these points.

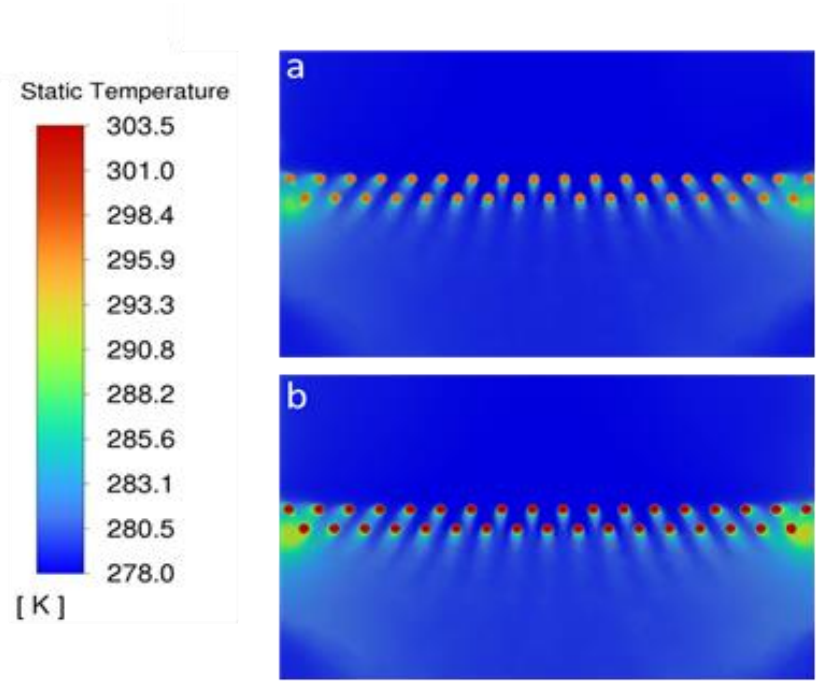

Figure 4-27 - Pre-heating of fresh air when inlet conditions are 2 m/s and 5 °C (278.15 K) and heat pipe temperature is a) 24 °C (297.15 K) and b) 30 °C (303.15 K)

When comparing the performance of the heat recovery system against that of similar studies, it was found to be comparable with a rotary thermal wheel when operating at a similar temperature difference between the inlet and outlet (O'Connor et al., 2016), and marginally below that of a wind tower with vertically arranged heat pipes (Calautit et al., 2016). By orienting the heat pipes vertically there is a larger surface area available for heat transfer, however this design required an intermediary system linking the heat pipes through the inlet and the outlets. In the current case, the addition of fins could be used to increase the surface area available for heat transfer, however, will further limit the flow of air through the wind tower.

In cases such as this where the wind direction results in a single inlet and three outlet quadrants, straight heat pipes are sufficient to transfer heat from the outlets to the inlet. However, under atmospheric boundary conditions different configurations of the heat pipes might be necessary to ensure that heat is effectively transferred from the outlets to the inlets regardless of wind direction (Figure 4-28). By changing the orientation of some of one pipe layer each quadrant is connected to every other quadrant, ensuring that a greater number of the heat pipes are exposed to both hot and cold fluid streams.

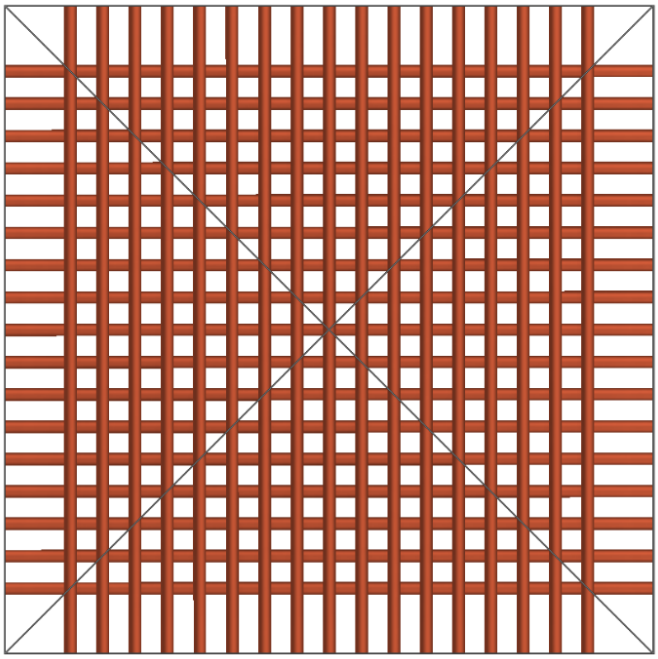

Figure 4-28 – Conceptual criss-crossed heat pipe arrangement

Although the current study did not evaluate the effects of an atmospheric boundary layer inlet condition onto the wind tower, previous investigations featuring similar wind tower designs have found that ventilation performance decreases, largely due to flow separation at the leading edge of the building. Finally, considering that the heat transfer to the air is dependent on the temperature difference between the pipe surface and the air, it could be assumed that for the same temperature difference between the inlet and outlet would result in a similar level of pre-cooling of fresh air during the summer.

4.6.2.1 Heating Energy Demand

The heating energy reduction associated with the pre-heating of fresh air can be estimated by finding the energy required to raise the temperature of the fresh air to that of the internal air temperature and comparing it against the baseline case with no pre-heating:

$$Q_H = \mathrm{V}\rho C_p \Delta T$$

Equation 4-3

Where Q_H is the decrease in energy to raise fresh air to room temperature in kJ/s, V is the volumetric flow rate of the air through the inlet of the wind tower, ρ is the density, C_p is the specific heat capacity, and ΔT is the temperature difference between the air and the proposed internal air temperature post heat pipes.

Figure 4-29 below shows the expected reduction in energy demand in kJ/s when compared against the baseline case of ventilation with no pre-heating. Energy demand is directly proportional to the temperature difference between the internal room temperature and the fresh air temperature below the heat pipes. Owing to the greater volumetric flow rate through the wind tower at higher wind speeds, a greater amount of energy is saved per second despite the lower amount of pre-heating achieved at higher velocities. At a maximum, a reduction of 1.03 kJ/s is achieved using 3 pipe layers at 4 m/s inlet velocity, while at a minimum approximately 0.2 kJ/s is saved using 1 pipe layer at 2 m/s inlet velocity.

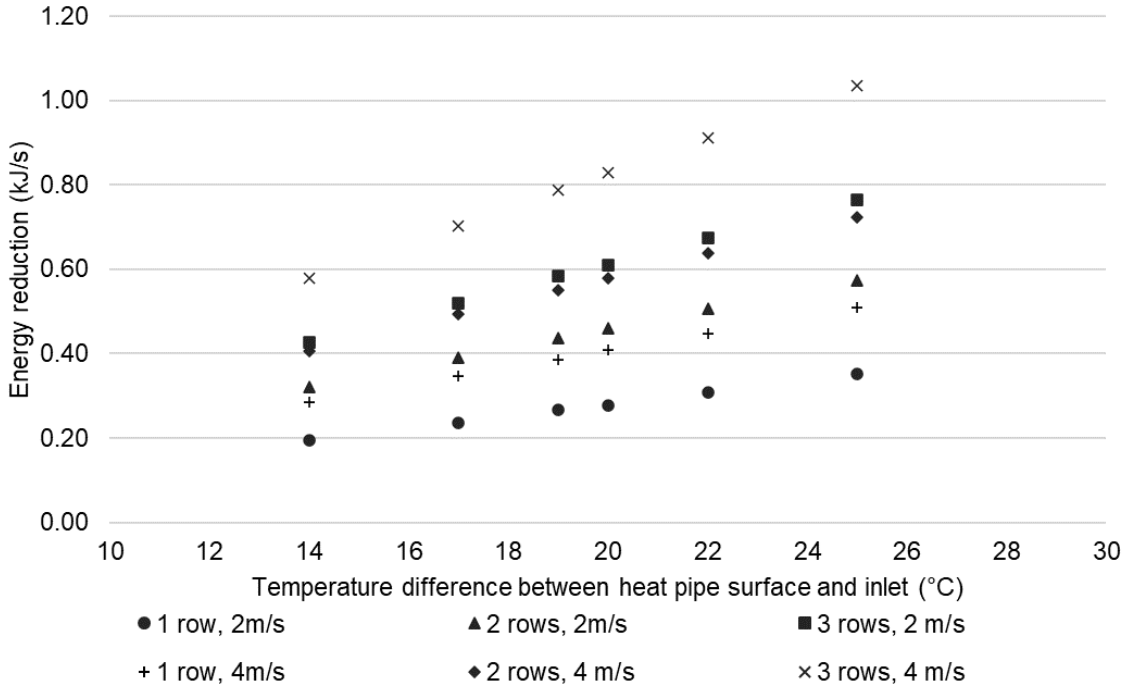

Figure 4-29 - Energy saving in kJ/s due to pre-heating of fresh air

The energy saved per m^3 of air was then calculated using Equation 4-4

$$Q_D = \frac{Q_H}{\mathrm{V}}$$

Equation 4-4

Where Q_D is the energy density in kJ/m^3. Figure 4-30 shows the resulting energy saved per m^3 of fresh air, with the chart now closely resembling the chart for pre-heating of fresh air (Figure 4-26).

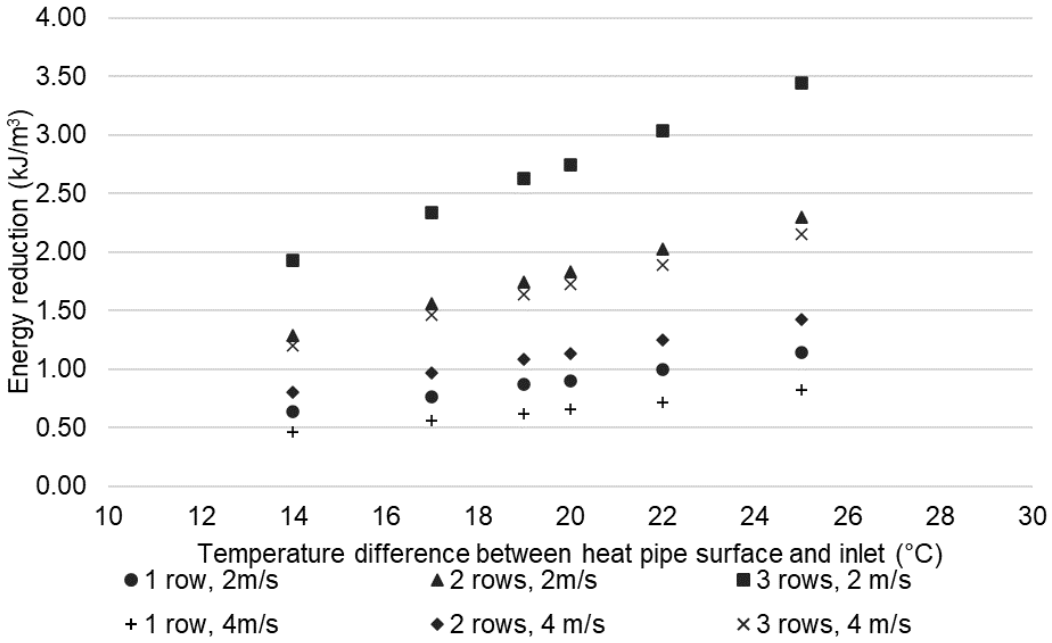

Figure 4-30 - Energy saved per m³ of fresh air

4.6.2.2 Ventilation heat loss

As previously discussed, wind towers are often closed though the winter of colder climates to prevent significant increases in building energy demand. This led rise to the inclusion of heat recovery devices within passive ventilation in efforts to limit the increase in building energy demand by increasing fresh air temperature prior to mixing throughout the room.

In addition to increasing building energy demand through the introduction of cool fresh air, energy demand can also be increased through over-ventilation, whereby the amount of fresh air supplied to the room is greater than is required. This increases the energy required to maintain the room at a comfortable temperature for the occupants as warm air within the room is constantly exhausted to the atmosphere. Equation 4-5 can be used to find the heat loss due to overventilation within a room (Liu *et al.*, 2024)**:**

$$Q = 0.33 \cdot ACH \cdot V_R \cdot (T_s - T_r)$$

Equation 4-5

Where Q is the energy lost in kW due to ventilation, 0.33 is the heat capacity of air per cubic meter, ACH is the number of air changes per hour within the room at the given volumetric flow rate, and T_s and T_r are the supply and room temperatures respectively.

A standard classroom for 20 occupants was used to find the ventilation heat loss, with a floor area of 35 m^2 (reference), and a ceiling height of 2.7 m, providing a total volume of 94.5 m^3. A minimum ventilation rate of 8 l/s per occupant was used to calculate the minimum number of air changes per hour (Equation 4-6):

$$ACH = \frac{3600 \cdot V}{V_R}$$

Equation 4-6

Where V is the volumetric flow rate through the wind tower and V_R is the volume of the classroom. A ventilation rate of 8 l/s per occupant was used to calculate the minimum number of ACH required for the classroom as well as the minimum ventilation heat loss expected at a given temperature difference between the indoors and ambient. This was compared against the ventilation heat loss through the wind tower with and without heat recovery at wind speeds of 2 and 4 m/s (Figure 4-31 and Figure 4-32):

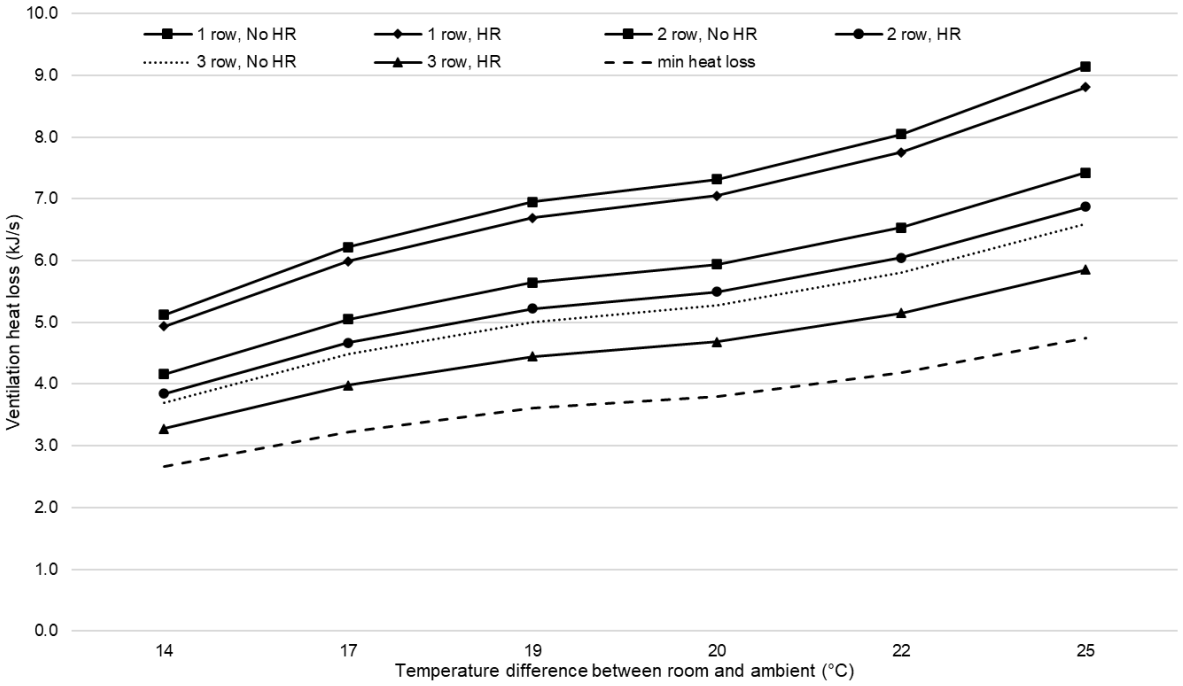

Figure 4-31 - Ventilation heat loss from building at 2 m/s wind speed

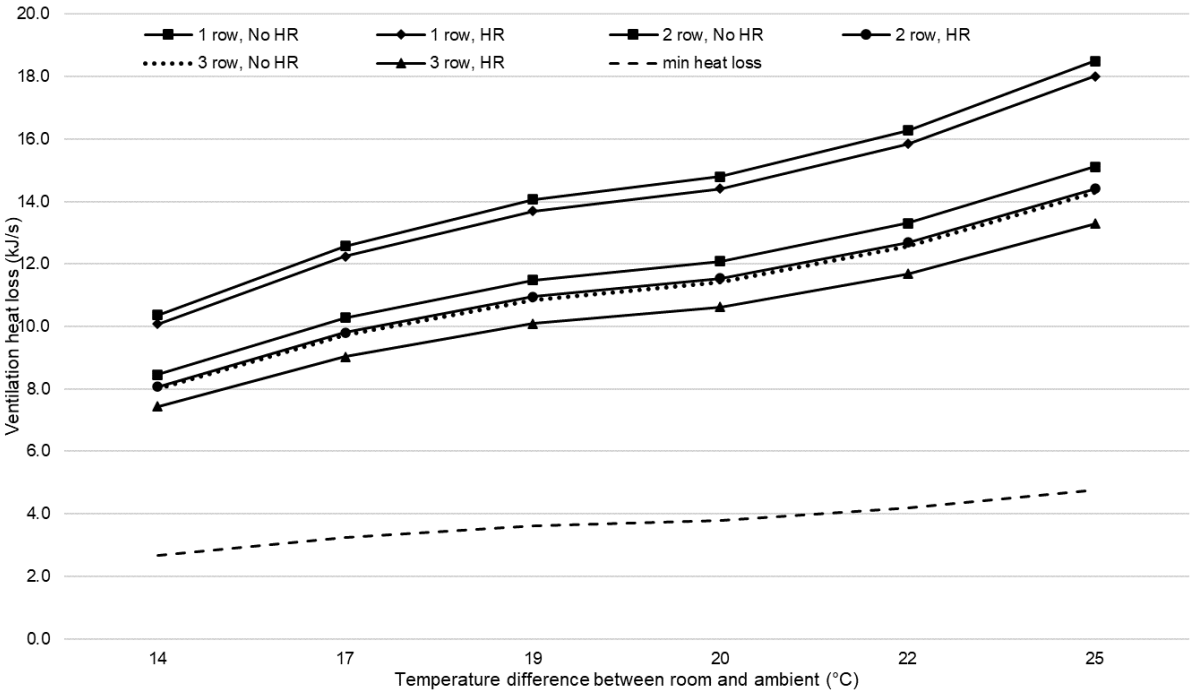

Figure 4-32 - Ventilation heat loss from building at 4 m/s wind speed

From the graphs it is seen that the ventilation heat loss greatly exceeds the minimum heat loss due to the volumetric flow rate through the wind tower exceeding the minimum 8 l/s per occupant, although the difference is much more pronounced at 4 m/s wind speed than 2 m/s. Comparing the cases of ventilation with and without heat

recovery, the increase in fresh air temperature due to heat recovered from the exhaust channels of the wind tower negates some of the excess heat loss, however is still in greater than the minimum. An increasing number of pipe layers serves to reduce the ventilation heat loss by increasing the fresh air temperature by a greater amount, but also by reducing the volumetric flow rate through the wind tower.

Installing heat recovery within passive ventilation is intended to increase the viable operational window of the wind tower into winter, however, issues with heat loss through over ventilation are still significant and would likely necessitate the closing of the system to prevent prohibitive increases to building energy demand at the current level of heat recovery. To limit the negative impacts of the ventilation system on building energy demand, the volumetric flow rates through the wind tower at higher wind speeds must be decreased, with automatic volume control dampers essential to reduce the volumetric flow rate depending on external wind speed. In addition, improving heat recovery and therefore the fresh air temperature prior to mixing throughout the room is necessary to further limit the increase in building energy demand. As it stands, the additional cost that would be incurred to install and operate a passive ventilation and heat recovery system would not make it competitive with mechanical HVAC systems.

4.7 Summary

This chapter has detailed the process followed for the evaluation of a wind tower with integrated heat pipes for heat recovery through a wind tunnel test and numerical model. Assessing several heat pipe arrangements the results produced the predicted volumetric flow rate through the wind tower with increasing inlet velocity as well as the potential for preheating of fresh air through heat recovered from exhaust air. In

addition, the reduction in energy because of the increased inlet air temperature was calculated.

4.7.1 Future Design Considerations

The results of the wind tunnel test and numerical modelling were used to inform design decisions when considering the integration of a water-based thermal loop to transfer waste thermal energy between the heat recovery system to a form of STES.

Firstly, it was established that a series of staggered pipe layers through a wind tower did not overly impede airflow into the room below, maintaining a volumetric flow rate of 100 L/s at an inlet velocity of 1 m/s. Although it is likely that by reducing the longitudinal and transversal pitch between pipes the pre-heating of fresh air would increase, this would be detrimental to the ventilation rate of the wind tower.

Secondly, the performance of the heat pipe heat recovery system is considered. Although the heat pipes increased the fresh air temperature, the increase achieved at temperature differences as large as 25 °C between the inlet and outlet fluid streams was 2.8 °C. To generate a more significant change in fresh air temperature through the wind tower would therefore require a heat source or sink at a greater temperature difference than the air temperatures simulated through the outlet of the wind tower.

Finally, consideration is given to the ease of integrating a thermal loop to extract and deliver waste thermal energy to and from the heat pipes for storage through STES. Studies have explored using a water tank installed within (Calautit & Hughes, 2016) and on top of (Calautit et al., 2017) a wind tower to act as a heat source or sink. Given the orientation and positioning of the pipes and the geometry of the wind tower, the heat source/sink for the current design would have to wrap around the outside of the wind tower so as not to impede the flow of air. It may also be necessary to have two

or more separate systems capable of delivering or extracting heat from each quadrant individually, depending upon the wind direction. This becomes further complicated when considering the implications of a pipe array with several orientations.

Considering all the above, it was determined that the subsequent design iteration would feature a run-around heat exchanger instead of heat pipes. The heat exchanger would resemble the heat pipe array installed through the wind tower, however, allows water to be passed directly through the pipes removing the need for an additional water tank attached to the wind tower, limiting the complexity of the operation, and decreasing the cost. Comparing the performance of heat pipes and run-arounds, the reported heat recovery efficiency of heat pipes was up to 80%, whereas run-arounds varied between 45 – 80% due to the varying designs of the integrated heat exchangers (Mardiana-Idayu and Riffat, 2012; O'connor, Calautit and Hughes, 2016). Comparing the measured drop, heat pipes were reported to incur a pressure drop between 1 – 5 Pa, whilst run-arounds delivered a pressure drop of approximately 1 Pa, however the velocities tested over the run-around heat exchangers were significantly lower than the velocities tested over the heat pipe arrays (Hviid and Svendsen, 2011; Davidsson et al., 2013; Calautit *et al.*, 2019; Liu and Calautit, 2023).

With regards to improving heat exchange, as water is constantly flowing through the pipes of the heat exchanger, heat is removed or supplied to the surface of the pipe at a greater rate than through the evaporation condensation cycle undergone within the heat pipes. Considering the addition of a form of STES to the system, the delivery temperature of the water can be controlled through a heat pump or chiller, providing a greater level of control over fresh air temperature as it enters the room. The flow rate through the run-around system can also be controlled as an additional way of

controlling thermal energy recovery. Negatively, there will be a significant amount of off-target heating and cooling delivered to the exhaust air passing through the outlet channels of the wind tower.

5 Far-field Testing

Using the wind tunnel test results to feed design considerations, a wind tower and run-around heat recovery system was installed at a demonstration site in Sheffield, UK, to explore the system's performance under real-world conditions. The field trial was conducted during the summer, focusing on the potential for pre-cooling fresh air and heat recovery through a wind tower. The field trial and subsequent numerical modelling focused on the performance of the Run-around Heat Exchanger (RAHE) within the wind tower, determining the potential for heating and cooling of fresh air as well as quantifying the thermal energy that could expect to be recovered.

5.1 System Design

The same wind tower design as was used for during wind tunnel testing was employed for the field trial, with a four-sided square frame, each with 7 louvres. As discussed in section 4.7.1, the heat pipe system was replaced with a run-around heat exchanger to improve the heating and cooling of fresh air as it passed through the wind tower.

When designing the heat exchanger for integration through the wind tower, several parameters were kept consistent to provide a fair comparison between the RAHE system and the heat pipe array. The outer diameter of the copper pipes that comprised the heat exchanger was 16 mm, equivalent to the outer diameter of the heat pipes. Likewise, the longitudinal and transversal pitches between the pipes was kept at 35

and 50 mm respectively. The positioning of the heat exchanger relative to the base of the wind tower ducting was also kept the same.

Given the intended operation of the wind tower and RAHE system within mild-cold climates, the system needs to be able to provide both heating and cooling using thermal energy recovered in the opposing season. To facilitate this the form of STES selected must be capable of storing both heat and cold on a seasonal basis. Of the available forms of STES, aquifer, tank, and pit thermal storage are all capable of storing heat and cold, although ATES is much more suited to the storage of both as the hot and cold wells can be separated geographically from one another within the aquifer to prevent excessive thermal losses due to interaction between the hot and cold regions.

As was reported through the literature review, the hot storage temperatures of both tanks and pits can reach up to 95 °C, while in low temperature ATES systems, hot well storage temperatures peak at approximately 25 °C. Given that summer temperatures in the UK rarely exceeding 30 °C, suitability for high temperatures is not considered as the hot water injection temperature will be lower than the ambient summer temperatures.

Finally, considering the relatively low temperature differences likely achieved through the RAHE system, it is desirable to store a larger volume of low temperature thermal energy. Aquifers are ideally placed to provide large amounts of cool water in the summer, with groundwater temperatures around 8 °C. In addition, aquifers are often located under large population centres, the areas which are most likely to generate large heating and cooling demands in occupied buildings. Using naturally available aquifers significantly reduces costs relative to purpose-built tanks or pits.

For the reasons listed above, ATES was selected as the most suitable form of STES for linking with a wind tower and RAHE system. Given the low injection temperatures during the summer, the hot water temperatures tested in the winter would be reliant on the use of heat pumps to increase the temperature of the water through the system so that a measurable amount of fresh-air heating is achieved.

5.2 System Description

The proposed system aims to combine a wind tower and a run-around heat exchanger to create a system capable of heating and cooling fresh air whilst recovering waste thermal energy for storage. Run-arounds traditionally link two heat exchangers placed within separate fluid streams. In this case, one heat exchanger was installed within the wind tower and the other would store and extract thermal energy through STES below ground.

Given the scale of the system, the need for both hot and cold storage, and the likely operating temperature range an ATES system is deemed to be the most suitable. Cold well injection temperatures in literature ranged between 3 and 17 °C while hot well injection temperatures ranged between 13 and 25 °C. In addition, ATES has been effectively adopted within energy systems, particularly throughout the Netherlands in smaller scale systems suitable for linking to single office buildings or a school. As a result, the temperature ranges explored corresponded to the temperatures reported in the literature for ATES. An insulated water tank was used within the experiment to imitate the delivery of stored hot or cold water from an ATES system at a near constant temperature.

Cold water is pumped from a tank throughout summer through a series of copper pipes installed horizontally through the base of the wind tower to pre-cool fresh air before

mixing throughout the room. Heat is transferred from the air to the water through the wall of the copper pipes as the air passes over the heat exchanger, increasing the temperature of the water flowing through the system. Cooled fresh air is discharged into the room where it can be cooled further if required using mechanical cooling systems and the water is discharged into the STES system. In the winter the stored heat can be used to provide heating via the same process, circulating hot water through the RAHE to increase air temperature, reducing the water temperature in the process before it is again stored for the following cooling season.

When considering the future composition and operation of the system, it may be necessary to circulate the water through the heat exchanger several times before the desired temperature for storage is reached. However, this study will only examine the temperature change achieved through a single pass. The use of a heat pump is anticipated in the winter to increase the water temperature prior to use for heating as the heat gained from the air in summer will be insufficient on its own.

For this experiment, water is circulated through the heat exchanger via an insulated water tank within the test room. A submersible pump and chiller supply water at a near-constant temperature throughout the testing period, imitating the water supply from a form of STES. The system's effectiveness in heating and cooling fresh air will be a function of the ambient air temperature, the wind velocity over the pipes, and the velocity and temperature of the water through the run-around. The thermal energy recovered will depend upon the effectiveness of the run-around system.

5.3 Experiment Design

An office site in Sheffield, UK, was used to conduct a field test of the full-scale wind tower and RAHE (Figure 5-1).

Figure 5-1 - Field trial location and surrounding buildings provided through Google Earth (Google, 2023)

The wind tower measured 1 x 1 x 2.5 m, where the height was measured from the tip of the roof to the base of the ducting through into the room below. The external configuration was the same as the wind tower used for the wind tunnel test, with each side featuring seven external louvres at a spacing of 100 mm. The internal x-frame divides the wind tower volume into four equal quadrants, extending to 120 mm above the bottom of the ducting to allow space for the heat exchanger to pass below. Dampers were installed at the base of the ducting to control the flow of air into the room, however for this experiment, they were left entirely open. The wind tower was installed through the pitched roof of an unused office space with an internal volume of 61.5 m^3. As the wind tower had to be fitted between existing roof joists it is placed slightly off-centre through the roof. A weather station was mounted to the side of the wind tower, recording wind speed, direction, and ambient temperature, recording values at five-minute intervals (Figure 5-2).

Figure 5-2 - Wind tower installation through the office roof

Eighteen copper pipes were installed in a single row horizontally through the base of the wind tower ducting (Figure 5-3).

Figure 5-3 - Copper pipes installed through the wind tower ducting inside the test room

The longitudinal (S_L) and transversal (S_T) pitches were 0.035 and 0.05 m respectively. The inner (D_i) and outer (D_o) pipe diameters were 0.014 and 0.016 m respectively. In the simulations featuring more than one pipe layer, a longitudinal pitch of 0.035 m was used maintaining similarity with the spacing used throughout the wind tunnel test and CFD study.

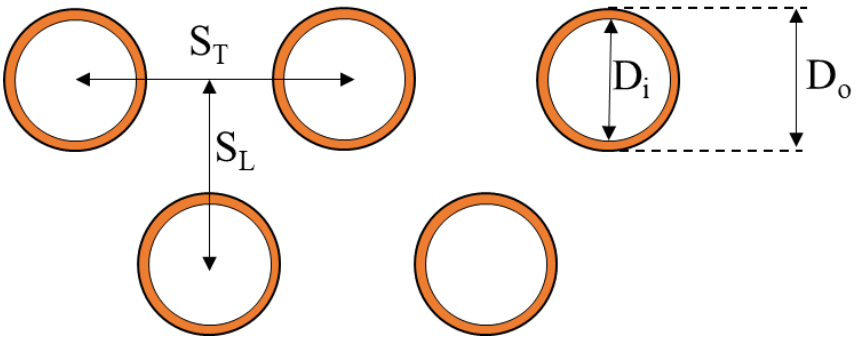

Figure 5-4 - Pipe configuration

A submersible water pump and a separate chiller unit were placed inside an insulated water tank. The chiller was used to maintain the water within the tank at a roughly constant temperature as without the water temperature rapidly increases with numerous passes through the heat exchanger. A digital flow meter recorded the flow rate of the water through the system (Figure 5-5).

Figure 5-5 - Insulated water tank and digital flow meter

5.3.1 Test Equipment

The field trial evaluated the potential for pre-cooling fresh air through a RAHE system. To measure the performance of the system, the following test equipment was used:

- Weather station
- Exposed tip k-type thermocouples
- Immersion tip k-type thermocouples
- Submersible pump
- Julabo chiller and heat exchanger
- Digital flow meter
- FLIR T640 thermal imaging camera

5.3.1.1 Bresser Weather Station

A Bresser 5-in-1 weather station was used to record ambient air temperature, wind speed and direction, where wind direction was broken down into 16 bands, each with a range of 22.5 degrees. Ambient pressure and rainfall were also recorded but not used for this experiment. The weather station wirelessly transmits measurement data from the weather station to an indoor hub via wi-fi which was uploaded to Weatherundergound, a public website used to record and process weather station data.

Figure 5-6 - Weather station

Weather readings through Weatherundergound were recorded every five minutes as the value at the beginning of each interval rather than the average value recorded throughout.

5.3.1.2 Thermocouples

Fluid temperatures were recorded using two types of k-type thermocouples. Exposed tip thermocouples with a temperature range of -75 to 250 °C and an uncertainty of ± 1% at 25 °C were used to record air temperature. Exposed tip thermocouples are characterised by fast response times but are limited to non-corrosive applications. Thermocouples with an immersion tip, a temperature range of -40 to 205 °C, and an uncertainty of ± 1% at 25 °C were used to record water temperature. The immersion tip prevents the corrosion of the metal wires over time.

Temperature data was recorded through a Picolog TC-08 Data logger connected to a laptop. Each data logger could record data from up to eight thermocouples simultaneously, offering a high-resolution and customisable interface to assess the

collected data. Temperature readings were taken every second throughout testing and averaged over five-minute intervals to provide consistency with the ambient weather conditions recorded through the weather station.

5.3.1.3 Submersible Pump

A 550 W submersible pump was used to circulate the water through the system, generating a volumetric flow rate of 0.087 L/s when pumping to a height of approximately 3 m. The pump drew water in through the base and discharged it vertically through the attached hose, with thermocouples placed within the inlet and outlets to record the fluid temperature.

5.3.1.4 Chiller

A Jubalo FL1201 recirculation chiller was used alongside the pump to cool the water within the tank (Figure 5-7). The chiller has a working temperature range of -20 to 40 °C at ambient temperatures between 5 and 40 °C, producing a cooling capacity of 1 kW at 10 °C. The temperature resolution can be changed in increments of 0.1 °C, delivering a stability of ± 0.5 °C.

Figure 5-7 - Julabo recirculation chiller

The chiller circulates a refrigerant through a heat exchanger submerged within the water tank to cool the water (Figure 5-8). The water discharge from the RAHE outlet generated enough mixing within the tank to cool the body of water sufficiently. The chiller uses a vapour compression cycle to reduce the refrigerant temperature through the system. To prevent the hot air expelled from the chiller from increasing the temperature within the test room, the chiller was placed outside the room and the tubing connecting the heat exchanger passed underneath the door.

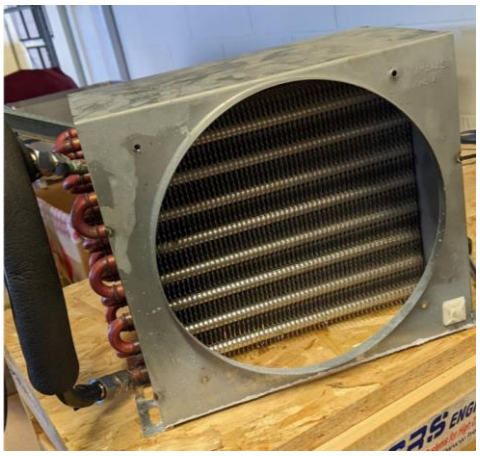

Figure 5-8 - Chiller heat exchanger submerged within the water tank

5.3.1.5 Digital Flow Meter

A digital flow meter with an accuracy of ± 1% when the fluid is between -10 °C and 40 °C was used to record the flow rate through the run-around (Figure 5-9).

Figure 5-9 - Digital flow meter

The flow rate was recorded in L/min through the flow meter which was then converted to L/s. The velocity of the fluid was found using the internal area of the pipes through which the water was flowing. The averaging function built into the flow meter was used to find the flow rate through the system during testing.

5.3.1.6 Thermal Imaging Camera

A thermal camera produces an image by measuring the infrared energy emitted from a surface and converting it into an image, relating differing temperatures to a colour scale for the user. A FLIR T640 thermal imaging camera was used to visualise the differences in temperature between the RAHE and the broader system. The camera has a temperature range of -40 up to 2000 °C and an accuracy of ± 2% or ± 2 °C, whichever is greater, at a nominal 25 °C. Figure 5-10 below shows an image taken using the camera before testing.

Figure 5-10 - Thermal imaging test using a portable radiator

5.3.2 Measurement Points

Temperature sensors were placed below the pipes in each wind tower quadrant. As the wind direction was predominantly westerly, more sensors were placed in the west-facing quadrant where the most cooling was likely to occur. As with the wind tunnel test, the average fresh air cooling was found by averaging the values at points 2 and 3 against the value at point 1. For the other quadrants, a single sensor was placed below the pipes in the centre of each quadrant (Figure 5-11). An additional thermocouple was used to measure pipe surface temperature.

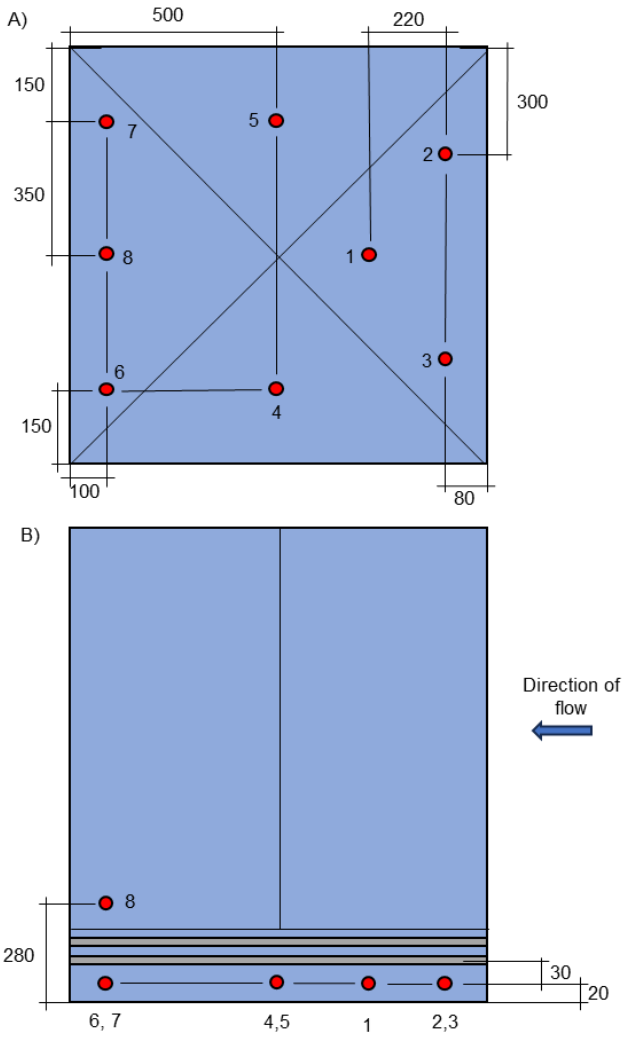

Figure 5-11 - Field trial temperature sensor placement in each quadrant of the wind tower, distances in mm

As there was only a single row of pipes the sensors are offset by 25 mm relative to the positioning used for the wind tunnel test, placing them directly below the pipes. These better measures the air temperature decrease due to the heat exchanger as the air passing between the pipes recorded little or no measurable temperature difference. This occurs as the spacing between the pipes was large enough to allow fresh air to pass between them without interacting with the surface of the pipe, indicating the need for at least two rows of pipes or a smaller transversal pitch in any heat exchanger.

Immersion tip thermocouples were placed inside the inlet of the submersible pump and at the outlet of the pipe system to record the change in water temperature through the RAHE. An additional thermocouple was left floating inside the body of water within the water tank to monitor the temperature of the bulk fluid.

Although wind speed was recorded through the weather station, no velocity measurements were recorded inside the test room. This was due to the variation in the inlet velocity with time and the reporting interval of the weather station, making it difficult to produce any consistent measurements of velocity below the heat exchanger referenced against the inlet velocity. This is a shortcoming of field trial testing of passive ventilation systems, with the difficulties of correlating measured field trial velocities against CFD results documented (Liu *et al.*, 2024). The velocity through the field trial wind tower was instead compared against the velocity measured through wind tunnel testing. CFD models are often validated using a single variable (O'Connor, Calautit and Hughes, 2015; Calautit and Hughes, 2016; Liu *et al.*, 2024), however this does not detract from the point that there is a lack of physical data for comparison with the CFD results and so the actual velocities through the wind tower inlet and outlets may vary from those reported through the CFD model.

5.3.3 Boundary Conditions

NASA's Prediction of Worldwide Energy Resources (POWER) program evaluated historical weather at the site between 2000 and 2021 (Sparks, 2018). Figure 5-12 shows the daily average historical temperature against the daily average temperature recorded by the weather station for the months it was active. The average temperature from July to August 2022 was higher than the historical average due to a heatwave that the UK was experiencing at the time. This weather behaviour may however become more common with climate change, resulting in an increased demand for cooling in residential and commercial spaces, emphasising the necessity for low-energy ventilation, heating, and cooling systems.

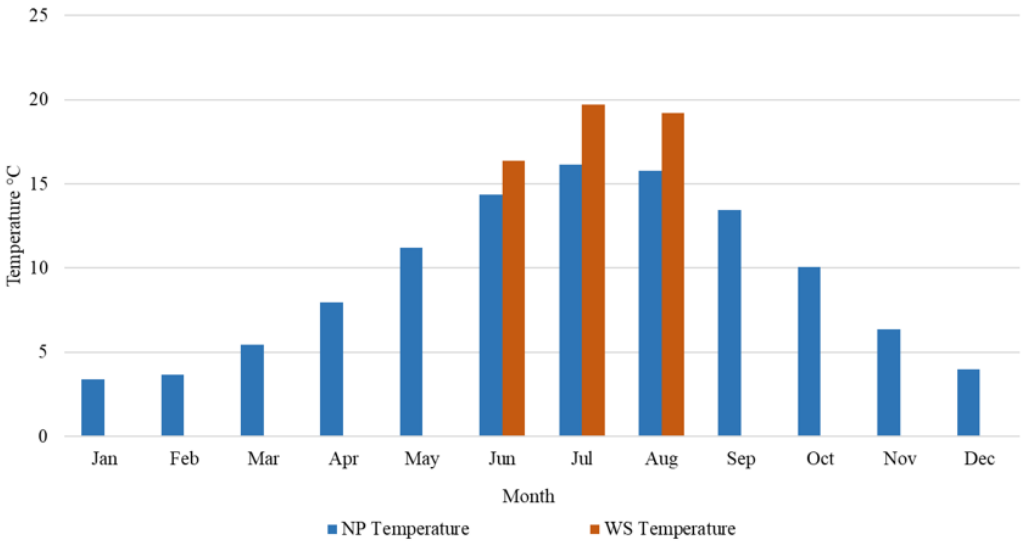

Figure 5-12 - Average daily temperature and wind speed by month in Sheffield (NASA Power (NP) vs. Weather Station (WS))

The wind velocity and direction recorded at the site were used to produce a wind rose (Figure 5-13).

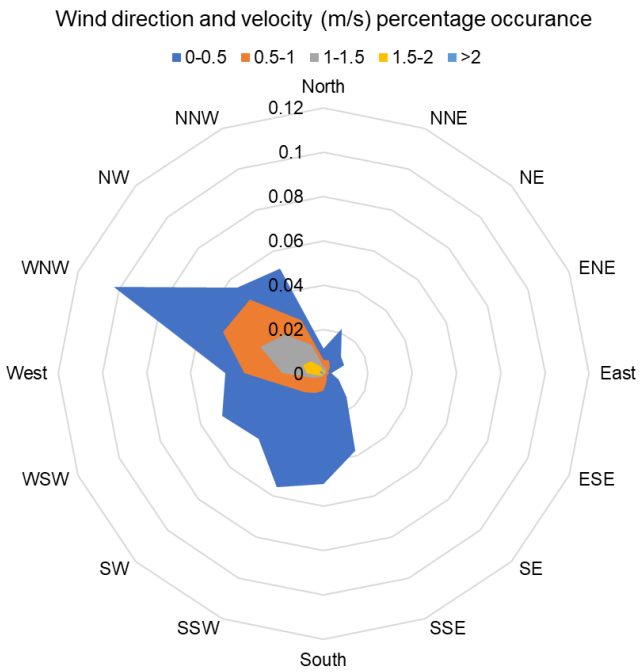

Figure 5-13 - Wind rose produced for June - August for field trial site

Due to the surrounding buildings and pitched roofs, the incident wind direction onto the wind tower is constrained mainly to a westerly direction. The wind velocity is typically also very low, falling between 0 - 0.5 m/s approximately 56% of the time.

Evaluating the wind speed daily, it is seen that the wind speed significantly falls overnight, with the weather station often recording zero wind for several hours (Figure 5-14). This phenomenon is often observed as ambient temperatures cool, reducing pressure gradients within the atmospheric boundary layer, contributing to much of the wind speed data below 0.5 m/s. As the anemometer is fixed to the side of the wind tower, the wind speed measured is taken as the inlet velocity into the wind tower inlet, however, may be lower than the free wind speed around the building.

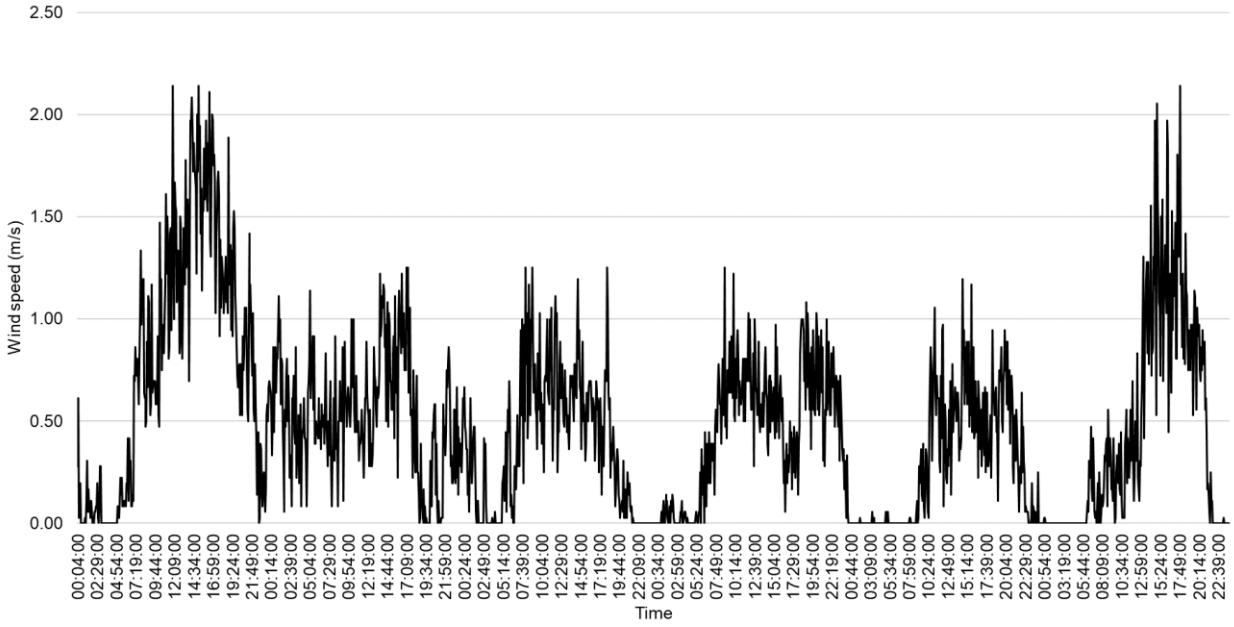

Figure 5-14 - Local wind speed from 15 - 20/06/22

Two days of testing were conducted on the 11th and 12th of August 2022 for three to four hours at a time. As seen in Figure 5-15 showing the ambient conditions on 12/08/22, the wind speed dropped to 0 m/s overnight, rising again throughout the day. Consistent with the wind rose, the wind direction falls almost exclusively from a westerly direction owing to the shape of the roof and surrounding buildings. The rise in wind speed coincides with the increase in ambient air temperature after sunrise, peaking at approximately 3.2 m/s.

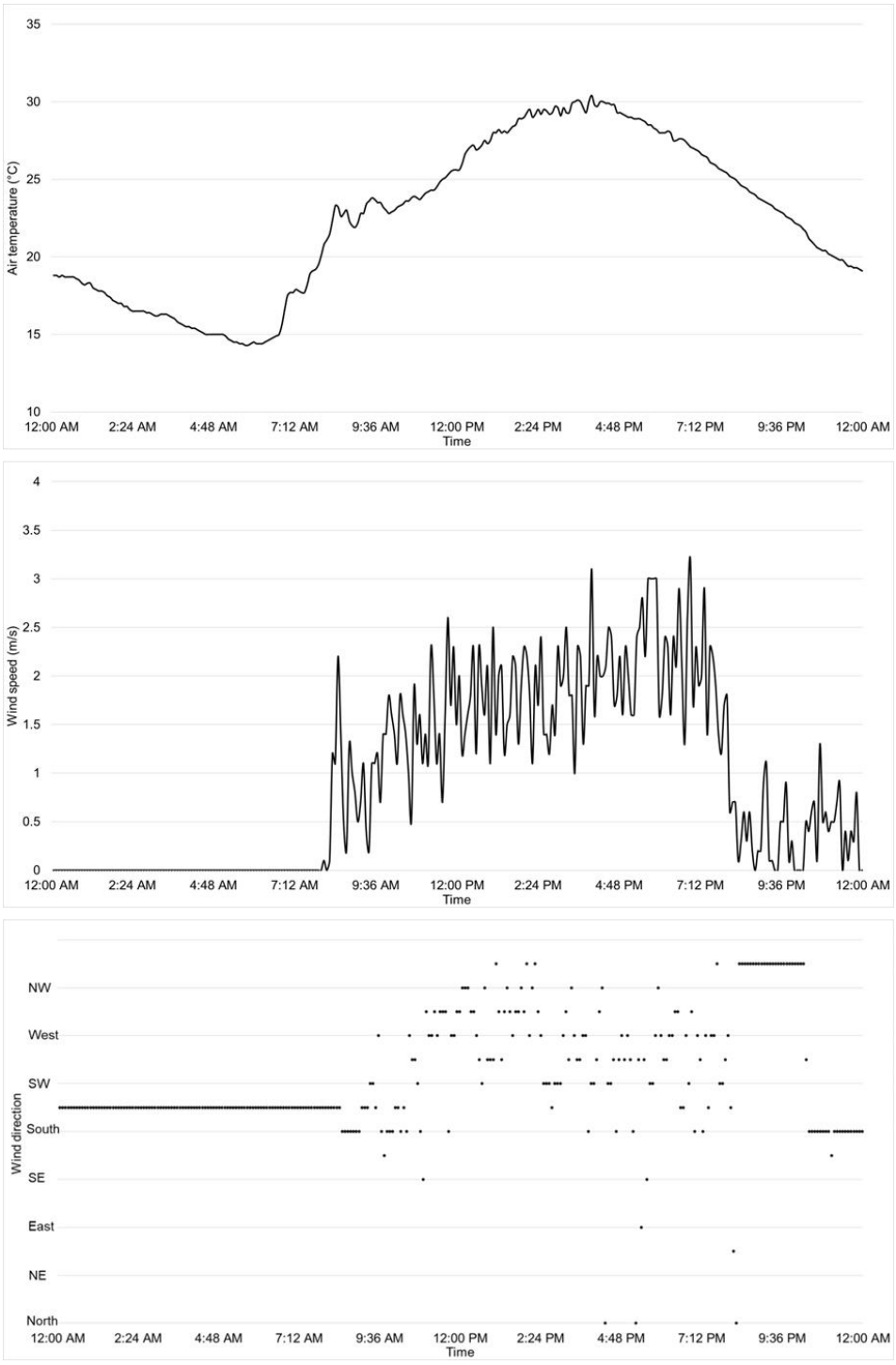

Figure 5-15 - Air temperature, wind speed, and wind direction recorded by the weather station on 12/08/23

The chiller was set to 10 °C, although, as seen below in the results this was insufficient to produce a constant inlet temperature to the RAHE as the limited volume of water within the tank didn't allow enough time for the chiller to cool the fluid before it was

recirculated through the system. The pump generated a flow rate of 0.087 L/s, equivalent to a velocity of 0.56 m/s through the system.

5.4 Results

Testing was conducted on the 11th and 12th of August 2022, using the RAHE to cool fresh air as it entered the room through the wind tower and recover waste heat in the process. Figure 5-16 shows the weather conditions experienced at the test site as recorded by the weather station on the 11th, with sunrise occurring at approximately 05:40 AM causing the sharp rise in ambient temperature.

The positioning of the wind tower in the roof and the sheltered location of the building contribute to the low wind speeds and a consistent westerly wind direction experienced as discussed. On the 11th, there is some discrepancy in the wind direction and velocity readings, with the weather station showing a changing wind direction but no wind speed indicating that the anemometer may have been temporarily stuck.

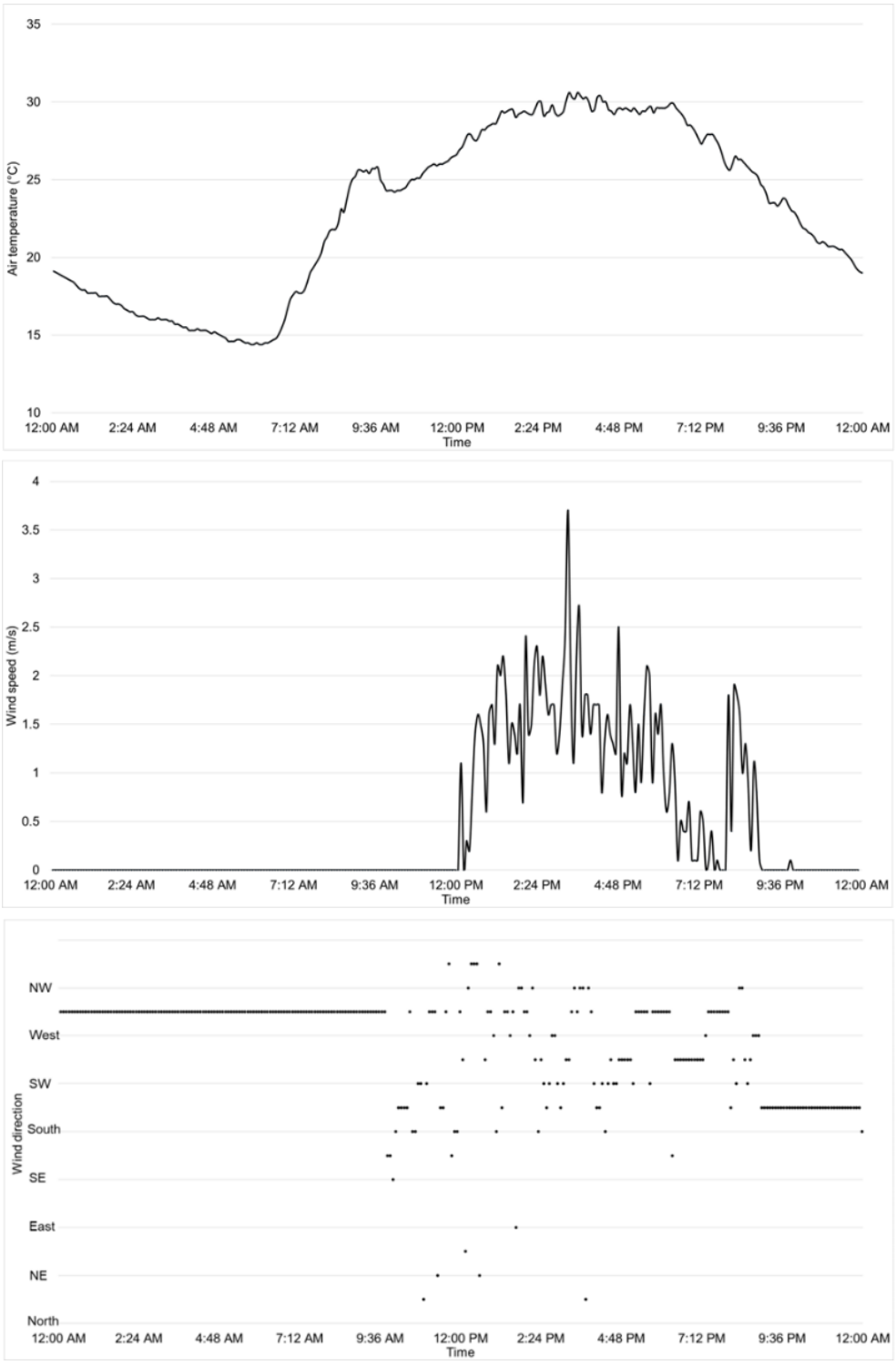

Figure 5-16 - Ambient air temperature, wind speed, and direction on 11/08/22

Taken directly from the data logging program, Figure 5-17 highlights the air and pipe surface temperature variation due to the changing ambient conditions when the reporting interval was 1 second.

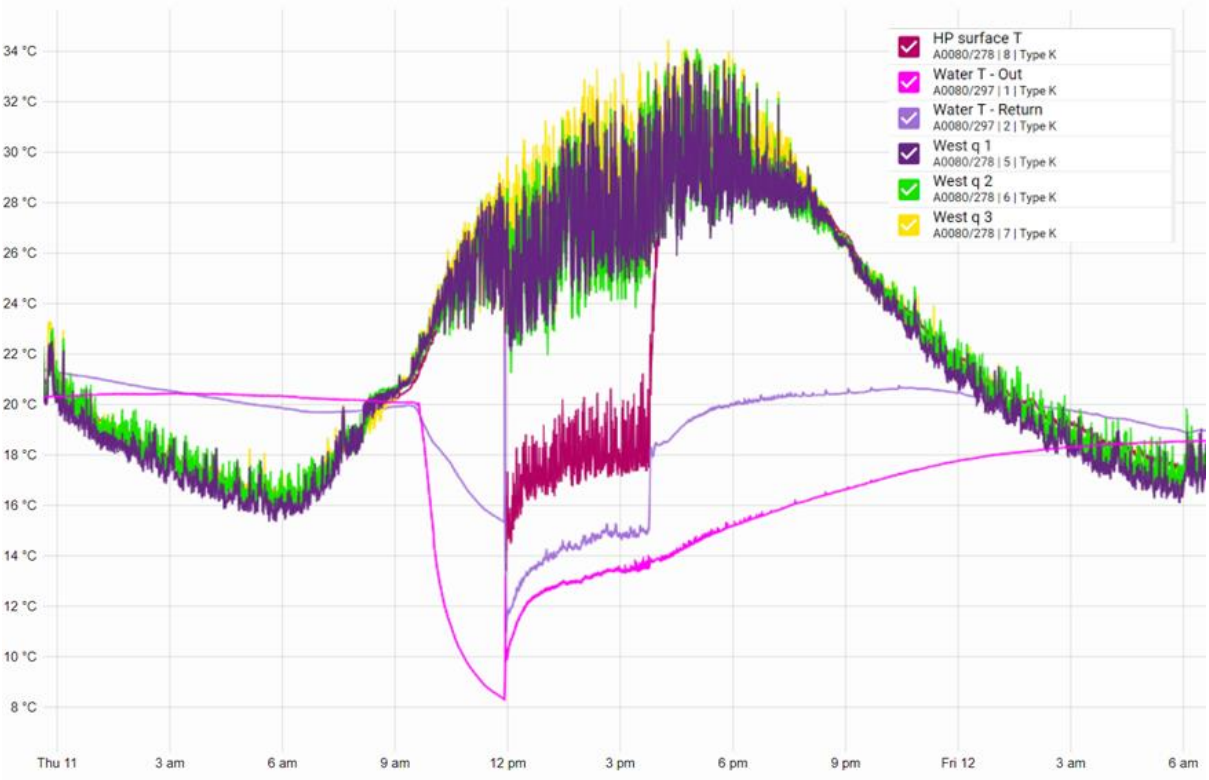

Figure 5-17 - Thermocouple temperature data prior to averaging

Figure 5-18 and Figure 5-19 then show select data from the weather station and thermocouples on both dates, with the weather data provided at five-minute intervals and the thermocouple data averaged over the same period. The chiller was first turned on without the pump to allow the temperature of the water within the tank to decrease, as seen by the steady decrease in temperature at the heat exchanger inlet and outlet which were both located within the tank.

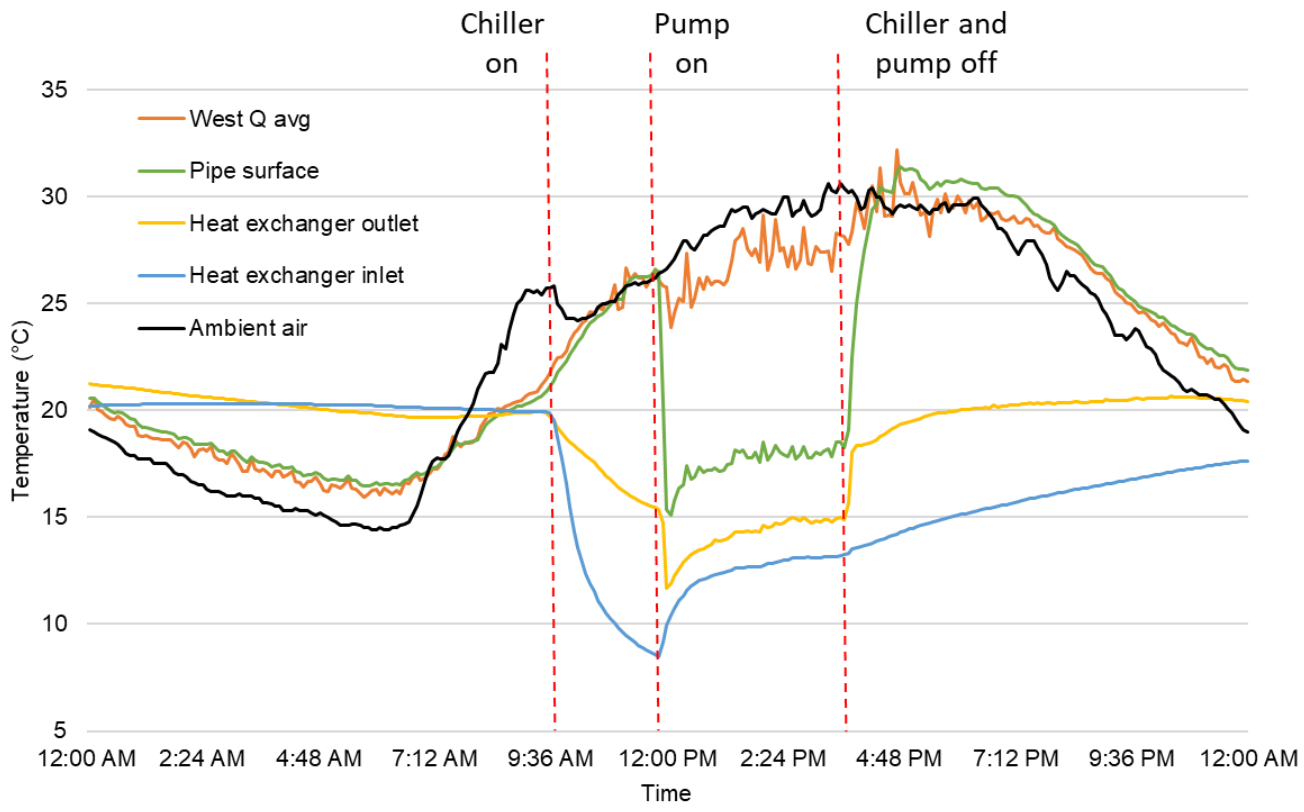

Figure 5-18 - Field trial experimental data from 11/08/22

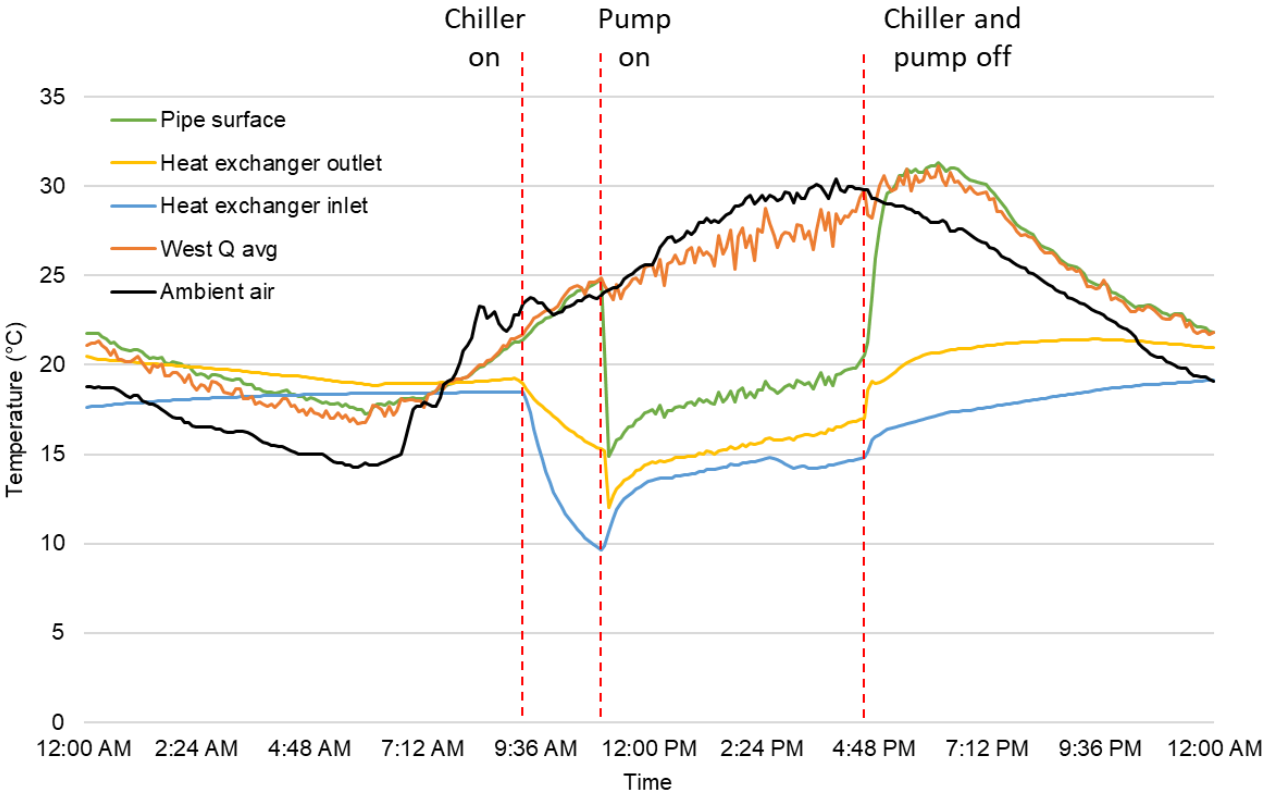

Figure 5-19 - Field trial experimental data from 12/08/22

As the wind speed increases into the day, the temperature of the air below the heat exchanger, the pipe surface, and the ambient air temperature are all similar indicating that fresh air is passing through the wind tower, but no cooling is occurring.

‘West Q avg’ is the average air temperature below the heat exchanger as measured through the average of points 1, 2, and 3 (Figure 5-11). To cool the water within the tank, the chiller was first turned on without the pump running, indicated by the steady reduction in heat exchanger inlet temperature without seeing any decrease in the pipe surface temperature. Once the water had reached a satisfactory temperature the submersible pump was activated to circulate the water through the heat exchanger, as shown by the rapid drop in pipe surface temperature on both dates. This correlates with a decrease in the air temperature below the pipes relative to the inlet air temperature, although this is more immediately noticeable on the 11th than the 12th. The water temperature at the heat exchanger inlet and outlet rapidly increases as heat stored within the walls of the pipes that constitute the heat exchanger is transferred to the water before the curve flattens out.

The west quadrant air temperature remains below the ambient air temperature as long as the pump and chiller remain active, with the amount of cooling varying with the ambient air temperature, wind speed, and direction. An average of 2.1 °C of cooling with a maximum of 3.7 °C was achieved on the 11th, whereas on the 12th an average of 1.6 °C and a maximum of 3.6 °C of cooling was measured. The lower cooling on the 12th is partially due to the higher average wind speed experienced throughout testing, 1.5 m/s on the 11th and 1.8 m/s on the 12th. The inlet temperature of the heat exchanger increased steadily with time as the chiller could not sufficiently cool the water as it was recirculated through the system. Despite this, the outlet temperature is approximately 1 °C higher than the inlet temperature consistently throughout testing.

Figure 5-20 shows a thermal image of the heat exchanger through the wind tower, clearly showing the contrast between the heat exchanger pipe wall temperature and the temperature of the wind tower.

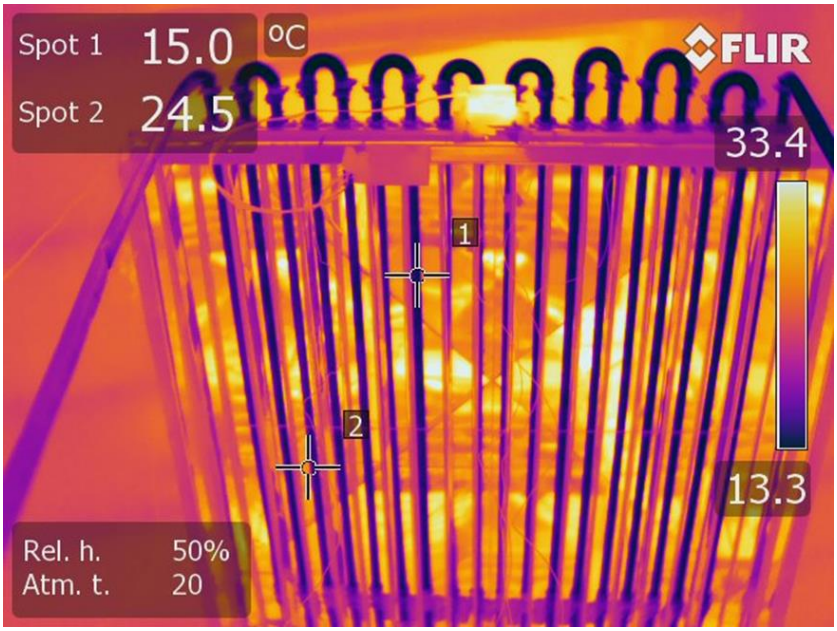

Figure 5-20 - Thermal image of the heat exchanger under operation

After switching off the pump and chiller simultaneously, the pipe surface temperature and heat exchanger inlet and outlet temperatures rapidly increase. Overnight, the air temperature inside the wind tower inlet quadrant remains higher than the ambient air temperature due to the warmth retained within the test room. As the wind speed drops to zero there is no ventilation occurring through the wind tower otherwise the ambient and west quadrant temperatures would be expected to be equal.

5.5 Field Trial Numerical Modelling

The following sections describe the development of the numerical model built to reflect the experimental design. The model was validated against experimental data through a transient simulation prior to completing steady-state simulations under a range of boundary conditions to predict the performance of the RAHE.

5.5.1 Geometry

A three-dimensional CAD model was first created to replicate the experimental design. The commercial wind tower design described in Section 4.3 was employed with ducting installed below to lower the height of the dampers and RAHE system within the test room. The wind tower and ducting were created as a single body within Autodesk Inventor with the dimensions indicated below in Figure 5-21. The internal x-frame extends from the top of the wind tower through the length of the ducting, finishing 120 mm above the base to allow space for the heat exchanger to pass below.

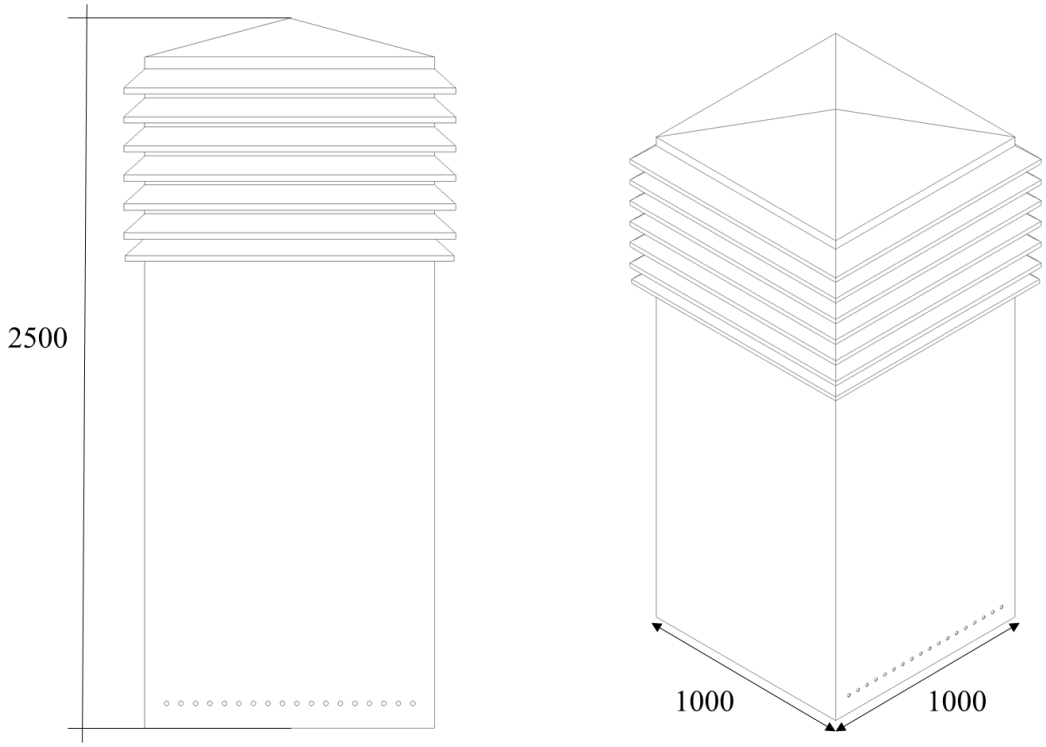

Figure 5-21 - Wind tower and ducting CAD model

To model the flow of water through the RAHE, two individual bodies representing the pipe system of the heat exchanger and the fluid passing through it were created. The heat exchanger is comprised of 18 copper pipes in a single row, each having an outer diameter of 16 mm, a wall thickness of 1 mm, and a transversal pitch of 50 mm from the centre of neighbouring pipes.

The thickness of the pipe wall created issues during the meshing process, whereby many small cells were required to model the pipe to avoid producing poor quality elements. In response the two bodies were combined, creating a single geometry with an outer diameter equal to the outer diameter of the pipes (Figure 5-22). A thin wall was created to separate the air and water fluid regions, where a thin wall is defined as having zero thickness.

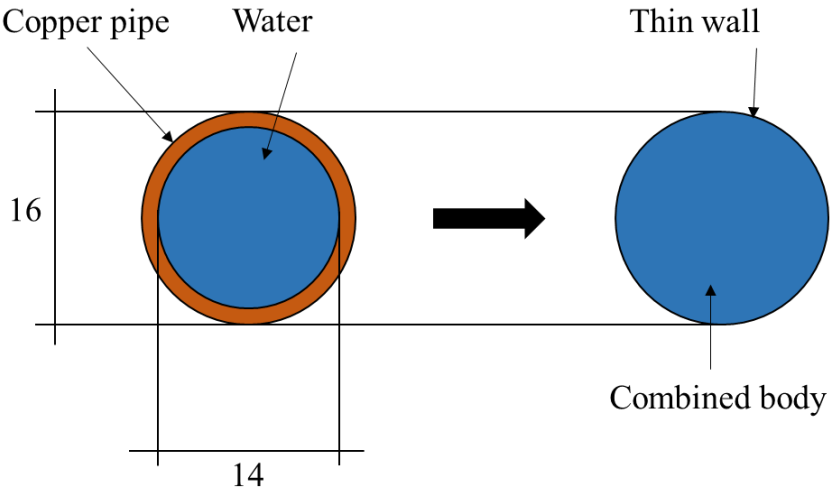

Figure 5-22 - Pipe and water bodies separate (left) and combined (right)

Upon loading the meshed model into ANSYS Fluent a wall thickness was retrospectively applied to the thin wall of the combined pipe and fluid body. In this way, the program computed the resistance to heat transfer through the pipe wall without physically modelling the pipe. Additional models were created featuring heat exchangers with two and three pipe layers, increasing the number of copper pipes to 35 and 52 respectively. As with the wind tunnel test the longitudinal pitch between rows was 35 mm.

The RAHE was assembled with the wind tower and ducting system and imported into Spaceclaim within the ANSYS workbench. Here, the fluid region within the test room

was extracted, accounting for large items that remained within the room such as a set of cupboards, a radiator, and the water tank used to provide water to the RAHE (Figure 5-23).

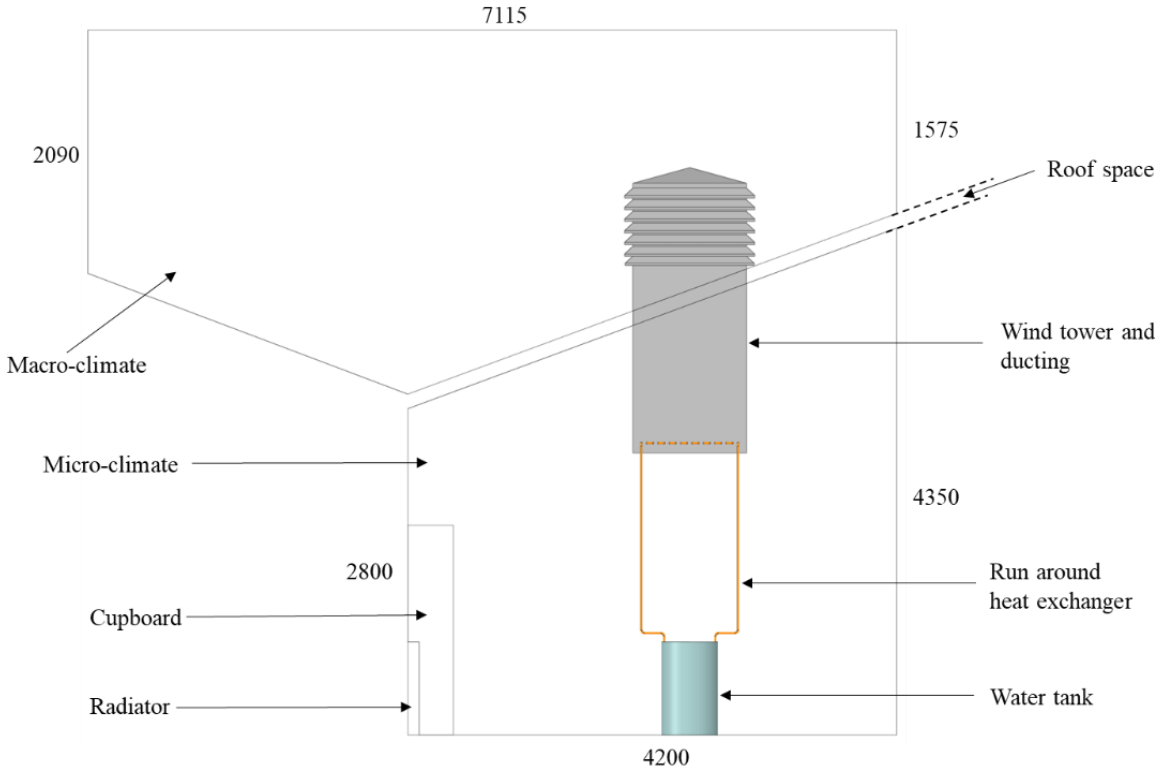

Figure 5-23 - Schematic of numerical model geometry

Figure 5-24 below indicates the region the macroclimate was extracted from relative to the surroundings, where the boundaries of the macroclimate were chosen to align with the roof geometry and adjoining building to limit the size of the domain.

Figure 5-24 - Macro-climate extraction from roof shape and surrounding buildings taken from Google Earth (Google, 2023)

It has previously been reported that neglecting to include the leading edge of the building within the simulated flow results in an increased flow rate through the wind tower relative to simulations where it is included. This arises from not accounting for the flow separation that occurs at the leading edge of the building which affects the velocity profile of the air onto the wind tower system (Ozmen et al., 2016; Wu *et al.*, 2021). In this instance it is difficult to predict the velocity distribution of the atmospheric boundary layer given the impact of the surrounding buildings, trees, car park, and changing wind direction. Consequently, a uniform boundary layer ignoring the leading edge of the building was applied with the understanding that the volumetric flow rate through the wind tower may be overestimated.

After creating the two separate fluid regions for the micro and macroclimates they were combined, first with each other to create one continuous fluid region throughout the domain, and then with the wind tower to subtract the body from the domain. By

subtracting the body of the wind tower from the surrounding fluids the physical wind tower geometry does not have to be meshed but the walls of the wind tower remain as solid boundaries within the model, affecting the flow without allowing any energy transfer through them. This prevents any conductive heat transfer through the walls of the wind tower, however there is limited contact between the heat exchanger and wind tower and therefore the impact is minimal. In physical testing, brass couples were used to hold the copper pipes in place within the wind tower, preventing any significant heat loss from the copper pipes to the aluminium body of the wind tower.

5.5.2 Materials

ANSYS Fluent contains the thermophysical properties of numerous materials for application to thermal models. The thermophysical properties of water, air, and copper were applied to the relevant bodies within the numerical model, with Table 5-1 indicating the values used for each material:

Table 5-1 - Material properties used for the field trial numerical model

Material	Density (kg/m^3)	Specific heat (J/kg·K)	Thermal conductivity (W/m·K)	Viscosity (Kg/m·s)
Water	998.2	4182	0.6	1.003×10^{-3}
Air	1.225	1006.43	0.024	1.789×10^{-5}
Copper	8960	380	401	N/A

5.5.3 Mesh Generation

Given the irregular shapes of the test room, roof, and wind tower, an unstructured mesh of tetrahedral elements was chosen to discretise the domain. Size functions were applied throughout to control cell size in areas of importance such as the wind tower louvres and x-frame walls, applying a growth rate of 1.2 to control the increase in cell size away from the wall.

Previous simulations showed that areas of recirculation and short-circuiting occur above and below the pipes installed through the wind tower. To help accurately model the flow in these regions two additional bodies were created within the ducting of the wind tower which were used as Bodies Of Influence (BOI)(Figure 5-25). BOI dictate the volume of the cells in the regions of the model they overlap with and were applied to increase the cell density in the regions where more complex flow regimes evolve.

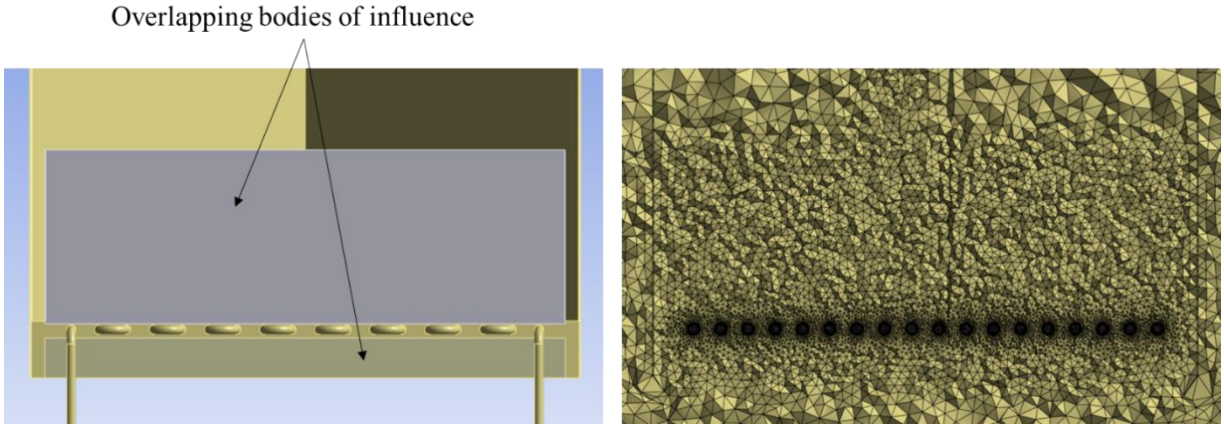

Figure 5-25 - Bodies of influence used to increase the mesh cell density

Tetrahedral elements were also used to mesh the RAHE, with inflation layers applied to the surface of the pipe through the wind tower ducting to resolve the flow properties close to the wall. Upon loading the unstructured tetrahedral mesh into ANSYS Fluent from the meshing program, all tetrahedral elements were converted to polyhedral (*Figure 5-26*). Polyhedral meshes have been shown to require fewer cells, reducing computation time whilst improving the accuracy of the results as each cell receives and provides information to a greater number of surrounding cells (Kim and Chung, 2015).

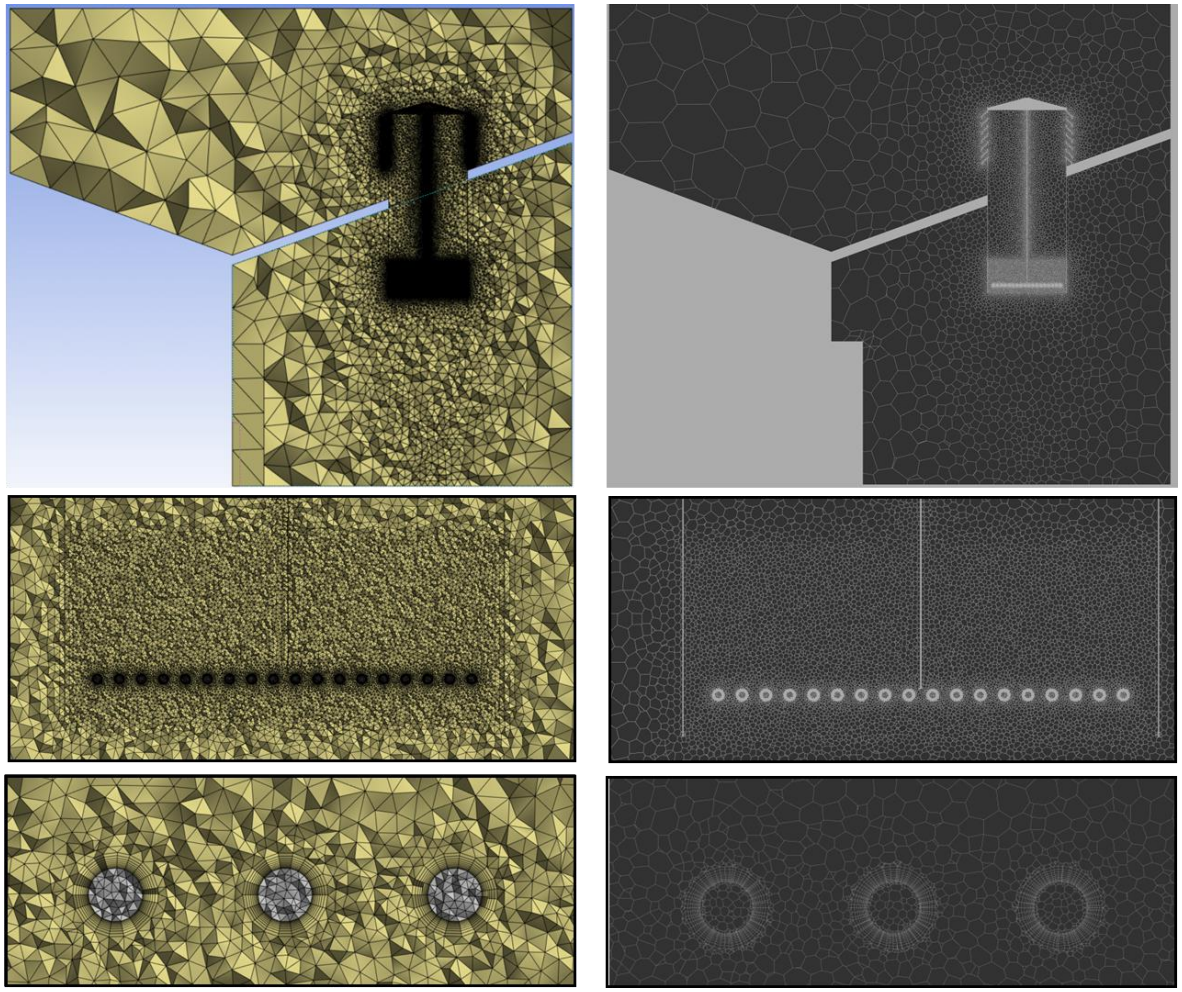

Figure 5-26 - Conversion of the fine mesh from tetrahedral (left) to polyhedral (right)

The wall y^+ was found to be 0.06 at the surface of the pipe, far below the recommended value of $30 < y^+ < 300$ for standard wall functions. Having a y^+ outside the recommended boundaries creates issues if the mesh is too coarse ($y^+ > 300$), as the wall functions may be unable to calculate the flow properties over the cell. However, having a particularly low y+ ignores the wall functions and results in the model calculating the values as is done throughout the rest of the domain, using the properties of the flow provided by the adjacent cells. As was shown by Celleck (2020), for standard wall functions a wall y^+ of approximately 0.1 marginally improved the accuracy of the numerical model relative to the model with a wall y^+ of 30.5. As a result, although the fine cells at the wall result in increased computational demand the mesh was deemed sufficient for further calculation. As is seen in section 5.5.5, the low y+

does not impact the ability of the model to predict the heat transfer away from the pipe surface, generating air and water temperatures within the bounds of expectation which are dependent on the heat transfer between the two fluids.

5.5.3.1 Mesh Independence Study

Following the process established in Section 3.1.9.1, a mesh independence study was undertaken to estimate the error throughout the domain resulting from discretisation by calculating the GCI. Three meshes were created using the h method for mesh refinement to increase mesh cell density throughout the domain progressively. The main areas of refinement included the face cell size on the louvres, x-frame, and heat exchanger, as well as the volume cell size dictated by the bodies of influence (*Figure 5-27*).

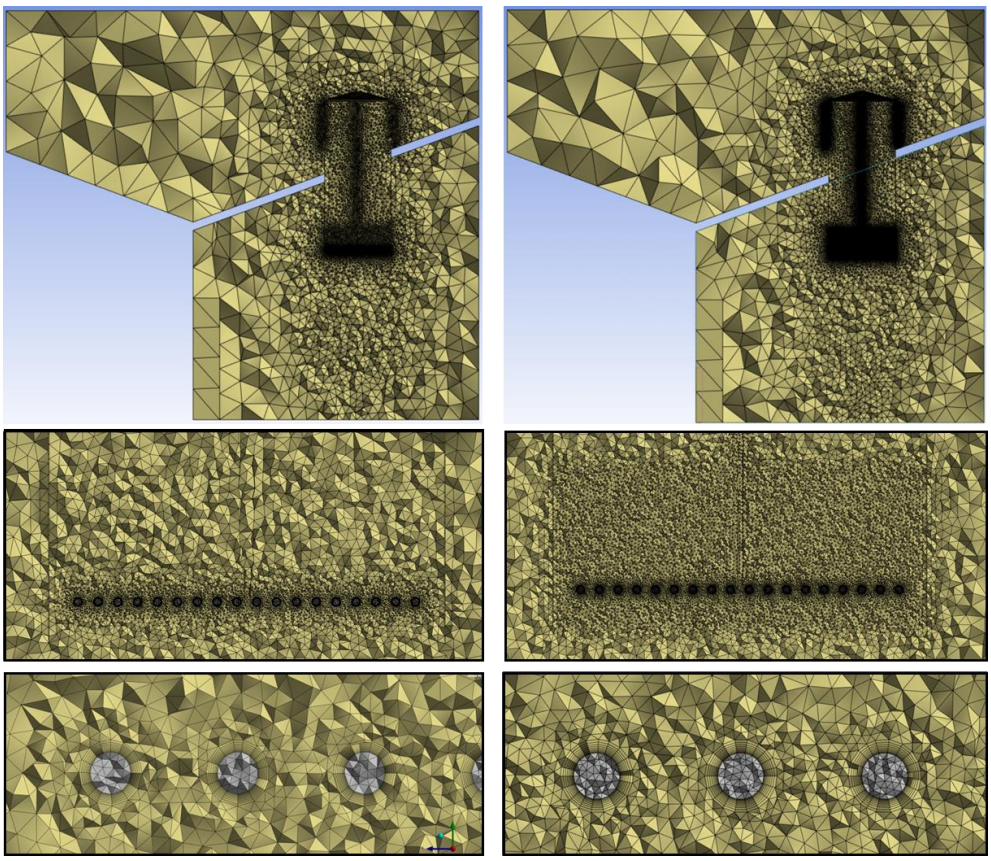

Figure 5-27 - Increasing the mesh cell density from coarse (left) to fine (right) grids

Coarse, medium, and fine tetrahedral meshes were initially created featuring 8,271, 364, 11,804,286, and 19,718,235 tetrahedral cells respectively, falling to 7,785,512, 10,799,507, and 14,967,695 cells once the domains were converted to polyhedral. Considering temperature measurements are used to validate the numerical model, temperature was selected as the most suitable parameter and was monitored at three points throughout the domain: below the pipes through the west quadrant, above the pipes through the east quadrant, and at the outlet of the RAHE.

Table 5-2 relays the results of the mesh independence study. The refinement ratio between meshes value was below the value recommended by Roache (1997), however, it is still within the bounds reported in studies that followed a similar process for establishing mesh independence (Volk et al., 2017; Pakari and Ghani, 2019; Carreto-Hernandez *et al.*, 2023). The conversion of tetrahedral to polyhedral cells is program controlled and the reduction ratio varies from mesh to mesh, limiting the control over the final mesh cell count.

Table 5-2 - Results of the mesh independence study for the field trial numerical model

	Heat exchanger outlet	Below heat exchanger (West quadrant)	Above heat exchanger (East quadrant)
N3	7,785,512	7,785,512	7,785,512
N2	10,799,507	10,799,507	10,799,507
N1	14,967,695	14,967,695	14,967,695
r_{32}	1.11	1.11	1.11
r_{21}	1.12	1.12	1.12
ϕ_3	281.74	291.23	290.25
ϕ_2	281.72	291.09	290.10
ϕ_1	281.71	291.05	290.02
p	7.92	11.65	5.89
$\phi_{21,ext}$	281.70	291.03	289.96
$\phi_{21,ext}$ error	0.003%	0.009%	0.021%
e_{21}	0.004%	0.013%	0.028%
GCI_{coarse}	0.015%	0.099%	0.116%
GCI_{fine}	0.003%	0.012%	0.026%

Figure 5-28 shows the measured and extrapolated values at each point used for the mesh independence study. The average of the local order of accuracies was 7.91,

which was used to calculate the GCI values. In this case, the coarse and fine GCI were low owing to the minimal temperature difference measured at the points between the coarse, medium, and fine meshes, inferring a high degree of confidence in the results. As a result, the medium mesh was selected for use throughout the rest of the simulations given the low temperature difference between the medium and fine mesh at each point and the high degree of confidence in the results indicated through the coarse GCI.

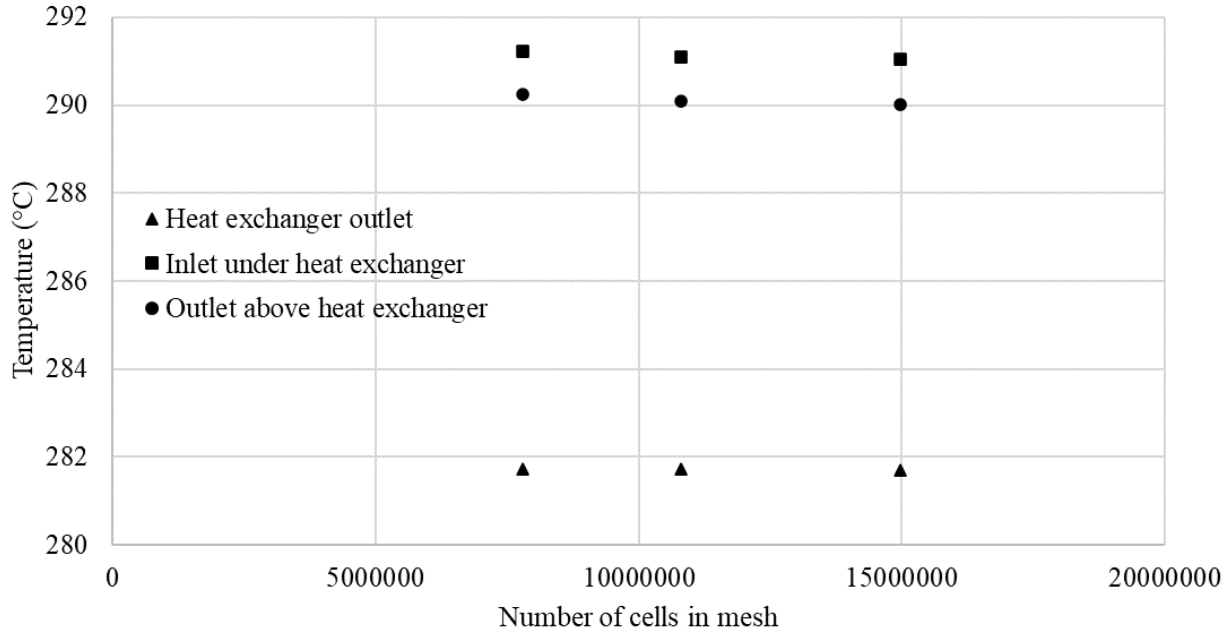

Figure 5-28 - Measured temperature with increasing grid resolution for the field trial numerical model

5.5.3.2 Mesh Quality

The mesh quality was evaluated through the orthogonal quality, skewness, and aspect ratio prior to the conversion of the tetrahedral to polyhedral elements. The average, maximum, and minimum values throughout the domain are shown below in *Table 5-3*.

Table 5-3 - Mesh quality assessment through chosen parameters for field trial numerical model

Parameter	Statistics
Aspect ratio	(max, avg) = (28.62, 2.45)
Orthogonal quality	(min, avg) = (0.08, 0.90)
Skewness	(max, avg) = (0.95, 0.30)

Removing the wind tower body from the model resulted in a higher minimum and average orthogonal quality within the mesh compared with the wind tunnel test numerical model which achieved minimum and average values of 0.03 and 0.69 respectively.

5.5.4 Boundary Conditions

Boundary conditions were applied to the numerical model to dictate thermal and physical properties throughout the domain. *Figure 5-29* shows the inlet and outlets applied to the model to control the respective fluid flows.

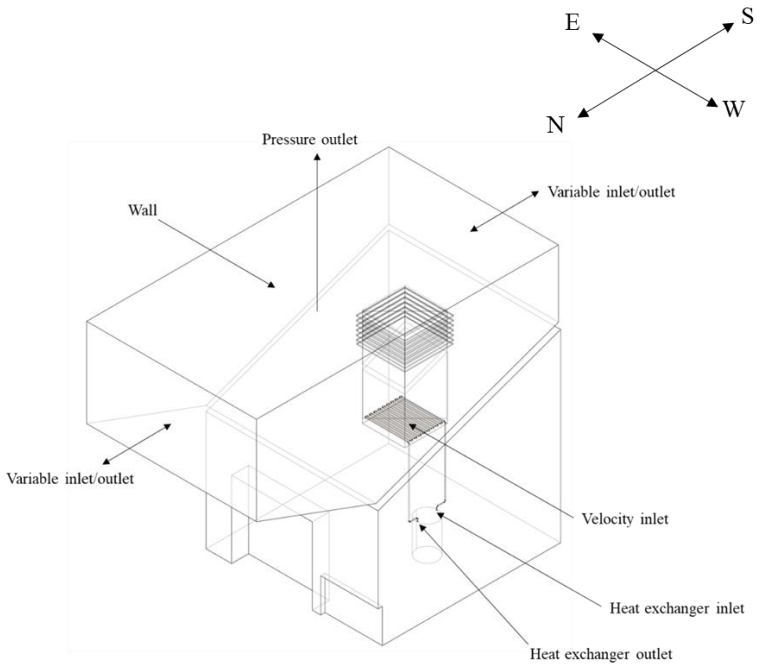

Figure 5-29 - Boundary conditions applied to the numerical model to control the flow of air and water through the domain

The wind direction is almost entirely constrained to a westerly direction due to the surrounding buildings. Consequently, while the west-facing boundary remains as an inlet throughout, the boundaries of the macro-climate on the north and south sides varied between velocity inlets and pressure outlets for each timestep depending upon the direction of the wind. The east-facing boundary is a solid wall representing the adjoining building.

The thin, two-sided wall separating the two fluid regions of the water passing through the RAHE and the air passing through the wind tower was set to coupled with a wall thickness of 1 mm. By coupling the wall, the heat transfer through it is calculated from the solution in the adjacent cells on either side, where the program applies the resistance to heat transfer through the wall according to the wall's thickness and the material's thermal conductivity.

To validate the numerical model a transient simulation was conducted using boundary conditions equal to those recorded throughout the field trial. Testing took place on two dates over several hours, with the inlet conditions and results between 12:04 – 14:09 PM on 12/08/22 selected to validate the numerical model. The transient simulation was conducted over 26 timesteps, each lasting five minutes to remain consistent with the inlet conditions provided by the weather station. The wind velocity, temperature, direction, water inlet temperature, and velocity measured throughout this period were applied as boundary conditions for each timestep of the transient simulation.

Table 5-4 indicates the values applied over each timestep. As the wind direction constantly changes, the velocity was resolved into the horizontal X and Z components to replicate the incident wind angle onto the wind tower (

Table 5-5). The model was oriented so that the positive X direction was due west and the positive Z direction was due north, where west is the zero angle.

Table 5-4 - Transient boundary conditions for numerical model validation

Time	Timestep No.	Air inlet temp (°C)	Air X velocity (m/s)	Air Z velocity (m/s)	Inlet water temp (°C)	Water velocity (m/s)
12:04	1	27.7	-1.41	-1.41	13.57	0.56
12:09	2	27.8	-0.85	-0.85	13.58	0.56
12:14	3	27.1	-0.99	-0.99	13.66	0.56
12:19	4	26.7	-1.48	-0.61	13.65	0.56
12:24	5	27.4	-1.66	-0.69	13.64	0.56
12:29	6	27.4	-2.30	0.00	13.67	0.56
12:34	7	27.5	-1.11	0.46	13.78	0.56
12:39	8	27.3	-1.63	1.63	13.80	0.56
12:44	9	28.4	-1.34	-1.34	13.82	0.56
12:49	10	27.1	-1.48	0.61	13.88	0.56
12:54	11	27.3	-1.94	0.80	13.88	0.56
12:59	12	28.6	-1.02	0.42	13.90	0.56
13:04	13	28.1	-0.96	-2.31	14.02	0.56
13:09	14	27.1	-1.29	-0.54	14.05	0.56
13:14	15	28.0	-1.85	0.77	14.13	0.56
13:19	16	28.0	-1.94	-0.80	14.17	0.56
13:24	17	28.8	-0.85	-0.85	14.12	0.56
13:29	18	29.3	-1.39	-0.57	14.18	0.56
13:34	19	28.6	-1.60	0.00	14.26	0.56
13:39	20	28.6	-2.03	-0.84	14.30	0.56
13:44	21	28.3	-1.94	-0.80	14.44	0.56
13:49	22	29.4	-0.92	-0.92	14.42	0.56
13:54	23	29.2	-1.76	-0.73	14.42	0.56
13:59	24	29.2	0.88	-2.12	14.54	0.56
14:04	25	29.2	-0.84	-2.03	14.53	0.56
14:09	26	29.4	-1.27	-1.27	14.61	0.56

Table 5-5 - Decomposition of wind velocity into X and Z components

Time	Timestep No.	Wind Velocity (m/s)	Wind Direction	Wind Angle (degrees)	X velocity component (m/s)	Z velocity component (m/s)
12:04	1	2	NW	45	-1.41	-1.41
12:09	2	1.2	NW	45	-0.85	-0.85
12:14	3	1.4	NW	45	-0.99	-0.99
12:19	4	1.6	WNW	22.5	-1.48	-0.61
12:24	5	1.8	WNW	22.5	-1.66	-0.69
12:29	6	2.3	West	0	-2.30	0.00
12:34	7	1.2	WSW	-22.5	-1.11	0.46
12:39	8	2.3	SW	-45	-1.63	1.63
12:44	9	1.9	NW	45	-1.34	-1.34
12:49	10	1.6	WSW	-22.5	-1.48	0.61
12:54	11	2.1	WSW	-22.5	-1.94	0.80
12:59	12	1.1	WSW	-22.5	-1.02	0.42
13:04	13	2.5	NNW	67.5	-0.96	-2.31
13:09	14	1.4	WNW	22.5	-1.29	-0.54
13:14	15	2	WSW	-22.5	-1.85	0.77
13:19	16	2.1	WNW	22.5	-1.94	-0.80
13:24	17	1.2	NW	45	-0.85	-0.85
13:29	18	1.5	WNW	22.5	-1.39	-0.57
13:34	19	1.6	West	0	-1.60	0.00
13:39	20	2.2	WNW	22.5	-2.03	-0.84
13:44	21	2.1	WNW	22.5	-1.94	-0.80
13:49	22	1.3	NW	45	-0.92	-0.92
13:54	23	1.9	WNW	22.5	-1.76	-0.73
13:59	24	2.3	NNW	-247.5	0.88	-2.12
14:04	25	2.2	West	67.5	-0.84	-2.03
14:09	26	1.8	NW	45	-1.27	-1.27

Following validation, simulations were conducted under steady-state conditions to evaluate the wind tower's and RAHE's performance when varying inlet air temperature, wind speed, water velocity, and water temperature (*Table 5-6*). A steady state model indicates performance under specific boundary conditions. The boundary conditions were varied to measure performance in a range of scenarios that could be expected in a typical summer or winter.

Table 5-6 - Summary of boundary conditions for field trial numerical model

Discretisation scheme	Second order upwind
Algorithm	SIMPLE
Time scheme	Steady State
Viscous model	k-epsilon
Wall functions	Standard
Air velocity (m/s)	1 - 5
Air temperature (°C)	0 - 35
Water velocity (m/s)	0.5 - 4.5
Water temperature (°C)	8 - 30

Simulations were conducted with heat exchanger models featuring one, two, and three pipe layers, exploring the impact on ventilation rates to compare with the wind tunnel test. Subsequently, the air inlet temperature was altered to represent ambient temperatures experienced throughout a UK summer and winter to determine the potential of the system to provide cooling and heating.

For the heat exchanger models featuring more than one pipe layer, the flow direction is such that the water travels laterally through the lowest row, moving upwards to create the greatest temperature difference between the fluids at all points throughout the heat exchanger. The impact of adding fins to the heat exchanger was also explored to increase the surface area available for heat transfer, recording the impact on

volumetric flow rate, pressure drop, cooling of fresh air, and thermal energy recovery through the RAHE.

5.5.5 Numerical Model Validation

The transient simulation and experiment results were compared throughout the selected testing period to determine if the numerical model could accurately replicate the experimental conditions. As insufficient velocity data points could be captured simultaneously under a constantly changing inlet velocity only temperature was used to validate the model, where the air temperature below the heat exchanger through the west quadrant of the wind tower and the water temperature at the outlet of the RAHE were selected as the most relevant data points.

5.5.5.1 Air Temperature

Figure 5-30 below shows the inlet air temperature versus the average air temperature below the heat exchanger at each timestep for the experimental and numerical results. Wind speed and direction are also shown to give some context to the variation in the amount of cooling achieved at each timestep.

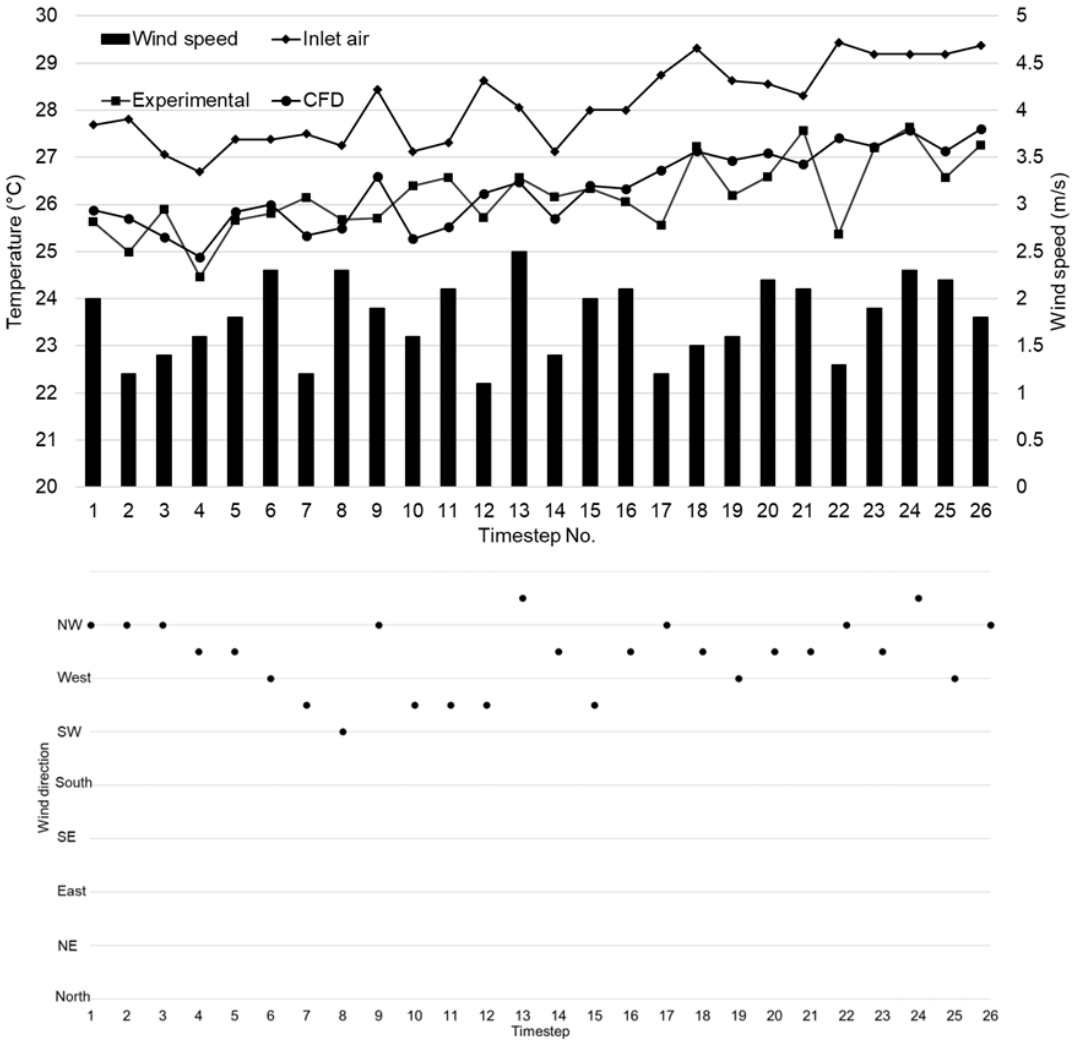

Figure 5-30 – Comparison between experimental and numerical air temperature below run-around heat exchanger (top) and wind direction at each timestep (bottom)

Dividing the average air temperature below the heat exchanger by the inlet temperature the dimensionless ratio between the two is found for the experimental and numerical results (*Figure 5-31*).

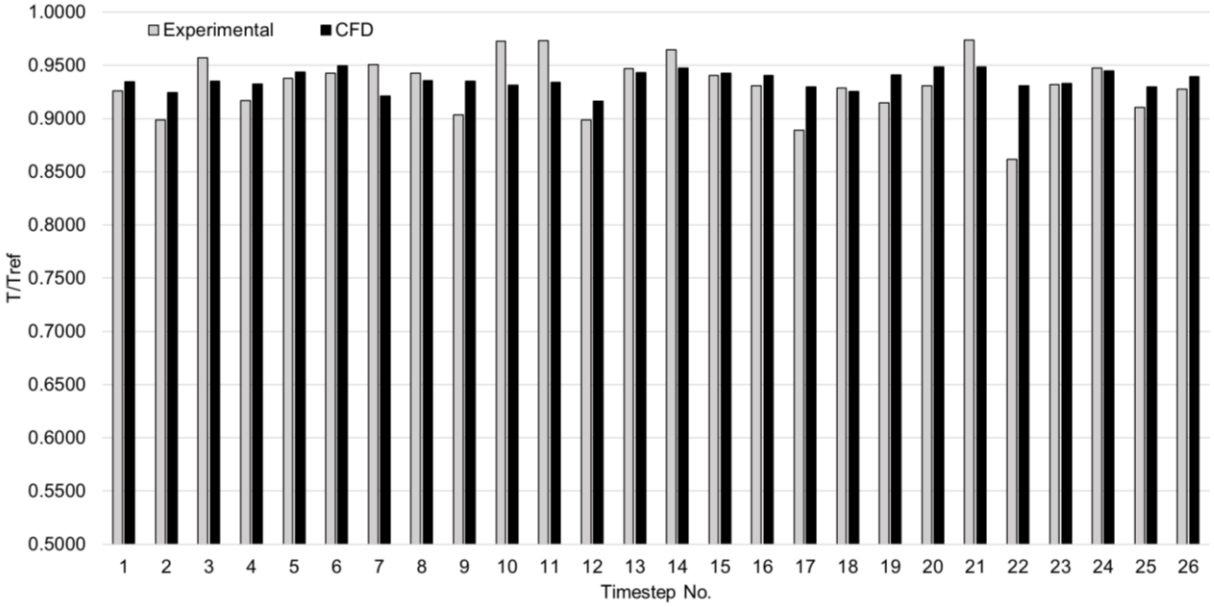

Figure 5-31 – T/T_{ref} for precooling of fresh air over the heat exchanger

The relative error between the temperatures measured at each timestep varied between -8% to 4.2%, giving a normalised average error of 2.1% over the data set. The greatest errors occur at timesteps 10, 11, 17, and 22, where timesteps 10 and 11 overestimate the amount of cooling and timesteps 17 and 22 underestimate the amount of cooling achieved. Overall, the numerical model underpredicted the amount of cooling on 16 of the 26 timesteps by an average of 2.2% and overpredicted on 10 of the 26 timesteps by an average of 2.0%.

Some discrepancy may occur due to changes in the wind velocity and direction after the weather station provides the initial reading. Air temperature, wind speed, and wind direction were measured at the start of each five-minute interval by the weather station, however each parameter was not constant throughout this period. As the numerical model assumes these boundary conditions are constant throughout each timestep differences can arise between the numerical and experimental results. This could be solved using a weather station that provides data at smaller time intervals but

would necessitate running transient simulations at much smaller timesteps, drastically increasing the simulation time.

5.5.5.2 Water Temperature

Figure 5-32 compares the experimental and numerical results of the outlet vs. inlet temperature. The inlet water temperature increased steadily throughout the experiment from 13.6 to 14.6 °C as the chiller could not sufficiently cool the body of water in the tank. The experimental results show a consistent temperature increase of around 1 °C between the inlet and outlet of the heat exchanger. In contrast, the CFD results show more variety, recording a minimum temperature increase of 0.54 °C and a maximum of 1.24 °C.

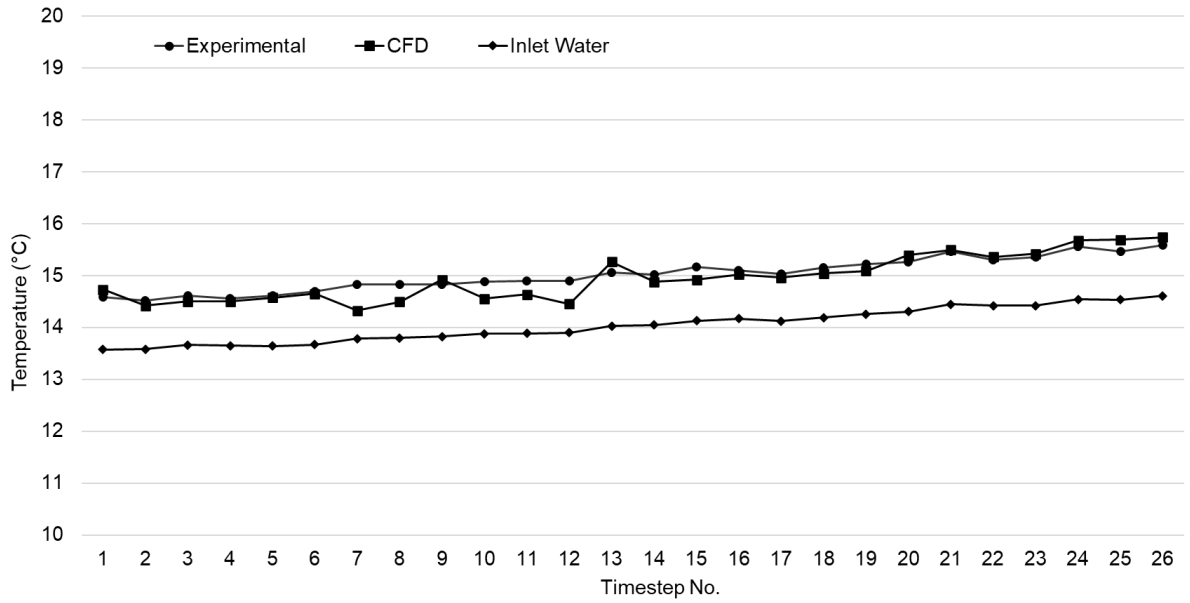

Figure 5-32 - Experimental vs. CFD results for run-around outlet temperature

Figure 5-33 shows the normalised results for the outlet temperature where the reference temperature is equal to the inlet temperature of the heat exchanger. The average error between the experimental and numerical results is 1.1%, peaking at 3.4% at timestep 7.

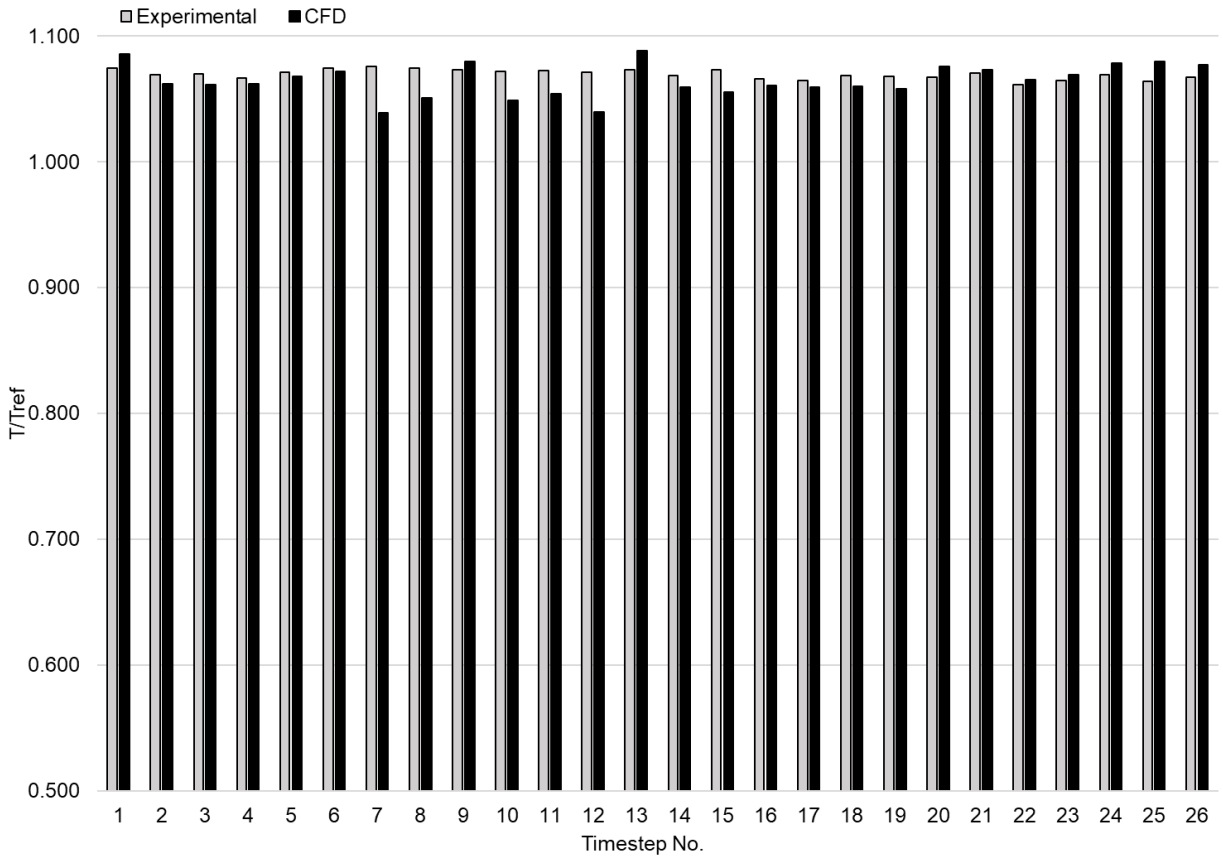

Figure 5-33 - T/T_{ref} at heat exchanger outlet

The increase in water temperature through the heat exchanger is more sensitive to changes in wind velocity and direction for the numerical model than for the experimental results. Experimentally, the likely variation of the boundary conditions over each five-minute period results in a consistent temperature increase through the heat exchanger as the walls of the copper pipes act as a buffer to any sudden changes. Applying constant boundary conditions over each five-minute timestep in the numerical model impacts the outlet temperature to a greater degree.

As has previously been shown, errors relating to passive ventilation simulations are often high given the low driving forces through the systems resulting in a greater degree of local variation. Therefore, trends and direct point-by-point comparisons are made. Across the results gathered for both the fresh air and heat exchanger

temperatures the general trends produced through the numerical model were sufficiently similar to those produced through physical testing and the percentage error was well within the reported range for passive ventilation simulations (Chen and Srebric, 2002; Hughes and Mak, 2011; Connor et al., 2019).

5.6 Results

Following the validation of the numerical model steady-state simulations were conducted using wind tower models with differing heat exchanger configurations. The impact of an increasing number of pipe layers on the volumetric flow rate was first explored before evaluating the pressure drop over the heat exchanger. Following this the potential to provide heating and cooling to fresh air whilst recovering thermal energy was determined, including the impact of the addition of fins on the performance of the heat exchanger.

5.6.1 Velocity

Inlet velocities of 1 – 5 m/s were applied to the model at a wind angle of zero degrees to understand how the heat exchanger installation impacts the volumetric flow rate into the room below. The air velocity was measured at six points below the heat exchanger through the wind tower inlet quadrant as described in section 4.3.3.1.

Figure 5-34 shows the effect of increasing inlet velocity on the volumetric flow rate through the wind tower for heat exchanger models featuring one, two, and three rows of pipes. It is predicted that for a wind tower featuring a heat exchanger with three pipe layers at an inlet velocity of 1 m/s the volumetric flow rate would be 0.09 m^3/s, equivalent to 90 L/s. As with the wind tunnel test, increasing the number of pipes through the wind tower decreases the volumetric flow rate through the inlet quadrant.

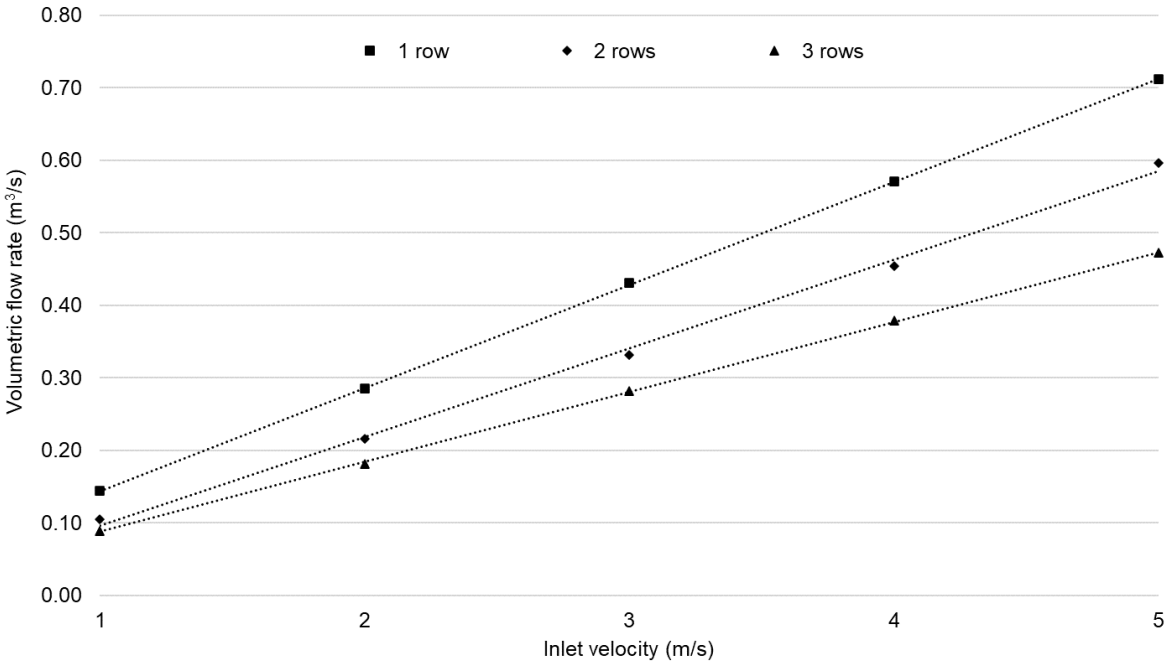

Figure 5-34 - Volumetric flow rate through the wind tower inlet with increasing inlet velocity

Comparing the simulated results of the wind tunnel test and field trial, the field trial numerical model reported volumetric flow rates between 5 and 22% lower than those reported through the wind tunnel test at the same inlet velocities (*Table 5-7*). The lower flow rates likely occur due to the length of the ducting installed for the field trial, allowing more time for natural interruptions to the flow such as recirculation areas to occur within the inlet quadrant and a dissipation of the wind-driven flow with decreasing height.

Table 5-7 – Simulated volumetric flow rates through the wind tower for the wind tunnel test and field trial

	Volumetric flow rate (m^3/s), 1 row		Volumetric flow rate (m^3/s), 2 rows		Volumetric flow rate (m^3/s), 3 rows	
Inlet velocity (m/s)	Field trial	Wind tunnel test	Field trial	Wind tunnel test	Field trial	Wind tunnel test
1	0.14	0.15	0.10	0.12	0.09	0.10
2	0.29	0.31	0.22	0.25	0.18	0.22
3	0.43	0.47	0.33	0.38	0.28	0.35
4	0.57	0.62	0.45	0.51	0.38	0.48
5	0.71	0.78	0.60	0.64	0.47	0.60

Figure 5-35 below compares the velocity distribution at points A – F (Figure 4-10) below the pipes through the wind tower inlet quadrant for models featuring a single

pipe layer at an inlet velocity of 1 m/s. The field trial model predicts a lower velocity at points B and C but higher at point E, whereas the values at A, D, and F are relatively similar.

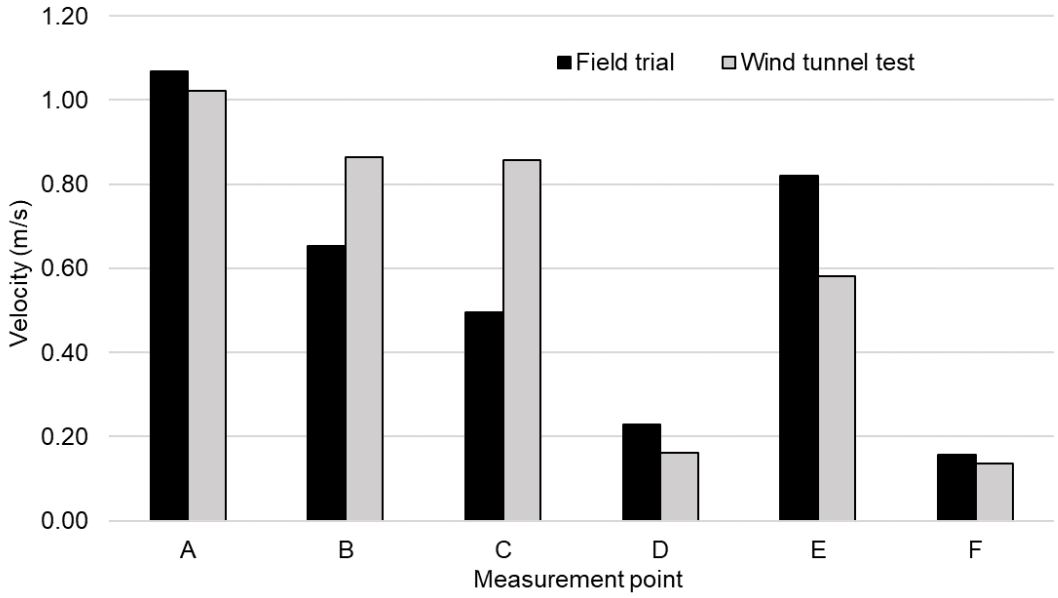

Figure 5-35 - Velocity at points below the heat exchanger for the wind tunnel test and field trial

Applying a wind angle of zero degrees ensures that one quadrant of the wind tower behaves as an inlet and the remaining three as outlets, representing the minimum volumetric flow rate through the wind tower relative to non-zero wind angles which will induce higher flow rates. Several studies have explored the impact of wind angle on volumetric flow rate through wind towers, where the maximum ventilation rate for a four-sided wind tower was achieved at a wind angle of 45 ° and was shown to be 47% higher than the volumetric flow rate at 0 ° for the same inlet velocity (Calautit and Hughes, 2014a). Using this prediction, the total volumetric flow rate for the three-row heat exchanger could be as high as 0.13 m^3/s at an inlet velocity of 1 m/s when the wind angle was 45 °.

Figure 5-36 shows the difference in the midplane velocity through the inlet quadrant between the 1 and 3 row heat exchangers at a wind speed of 5 m/s. The interruption to the flow by the heat exchanger is limited for the single row, resulting in a fast-moving air jet down into the room below. In comparison, the three-row heat exchanger incurs a more significant reduction in velocity but retains the air jet down into the room below. Owing to the water tank's placement, the air jet makes contact with it and spreads throughout the room. If this were a person, they would likely experience some discomfort due to the draught created directly onto them.

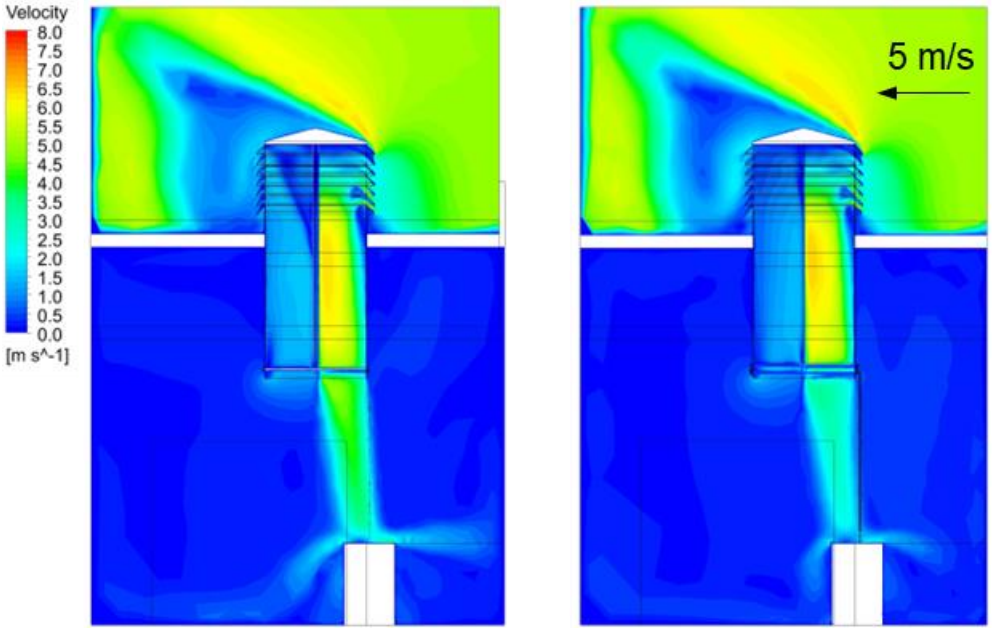

Figure 5-36 - Midplane velocity through the wind tower at 5 m/s wind speed for 1 row (left) and three rows (right) heat exchangers

Referring to British Standards 5925:1991 for 'Ventilation principles and designing for ventilation', minimum ventilation rates of 0.8 and 1.3 L/s per m^2 of floor area are established for factories and offices/schools respectively (British Standards, 1991). For occupants within these spaces a minimum ventilation rate of 5 L/s per occupant is stipulated

The recommended secondary school classroom size for 20 occupants is 35 m^2 (Department for Education, 2014) which is used to find the ventilation rate in L/s/m^2 and the L/s per occupant for the wind tower and heat exchanger comprised of three rows of pipes. Table 5-8 below shows the ventilation rates in L/s/m^2 and L/s per occupant produced by the wind tower against the levels stipulated in BS5952:1991.

Table 5-8 - BS5952:1991 recommendations vs. CFD

	BS5952:1991				
Wind velocity (m/s)	Factory (L/s/m^2)	Office/School (L/s/m^2)	CFD (L/s/m^2)	BS5952:1991 (L/s per occupant)	CFD (L/s per occupant)
1	0.8	1.3	2.54	5	4.35
2	0.8	1.3	5.18	5	8.65
3	0.8	1.3	8.06	5	12.68
4	0.8	1.3	10.83	5	17.34
5	0.8	1.3	13.50	5	21.84

The wind tower provides sufficient air per m^2 for factories and offices/schools at all simulated wind speeds. For a small classroom with 20 occupants, the ventilation rate falls below the minimum 5 L/s per occupant at 1 m/s wind speed, however, it easily exceeds this as external wind speed increases (Figure 5-37). In such environments a backup mechanical ventilation system is required to ensure compliance with regulations when wind speeds are low. The average UK wind speed is approximately 4.5 m/s depending on the location (Hughes and Ghani, 2008). At this velocity, for a 35 m^2 classroom with 20 occupants, the wind tower produces an approximate ventilation rate of 12.1 L/s/m^2 or 19.6 L/s per occupant, 12 and 20 times higher respectively than the minimum requirements.

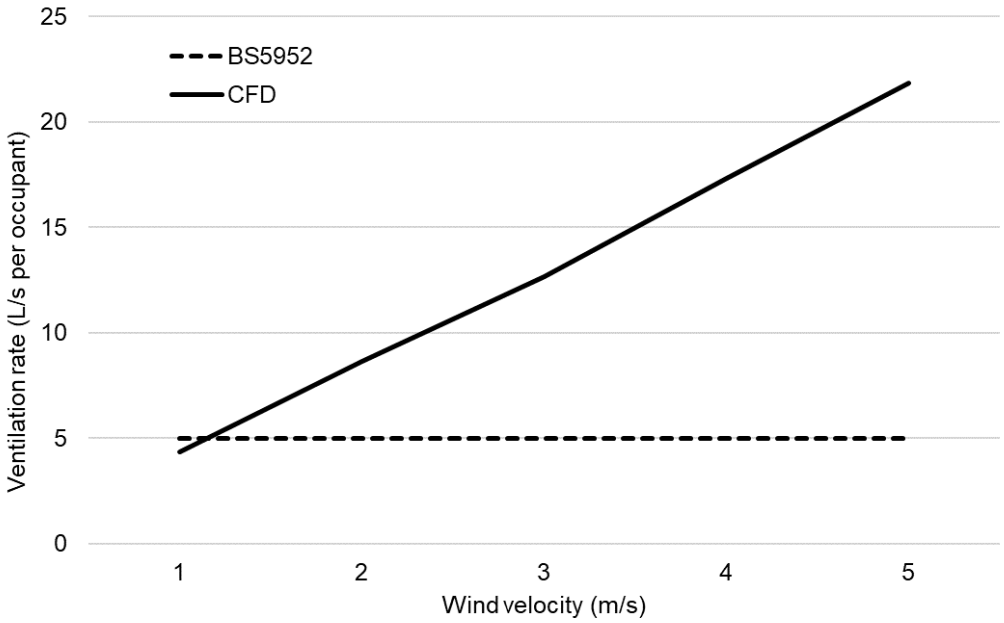

Figure 5-37 - Recommended ventilation rate per occupant versus CFD results

Although the system can consistently exceed required ventilation rates, at higher velocities an airflow can negatively impact the thermal comfort of the occupants. In case of high winds, automated dampers are necessary to restrict airflow into the indoor environment.

Upon establishing the volumetric flow rate through the wind tower and three-row heat exchanger model was sufficient, further simulations and analysis were conducted using this model to maximise the heating, cooling, and thermal energy recovery through the RAHE whilst saving time on the number of simulations required.

5.6.2 Pressure

Figure 5-38 shows the contour for static pressure through the centre of the wind tower when the inlet velocity is 5 m/s. A region of high pressure occurs at the windward face of the wind tower and in the upper section of the inlet quadrant as the flow makes contact with the louvres and internal x-frame. A corresponding region of low pressure occurs on the leeward face of the wind tower, lower than the pressure within the room,

drawing air through the east facing exhaust quadrant. A region of low pressure also occurs near the inside wall of the wind tower inlet quadrant as the fast-moving air moves towards the centre of the channel.

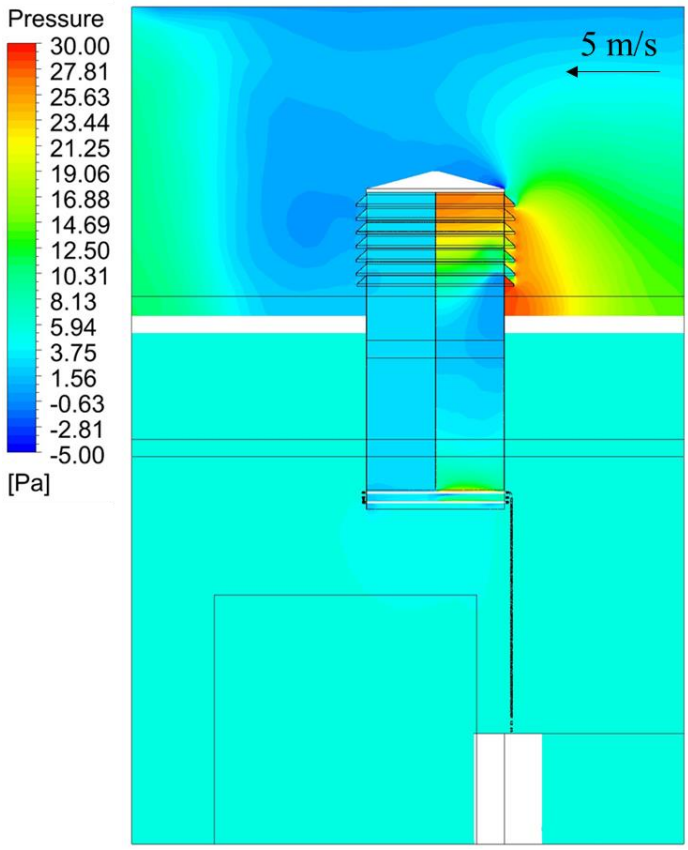

Figure 5-38 - Pressure contour through the midplane of the wind tower and three-row heat exchanger model

Figure 5-39 shows the average pressure through the inlet quadrant with decreasing height where 0 m is in line with the base of the wind tower, just below the bottom row of the heat exchanger.

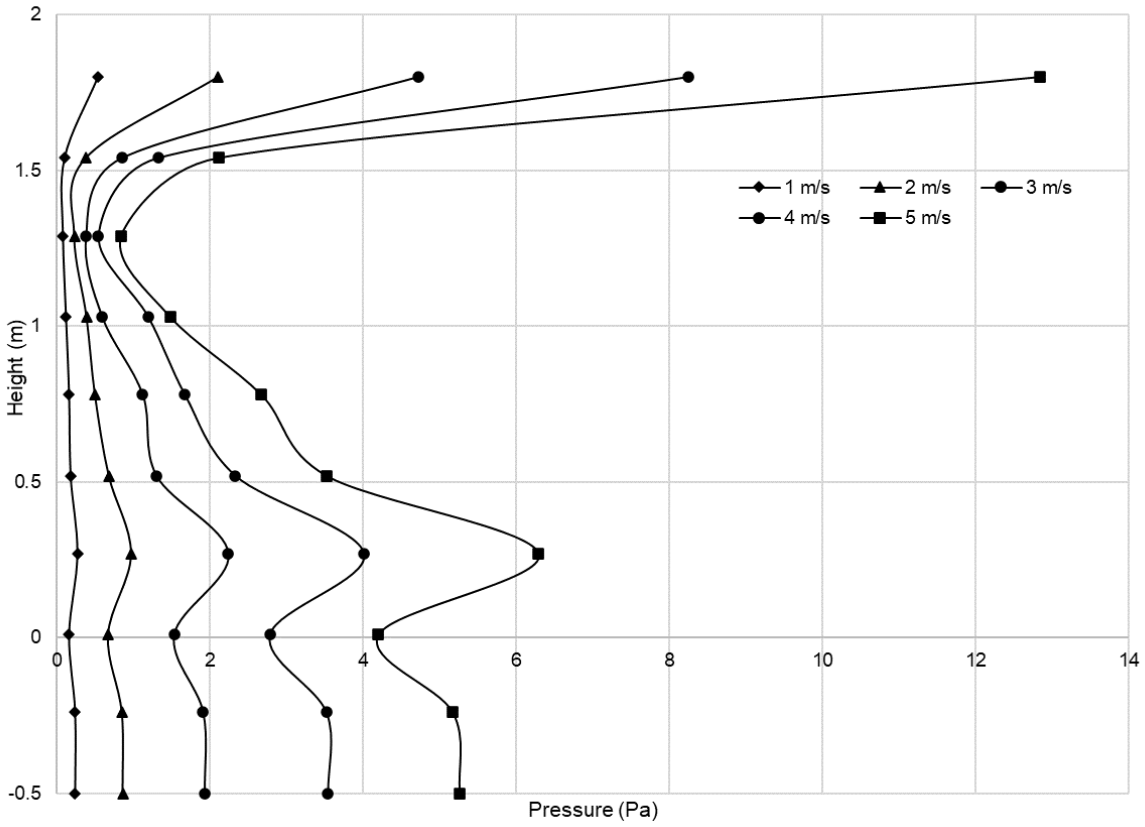

Figure 5-39 - Pressure gradient through the wind tower inlet quadrant with three pipe layers

The pressure is seen to fall quickly below the louvres before rapidly increasing just above the heat exchanger due to the blockage of the channel. The pressure drop over the heat exchanger from 0.25 m to 0 m increases from 0.11 Pa at 1 m/s to 2.09 Pa at 5 m/s, resulting in supply pressures of 0.24 and 5.26 Pa respectively. The pressure drop over the heat exchanger is comparable with the pressure loss calculated by Hviid and Svenson (2011) for a heat exchanger designed for use within a passive ventilation system.

Figure 5-40 and Figure 5-41 compare the pressure through the inlet channel for the heat exchangers with two and three pipe layers.

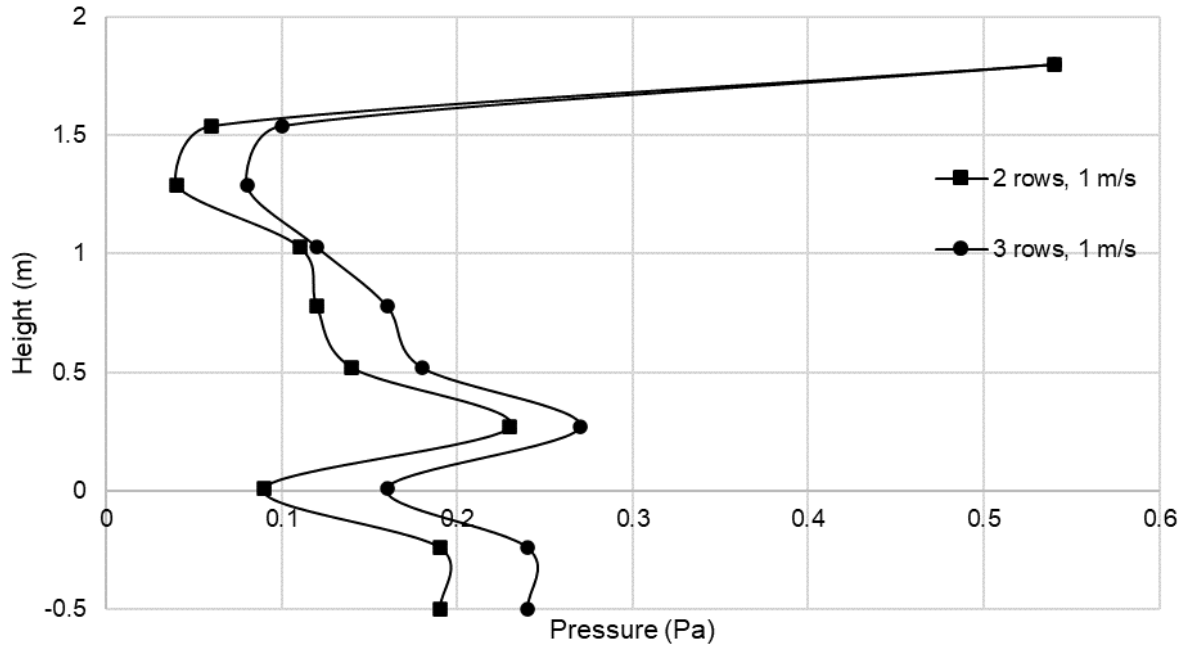

Figure 5-40 - Pressure through the wind tower inlet channel for the heat exchanger models with two and three pipe layers under 1 m/s wind speed

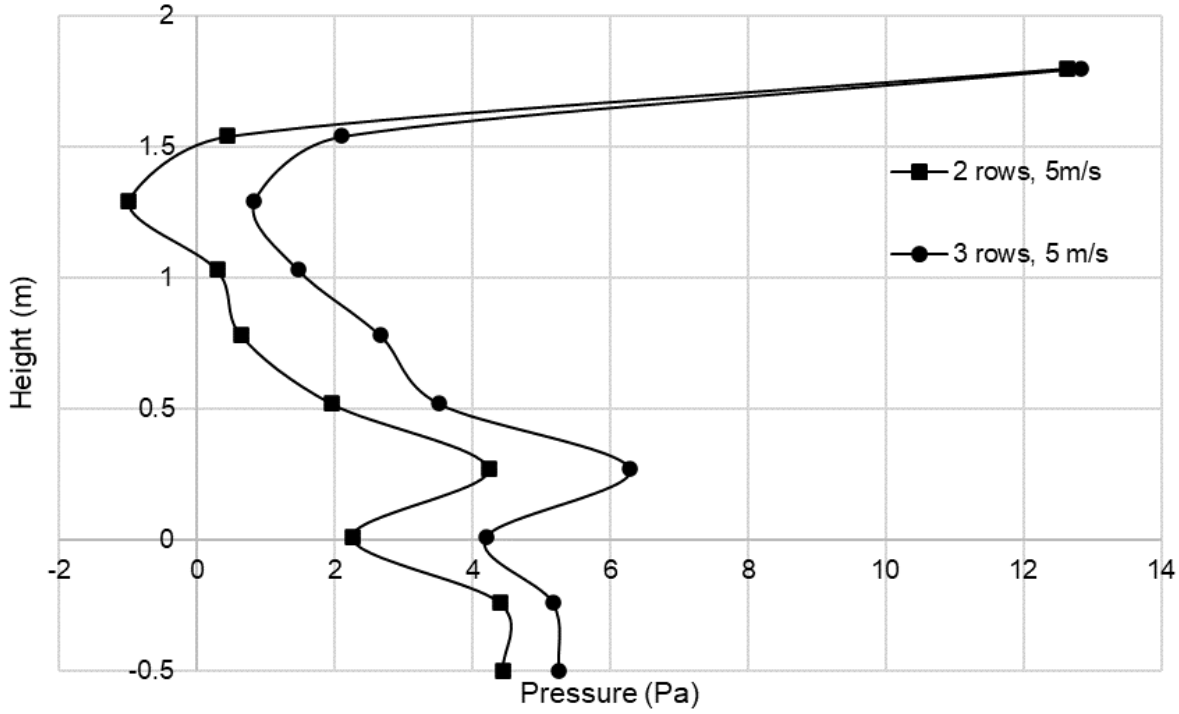

Figure 5-41 - Comparison of the pressure through the wind tower inlet channel for the heat exchanger models with two and three pipe layers under 5 m/s wind speed

When the inlet velocity was 1 m/s, the difference in pressure through the inlet channel between the two models was minimal, with the average pressure through the two-layer

model marginally lower due to the higher velocity. Under a wind speed of 5 m/s the difference between the two- and three-layer models is much more significant. Despite the differences in pressure above the heat exchanger, the decrease in pressure over the heat exchanger remained relatively consistent between the two models. At a wind speed of 5 m/s, a pressure drop of 1.98 and 2.09 Pa was recorded for the two- and three-layer heat exchanger models respectively. At a wind speed of 1 m/s, the pressure drop was 0.14 and 0.11 Pa for the two- and three-layer models respectively.

5.6.3 Heating and Cooling

Simulations were conducted to predict the increase or decrease in fresh air temperature over the heat exchanger. For all simulations the inlet air velocity was 3 m/s and the volumetric flow rate of water through the run-around was 0.077 L/s at a velocity of 0.5 m/s. For the cooling simulations, air temperature was increased from 20 to 35 °C in increments of 3 °C while water temperature remained constant at 8 °C. For the heating simulations air temperature was increased from 0 to 15 °C while water temperature remained at 30 °C. The air temperatures were chosen to represent the temperatures experienced throughout a typical UK summer or winter. The cold-water temperature was within the cold injection temperatures reported in the literature. The hot water temperature is above the typical warm well injection temperature for ATES which would necessitate using a heat pump to increase the water temperature after extraction.

A wind angle of 0 ° was applied ensuring a single quadrant behaves as an inlet with the other three as outlets. *Figure 5-33* indicates the average change in fresh air temperature over the heat exchanger with three rows of pipes. The change in air

temperature over the heat exchanger is plotted against the difference in temperature between the inlet temperatures of the air and water.

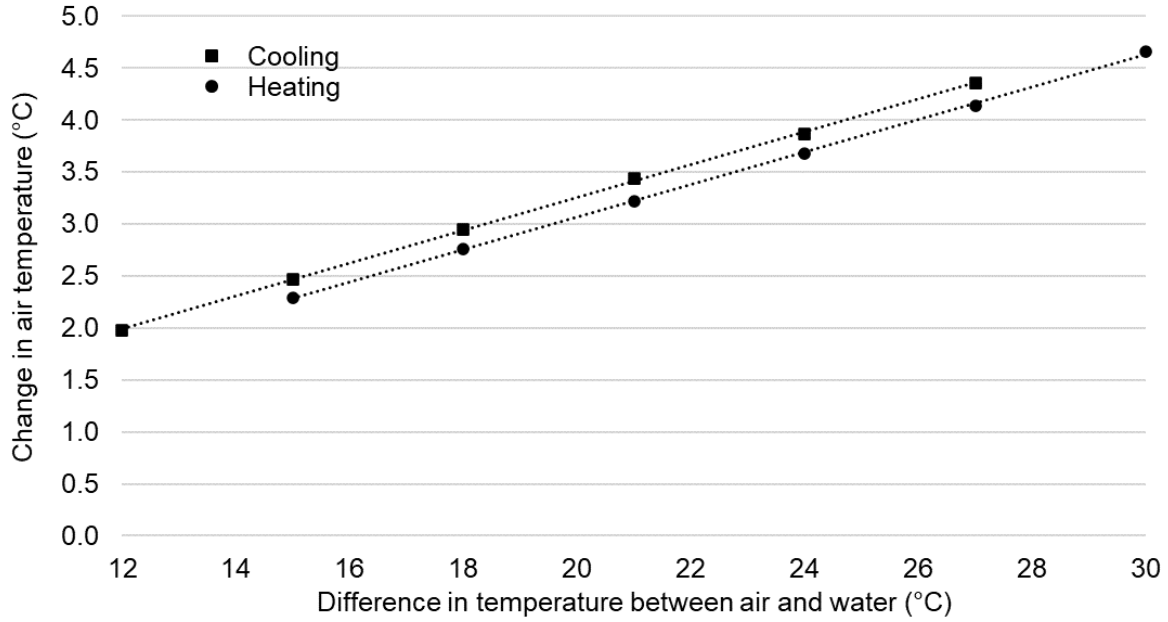

Figure 5-42 - Heating and cooling of fresh air through the RAHE

At a temperature difference of 27 °C the air temperature is increased by 4.14 °C when heating and reduced by 4.36 °C when cooling. Although only a small difference this is consistent throughout the corresponding heating and cooling simulations, likely due to the minor differences in air density arising from the differences in air temperature. The change in temperature over the heat exchanger increases linearly with an increasing temperature difference between the fluids, with a 3 °C increase resulting in an additional 0.48 °C of heating or cooling on average.

Figure 5-43 shows a temperature contour through the wind tower inlet when the inlet air and water temperatures are 35 and 8 °C respectively. A greater amount of cooling occurs towards the outer edges of the quadrant as the velocity is lower here than through the centre. Some short-circuiting occurs whereby fresh air exits directly through the adjacent wind tower quadrants without mixing throughout the room.

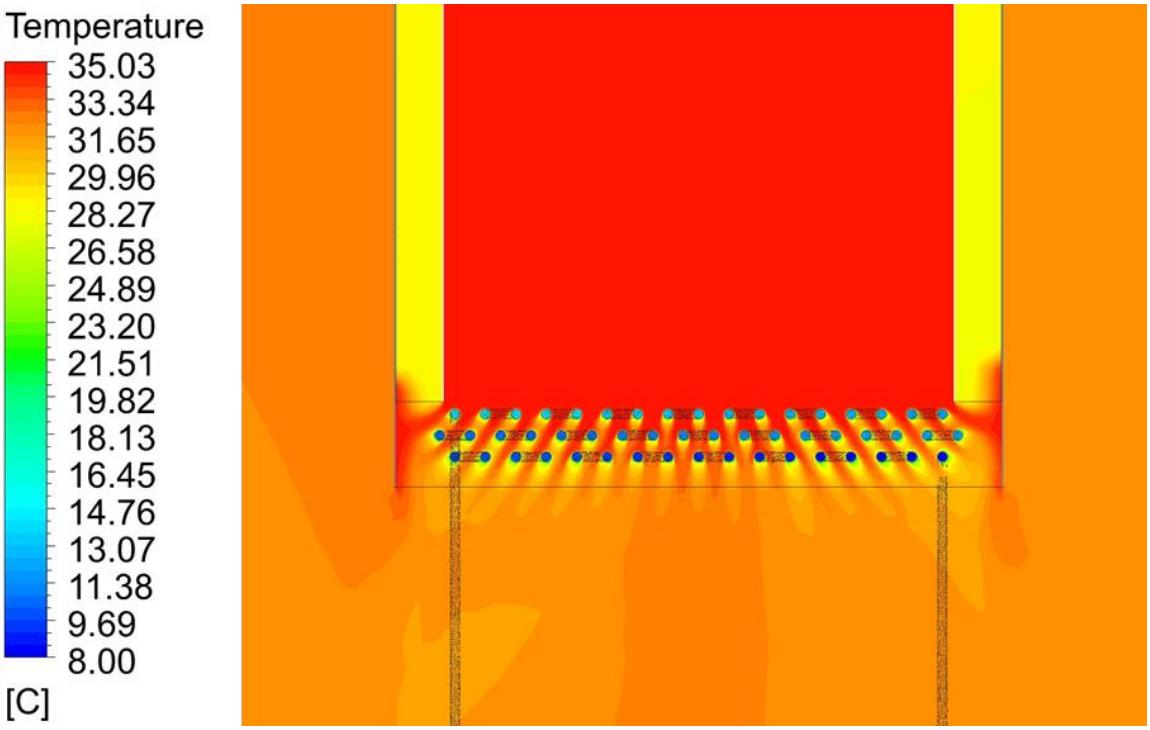

Figure 5-43 - Pre-cooling of fresh air over the heat exchanger

Figure 5-44 shows the cooling through all four quadrants under the same boundary conditions. Despite the temperature difference between the two fluids being lower through the exhaust channels than through the inlet quadrant, the lower velocity compensates for this resulting in a comparable temperature decrease to the stale air exiting through the wind tower.

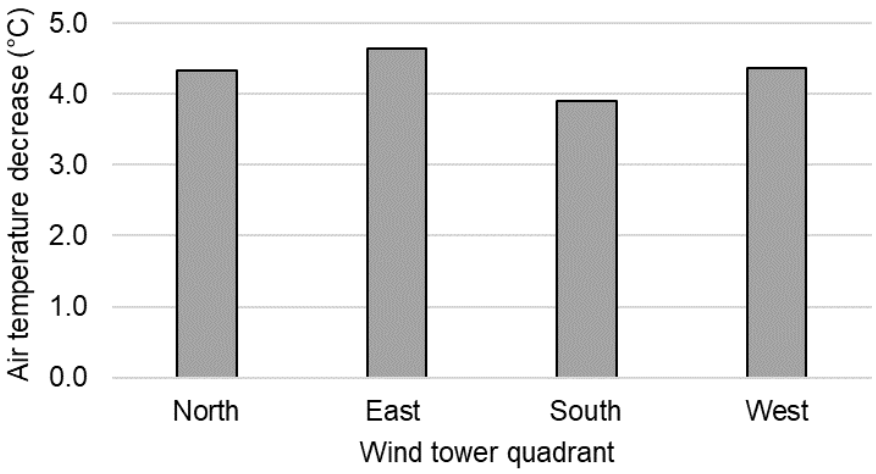

Figure 5-44 - Fresh air temperature decrease through each wind tower quadrant

Figure 5-45 shows the difference in water temperature between the inlet and outlet of the RAHE under the same boundary conditions. At a temperature difference of 27 °C the water temperature was increased by 6.15 °C for both heating and cooling simulations in contrast to the difference in air temperature that was reported. The change in water temperature through the RAHE depends on the inlet and exhaust air temperature through the wind tower. Given that more quadrants behave as outlets, the exhaust temperature significantly impacts the change in water temperature through the RAHE.

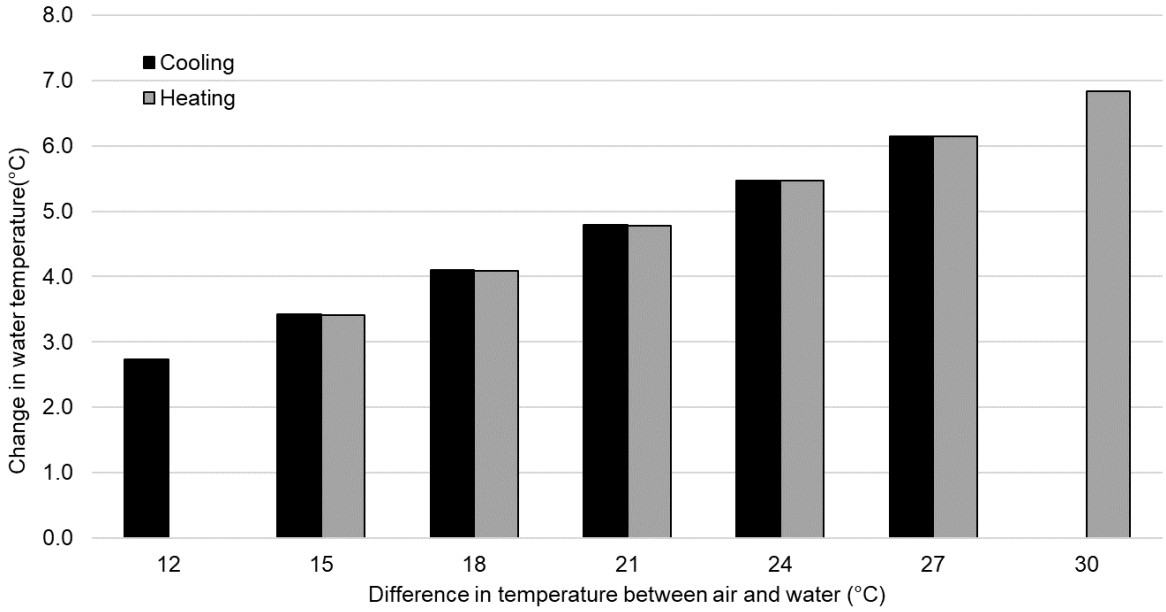

Figure 5-45 – Water temperature increase through the RAHE

When cooling the greater temperature decrease to the fresh air through the inlet results in a marginally lower air temperature within the room and therefore a smaller temperature difference between the two fluids through the outlets, resulting in less heat transfer through the exhaust quadrants. In contrast, the change in fresh air temperature when heating was smaller, resulting in a greater temperature difference between the two fluids through the wind tower outlet and a greater amount of heat transfer between them. Consequently, the total heat transfer to or away from the water

passing through the RAHE is balanced between all four quadrants resulting in approximately the same temperature change under both heating and cooling conditions.

The change in water temperature is greater than the change in air temperature resulting from the additional thermal energy transferred through the outlet quadrants of the wind tower. Given the widespread use of HVAC systems towards creating thermally comfortable environments, it would be anticipated that the exhaust temperature through the wind tower would be higher or lower than the fresh air delivery temperature from the wind tower in the winter and summer respectively. As the change in water temperature is also dependent upon the outlet temperature through the wind tower this would result in a smaller measurable temperature difference between the inlet and outlet of the heat exchanger and less thermal energy recovered in a single pass. In this case, imposing a system control whereby water was recirculated until it reached a specific temperature would increase the sensible energy recovery, as with each pass through the RAHE the amount of cooling or heating affected to the fresh air would decrease.

5.6.4 Wind Speed

The wind speed onto the wind tower was increased from 1 to 5 m/s to determine the impact on the cooling of fresh air and the sensible energy recovery through the heat exchanger. As well as measuring the change in temperature through the inlet quadrant, the temperature through each of the three outlet quadrants (north, east, and south) was also measured. The inlet air and water temperatures were kept constant at 35 and 8 °C respectively, with the velocity of the water through the RAHE at 0.5

m/s. Table 5-9 below shows the temperature change to the fresh air through each quadrant and the increase in water temperature through the heat exchanger.

Table 5-9 – Change in fluid temperatures throughout wind tower and RAHE

Inlet velocity (m/s)	West (°C)	North (°C)	East (°C)	South (°C)	Thermal loop outlet (°C)
1	-6.70	-6.14	-7.18	-6.17	2.84
2	-5.32	-5.00	-4.83	-5.13	4.78
3	-4.36	-4.34	-3.90	-4.22	6.15
4	-3.84	-3.59	-3.96	-3.91	7.41
5	-3.75	-3.02	-3.68	-3.42	8.43

As with the wind tunnel test, the cooling of fresh air decreases with increasing wind speed, reaching a minimum and maximum of 3.75 and 6.70 °C of cooling at 5 and 1 m/s respectively (Figure 5-46).

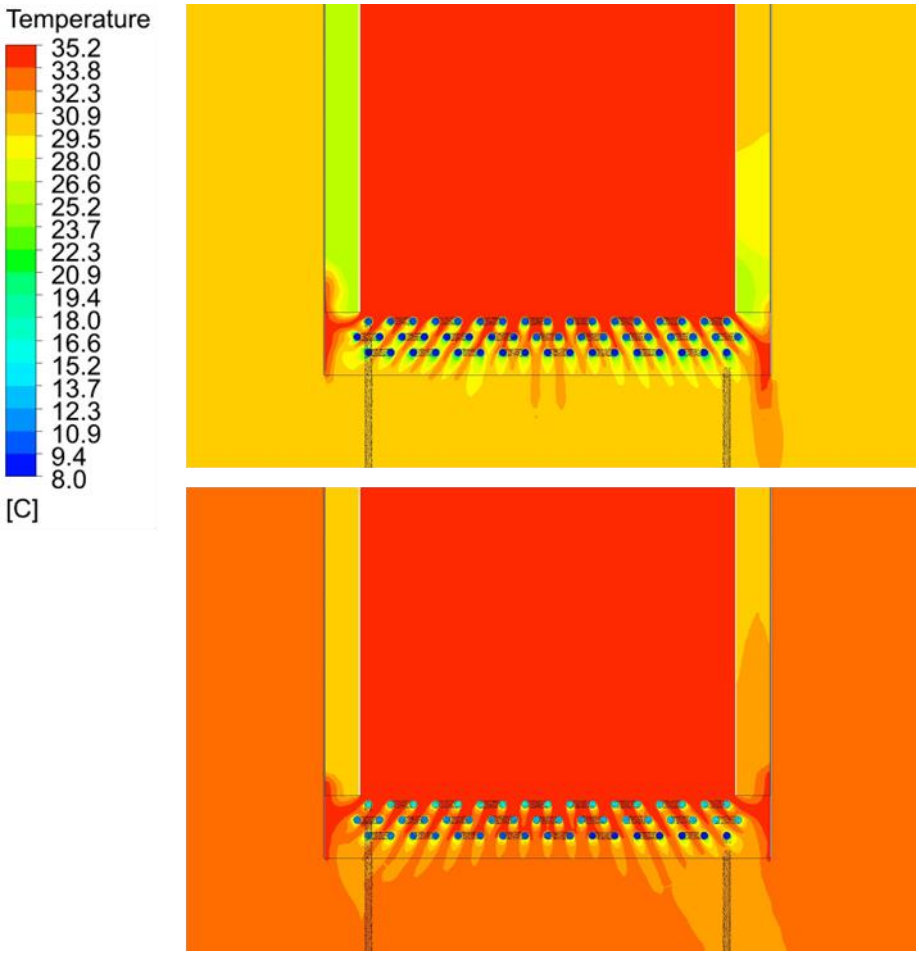

Figure 5-46 - Cooling over heat exchanger when wind speed is 1 m/s (top) and 5 m/s (bottom)

Conversely, the RAHE outlet temperature increases with increasing wind speed due to a greater volume of cool air passing over the heat exchanger in the same time frame, reaching a maximum temperature increase of 8.43 °C at 5 m/s. Despite the lower temperature difference between the fluids through the outlet channels, the amount of cooling is similar to that measured through the inlet quadrant owing to the much lower air velocity through the outlets (Figure 5-47). The room's shape and the water tank below the wind tower inlet impact the airflow around the room, resulting in unequal volumetric flow rates and average velocities through each outlet channel.

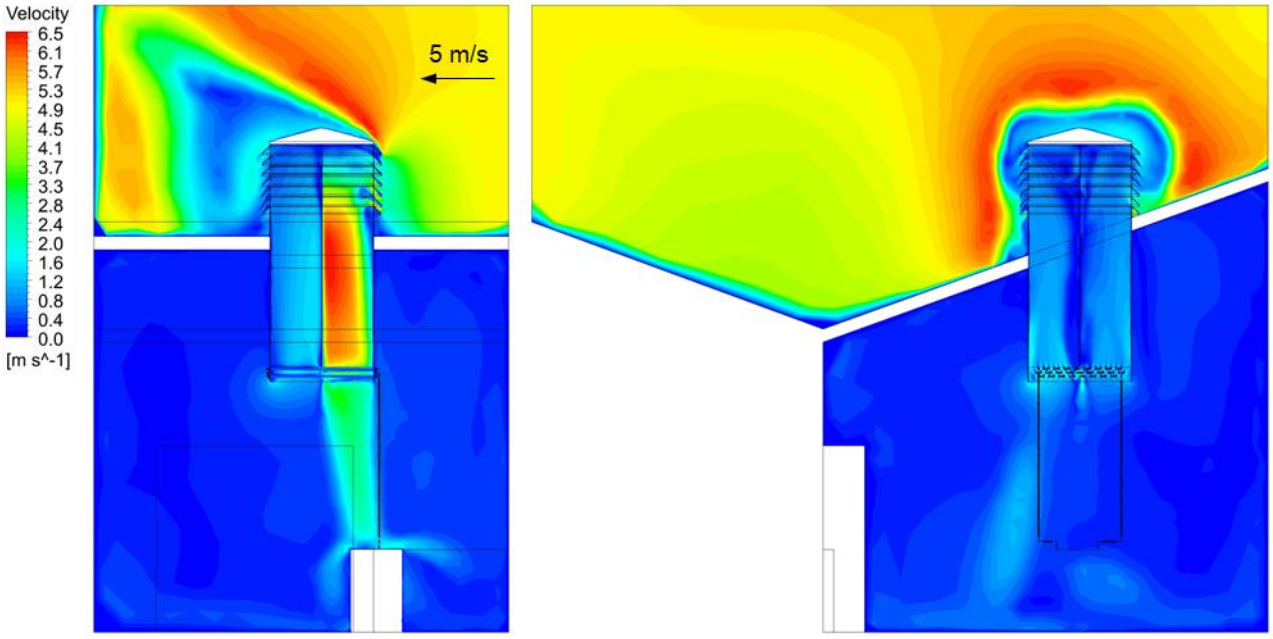

Figure 5-47 - Velocity through east and west quadrants (left) and north and south quadrants (right)

Plotting the decrease in air temperature and increase in water temperature against the wind speed, the there is a clear trade-off between sensible energy recovery and fresh air cooling with increasing wind speed (Figure 5-48). As the wind tower system is passive, the performance of the system is largely dictated by the ambient weather conditions and so the amount of heating, cooling, and sensible energy recovery cannot easily be controlled by the user.

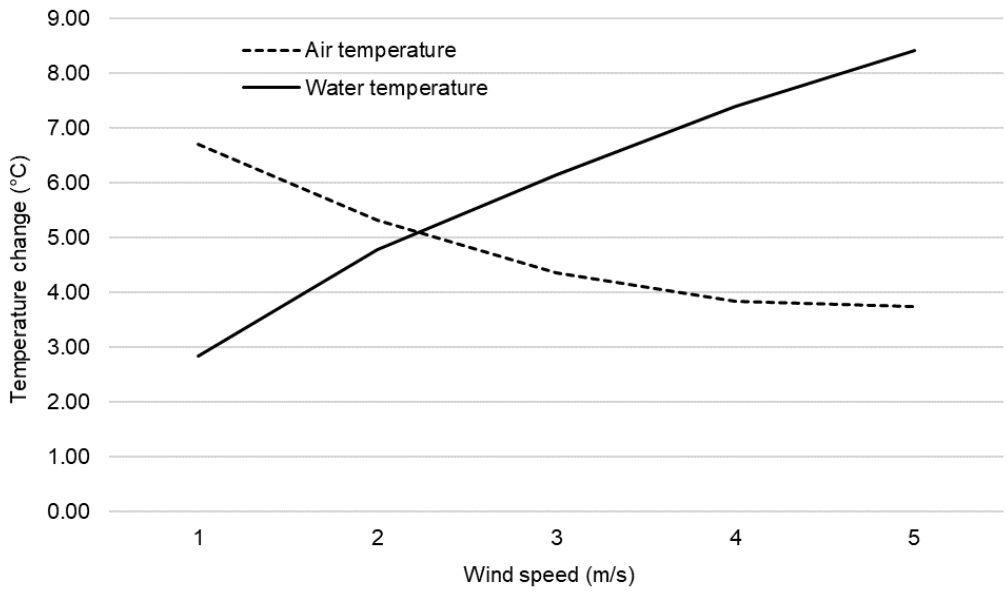

Figure 5-48 - Change in air temperature through wind tower inlet and water temperature through the RAHE

5.6.5 Run-around Heat Exchanger Volumetric Flow Rate

The velocity of the fluid through the RAHE was increased from 0.5 to 3.5 m/s to determine the impact on pre-cooling of fresh air and heat recovery. Using a heat exchanger with three rows of pipes, an inlet air temperature of 35 °C, velocity of 3 m/s, and water temperature of 8 °C, an increase in water velocity was shown to marginally increase the drop in air temperature over the heat exchanger and reduce the recovery of heat by the water flowing through the heat exchanger (*Figure 5-49*).

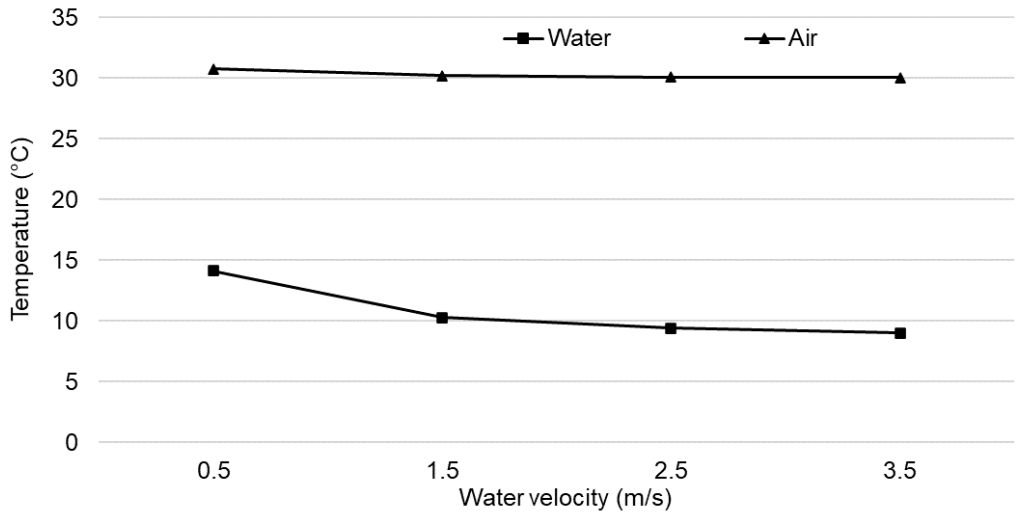

Figure 5-49 - Impact of increasing fluid velocity through the RAHE on inlet air temperature and heat recovery

Increasing the velocity of the water through the RAHE reduces the time available for heat transfer between the two fluids. This results in a greater decrease in air temperature with increasing water velocity as there is less time for heat to transfer from the air to the water, creating a greater temperature difference between the two fluids throughout the inlet quadrant and heat exchanger. Increasing the velocity of the water from 2.5 to 3.5 m/s had a minimal effect on the fluid temperatures. However, larger velocities would likely continue influencing the fluid temperatures if the initial temperature difference between the two fluids was higher.

5.6.6 Fin Addition

Using the information from the reviewed studies (Section 2.4.5.1), a heat exchanger with three rows of pipes and back side fins was created. The fin length and thickness were 20 and 4 mm respectively, with a wall angle of 0 ° parallel to the direction of flow to minimise the increase in pressure drop over the heat exchanger that is associated with the use of fins (*Figure 5-50*).

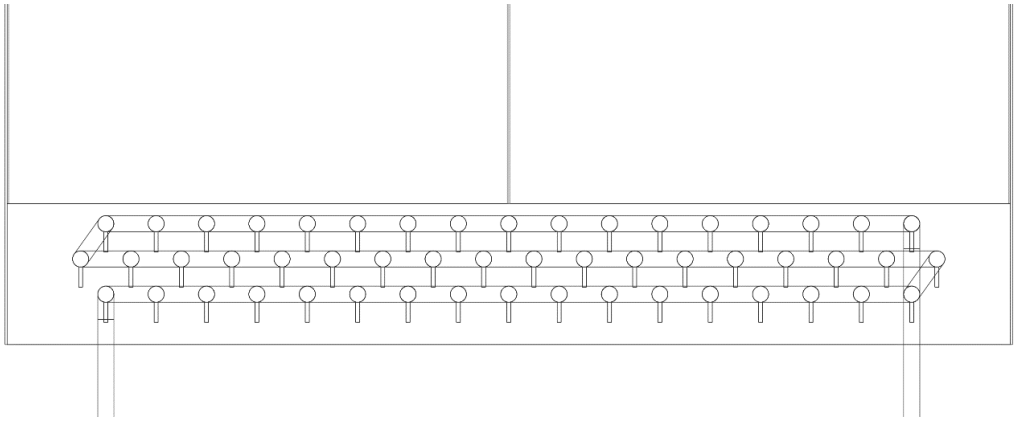

Figure 5-50 - Heat exchanger with finned pipes

Figure 5-51 shows the difference in volumetric flow rate through the wind tower inlet for the finned and standard heat exchangers. As anticipated, the introduction of fins reduces the volumetric flow rate due to the increased resistance to the airflow, falling between 12 and 22% compared to the standard model.

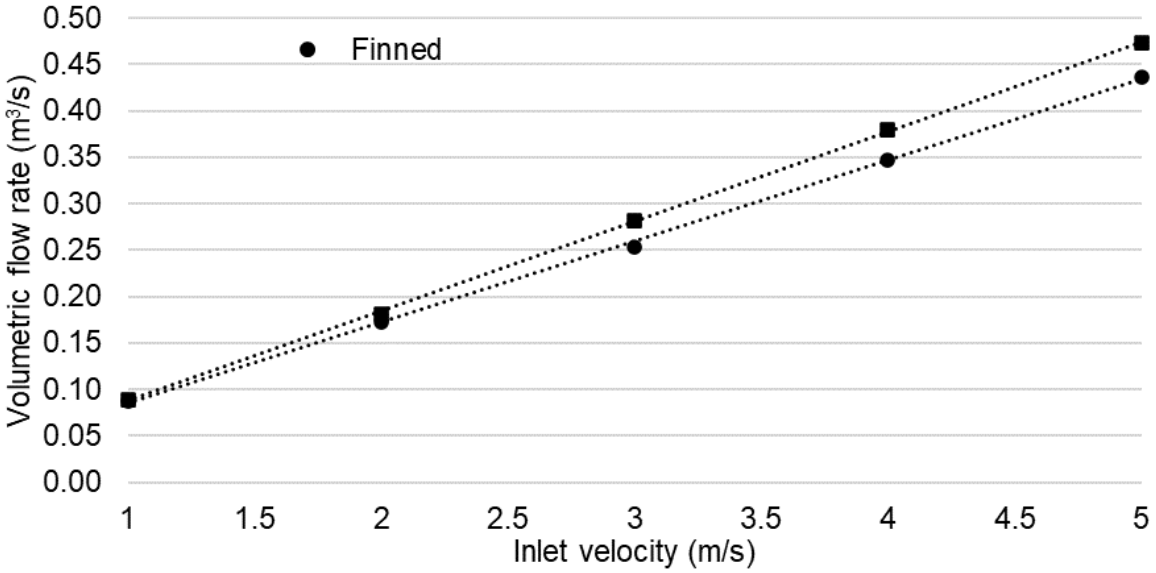

Figure 5-51 - Finned vs. standard volumetric flow rate for three-row heat exchanger model

Figure 5-52 displays velocity contours through the finned and standard heat exchangers. As was observed by Sparrow and Kang (Sparrow and Kang, 1985), the introduction of longitudinal fins results in some channelling of the flow, creating a

narrower jet of air into the room below, evidenced primarily towards the centre of the wind tower.

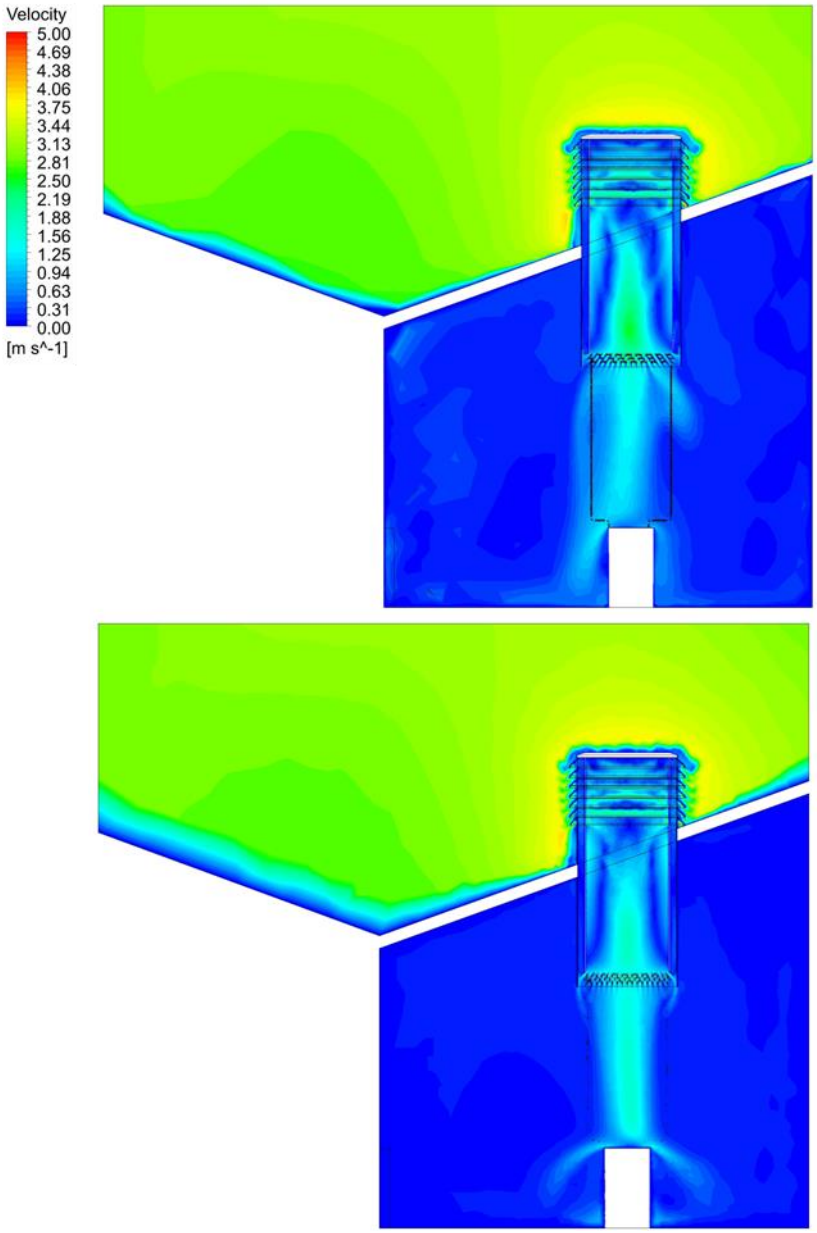

Figure 5-52 - Cross-sectional velocity contour through standard (top) and finned (bottom) heat exchanger models

Figure 5-53 compares the pressure gradient over the finned and standard heat exchangers. The pressure is much the same on the windward face of the wind tower and in the upper section of the inlet quadrant.

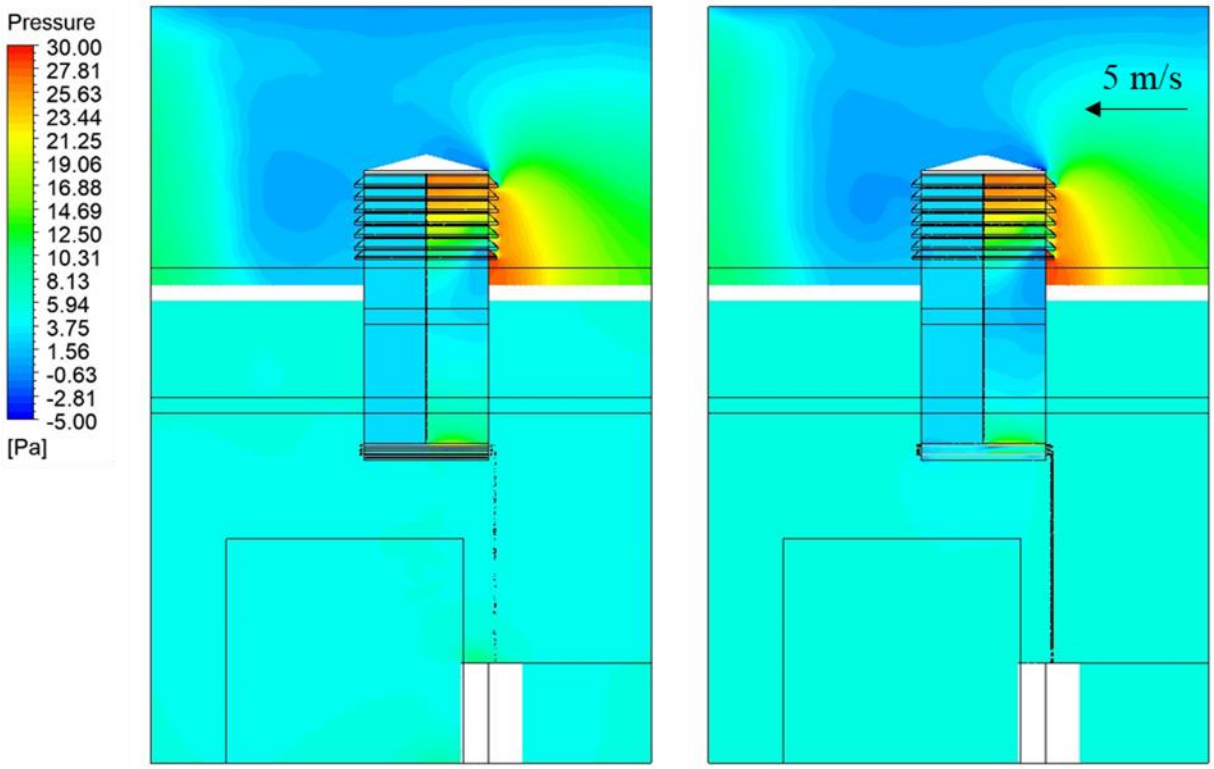

Figure 5-53 - Contour of static pressure through cross-sectional plane for finned (left) and standard (right) wind tower and heat exchanger models

Following the pressure change through the inlet quadrant, for both the finned and standard models a region of high pressure occurs inside the inlet quadrant level with the louvres (*Figure 5-54*). In the finned heat exchanger case, the decrease in pressure below the level of the louvres is less than the decrease for the standard model. The increased resistance to the flow of air caused by the addition of fins results in a greater build-up of pressure above the heat exchanger, in turn resulting in a greater pressure drop of 3.71 Pa at 5 m/s inlet velocity versus 2.09 Pa for the standard heat exchanger. Below the heat exchanger, as the air enters the room the pressure is seen to equalise for the finned and standard models, with a marginally higher supply pressure for the finned model, in line with the lower supply volumetric flow rate.

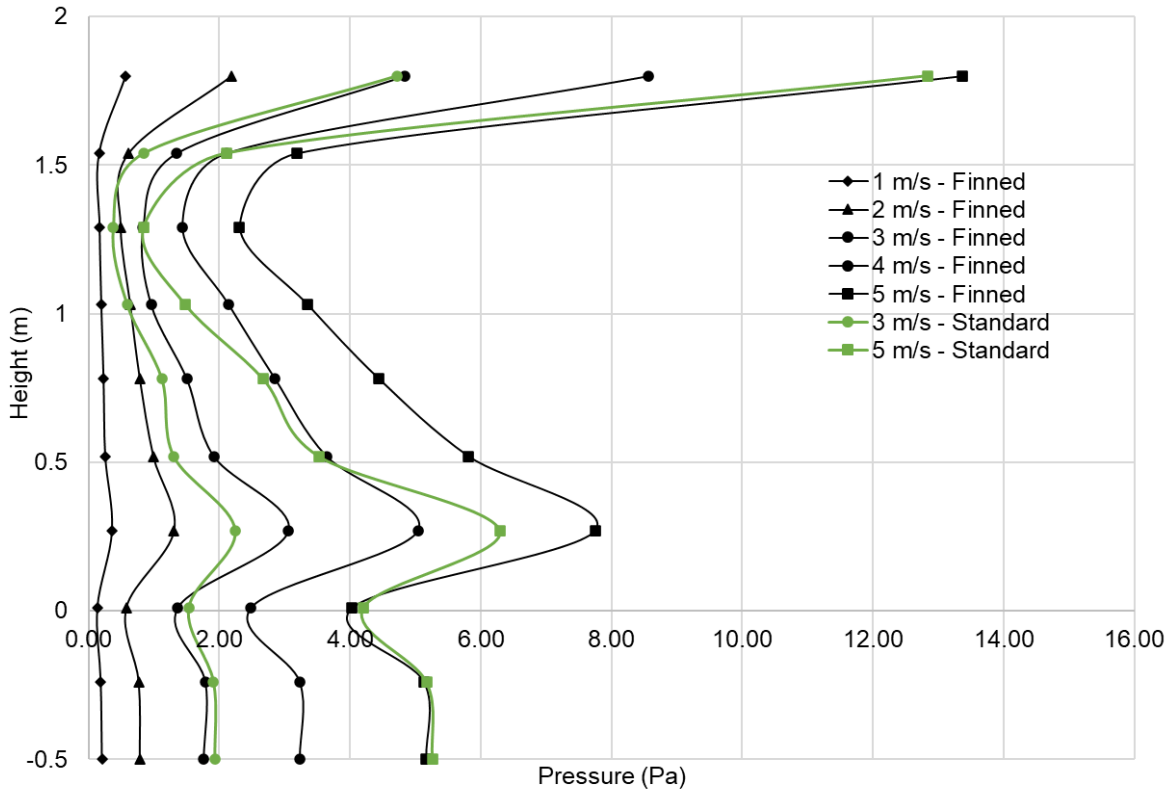

Figure 5-54 - Pressure through wind tower inlet quadrant for finned and standard wind tower and heat exchanger models

Measuring the temperature decrease of the fresh air over the heat exchanger, adding fins to the model further decreased air temperature by an average of 15% when the temperature difference between the fluids increased from 12 to 27 °C (*Figure 5-55*).

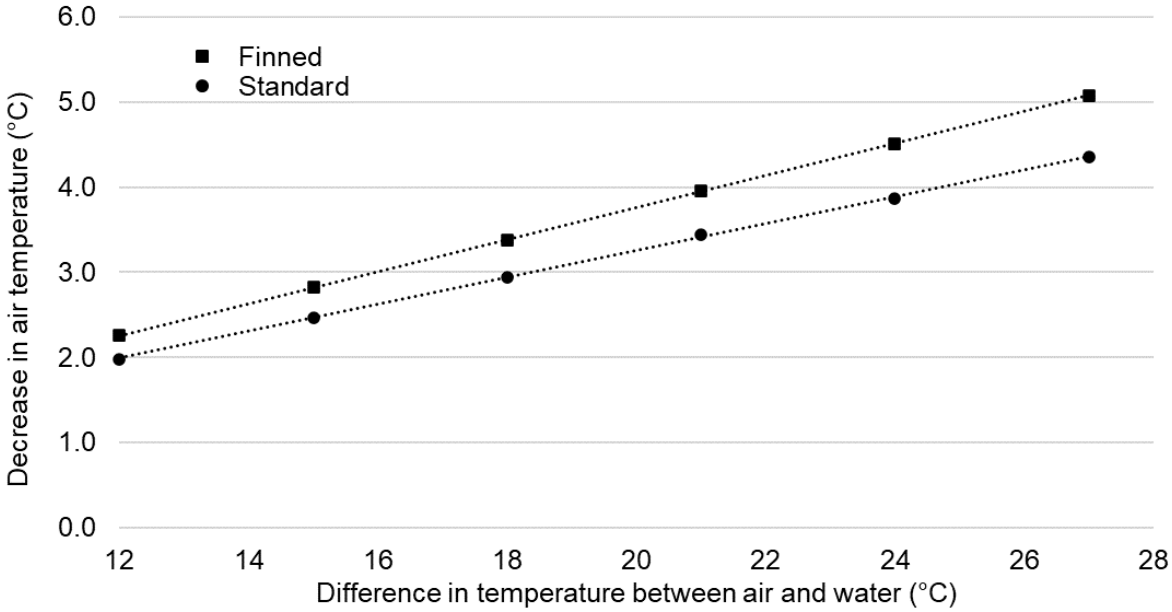

Figure 5-55 - Finned vs. standard air temperature decrease for three-row heat exchanger model.

At a temperature difference of 27 °C and an inlet velocity of 3 m/s, the standard and finned heat exchangers reduce the fresh air temperature by 4.36 and 5.07 °C respectively. As a result of the fins, at an inlet velocity of 3 m/s the volumetric flow rate into the room over the finned heat exchanger was 0.25 m^3/s whereas the flow rate through the standard heat exchanger was 0.28 m^3/s. When the volumetric flow rate is 0.25 m^3/s through the standard heat exchanger model, the fresh air temperature would be expected to be reduced by approximately 4.65 °C, indicating that the remaining difference between the standard and finned heat exchanger models results from the increased surface area.

Similarly, the difference in temperature between the inlet and outlet of the RAHE increased by up to 1.38 °C, with an average increase of 23% (*Figure 5-56*).

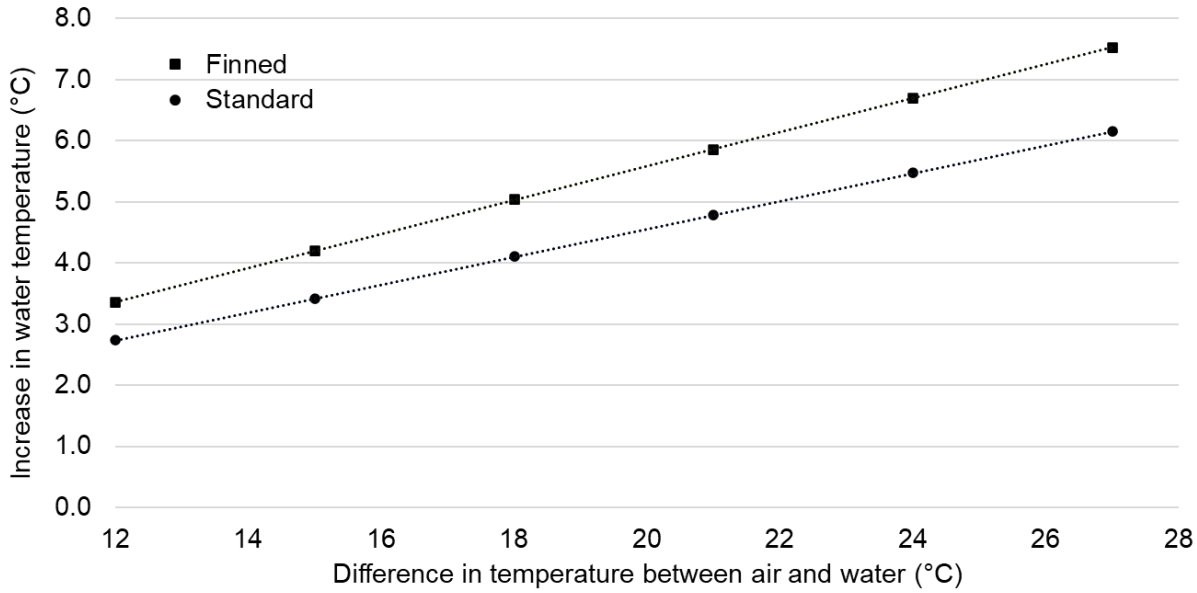

Figure 5-56 - Finned vs. standard water temperature increase for three-row heat exchanger model

Figure 5-57 compares the temperature contours over the finned and standard heat exchangers when the fresh air and water temperatures were 35 and 8 °C respectively. The channelling of the flow through the centre of the inlet quadrant by the fins further reduces the velocity of the air towards the outer edges of the quadrant creating a greater amount of cooling in these regions. Little difference was observed in short-circuiting between the inlet and outlet quadrants above the heat exchanger. If the dividing cross frame was extended to in line with the base of the wind tower and the heat exchanger fitted through it, the channelling of the air via the fins may help reduce the short-circuiting that occurs.

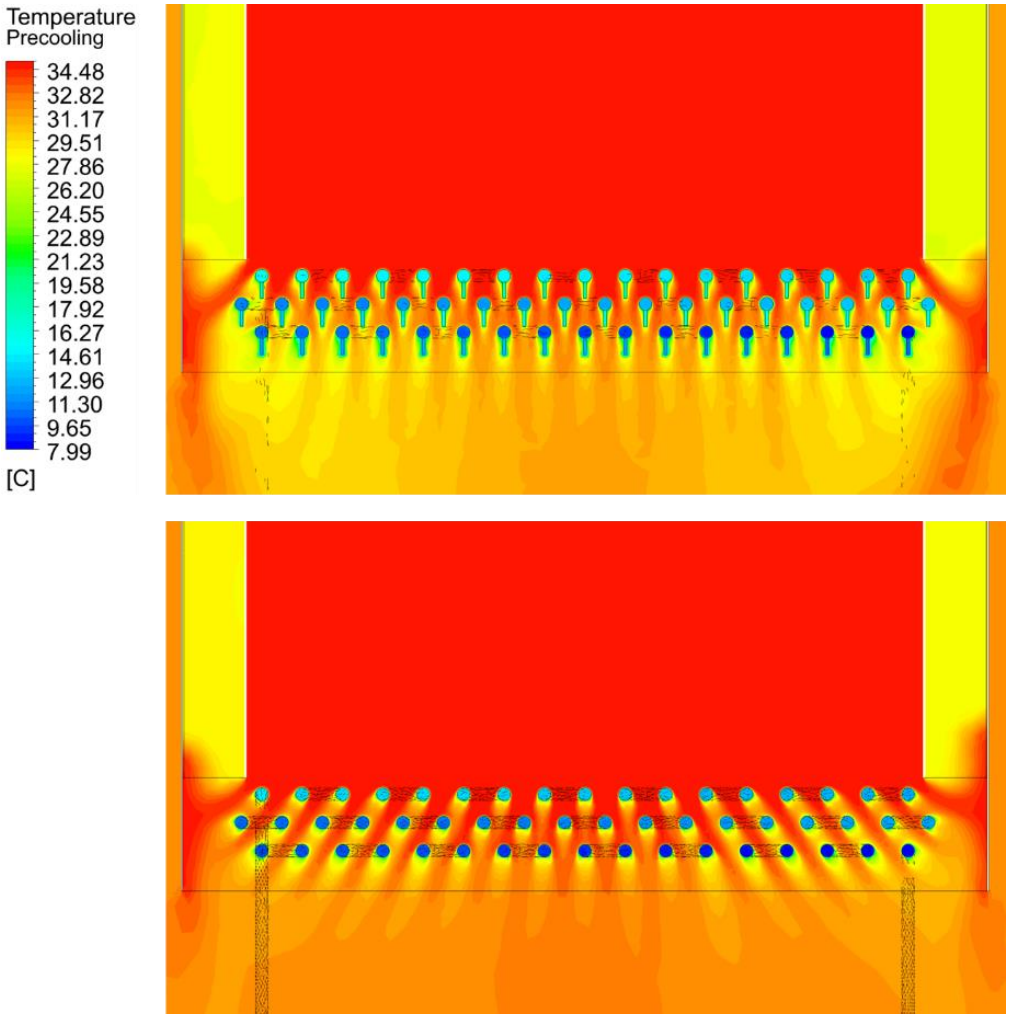

Figure 5-57 - Decrease in air temperature for finned (top) and standard (bottom) heat exchanger models

5.6.7 Thermal Energy Recovery

Using the temperature change of the water between the inlet and outlet of the RAHE, the sensible energy gained or lost by the water through heat exchanger can be calculated. Using Equation 5-1, the energy Q in kW is found:

$$Q = V\rho C_p \Delta T$$

Equation 5-1

Where V is the volumetric flow rate, ρ is the density, C_p is the specific heat capacity, and ΔT is the change in temperature between the inlet and outlet. The density and specific heat capacity were evaluated at the average temperature of the water through the RAHE. The volumetric flow rate was 0.077 L/s. Figure 5-58 shows the sensible

energy gained or lost by the water through the RAHE in a single pass, where the water is gaining heat when cooling and losing heat when heating the fresh air. Owing to the water experiencing the same temperature change through the RAHE when both heating and cooling, the sensible energy recovered or lost is approximately equal, with the difference in density and specific heat at different water temperatures having a minimal effect. At a temperature difference of 27 °C between the two fluids, approximately 2 kW of sensible energy could be expected to be recovered in a single pass. It is important to note that not all of the sensible energy lost or gained by the water is transferred to the room, as a large portion is transferred to the air passing through the wind tower outlets.

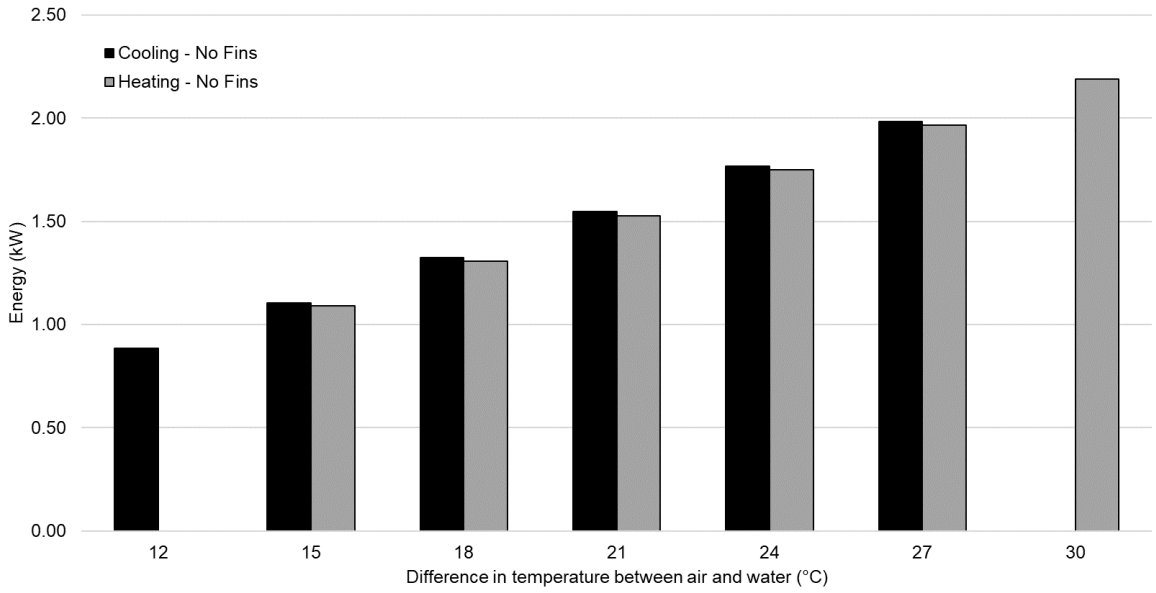

Figure 5-58 - Sensible energy recovered and lost through the heat exchanger when heating and cooling fresh air

Figure 5-59 then compares the difference in sensible energy recovery between the finned and standard heat exchanger models when cooling fresh air.

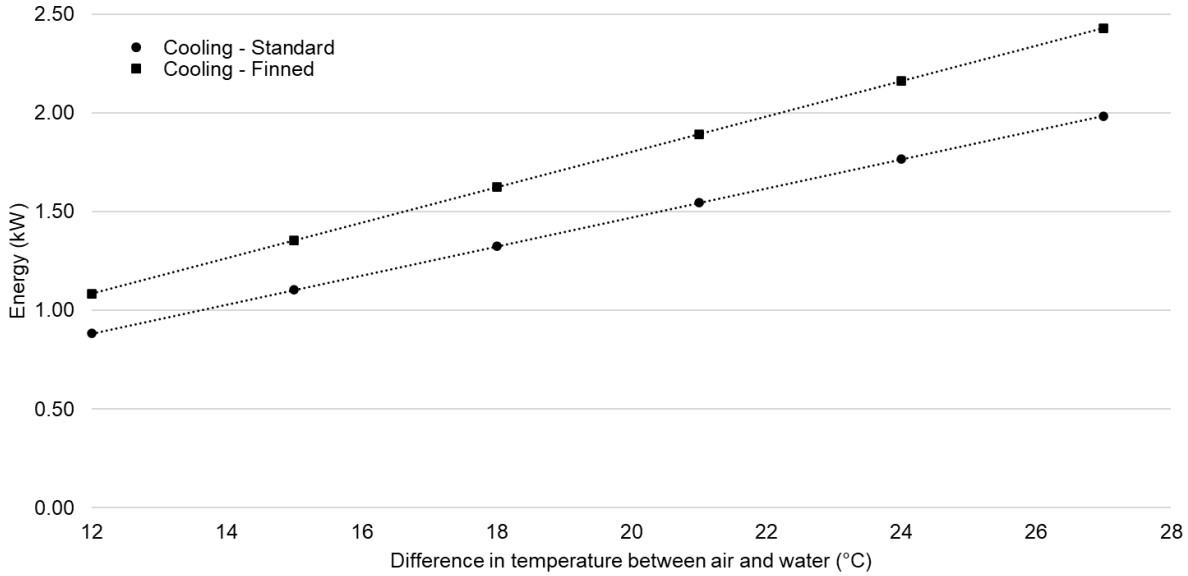

Figure 5-59 - Sensible energy recovered through the heat exchanger for finned and standard models when cooling fresh air

The larger change in fluid temperature through the heat exchanger due to adding fins directly increases the sensible energy recovered from 2.0 to 2.4 kW. The impact of the water velocity through the RAHE on the sensible energy recovery was then evaluated (Figure 5-60).

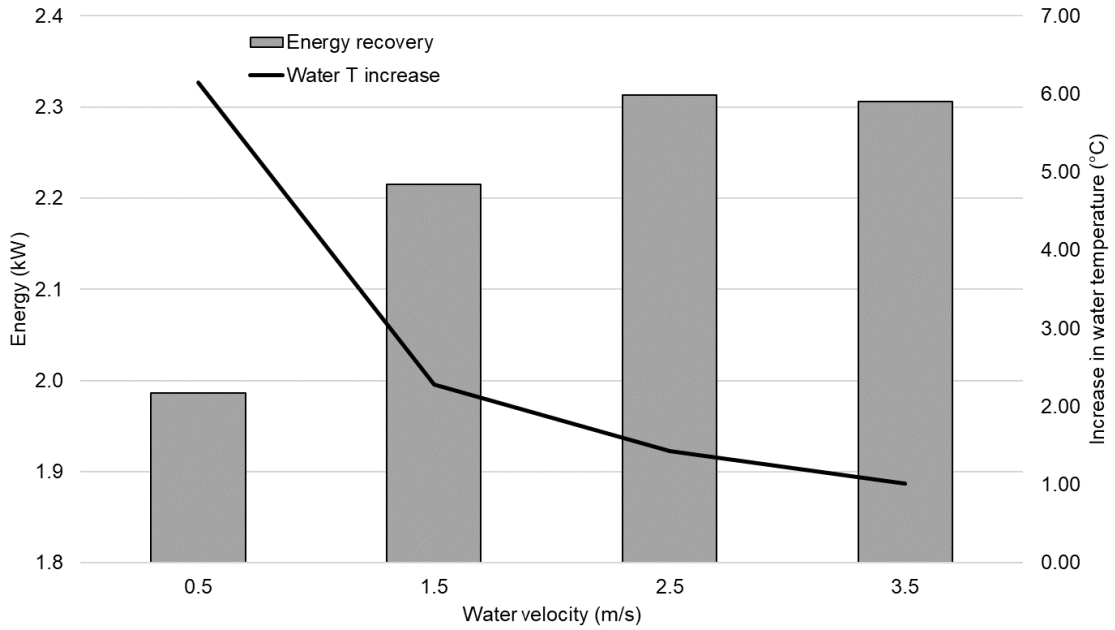

Figure 5-60 - Sensible energy recovery with increasing flow rate through the heat exchanger

At a velocity of 0.5 m/s the volumetric flow rate was 0.077 L/s, increasing to 0.54 L/s when the inlet velocity was 3.5 m/s. Although increasing the velocity through the heat exchanger resulted in a decrease in water temperature at the heat exchanger outlet, the increase in volumetric flow rate through the system means that a greater amount of sensible energy was recovered.

5.6.8 Efficiency

Table 5-10 and Table 5-11 show the efficiency of the heat exchanger with and without fins calculated according to the process laid out in section 3.2.1 with increasing temperature difference between the two fluids. The air inlet and water velocities were kept constant at 3 and 0.5 m/s respectively. The efficiency reflects heat transfer from the air to the water through a combination of convective and conductive heat transfer.

Table 5-10 - Standard heat exchanger efficiency with increasing temperature difference between the fluids

Standard					
Air Inlet Temp (°C)	Air outlet temp (°C)	Water inlet temp (°C)	Water outlet temp (°C)	LMTD (°C)	Efficiency
20	18.0	8	10.7	9.6	0.21
23	20.5	8	11.4	12.0	0.20
26	23.1	8	12.1	14.5	0.20
29	25.6	8	12.8	16.9	0.20
32	28.1	8	13.5	19.3	0.20
35	30.6	8	14.1	21.7	0.20

Table 5-11 - Finned heat exchanger efficiency with increasing temperature difference between the fluids

Finned					
Air Inlet Temp (°C)	Air outlet temp (°C)	Water inlet temp (°C)	Water outlet temp (°C)	LMTD (°C)	Efficiency
20	17.7	8	11.4	9.2	0.25
23	20.2	8	12.2	11.5	0.25
26	22.6	8	13.0	13.8	0.25
29	25.0	8	13.9	16.1	0.25
32	27.5	8	14.7	18.4	0.25
35	29.9	8	15.5	20.7	0.25

The efficiency was calculated to be an average of 20% and 25% for the standard and finned models respectively. The amount of cooling increases proportionally with the

LMTD between the two fluids, maintaining the efficiency of the heat exchanger. The air temperature results under increasing wind speed were then used to calculate the efficiency from 1 to 5 m/s for the standard heat exchanger model (Table 5-12).

Table 5-12 - Heat exchanger efficiency through inlet quadrant with increasing wind speed

Inlet velocity (m/s)	Air Inlet Temp (°C)	Air outlet temp (°C)	Water inlet temp (°C)	Water outlet temp (°C)	LMTD (°C)	Efficiency
1	35	28.3	8	10.8	22.2	0.30
2	35	29.7	8	12.8	22.0	0.24
3	35	30.6	8	14.1	21.7	0.20
4	35	31.2	8	15.4	21.3	0.18
5	35	31.3	8	16.4	20.8	0.18

Heat transfer efficiency between the fluids reaches a maximum of 30% at an inlet velocity of 1 m/s. Previously published studies involving run-around heat exchangers reported efficiencies of 75.6 % (Hviid and Svendsen, 2011) and 70 % (Davidsson et al., 2013) at pressure drops of 0.74 Pa and 1 Pa respectively, although both studies involved small-scale experimental setups replicating passive ventilation systems and so the actual performance may vary. To achieve these efficiencies, Hviid and Svendsen (2011) used 28, 3m long tube layers, generating a heat exchanger surface area 7.5x larger than the heat exchanger installed in this study. The air velocity onto the heat exchanger was also only 0.1 m/s, much lower than any wind speeds simulated within this study. Likewise, Davidsson et al. (2013) used a lengthways counterflow heat exchanger with fins on the top and bottom of the pipes, also generating a larger surface area for heat transfer when the air inlet velocity was 0.34 m/s. Both studies also use narrower pipes in the heat exchanger, with outer diameters of 8 mm (Hviid and Svendsen, 2011) and 9.5 mm (Davidsson et al., 2013) to help reduce the pressure drop over the heat exchanger.

There is clearly scope to improve the performance of the heat exchanger within the passive ventilation system. At the cost of reducing the volumetric flow rate of air

through the wind tower, the efficiency could be improved by decreasing the distance between the copper pipes, using a greater number of pipes, or increasing the length/changing the geometry of the fins. As the heat exchanger has to traverse all four quadrants to account for changes in wind direction, installing vertical pipes through each quadrant is not viable to increase the surface area of the heat exchanger within each quadrant.

5.6.9 Overall Heat Transfer Coefficient

The overall heat transfer coefficient between the two fluids was calculated analytically using the process described in section 3.2.2. The analytical values calculated for the Nusselt number and Reynolds numbers of the water were compared with values found through the numerical model to determine the accuracy of the analytical solution.

The overall heat transfer coefficient was calculated for inlet velocities between 1 – 5 m/s. The inlet air and water temperatures remained constant at 35 and 8 °C, respectively. Likewise, the inlet velocity to the RAHE remained at 0.5 m/s.

Table 5-13 and Table 5-14 show the mean fluid temperature, Reynolds number, Nusselt number, and heat transfer coefficient for the water passing through the RAHE calculated analytically and using values provided through ANSYS.

Table 5-13 - Heat transfer coefficient for water flowing through the RAHE calculated analytically

Analytical			
Mean Water T (°C)	Reynolds number	Nusselt number	Heat transfer coefficient (W/m^2- K)
9.4	5280.1	53.7	2207.9
10.4	5412.9	54.2	2241.6
11.1	5510.8	54.5	2265.9
11.7	5604.0	54.9	2288.7
12.2	5681.8	55.1	2307.4

Table 5-14 - Heat transfer coefficient for water flowing through the RAHE calculated through ANSYS

CFD			
Mean Water T (°C)	Reynolds number	Nusselt number	Heat transfer coefficient (W/m^2- K)
9.5	5216.7	53.1	2186.3
10.5	5345.8	53.6	2218.2
11.2	5442.8	53.9	2241.6
11.9	5538.7	54.2	2264.5
12.5	5615.4	54.4	2281.9

Analytically, the average fluid velocity was taken as 0.5 m/s, with all fluid properties evaluated at the mean fluid temperature, taken as the average between the temperatures recorded at the inlet and the outlet. The average properties of an entire fluid volume can be calculated through ANSYS. Through this the average velocity within the fluid body was reported as 0.49 m/s, with the average temperature shown to be very close to the analytical method with increasing inlet velocity.

As a result of the minor differences in velocity and temperature between the two approaches, the Reynolds number, Nusselt number, and heat transfer coefficient calculated using the CFD values were, on average, 1% smaller than the analytical values. The accuracy of the analytical method for the air could not be verified via the same process due to the numerical model's composition. The analytical calculations only concern the air in the vicinity of the heat exchanger. The air volume is continuous throughout the entire model and therefore it is not possible to use the program to calculate the average Reynolds and Nusselt numbers in just the region of interest.

The U value was then calculated for increasing wind speeds (Table 5-15). On the air side the average temperature and flow properties were taken from the conditions through the inlet quadrant.

Table 5-15 - Analytical calculations used to find the overall heat transfer coefficient of the heat exchanger

Air				
Air Inlet Velocity (m/s)	Mean air T (°C)	Reynolds number	Nusselt number	Heat transfer coefficient (W/m^2 - K)
1	31.7	1449	30	48
2	32.3	2887	42	68
3	32.8	4319	51	83
4	33.1	5750	59	96
5	33.1	7185	66	108

Water				
Water Inlet Velocity (m/s)	Mean water T (°C)	Reynolds number	Nusselt number	Heat transfer coefficient (W/m^2 - K)
0.5	9.4	5280	54	2208
0.5	10.4	5413	54	2242
0.5	11.1	5511	55	2266
0.5	11.7	5604	55	2289
0.5	12.2	5682	55	2307

Air Inlet Velocity (m/s)	Overall heat transfer coefficient (W/m^2 - K)
1	2.4
2	3.3
3	4.0
4	4.6
5	5.1

The Reynolds and Nusselt numbers increase with increasing inlet velocity on the air side, indicating increasing turbulence and convective heat transfer. The values for the water remain comparatively stable, only varying slightly due to the changing properties of the fluid with increasing average temperature. The U value increased from 2.4 to 5.1 W/m^2-K as the inlet velocity increased from 1 to 5 m/s, reflecting the increased water temperature recorded with increasing wind speed. It is common that one of the fluids largely dictates the rate of heat transfer between the two. Given that the heat transfer coefficient for the air is much lower than that of the water the flow properties of the air dominate the U value.

5.7 Limitations

Due to the experimental design and the impacts on the numerical modelling, there are several limitations to the results produced herein. It is acknowledged that because the whole building is not subject to the boundary layer, it is likely that for a given inlet velocity, the velocity and volumetric flow rate of air through the wind tower would be

lower than reported. Although this may result in an overestimation of the ventilation rate provided to the test room, lower velocities have been shown to result in a more significant fresh air temperature increase or decrease. Given the location of the field trial site, surrounding buildings, and local topography, it is difficult to predict the shape of the boundary layer that the building and wind tower system would be subject to. Therefore, simulations remained with just the wind tower immersed within the flow.

Related to this, constantly changing ambient conditions are discretised and applied as constant boundary conditions over each timestep of the transient validation. Wind velocity and direction constantly change, resulting in lulls and gusts of wind-driven flow through the wind tower. These lulls allow more time for the air within the quadrant to heat or cool as it circulates within the enclosed space. Similarly, changes in wind direction create constantly changing areas of recirculation that affect the velocity and direction of the air over the pipes and hence the heat transfer to and away from the heat exchanger.

5.8 Summary and Discussion

A wind tower and RAHE field trial was conducted to explore the potential for pre-heating and cooling fresh air whilst recovering waste thermal energy for storage through STES. The boundary conditions and results of the field trial were used to validate a numerical model developed through ANSYS Fluent using a transient simulation. The numerical model showed good agreement between the two sets of results, accurately predicting the temperature change of the fresh air through the wind tower and the water flowing through the run-around. Subsequently, steady-state simulations were conducted, varying boundary conditions including the fluid temperatures and velocities.

Through these simulations the wind tower was shown to sustain a volumetric flow rate of 0.09 m^3/s into the room below at inlet velocities as low as 1 m/s for a heat exchanger model featuring 52 pipes arranged into three staggered rows. The volumetric flow rates from the field trial and wind tunnel test were first compared, showing that increasing the length of the wind tower marginally decreased the volumetric flow rate through the inlet quadrant as the driving pressure through the inlet quadrant dissipated. Despite this, the wind tower was shown to supply above the required 0.8 $L/s/m^2$ for factories and 1.3 $L/s/m^2$ for offices and schools at wind speeds between 1 – 5 m/s, although it fell marginally short of the 5 L/s per occupant required for a classroom of 20 occupants and a floor area of 35 m^2. Simulations were conducted with only the wind tower exposed to the airflow. The impact of including the building in the boundary layer has been shown to reduce the flow rate through a wind tower by 15 – 40% due to the flow separation at the leading edge (Wu et al., 2021), however, the magnitude of the impact is also dependent on the angle of the roof, the wind speed, and the proximity of the wind tower to the leading edge.

Simulations were conducted at a wind angle of 0 °, generating one inlet and three outlets through the four-sided wind tower. This represents the minimum possible ventilation rate through the wind tower, with ventilation rates increasing up to 47% when the wind angle is 45 °. It is also possible to install several wind towers in the same room to increase the fresh air supply rate. If several wind towers are installed it may be possible to further increase the number of pipe layers in the heat exchanger as the fresh air supply from an additional wind tower or towers can compensate for the reduction in flow through each. The positioning of multiple wind towers must be considered to prevent the recirculation of expunged CO_2 through the room below (Calautit et al., 2014).

Dampers and diffusers are also recommended for any wind tower installation. As was seen through the velocity contours produced through simulation, a jet of air occurs below the inlet quadrant of the wind tower. Increased air velocity inside the room can cause thermal discomfort for the occupants, especially directly below the wind tower. It is therefore important to restrict or distribute the airflow throughout the room to prevent thermal discomfort, particularly at higher wind speeds. This also generates better mixing of fresh air throughout the room.

Through the same heat exchanger model, at an inlet velocity of 3 m/s and a temperature difference of 27 °C between the air and water, the air temperature was increased by 4.2 °C and decreased by 4.4 °C when heating and cooling respectively. Under the same boundary conditions the water temperature increased and decreased by 6.2 °C for both heating and cooling due to the heat transfer that also occurs through the exhaust channels of the wind tower. This represents a modest improvement in fresh air treatment compared to the wind tower and heat pipe system. By running water through the heat exchanger pipes, heat is removed or delivered to the pipe at a greater rate than was achieved through the evaporation-condensation cycle within the heat pipes, affecting a more significant change in fresh air temperature. Increasing or decreasing the water temperature through the RAHE would result in a greater temperature difference to the fresh air, however, it would incur additional energy demand from chillers and heat pumps to do so.

The sensible energy recovered through the heat exchanger was directly related to the change in water temperature between the inlet and outlet of the fluid loop, where the system is seeking to recover heat from the fresh air in the summer to provide heating in the winter, and cold in the winter to provide cooling in the summer. An increase or

decrease in water temperature of 6.2 °C correlated to an approximate gain or loss of 2 kW in a single pass.

As the heat exchanger traverses all four quadrants of the wind tower through the winter a significant portion of the heat delivered through the heat exchanger is lost to the exhaust air passing through the wind tower outlets. In an occupied building, the heat transferred to the exhaust air would be reduced as stale air would leave the room within the comfortable range for the occupants rather than at the delivery temperature through the wind tower. Likewise, in the summer less heat would be transferred to the water flowing through the heat exchanger as the exhaust air temperature would be lower than the delivery temperature from the wind tower considering the use of mechanical HVAC systems in conjunction with the passive ventilation system. Ideally, each quadrant would contain an individual heat exchanger so that only fresh air received heating or cooling, however this would generate an overly complex system that would struggle to keep pace with the constant changes in wind direction experienced under ambient conditions.

The reduction of fresh air temperature was maximised at lower wind speeds, reaching 6.7 °C at 1 m/s and falling to 3.8 °C at 5 m/s. In contrast, heat recovery through the heat exchanger was maximised at higher wind speeds, increasing the water temperature to 8.4 °C at 5 m/s and falling to 2.8 °C at 1 m/s. Increasing the volumetric flow rate through the RAHE had little impact on the fresh air temperature but resulted in a significant decrease in the sensible energy recovered through the water, indicating a preference for a low volumetric flow rate where possible.

Adding fins to the heat exchanger decreased the volumetric flow rate through the wind tower by between 12 and 22%, simultaneously increasing the pressure drop from 2.09

to 3.71 Pa at an inlet velocity of 5 m/s. Reducing the flow rate and increasing the heat exchanger's surface area resulted in a 15% increase in fresh air cooling and a 23% increase in the water temperature through the RAHE. This increased the sensible energy recovered in a single pass to 2.4 kW. Backside-only fins were used to limit the pressure drop over the heat exchanger, however both front and backside fins have been used (Sparrow and Kang, 1985).

Evaluating the performance of the heat exchanger, the efficiency was found to be 20% and 25% for the standard and finned models respectively under increasing fresh air temperatures and a constant wind speed of 3 m/s. When increasing the wind speed from 1 to 5 m/s the efficiency fell from 30% to 18%, reflecting the reduction in pre-cooling as wind speed increases. The overall heat transfer coefficient increased with increasing wind speed, rising from 2.4 to 5.1 W/m^2-K when the wind speed increased from 1 to 5 m/s, reflecting the increase in thermal energy transfer from the air to the water. The performance of the heat exchanger fell short of the performance of other heat exchangers designed for use in passive ventilation systems that incurred similar pressure drops (Hviid and Svendsen, 2011; Davidsson et al., 2013). The improved performance of the heat exchangers in the literature was primarily due to the increased surface area of each heat exchanger relative to the installation applied in this study and the much lower air velocities tested. It is still determined that there is scope to improve the performance of the heat exchanger by optimising the fin design and altering the spacing and dimensions of the pipe layers. This would ideally maintain a low-pressure drop while increasing the number of pipe layers that constitute the heat exchanger.

Li et al (2022) completed a thermo-economic analysis for a run-around heat recovery system installed within a mechanical ventilation unit in a building in northern China.

They used sets of finned tube heat exchangers, each with 6 tube layers of copper pipes in a staggered arrangement. Each pipe had an outer diameter of 12.7 mm and a wall thickness of 1 mm, with a transversal and longitudinal pitch of 50 and 20 mm between pipe centres respectively. An antifreeze solution linking the exhaust and inlet heat exchangers served to increase fresh air temperature through heat recovered from exhaust air. After monitoring the performance of the system, the exhaust air temperature was found to fall between 14 and 18 °C, leading to an increase in fresh air temperature between 7.7 - 19.2 °C. This high temperature increase was due to the low ambient temperatures experienced in the area, generating large temperature differences between the exhaust and fresh air, which ranged from 8 – 35 °C, approximately. As a result, the heat recovery efficiency fell between 40 and 85%, with an average of 60%.

The performance of the system can also be compared against commercially available systems. Ventive produce passive and active ventilation systems, with and without heat recovery (Vivian Dorizas *et al.*, 2017). The Windhive system employs a wind tower and heat recovery system designed to provide up to 200 L/s of air, where the heat recovery is comprised of two coaxial heat exchangers with aluminium fins to exchange heat between exhaust and fresh air. Although the information on the performance of the system is limited, it is claimed that the thermal efficiency when combined with a wind tower is as high as 72%, saving up to 1500 kWh per year for the building. For an alternative passive system, two wall ventilators are integrated into the facade, with fresh air entering through the lower unit and stale air exiting through the higher unit. In addition to heat recovery, the system makes use of a heat pump to further increase the fresh air temperature into the room, achieving up to 2.2 kW of

cooling when the ambient temperature is 18 °C. The flow rate through the system was limited to 30 – 150 L/s, generating a heat recovery efficiency of 55%.

Compared against the proposed wind tower and RAHE system explored, the designed flow rates through the commercial passive ventilation systems are much lower, with the wind tower and RAHE system predicted to provide over 200 L/s when the wind speed was only 2 m/s. Although limited information is available around the performance of the commercial heat recovery system, the reported efficiencies are beyond those reported herein, indicating significant work would have to be done to make the proposed system competitive with commercially available products. Likewise, compared against the performance of a RAHE within a mechanical ventilation system, the heat recovery efficiency falls below the reported values although the structure of the heat exchangers offered greater heat recovery due to an increased number of pipe layers.

Several limitations to passive ventilation were identified throughout the study. The issue with overventilation leading to large heat losses from the occupied environment necessitates some form of volume control to limit the flow rate into the room under high winds. This can be achieved through volume control dampers which are correlated to open and close with inlet velocity. A method for achieving this passively is yet to be developed but would be an important addition to help improve the viability of passive ventilation systems when compared with mechanical ventilation. As a consequence of uncontrolled ventilation rate through the system, the amount of heat transfer is also variable, meaning that the pre-heating or cooling of fresh air is unpredictable. Employing a run-around rather than direct heat recovery allows for some degree of control over the temperature of the fluid flowing through the RAHE

system, but would require an active control system to monitor the wind speed, temperature, and direction to adjust accordingly.

Although passive ventilation systems can provide fresh air with zero energy demand, to generate a significant enough increase in fresh air temperature in the winter prior to entering the room direct heat recovery is likely to be insufficient. A run-around system was shown to generate a more significant increase in fresh air temperature, however, requires a pump to circulate the fluid through the system and a heat pump to generate sufficiently high temperatures. This negates the impact of removing the fan from the ventilation system. A full system analysis that accounts for the widening of set-points for thermal comfort may offer some additional decrease in energy demand relative to mechanical systems, however, would require a more comprehensive study to fully evaluate this.

As it stands, it may still be necessary to combine any such system with mechanical HVAC systems to ensure ventilation rates and thermal comfort are maintained independent from external conditions. Regarding the linking of STES, the system is well suited for integration into an ATES system due to the demand for both hot and cold storage and the precited operation temperature range. The natural extraction temperature of groundwater is well suited to provide cooling to fresh air in the summer, with the hot well re-injection temperature falling well within the range reported in the literature. To recover a significant amount of thermal energy, installing several systems in proximity may be necessary.

6 Conclusions and Future Work

This final chapter concludes the experimental and computational investigations discussed throughout this thesis. As discussed, the overarching aim of this research

was to design a passive ventilation and heat recovery system for pre-heating and cooling fresh air whilst recovering waste thermal energy. Achieving this would result in a low-energy alternative to mechanical HVAC systems suitable for integration within a range of buildings, lowering building energy demand whilst generating thermally comfortable environments for the occupants.

6.1 Main Findings

Due to the work carried out in this thesis, the following findings were generated:

1. A literature review was conducted to identify gaps in the existing body of research. The review individually covered passive ventilation, heat recovery devices, seasonal thermal energy storage, and instances where efforts had been made to combine several technologies. Through this it was established that passive ventilation systems are suitable for ventilating indoor spaces with zero energy demand, helping to reduce energy demand by broadening the range at which the occupants achieve thermal comfort. Of the heat recovery devices reviewed, heat pipes and run-arounds were the most suitable for integration within passive ventilation owing to their high heat recovery rate and low-pressure drop. Aquifer thermal energy storage was determined to be most suitable for use in a mild cold climate as it could effectively store both heat and cold depending upon the season.
2. A numerical model produced to replicate the wind tunnel test was validated using experimental data under steady-state conditions, establishing an average error of 24.3% between the experimental and numerical velocities. The agreement between the temperature results was much closer, showing an average error of 7.5% despite the dependence of temperature on the air velocity. The accuracy of the numerical model was within a satisfactory range

for natural ventilation flows, also showing good agreement between the trends established at individual measurement points. Applying surface temperature as a boundary condition across the heat pipe was also shown to give a reasonable prediction of the heat transfer between the heat pipe and fresh air.

3. The study sought to maximise the heat recovery from the exhaust to inlet quadrants by increasing the number of pipes installed through the wind tower. When using 52 thermosyphon heat pipes arranged into three staggered rows, a volumetric flow rate of 0.1 m^3/s (100 L/s) was maintained through the wind tower when the inlet velocity was 1 m/s. An increasing number of pipe layers had a decreasing impact on the volumetric flow rate due to the staggered arrangement.
4. By recovering heat from warm exhaust to cool fresh air through the heat pipes, the incoming air temperature was increased by up to 2.8 °C when the difference in temperature between the fresh and exhaust air was 25 °C. By increasing the fresh air temperature, the additional energy required by mechanical systems to raise the fresh air temperature to room temperature was reduced by up to 1 kJ/s. These values were achieved at a wind angle of zero degrees, with one of the four wind tower quadrants behaving as an inlet and the remaining three as outlets.
5. A field trial of a run-around heat exchanger installed within a commercial wind tower was conducted to determine the potential for pre-heating and cooling fresh air whilst recovering waste thermal energy. The heat exchanger was comprised of a single row of linked copper pipes using the same transversal pitch as was applied in the wind tunnel test. A submersible pump and separate chiller were used to circulate water through the system at an approximately

constant temperature, simulating the seasonal thermal energy storage supply. Temperature measurements taken throughout the wind tower were correlated against ambient conditions recorded through a weather station to monitor the system's performance.

Conducted during summer, physical testing showed the ability of the heat exchanger to reduce fresh air temperature by up to 3.7 °C, however the amount of cooling was found to be highly dependent on the wind speed and direction.

6. A second numerical model was developed corresponding to the experimental design of the field trial, validated against the decrease in fresh air temperature over the heat exchanger and the increase in water temperature through the run-around. Comparing the experimental and numerical results the average error between the air temperature below the heat exchanger was found to be 2.1% between the two datasets. For the water temperature at the outlet of the run-around heat exchanger the average error was found to be 1.1%.
7. To ensure compliance with BS5952:1991 the volumetric flow rate into the room was measured. The wind tower produced a flow rate of 0.09 m^3/s (90 L/s) for the heat exchanger model featuring 52 pipes in three staggered rows at an inlet velocity of 1 m/s, corresponding to a pressure drop of 0.11 Pa. For a classroom with 20 occupants and a floor area of 35 m^2, a flow rate of 2.54 $L/s/m^2$ or 4.35 L/s per occupant was maintained. This was higher than the 0.8 and 1.3 $L/s/m^2$ stipulated for factories and offices/schools respectively but fell marginally below the 5 L/s per occupant required for the classroom with 20 occupants, although as the external wind speed increased this value was easily exceeded. It is indicated that a mechanical ventilation system would be required alongside any passive ventilation system to ensure ventilation rates are always maintained.

8. The RAHE was shown to decrease and increase the fresh air temperature by 4.4 and 4.2 °C respectively, when the temperature difference between the two fluids was 27 °C and the inlet velocity was 3 m/s. The amount of heating or cooling was directly proportional to the temperature difference between the two fluids, with an increase of 3 °C worth an additional 0.5 °C of heating or cooling. The water temperature through the heat exchanger increased and decreased by 6.15 °C under the same boundary conditions due to the additional thermal energy exchanged through the exhaust quadrants of the wind tower.
9. Increasing wind speed negatively impacted fresh air cooling but positively impacted the sensible energy recovery through the RAHE. Fresh air temperature was reduced by 6.70 C at 1 m/s and 3.75 C at 5 m/s. Water temperature increased by 2.84 C at 1 m/s and 8.43 C at 5 m/s. Increasing the volumetric flow rate through the RAHE had little impact on the fresh air temperature but resulted in a significant decrease in the water temperature at the outlet of the RAE. Despite this, the sensible energy recovered increased due to the increased flow rate through the heat exchanger.
10. Adding fins to the surface of the heat exchanger reduced the volumetric flow rate through the wind tower, increasing the pressure drop over the heat exchanger from 2.09 Pa to 3.71 Pa at 5 m/s inlet velocity. The heating or cooling of the fresh air was increased by an average of 15% whereas the temperature of the water and therefore the thermal energy recovered was increased by an average of 23%. The sensible energy recovered through the RAHE in a single pass increased from 2.0 to 2.4 kW when the wind speed was 3 m/s and the temperature difference between the two fluids was 27 C.

11. The average efficiency of the heat exchanger was calculated when changing the wind speed and air temperature. The standard heat exchanger maintained an average efficiency of 20% as the temperature difference between the fluids increased, rising to 25% with the addition of fins. When altering the wind speed, the efficiency fell from 30% to 18% when the wind speed increased from 1 to 5 m/s.
12. The heat exchanger's overall heat transfer coefficient (U value) was then calculated through the individual heat transfer coefficients for the air, water, and copper pipe. The U value increased from 2.4 to 5.1 W/m^2-K as the wind speed increased from 1 to 5 m/s. The increase in the U value reflects the increased heat transfer from the air to the water in the RAHE.

6.2 Contribution to Knowledge

The following is a summary of the main contributions to knowledge made in this thesis:

1. Two numerical models were created and used to generate simulation data on the application of commercial wind tower designs in mild-cold climates.

2. CFD models were validated using experimental data for both velocity and temperature (Wind tunnel test) and temperature (field trial), achieving levels of accuracy comparable to other studies exploring passive ventilation.

3. The numerical models showed that heat pipes could be integrated to directly recover heat from exhaust to inlet air streams, reducing the energy required to raise fresh air to a comfortable temperature.

4. A run-around heat exchanger integrated into a four-sided wind tower can be used to pre-heat and cool fresh air whilst recovering thermal energy, however the amount of heating, cooling, and heat recovery is highly dependent upon ambient conditions.

5. The use of fins to increase the surface area of the heat exchanger improved the system's performance without overly impacting the volumetric flow rate through the wind tower.

6.3 Future Work

To complement the work completed herein the following work is suggested:

1. The numerical studies only subjected the wind tower to the airflow, neglecting the impact of the leading edge of the building on the flow rate through the wind tower. Further studies broadening the scope of the model to explore the impact of a full atmospheric boundary layer on the performance of the heat exchanger should be carried out, especially as the lower velocities predicted through the wind tower would improve the performance of the heat exchanger. To complement this, it would also be beneficial to measure the performance of the wind tower under different wind angles. Using one quadrant as an inlet and three as outlets effectively represents the minimum performance of the system with regard to thermal energy recovery through the RAHE.
2. Further investigation is required to optimise the orientation of the heat pipes through a wind tower to effectively recover waste heat from each quadrant to every other quadrant regardless of wind direction.
3. Installing a run-around heat exchanger into a four-sided wind tower was effective at pre-heating and cooling fresh air whilst recovering waste thermal energy. The performance could be improved by altering the composition and

design of the heat exchanger, including the number of pipe layers, pipe spacing, pipe diameter, and fin design. By optimising the heat exchanger design the pressure drop could be further reduced, allowing for more pipe layers in the heat exchanger and therefore improving the heat recovery and treatment of fresh air.

4. To fully characterise the potential for linking a form of STES, it is crucial to calculate the sensible energy recovery over an entire heating or cooling season. This would also enable a calculation of the predicted reduction in building heating or cooling energy demand by linking the thermal energy delivered through the heat exchanger to the increase or decrease in fresh air temperature.
5. The work focussed mainly on the performance of the heat exchanger within the wind tower. These results could be used to investigate the impacts on the thermal comfort of the building occupants using approaches such as the Predicted Mean Vote (PMV) and the impacts on Indoor Air Quality (IAQ) before any commercialisation.

7 References

Abd El-Baky, M.A. and Mohamed, M.M. (2007) ‘Heat pipe heat exchanger for heat recovery in air conditioning’, *Applied Thermal Engineering*, 27(4), pp. 795–801. Available at: https://doi.org/10.1016/j.applthermaleng.2006.10.020.

Abraham, S. and Li, X. (2014) ‘A cost-effective wireless sensor network system for indoor air quality monitoring applications’, in *Procedia Computer Science*. Elsevier B.V., pp. 165–171. Available at: https://doi.org/10.1016/j.procs.2014.07.090.

Adamu, Z.A. and Price, A.D.F. (2015) ‘Natural ventilation with heat recovery: A biomimetic concept’, *Buildings*, 5(2), pp. 405–423. Available at: https://doi.org/10.3390/buildings5020405.

Ahmed Abdul–Wahab, S.A. *et al.* (2015) ‘A review of standards and guidelines set by international bodies for the parameters of indoor air quality’, *Atmospheric Pollution Research*, 6(5), pp. 751–767. Available at: https://doi.org/10.5094/APR.2015.084.

Ahmed, T., Kumar, P. and Mottet, L. (2021) ‘Natural ventilation in warm climates: The challenges of thermal comfort, heatwave resilience and indoor air quality’, *Renewable and Sustainable Energy Reviews*. Elsevier Ltd. Available at: https://doi.org/10.1016/j.rser.2020.110669.

Ahrens, M.U. *et al.* (2021) ‘Integrated high temperature heat pumps and thermal storage tanks for combined heating and cooling in the industry’, *Applied Thermal Engineering*, 189(February), p. 116731. Available at: https://doi.org/10.1016/j.applthermaleng.2021.116731.

Alammar, A.A., Al-Dadah, R.K. and Mahmoud, S.M. (2016) ‘Numerical investigation of effect of fill ratio and inclination angle on a thermosiphon heat pipe thermal performance’, *Applied Thermal Engineering*, 108, pp. 1055–1065. Available at: https://doi.org/10.1016/j.applthermaleng.2016.07.163.

Alizadehdakhel, A., Rahimi, M. and Alsairafi, A.A. (2010) ‘CFD modeling of flow and heat transfer in a thermosyphon’, *International Communications in Heat and Mass Transfer*, 37(3), pp. 312–318. Available at: https://doi.org/10.1016/j.icheatmasstransfer.2009.09.002.

Al-Sallal, K.A. and Al-Rais, L. (2012) ‘Outdoor airflow analysis and potential for passive cooling in the modern urban context of Dubai’, *Renewable Energy*, 38(1), pp. 40–49. Available at: https://doi.org/10.1016/j.renene.2011.06.046.

Alwetaishi, M. and Gadi, M. (2020) ‘New and Innovative Wind Catcher Designs to Improve Indoor Air Quality in Buildings’, *Energy and Built Environment* [Preprint]. Available at: https://doi.org/10.1016/j.enbenv.2020.06.009.

Amasyali, K. and El-Gohary, N.M. (2018) ‘A review of data-driven building energy consumption prediction studies’, *Renewable and Sustainable Energy Reviews*, 81(September 2017), pp. 1192–1205. Available at: https://doi.org/10.1016/j.rser.2017.04.095.

Anastasovski, A., Rasković, P. and Guzović, Z. (2020) 'A review of heat integration approaches for organic rankine cycle with waste heat in production processes', *Energy Conversion and Management*, 221. Available at: https://doi.org/10.1016/j.enconman.2020.113175.

Ann Cruickshank, C. and Baldwin, C. (2016) *Sensible Thermal Energy Storage: Diurnal and Seasonal*, *Storing Energy: With Special Reference to Renewable Energy Sources*. Elsevier Inc. Available at: https://doi.org/10.1016/B978-0-12-803440-8.00015-4.

Ansys (2020) 'ANSYS FLUENT Theory Guide', (January).

ANSYS Inc. (2015) 'ANSYS Fluent Meshing User's Guide', 15317(April), pp. 724–746.

de Antonellis, S. *et al.* (2014) 'Design optimization of heat wheels for energy recovery in HVAC systems', *Energies*, 7(11), pp. 7348–7367. Available at: https://doi.org/10.3390/en7117348.

Arce, J. *et al.* (2009) 'Experimental study for natural ventilation on a solar chimney', *Renewable Energy*, 34(12), pp. 2928–2934. Available at: https://doi.org/10.1016/j.renene.2009.04.026.

Arshi Banu, P.S. *et al.* (2022) 'Simulation of fin and tube heat exchanger and validation with CFD analysis', *Materials Today: Proceedings*, 66, pp. 1471–1476. Available at: https://doi.org/10.1016/j.matpr.2022.05.552.

Babaei, M. and Nick, H.M. (2019) 'Performance of low-enthalpy geothermal systems: Interplay of spatially correlated heterogeneity and well-doublet spacings', *Applied Energy*, 253(July), p. 113569. Available at: https://doi.org/10.1016/j.apenergy.2019.113569.

Bai, Y. *et al.* (2020) 'Numerical and experimental study of an underground water pit for seasonal heat storage', *Renewable Energy* [Preprint]. Available at: https://doi.org/10.1016/j.renene.2019.12.080.

Bakhtiari, H. *et al.* (2020) 'On the performance of night ventilation in a historic office building in nordic climate', *Energies*, 13(6). Available at: https://doi.org/10.3390/en13164159.

Baloch, R.M. *et al.* (2020) 'Indoor air pollution, physical and comfort parameters related to schoolchildren's health: Data from the European SINPHONIE study', *Science of the Total Environment*, 739. Available at: https://doi.org/10.1016/j.scitotenv.2020.139870.

Baradol, O. *et al.* (2019) 'Experimental Study on the Heat Transfer Enhancement In The Electronics Devices By Using Php'. Available at: www.ijsrset.com.

Başer, T. and McCartney, J.S. (2020) 'Transient evaluation of a soil-borehole thermal energy storage system', *Renewable Energy*, 147, pp. 2582–2598. Available at: https://doi.org/10.1016/j.renene.2018.11.012.

Becker, R. and Paciuk, M. (2002) *Inter-related effects of cooling strategies and building features on energy performance of office buildings*.

Beier, R.A. (2020) 'Thermal response tests on deep borehole heat exchangers with geothermal gradient', *Applied Thermal Engineering*, 178(February), p. 115447. Available at: https://doi.org/10.1016/j.applthermaleng.2020.115447.

Beier, R.A. and Ewbank, G.N. (2012) 'In-Situ Test Thermal Response Tests Interpretations OG&E Ground Source Heat Exchange Study', (August).

Ben-David, T. and Waring, M.S. (2016) 'Impact of natural versus mechanical ventilation on simulated indoor air quality and energy consumption in offices in fourteen U.S. cities', *Building and Environment*, 104, pp. 320–336. Available at: https://doi.org/10.1016/j.buildenv.2016.05.007.

Bloemendal, M. and Hartog, N. (2018) 'Analysis of the impact of storage conditions on the thermal recovery efficiency of low-temperature ATES systems', *Geothermics*, 71(October 2017), pp. 306–319. Available at: https://doi.org/10.1016/j.geothermics.2017.10.009.

Bloemendal, M., Olsthoorn, T. and van de Ven, F. (2015) 'Combining climatic and geo-hydrological preconditions as a method to determine world potential for aquifer thermal energy storage', *Science of the Total Environment* [Preprint]. Available at: https://doi.org/10.1016/j.scitotenv.2015.07.084.

Boache, P.J. (1994) 'Perspective: A method for uniform reporting of grid refinement studies', *Journal of Fluids Engineering, Transactions of the ASME*, 116(3), pp. 405–413. Available at: https://doi.org/10.1115/1.2910291.

Bonte, M. (2013) *Impacts of shallow geothermal energy on groundwater quality*.

Borjigin, S. *et al.* (2020) 'Performance enhancement of cabinet cooling system by utilizing cross-flow plate heat exchanger', *Energy Conversion and Management*, 213. Available at: https://doi.org/10.1016/j.enconman.2020.112854.

Bozkaya, B. and Zeiler, W. (2019) 'The effectiveness of night ventilation for the thermal balance of an aquifer thermal energy storage', *Applied Thermal Engineering*, 146(August 2018), pp. 190–202. Available at: https://doi.org/10.1016/j.applthermaleng.2018.09.106.

British Standards (1991) 'Ventilation principles and designing for natural ventilation.', ((BS 5925: 1991)).

Cabeza, L.F. *et al.* (2015) *Introduction to thermal energy storage (TES) systems*, *Advances in Thermal Energy Storage Systems: Methods and Applications*. Woodhead Publishing Limited. Available at: https://doi.org/10.1533/9781782420965.1.

Calautit, J.K. *et al.* (2013) 'Comparison between evaporative cooling and a heat pipe assisted thermal loop for a commercial wind tower in hot and dry climatic conditions', *Applied Energy*, 101, pp. 740–755. Available at: https://doi.org/10.1016/j.apenergy.2012.07.034.

Calautit, J.K. *et al.* (2017) 'Numerical and experimental analysis of a multi-directional wind tower integrated with vertically-arranged heat transfer devices (VHTD)', *Applied Energy* [Preprint]. Available at: https://doi.org/10.1016/j.apenergy.2016.02.025.

Calautit, J.K., O'Connor, D., *et al.* (2020) 'Development of a natural ventilation windcatcher with passive heat recovery wheel for mild-cold climates: CFD and experimental analysis', *Renewable Energy*, 160, pp. 465–482. Available at: https://doi.org/10.1016/j.renene.2020.05.177.

Calautit, J.K., Tien, P.W., *et al.* (2020) 'Numerical and experimental investigation of the indoor air quality and thermal comfort performance of a low energy cooling windcatcher with heat pipes and extended surfaces', *Renewable Energy* [Preprint]. Available at: https://doi.org/10.1016/j.renene.2019.06.040.

Calautit, J.K. and Hughes, B.R. (2014a) 'Measurement and prediction of the indoor airflow in a room ventilated with a commercial wind tower', *Energy and Buildings*, 84, pp. 367–377. Available at: https://doi.org/10.1016/j.enbuild.2014.08.015.

Calautit, J.K. and Hughes, B.R. (2014b) 'Wind tunnel and CFD study of the natural ventilation performance ofa commercial multi-directional wind tower', *Building and Environment*, 80, pp. 71–83. Available at: https://doi.org/10.1016/j.buildenv.2014.05.022.

Calautit, J.K. and Hughes, B.R. (2016) 'A passive cooling wind catcher with heat pipe technology: CFD, wind tunnel and field-test analysis', *Applied Energy*, 162, pp. 460–471. Available at: https://doi.org/10.1016/j.apenergy.2015.10.045.

Calautit, J.K., O'Connor, D. and Hughes, B.R. (2014) 'Determining the optimum spacing and arrangement for commercial wind towers for ventilation performance', *Building and Environment*, 82, pp. 274–287. Available at: https://doi.org/10.1016/j.buildenv.2014.08.024.

Calautit, J.K., O'Connor, D. and Hughes, B.R. (2016) 'A natural ventilation wind tower with heat pipe heat recovery for cold climates', *Renewable Energy*, 87, pp. 1088–1104. Available at: https://doi.org/10.1016/j.renene.2015.08.026.

Carreto-Hernandez, L.G. *et al.* (2023) 'Numerical-experimental study of mixed convection in a wind tower-room system', *Building and Environment*, 237. Available at: https://doi.org/10.1016/j.buildenv.2023.110294.

Carrillo, A.J. *et al.* (2019) 'Solar Energy on Demand: A Review on High Temperature Thermochemical Heat Storage Systems and Materials', *Chemical Reviews*, 119(7), pp. 4777–4816. Available at: https://doi.org/10.1021/acs.chemrev.8b00315.

Cellek, M.S. (2020) 'Turbulent flames investigation of methane and syngas fuels with the perspective of near-wall treatment models', *International Journal of Hydrogen Energy*, 45(60), pp. 35223–35234. Available at: https://doi.org/10.1016/j.ijhydene.2020.05.039.

Chang, C., Wu, Z., *et al.* (2017) 'Comparative study of the transient natural convection in an underground water pit thermal storage', *Applied Energy*, 208(August), pp. 1162–1173. Available at: https://doi.org/10.1016/j.apenergy.2017.09.036.

Chang, C., Nie, B., *et al.* (2017) 'Influences of the key characteristic parameters on the thermal performance of a water pit seasonal thermal storage', *Energy Procedia*, 142, pp. 495–500. Available at: https://doi.org/10.1016/j.egypro.2017.12.077.

Chang, C., Leng, G., *et al.* (2017) 'Investigation on transient cooling process in a water heat storage tank with inclined sidewalls', *Energy Procedia*, 142, pp. 142–147. Available at: https://doi.org/10.1016/j.egypro.2017.12.023.

Chaudhry, H.N., Hughes, B.R. and Ghani, S.A. (2012) 'A review of heat pipe systems for heat recovery and renewable energy applications', *Renewable and Sustainable Energy Reviews*, 16(4), pp. 2249–2259. Available at: https://doi.org/10.1016/j.rser.2012.01.038.

Chen, Q. and Srebric, J. (2002) 'A procedure for verification, validation, and reporting of indoor environment CFD analyses', *HVAC and R Research*, 8(2), pp. 201–216. Available at: https://doi.org/10.1080/10789669.2002.10391437.

Cheng, Y. *et al.* (2003) 'A comparison of large Eddy simulations with a standard k-ε Reynolds-averaged Navier-Stokes model for the prediction of a fully developed turbulent flow over a matrix of cubes', *Journal of Wind Engineering and Industrial Aerodynamics*, 91(11), pp. 1301–1328. Available at: https://doi.org/10.1016/j.jweia.2003.08.001.

Cheruy, F. *et al.* (2017) 'Role of Soil Thermal Inertia in Surface Temperature and Soil Moisture-Temperature Feedback', *Journal of Advances in Modeling Earth Systems*, 9(8), pp. 2906–2919. Available at: https://doi.org/10.1002/2017MS001036.

Choi, Y. hee *et al.* (2018) 'Analysis of the variable heat exchange efficiency of heat recovery ventilators and the associated heating energy demand', *Energy and Buildings*, 172, pp. 152–158. Available at: https://doi.org/10.1016/j.enbuild.2018.04.066.

Chung, T.J. (2002) 'Adaptive Methods', in *Computational Fluid Dynamics*. Cambridge University Press, pp. 607–643. Available at: https://doi.org/10.1017/CBO9780511606205.024.

CIBSE Guide A: Environmental Design, Chartered Institution of Building Service Engineers London (2015).

Claudia Klein, A. *et al.* (2018) 'About the suitability of different numerical methods to reproduce model wind turbine measurements in a wind tunnel with a high blockage ratio', *Wind Energy Science*, 3(1), pp. 439–460. Available at: https://doi.org/10.5194/wes-3-439-2018.

Collignon, M. *et al.* (2020) 'Evaluating thermal losses and storage capacity in high-temperature aquifer thermal energy storage (HT-ATES) systems with well operating limits: insights from a study-case in the Greater Geneva Basin, Switzerland', *Geothermics*, 85(November 2019), p. 101773. Available at: https://doi.org/10.1016/j.geothermics.2019.101773.

Connor, D.O. *et al.* (2019) ‘Analysis of a rotary passive heat recovery device for natural ventilation windcatcher’, *IOP Conference Series: Materials Science and Engineering*, 556(1). Available at: https://doi.org/10.1088/1757-899X/556/1/012001.

Davidsson, H., Bernardo, R. and Hellström, B. (2013) ‘Theoretical and experimental investigation of a heat exchanger suitable for a hybrid ventilation system’, *Buildings*, 3(1), pp. 18–38. Available at: https://doi.org/10.3390/buildings3010018.

De Dear, R.J. *et al.* (2013) ‘Progress in thermal comfort research over the last twenty years’, *Indoor Air*, pp. 442–461. Available at: https://doi.org/10.1111/ina.12046.

De Dear, R.J. and Brager, G.S. (2002) *Thermal comfort in naturally ventilated buildings: revisions to ASHRAE Standard 55*.

Deng, J. *et al.* (2019) ‘Field test on energy performance of medium-depth geothermal heat pump systems (MD-GHPs)’, *Energy and Buildings*, 184, pp. 289–299. Available at: https://doi.org/10.1016/j.enbuild.2018.12.006.

Department for Education (2014) ‘Briefing Framework for Secondary School Projects. Revision of BB82: Area Guidelines for Schools (Secondary section)’, pp. 1–66.

Djongyang, N., Tchinda, R. and Njomo, D. (2010) ‘Thermal comfort: A review paper’, *Renewable and Sustainable Energy Reviews*. Elsevier Ltd. Available at: https://doi.org/10.1016/j.rser.2010.07.040.

Drach, P.R.C. (2009) ‘A study on air circulation: The case of House VI of “Vila” 37 with the application of wind-catch’, *Building Simulation*, 2(4), pp. 307–316. Available at: https://doi.org/10.1007/s12273-009-9415-6.

Eça, L. and Hoekstra, M. (2006) *Discretization Uncertainty Estimation based on a Least Squares version of the Grid Convergence Index*.

Eça, L. and Hoekstra, M. (2014) ‘A procedure for the estimation of the numerical uncertainty of CFD calculations based on grid refinement studies’, *Journal of Computational Physics*, 262, pp. 104–130. Available at: https://doi.org/10.1016/j.jcp.2014.01.006.

Elmualim, A.A. (2006) ‘Verification of design calculations of a wind catcher/tower natural ventilation system with performance testing in a real building’, *International Journal of Ventilation*, 4(4), pp. 393–404. Available at: https://doi.org/10.1080/14733315.2005.11683717.

Elmualim, A.A. and Awbi, H.B. (2002) ‘Wind Tunnel and CFD Investigation of the Performance of “Windcatcher” Ventilation Systems’, *International Journal of Ventilation*, 1(1), pp. 53–64. Available at: https://doi.org/10.1080/14733315.2002.11683622.

Engarnevis, A. *et al.* (2017) ‘Particulate fouling assessment in membrane based air-to-air energy exchangers’, *Energy and Buildings*, 150, pp. 477–487. Available at: https://doi.org/10.1016/j.enbuild.2017.05.046.

Engarnevis, A. *et al.* (2018) ‘Heat and mass transfer modeling in enthalpy exchangers using asymmetric composite membranes’, *Journal of Membrane Science*, 556(March), pp. 248–262. Available at: https://doi.org/10.1016/j.memsci.2018.03.007.

EPA (1991) *Indoor Air Facts No. 4 Sick Building Syndrome*.

European Commission (2020) *Stepping up Europe’s 2030 climate ambition*.

European Council (2014) ‘European Council 23-24 October 2014 - Conclusions’.

Fernández-Seara, J. *et al.* (2011) ‘Experimental analysis of an air-to-air heat recovery unit for balanced ventilation systems in residential buildings’, *Energy Conversion and Management*, 52(1), pp. 635–640. Available at: https://doi.org/10.1016/j.enconman.2010.07.040.

Flaga-Maryanczyk, A. *et al.* (2014) ‘Experimental measurements and CFD simulation of a ground source heat exchanger operating at a cold climate for a passive house ventilation system’, *Energy and Buildings*, 68(PARTA), pp. 562–570. Available at: https://doi.org/10.1016/j.enbuild.2013.09.008.

Fleuchaus, P. *et al.* (2018) ‘Worldwide application of aquifer thermal energy storage – A review’, *Renewable and Sustainable Energy Reviews* [Preprint]. Available at: https://doi.org/10.1016/j.rser.2018.06.057.

Gao, L. *et al.* (2017) ‘A review on system performance studies of aquifer thermal energy storage’, *Energy Procedia*, 142, pp. 3537–3545. Available at: https://doi.org/10.1016/j.egypro.2017.12.242.

Geros, V. *et al.* (1999) *Experimental evaluation of night ventilation phenomena*, *Energy and Buildings*.

Ghadiri, M. (2011) *The Effect of Tower Height in Square Plan Wind catcher on its Thermal Behavior*. Available at: https://www.researchgate.net/publication/281773494.

Ghoreishi-Madiseh, S.A. *et al.* (2017) ‘Performance evaluation of large scale rock-pit seasonal thermal energy storage for application in underground mine ventilation’, *Applied Energy*, 185, pp. 1940–1947. Available at: https://doi.org/10.1016/j.apenergy.2016.01.062.

Google (2023) *Google Earth*.

Hähnlein, S. *et al.* (2013) ‘Sustainability and policy for the thermal use of shallow geothermal energy’, *Energy Policy*, 59, pp. 914–925. Available at: https://doi.org/10.1016/j.enpol.2013.04.040.

Hakkarainen, E., Hannula, I. and Vakkilainen, E. (2019) ‘Bioenergy RES hybrids − assessment of status in Finland, Austria, Germany, and Denmark’, *Biofuels, Bioproducts and Biorefining*, 13(6), pp. 1402–1416. Available at: https://doi.org/10.1002/bbb.2019.

Han, C. and Yu, X. (2016) ‘Sensitivity analysis of a vertical geothermal heat pump system’, *Applied Energy*, 170, pp. 148–160. Available at: https://doi.org/10.1016/j.apenergy.2016.02.085.

He, G. *et al.* (2021) ‘Ventilation performance of solar chimney in a test house: Field measurement and validation of plume model’, *Building and Environment*, 193. Available at: https://doi.org/10.1016/j.buildenv.2021.107648.

Herath, H.M.D.P. *et al.* (2020) ‘Applicability of rotary thermal wheels to hot and humid climates’, *Energy Reports*, 6, pp. 539–544. Available at: https://doi.org/10.1016/j.egyr.2019.11.116.

Hosseini, S.H. *et al.* (2016) ‘Evaluation of airflow and thermal comfort in buildings ventilated with wind catchers: Simulation of conditions in Yazd City, Iran’, *Energy for Sustainable Development*, 35, pp. 7–24. Available at: https://doi.org/10.1016/j.esd.2016.09.005.

Hosseinnia, S.M., Saffari, H. and Abdous, M.A. (2013) ‘Effects of different internal designs of traditional wind towers on their thermal behavior’, *Energy and Buildings*, 62, pp. 51–58. Available at: https://doi.org/10.1016/j.enbuild.2012.10.058.

Hughes, B.R., Calautit, J.K. and Ghani, S.A. (2012) ‘The development of commercial wind towers for natural ventilation: A review’, *Applied Energy* [Preprint]. Available at: https://doi.org/10.1016/j.apenergy.2011.11.066.

Hughes, B.R., Chaudhry, H.N. and Calautit, J.K. (2014) ‘Passive energy recovery from natural ventilation air streams’, *Applied Energy*, 113, pp. 127–140. Available at: https://doi.org/10.1016/j.apenergy.2013.07.019.

Hughes, B.R., Chaudhry, H.N. and Ghani, S.A. (2011) ‘A review of sustainable cooling technologies in buildings’, *Renewable and Sustainable Energy Reviews*. Elsevier Ltd, pp. 3112–3120. Available at: https://doi.org/10.1016/j.rser.2011.03.032.

Hughes, B.R. and Ghani, S.A. (2011) ‘A numerical investigation into the feasibility of a passive-assisted natural ventilation stack device’, *International Journal of Sustainable Energy*, 30(4), pp. 193–211. Available at: https://doi.org/10.1080/1478646X.2010.503275.

Hughes, B.R. and Ghani, S.A.A.A. (2008) ‘Investigation of a windvent passive ventilation device against current fresh air supply recommendations’, *Energy and Buildings*, 40(9), pp. 1651–1659. Available at: https://doi.org/10.1016/j.enbuild.2008.02.024.

Hughes, B.R. and Ghani, S.A.A.A. (2010) ‘A numerical investigation into the effect of Windvent louvre external angle on passive stack ventilation performance’, *Building and Environment* [Preprint]. Available at: https://doi.org/10.1016/j.buildenv.2009.10.010.

Hughes, B.R. and Mak, C.M. (2011) ‘A study of wind and buoyancy driven flows through commercial wind towers’, *Energy and Buildings*, 43(7), pp. 1784–1791. Available at: https://doi.org/10.1016/j.enbuild.2011.03.022.

Huo, X. *et al.* (2020) ‘Sick building syndrome symptoms among young parents in Chinese homes’, *Building and Environment*, 169. Available at: https://doi.org/10.1016/j.buildenv.2019.106283.

Hviid, C.A. and Svendsen, S. (2011) ‘Analytical and experimental analysis of a low-pressure heat exchanger suitable for passive ventilation’, *Energy and Buildings*, 43(2–3), pp. 275–284. Available at: https://doi.org/10.1016/j.enbuild.2010.08.003.

Jing, R. *et al.* (2022) ‘Cost-efficient decarbonization of local energy systems by whole-system based design optimization’, *Applied Energy*, 326(August), p. 119921. Available at: https://doi.org/10.1016/j.apenergy.2022.119921.

Jones, B. and Molina, C. (2017) *Indoor Air Quality*, *Encyclopedia of Sustainable Technologies*. Elsevier. Available at: https://doi.org/10.1016/B978-0-12-409548-9.10198-8.

Jouhara, H. *et al.* (2017) ‘Heat pipe based systems - Advances and applications’, *Energy*. Elsevier Ltd, pp. 729–754. Available at: https://doi.org/10.1016/j.energy.2017.04.028.

Jouhara, H. *et al.* (2018) ‘Waste heat recovery technologies and applications’, *Thermal Science and Engineering Progress*, 6(January), pp. 268–289. Available at: https://doi.org/10.1016/j.tsep.2018.04.017.

Kallesøe, A.J. *et al.* (2021) *HEATSTORE-Underground Thermal Energy Storage (UTES)-State of the Art, Example Cases and Lessons Learned*.

Kallesøe, A.J. and Vangkilde-Pedersen, T. (2019) *HEATSTORE. Underground Thermal Energy Storage (UTES) – state-of-the-art, example cases and lessons learned.*, *HEATSTORE project report, GEOTHERMICA – ERA NET Cofund Geothermal.* Available at: https://www.heatstore.eu/documents/HEATSTORE_UTES State of the Art_WP1_D1.1_Final_2019.04.26.pdf.

Karniadakis, G.E. (2002) ‘Quantifying uncertainty in CFD’, *Journal of Fluids Engineering, Transactions of the ASME*, 124(3).

Kasaeian, A.B. *et al.* (2017) ‘A review on solar chimney systems’, *Renewable and Sustainable Energy Reviews*. Elsevier Ltd, pp. 954–987. Available at: https://doi.org/10.1016/j.rser.2016.09.081.

Kassaei, F. *et al.* (2022) ‘Experimental studies on solar chimneys for natural ventilation in domestic applications: a comprehensive review’, *Environmental Science and Pollution Research*. Springer Science and Business Media Deutschland GmbH, pp. 73842–73855. Available at: https://doi.org/10.1007/s11356-022-22956-3.

Khan, N., Su, Y. and Riffat, S.B. (2008) ‘A review on wind driven ventilation techniques’, *Energy and Buildings* [Preprint]. Available at: https://doi.org/10.1016/j.enbuild.2008.02.015.

Khan, W.A., Culham, J.R. and Yovanovich, M.M. (2006) ‘Convection heat transfer from tube banks in crossflow: Analytical approach’, *International Journal of Heat and Mass Transfer*, 49(25–26), pp. 4831–4838. Available at: https://doi.org/10.1016/j.ijheatmasstransfer.2006.05.042.

Khanmohammadi, S. and Shahsavar, A. (2018) ‘Energy analysis and multi-objective optimization of a novel exhaust air heat recovery system consisting of an air-based

building integrated photovoltaic/thermal system and a thermal wheel', *Energy Conversion and Management*, 172(July), pp. 595–610. Available at: https://doi.org/10.1016/j.enconman.2018.07.057.

Khosravi, M., Fazelpour, F. and Rosen, M.A. (2019) 'Improved application of a solar chimney concept in a two-story building: An enhanced geometry through a numerical approach', *Renewable Energy*, 143, pp. 569–585. Available at: https://doi.org/10.1016/j.renene.2019.05.042.

Kim, J. and Chung, J. (2015) 'Untangling polygonal and polyhedral meshes via mesh optimization', *Engineering with Computers*, 31(3), pp. 617–629. Available at: https://doi.org/10.1007/s00366-014-0379-5.

Kocijel, L., Mrzljak, V. and Glažar, V. (2020) 'Numerical analysis of geometrical and process parameters influence on temperature stratification in a large volumetric heat storage tank', *Energy*, 194. Available at: https://doi.org/10.1016/j.energy.2019.116878.

Kubiński, K. and Szabłowski, Ł. (2020) 'Dynamic model of solar heating plant with seasonal thermal energy storage', *Renewable Energy*, 145, pp. 2025–2033. Available at: https://doi.org/10.1016/j.renene.2019.07.120.

Lagoeiro, H. *et al.* (2022) *Integrating Waste Heat Recovery from Railway Tunnels into Flexible Heat Networks*.

Languri, E.M. and Cunningham, G. (2019) 'Thermal Energy Storage Systems', *Lecture Notes in Energy*, 70(November), pp. 169–176. Available at: https://doi.org/10.1007/978-3-030-05636-0_9.

Li, C. *et al.* (2017) 'Effects of load optimization and geometric arrangement on the thermal performance of borehole heat exchanger fields', *Sustainable Cities and Society*, 35(May), pp. 25–35. Available at: https://doi.org/10.1016/j.scs.2017.07.018.

Lim, H.S. *et al.* (2020) 'Efficiency improvement of energy storage and release by the inlet position control for seasonal thermal energy storage', *International Journal of Heat and Mass Transfer*, 151. Available at: https://doi.org/10.1016/j.ijheatmasstransfer.2020.119435.

Liu, M. and Calautit, J.K. (2023) 'A parametric investigation of the heat transfer enhancement of tube bank heat exchanger with reversed trapezoidal profile fins', *Thermal Science and Engineering Progress*, 42. Available at: https://doi.org/10.1016/j.tsep.2023.101914.

Liu, P. *et al.* (2016) 'A theoretical model to predict frosting limits in cross-flow air-to-air flat plate heat/energy exchangers', *Energy and Buildings*, 110, pp. 404–414. Available at: https://doi.org/10.1016/j.enbuild.2015.11.007.

Liu, S., Mak, C.M. and Niu, J.L. (2011) 'Numerical evaluation of louver configuration and ventilation strategies for the windcatcher system', *Building and Environment*, 46(8), pp. 1600–1616. Available at: https://doi.org/10.1016/j.buildenv.2011.01.025.

Lu, H., Tian, P. and He, L. (2019) 'Evaluating the global potential of aquifer thermal energy storage and determining the potential worldwide hotspots driven by socio-economic, geo-hydrologic and climatic conditions', *Renewable and Sustainable Energy Reviews* [Preprint]. Available at: https://doi.org/10.1016/j.rser.2019.06.013.

Lu, T. *et al.* (2016) 'The application of linear regression and the power law relationship of air-side heat transfer with field measurements to model the performance of run-around heat recovery systems', *Energy and Buildings*, 110, pp. 453–467. Available at: https://doi.org/10.1016/j.enbuild.2015.10.028.

Ma, N. *et al.* (2021) 'Measuring the right factors: A review of variables and models for thermal comfort and indoor air quality', *Renewable and Sustainable Energy Reviews*. Elsevier Ltd. Available at: https://doi.org/10.1016/j.rser.2020.110436.

Maasoumy, M. and Sangiovanni-Vincentelli, A. (2016) 'Smart connected buildings design automation: Foundations and trends', *Foundations and Trends in Electronic Design Automation*, 10(1–2), pp. 1–143. Available at: https://doi.org/10.1561/1000000043.

MacNaughton, P. *et al.* (2016) 'Environmental perceptions and health before and after relocation to a green building', *Building and Environment*, 104, pp. 138–144. Available at: https://doi.org/10.1016/j.buildenv.2016.05.011.

Maghrabie, H.M. *et al.* (2022) 'A review of solar chimney for natural ventilation of residential and non-residential buildings', *Sustainable Energy Technologies and Assessments*, 52. Available at: https://doi.org/10.1016/j.seta.2022.102082.

Mahon, H. *et al.* (2022) 'A review of thermal energy storage technologies for seasonal loops', *Energy*, 239, p. 122207. Available at: https://doi.org/10.1016/j.energy.2021.122207.

Mansi, S.A. *et al.* (2021) 'Measuring human physiological indices for thermal comfort assessment through wearable devices: A review', *Measurement: Journal of the International Measurement Confederation*, 183. Available at: https://doi.org/10.1016/j.measurement.2021.109872.

Mardiana-Idayu, A. and Riffat, S.B. (2011) 'An experimental study on the performance of enthalpy recovery system for building applications', *Energy and Buildings*, 43(9), pp. 2533–2538. Available at: https://doi.org/10.1016/j.enbuild.2011.06.009.

Mardiana-Idayu, A. and Riffat, S.B. (2012) 'Review on heat recovery technologies for building applications', *Renewable and Sustainable Energy Reviews*, 16(2), pp. 1241–1255. Available at: https://doi.org/10.1016/j.rser.2011.09.026.

Matos, C.R., Carneiro, J.F. and Silva, P.P. (2019) 'Overview of Large-Scale Underground Energy Storage Technologies for Integration of Renewable Energies and Criteria for Reservoir Identification', *Journal of Energy Storage* [Preprint]. Available at: https://doi.org/10.1016/j.est.2018.11.023.

Mehmood, S. *et al.* (2022) 'Resilient cooling pathway for extremely hot climates in southern Asia', *Applied Energy*, 325. Available at: https://doi.org/10.1016/j.apenergy.2022.119811.

Meister, C. and Beausoleil-Morrison, I. (2021) ‘Experimental and modelled performance of a building-scale solar thermal system with seasonal storage water tank’, *Solar Energy*, 222(May), pp. 145–159. Available at: https://doi.org/10.1016/j.solener.2021.05.025.

Mesquita, L. *et al.* (2017) ‘Drake Landing solar community: 10 years of operation’, *ISES Solar World Congress 2017 - IEA SHC International Conference on Solar Heating and Cooling for Buildings and Industry 2017, Proceedings*, pp. 333–344. Available at: https://doi.org/10.18086/swc.2017.06.09.

Montazeri, H. (2011) ‘Experimental and numerical study on natural ventilation performance of various multi-opening wind catchers’, *Building and Environment*, 46(2), pp. 370–378. Available at: https://doi.org/10.1016/j.buildenv.2010.07.031.

Moosavi, L. *et al.* (2020) ‘New design for solar chimney with integrated windcatcher for space cooling and ventilation’, *Building and Environment*, 181. Available at: https://doi.org/10.1016/j.buildenv.2020.106785.

Morchio, S. and Fossa, M. (2020) ‘On the ground thermal conductivity estimation with coaxial borehole heat exchangers according to different undisturbed ground temperature profiles’, *Applied Thermal Engineering*, 173(December 2019), p. 115198. Available at: https://doi.org/10.1016/j.applthermaleng.2020.115198.

Mroue, H. *et al.* (2015) ‘Experimental and numerical investigation of an air-to-water heat pipe-based heat exchanger’, *Applied Thermal Engineering*, 78, pp. 339–350. Available at: https://doi.org/10.1016/j.applthermaleng.2015.01.005.

Natarajan, S., Rodriguez, J. and Vellei, M. (2015) ‘A field study of indoor thermal comfort in the subtropical highland climate of Bogota, Colombia’, *Journal of Building Engineering*, 4, pp. 237–246. Available at: https://doi.org/10.1016/j.jobe.2015.10.003.

Nejat, P. *et al.* (2016) ‘Anti-short-circuit device: A new solution for short-circuiting in windcatcher and improvement of natural ventilation performance’, *Building and Environment*, 105, pp. 24–39. Available at: https://doi.org/10.1016/j.buildenv.2016.05.023.

Nielsen, T.R., Rose, J. and Kragh, J. (2009) ‘Dynamic model of counter flow air to air heat exchanger for comfort ventilation with condensation and frost formation’, *Applied Thermal Engineering*, 29(2–3), pp. 462–468. Available at: https://doi.org/10.1016/j.applthermaleng.2008.03.006.

Nithyanandam, K., Stekli, J. and Pitchumani, R. (2017) *High-temperature latent heat storage for concentrating solar thermal (CST) systems*, *Advances in Concentrating Solar Thermal Research and Technology*. Elsevier Ltd. Available at: https://doi.org/10.1016/B978-0-08-100516-3.00010-1.

Nordell, B. *et al.* (2015) ‘Long-term Performance of the HT-BTES in Emmaboda, Sweden’.

Novo, A. V. *et al.* (2010) ‘Review of seasonal heat storage in large basins: Water tanks and gravel-water pits’, *Applied Energy* [Preprint]. Available at: https://doi.org/10.1016/j.apenergy.2009.06.033.

O'Connor, D., Calautit, J. and Hughes, B.R. (2015) 'Effect of Rotation Speed of a Rotary Thermal Wheel on Ventilation Supply Rates of Wind Tower System', *Energy Procedia*, 75, pp. 1705–1710. Available at: https://doi.org/10.1016/j.egypro.2015.07.432.

O'Connor, D., Calautit, J.K. and Hughes, B.R. (2014) 'A study of passive ventilation integrated with heat recovery', *Energy and Buildings* [Preprint]. Available at: https://doi.org/10.1016/j.enbuild.2014.05.050.

O'Connor, D., Calautit, J.K. and Hughes, B.R. (2016) 'A novel design of a desiccant rotary wheel for passive ventilation applications', *Applied Energy*, 179, pp. 99–109. Available at: https://doi.org/10.1016/j.apenergy.2016.06.029.

O'connor, D., Calautit, J.K.S. and Hughes, B.R. (2016) 'A review of heat recovery technology for passive ventilation applications', *Renewable and Sustainable Energy Reviews*, 54, pp. 1481–1493. Available at: https://doi.org/10.1016/j.rser.2015.10.039.

Omrani, S. *et al.* (2017) 'Effect of natural ventilation mode on thermal comfort and ventilation performance: Full-scale measurement', *Energy and Buildings*, 156, pp. 1–16. Available at: https://doi.org/10.1016/j.enbuild.2017.09.061.

Ozmen, Y., Baydar, E. and van Beeck, J.P.A.J. (2016) 'Wind flow over the low-rise building models with gabled roofs having different pitch angles', *Building and Environment*, 95, pp. 63–74. Available at: https://doi.org/10.1016/j.buildenv.2015.09.014.

Pakari, A. and Ghani, S. (2019) 'Airflow assessment in a naturally ventilated greenhouse equipped with wind towers: numerical simulation and wind tunnel experiments', *Energy and Buildings*, 199, pp. 1–11. Available at: https://doi.org/10.1016/j.enbuild.2019.06.033.

Paksoy, H.O. *et al.* (2004) 'Aquifer thermal storage (ATES) for air-conditioning of a supermarket in Turkey', *Renewable Energy*, 29(12), pp. 1991–1996. Available at: https://doi.org/10.1016/j.renene.2004.03.007.

Papapetrou, M. *et al.* (2018) 'Industrial waste heat: Estimation of the technically available resource in the EU per industrial sector, temperature level and country', *Applied Thermal Engineering*, 138(April), pp. 207–216. Available at: https://doi.org/10.1016/j.applthermaleng.2018.04.043.

Pardo, P. *et al.* (2014) 'A review on high temperature thermochemical heat energy storage', *Renewable and Sustainable Energy Reviews*, 32, pp. 591–610. Available at: https://doi.org/10.1016/j.rser.2013.12.014.

Paudel, S. and Saenger, N. (2017) 'Grid refinement study for three dimensional CFD model involving incompressible free surface flow and rotating object', *Computers and Fluids*, 143, pp. 134–140. Available at: https://doi.org/10.1016/j.compfluid.2016.10.025.

Pavlov, G.K. and Olesen, B.W. (2011) 'Seasonal ground solar thermal energy storage - Review of systems and applications', *30th ISES Biennial Solar World Congress 2011, SWC 2011*, 6, pp. 4864–4874. Available at: https://doi.org/10.18086/swc.2011.29.24.

Pellegrini, M. *et al.* (2019) ‘Classification through analytic hierarchy process of the barriers in the revamping of traditional district heating networks into low temperature district heating: An Italian case study’, *International Journal of Sustainable Energy Planning and Management*, 20(April), pp. 51–66. Available at: https://doi.org/10.5278/ijsepm.2019.20.5.

Perén, J.I. *et al.* (2015) ‘CFD analysis of cross-ventilation of a generic isolated building with asymmetric opening positions: Impact of roof angle and opening location’, *Building and Environment*, 85, pp. 263–276. Available at: https://doi.org/10.1016/j.buildenv.2014.12.007.

Pérez-Lombard, L., Ortiz, J. and Pout, C. (2008) ‘A review on buildings energy consumption information’, *Energy and Buildings*, 40(3), pp. 394–398. Available at: https://doi.org/10.1016/j.enbuild.2007.03.007.

Qian, F. *et al.* (2020) ‘Potential analysis of the transfer learning model in short and medium-term forecasting of building HVAC energy consumption’, *Energy*, 193, p. 116724. Available at: https://doi.org/10.1016/j.energy.2019.116724.

Ramos, J., Chong, A. and Jouhara, H. (2016a) ‘Experimental and numerical investigation of a cross flow air-to-water heat pipe-based heat exchanger used in waste heat recovery’, *International Journal of Heat and Mass Transfer*, 102, pp. 1267–1281. Available at: https://doi.org/10.1016/j.ijheatmasstransfer.2016.06.100.

Ramos, J., Chong, A. and Jouhara, H. (2016b) ‘Experimental and numerical investigation of a cross flow air-to-water heat pipe-based heat exchanger used in waste heat recovery’, *International Journal of Heat and Mass Transfer* [Preprint]. Available at: https://doi.org/10.1016/j.ijheatmasstransfer.2016.06.100.

Reji, A.K. *et al.* (2021) ‘Performance analysis of thermosyphon heat pipe using aluminum oxide nanofluid under various angles of inclination’, in *Materials Today: Proceedings*. Elsevier Ltd, pp. 1211–1216. Available at: https://doi.org/10.1016/j.matpr.2020.04.247.

Renaldi, R. and Friedrich, D. (2019) ‘Techno-economic analysis of a solar district heating system with seasonal thermal storage in the UK’, *Applied Energy*, 236(August 2018), pp. 388–400. Available at: https://doi.org/10.1016/j.apenergy.2018.11.030.

Reuss, M. (2015) *The use of borehole thermal energy storage (BTES) systems*, *Advances in Thermal Energy Storage Systems: Methods and Applications*. Woodhead Publishing Limited. Available at: https://doi.org/10.1533/9781782420965.1.117.

Riffat, S.B. and Gan, G. (1998) ‘Determination of effectiveness of heat-pipe heat recovery for naturally-ventilated buildings’, *Applied Thermal Engineering*, 18(3–4), pp. 121–130. Available at: https://doi.org/10.1016/s1359-4311(97)00033-1.

Rigas, F. and Sklavounos, S. (2005) ‘Experimentally validated 3-D simulation of shock waves generated by dense explosives in confined complex geometries’, *Journal of Hazardous Materials*, 121(1–3), pp. 23–30. Available at: https://doi.org/10.1016/j.jhazmat.2005.01.031.

Roache, P.J. (1997) ‘Quantification of uncertainty in computational fluid dynamics’, *Annual Review of Fluid Mechanics*, 29, pp. 123–160. Available at: https://doi.org/10.1146/annurev.fluid.29.1.123.

Roache, P.J. (1998) ‘Fundamentals of Computational Fluid Dynamics’.

Root, W., Bechtold, T. and Pham, T. (2020) ‘Textile-Integrated thermocouples for temperature measurement’, *Materials*, 13(3). Available at: https://doi.org/10.3390/ma13030626.

Saadatian, O. *et al.* (2012) ‘Review of windcatcher technologies’, *Renewable and Sustainable Energy Reviews*, 16(3), pp. 1477–1495. Available at: https://doi.org/10.1016/j.rser.2011.11.037.

Sabek, S. *et al.* (2016) ‘Experimental investigation and numerical validation of total heat exchanger and membrane phenomena’, *Energy and Buildings*, 133, pp. 131–140. Available at: https://doi.org/10.1016/j.enbuild.2016.09.045.

Salim, S.M. and Cheah, S.C. (2009) *Wall y+ Strategy for Dealing with Wall-bounded Turbulent Flows*. Newswood Ltd.

Sanner, B. (2017) ‘Ground Source Heat Pumps – history , development , current status , and future prospects’, *12th IEA Heat Pump Conference 2017*, pp. 1–14. Available at: http://hpc2017.org/wp-content/uploads/2017/05/K.2.9.1-Ground-Source-Heat-Pumps-history-development-current-status-and-future-prospects.pdf.

Sarkar, J. and Bhattacharyya, S. (2012) ‘Characteristics of medium deep borehole thermal energy storage’, *Archives of Thermodynamics*, 33(4), pp. 23–40. Available at: https://doi.org/10.1002/er.

Sarkhosh, M. *et al.* (2021) ‘Indoor Air Quality associations with sick building syndrome: An application of decision tree technology’, *Building and Environment*, 188. Available at: https://doi.org/10.1016/j.buildenv.2020.107446.

Sauer, H.J. and Howell, R.H. (1981) ‘Promise and potential of air-to-air energy recovery systems’, *International Journal of Refrigeration*, 4(4), pp. 182–194. Available at: https://doi.org/10.1016/0140-7007(81)90049-9.

Schmidt, T. (2016) ‘Monitoring results from large-scale solar thermal plants with long term storage in Marstal, Brædstrup and Dronninglund, Denmark’, *4th International Solar District Heating Conference* [Preprint]. Available at: http://solar-district-heating.eu/Portals/0/SDH Conference 2016/Presentations_SDH2016_day2.zip.

Schmidt, T. *et al.* (2018) ‘Design Aspects for Large-scale Pit and Aquifer Thermal Energy Storage for District Heating and Cooling’, in *Energy Procedia*. Elsevier Ltd, pp. 585–594. Available at: https://doi.org/10.1016/j.egypro.2018.08.223.

Schmidt, T. and Miedaner, O. (2005) ‘Solar district heating guidelines, Fact sheet 7.2’, *Food Engineering Series*, pp. 93–123. Available at: https://doi.org/10.1007/0-387-27613-0_4.

Schmidt, T. and Miedaner, O. (2012) ‘Solar district heating guidelines’, *30th ISES Biennial Solar World Congress 2011, SWC 2011*, 4(August), pp. 3058–3065. Available at: https://doi.org/10.18086/swc.2011.21.08.

Schout, G., Drijver, B. and Schotting, R. (2016) ‘The influence of the injection temperature on the recovery efficiency of high temperature aquifer thermal energy storage: Comment on Jeon et al., 2015’, *Energy*, 103, pp. 107–109. Available at: https://doi.org/10.1016/j.energy.2016.02.122.

Schulte, D.O. *et al.* (2016) ‘Optimization of Medium-Deep Borehole Thermal Energy Storage Systems’, *Energy Technology*, 4(1), pp. 104–113. Available at: https://doi.org/10.1002/ente.201500254.

Schwer, L.E. (2008) ‘Is your mesh refined enough? Estimating Discretization Error using GCI’, *7th LS-DYNA Anwenderforum*, 1(1), pp. 45–54. Available at: https://www.dynamore.eu/en/downloads/papers/dynamore/de/download/papers/forum08/dokumente/I-I-03.pdf.

Seo, J.W., Lee, D.Y. and Kim, D.S. (2018) ‘A simple effectiveness model for heat wheels’, *International Journal of Heat and Mass Transfer*, 120, pp. 1358–1364. Available at: https://doi.org/10.1016/j.ijheatmasstransfer.2017.12.102.

Seppanen, O. and Fisk, W.J. (2001) *Association of ventilation system type with SBS symptoms in office workers Publication Date*.

Serageldin, A.A. *et al.* (2020) ‘Solar chimney combined with earth to-air heat exchanger for passive cooling of residential buildings in hot areas’, *Solar Energy*, 206, pp. 145–162. Available at: https://doi.org/10.1016/j.solener.2020.05.102.

Seyed-Ahmadi, M. *et al.* (2009a) ‘Transient behavior of run-around heat and moisture exchanger system. Part I: Model formulation and verification’, *International Journal of Heat and Mass Transfer*, 52(25–26), pp. 6000–6011. Available at: https://doi.org/10.1016/j.ijheatmasstransfer.2009.07.012.

Seyed-Ahmadi, M. *et al.* (2009b) ‘Transient behavior of run-around heat and moisture exchanger system. Part II: Sensitivity studies for a range of initial conditions’, *International Journal of Heat and Mass Transfer*, 52(25–26), pp. 6012–6020. Available at: https://doi.org/10.1016/j.ijheatmasstransfer.2009.06.037.

Shabgard, H. *et al.* (2015) ‘Heat pipe heat exchangers and heat sinks: Opportunities, challenges, applications, analysis, and state of the art’, *International Journal of Heat and Mass Transfer*, 89, pp. 138–158. Available at: https://doi.org/10.1016/j.ijheatmasstransfer.2015.05.020.

Shah, S.K., Aye, L. and Rismanchi, B. (2018) ‘Seasonal thermal energy storage system for cold climate zones: A review of recent developments’, *Renewable and Sustainable Energy Reviews*, 97(August), pp. 38–49. Available at: https://doi.org/10.1016/j.rser.2018.08.025.

Shao, L. and Riffat, S.B. (1997) ‘Flow loss caused by heat pipes in natural ventilation stacks’, *Applied Thermal Engineering*, 17(4), pp. 393–399. Available at: https://doi.org/10.1016/s1359-4311(96)00029-4.

Shao, L., Riffat, S.B. and Gan, G. (1998) ‘Heat recovery with low pressure loss for natural ventilation’, *Energy and Buildings* [Preprint]. Available at: https://doi.org/10.1016/s0378-7788(98)00016-4.

Siegele, D. and Ochs, F. (2019) ‘Effectiveness of a membrane enthalpy heat exchanger’, *Applied Thermal Engineering*, 160(April). Available at: https://doi.org/10.1016/j.applthermaleng.2019.114005.

Skarphagen, H. *et al.* (2019) ‘Design Considerations for Borehole Thermal Energy Storage (BTES): A Review with Emphasis on Convective Heat Transfer’, *Geofluids*, 2019. Available at: https://doi.org/10.1155/2019/4961781.

Sodja, J. (2007) ‘Turbulence models in CFD’, *University of Ljubljana*, (March), pp. 1–18. Available at: http://mafija.fmf.uni-lj.si/seminar/files/2006_2007/Turbulence_models_in_CFD.pdf.

Sofotasiou, P. (2017) ‘Aerodynamic optimisation of sports stadiums towards wind comfort’, (January). Available at: http://etheses.whiterose.ac.uk/17820/.

Solgi, E. *et al.* (2019) ‘A parametric study of phase change material behaviour when used with night ventilation in different climatic zones’, *Building and Environment*, 147, pp. 327–336. Available at: https://doi.org/10.1016/j.buildenv.2018.10.031.

Sparks, A. (2018) ‘nasapower: A NASA POWER Global Meteorology, Surface Solar Energy and Climatology Data Client for R’, *Journal of Open Source Software*, 3(30), p. 1035. Available at: https://doi.org/10.21105/joss.01035.

Sparrow, E.M. and Kang, S.S. (1985) *Longitudinally-finned cross-flow tube banks and their heat transfer and pressure drop characteristics*, *hr. J. Hear Mass Transfer*.

Srimuang, W. and Amatachaya, P. (2012) ‘A review of the applications of heat pipe heat exchangers for heat recovery’, *Renewable and Sustainable Energy Reviews* [Preprint]. Available at: https://doi.org/10.1016/j.rser.2012.03.030.

Stern, F. *et al.* (2001a) ‘Comprehensive approach to verification and validation of CFD simulations—Part 1: Methodology and procedures’, *Journal of Fluids Engineering, Transactions of the ASME*, 123(4), pp. 793–802. Available at: https://doi.org/10.1115/1.1412235.

Stern, F. *et al.* (2001b) ‘Comprehensive approach to verification and validation of CFD simulations—Part 1: Methodology and procedures’, *Journal of Fluids Engineering, Transactions of the ASME*, 123(4), pp. 793–802. Available at: https://doi.org/10.1115/1.1412235.

Sun, S. and Zhang, T. (2020) ‘Review of classical reservoir simulation’, in *Reservoir Simulations*. Elsevier, pp. 23–86. Available at: https://doi.org/10.1016/b978-0-12-820957-8.00002-2.

Sundell, J. (2004) *On the history of indoor air quality and health History*. Available at: www.blackwellpublishing.com/ina.

Taler, D. and Taler, J. (2017) *Simple heat transfer correlations for turbulent tube flow*.

Tiskatine, R. *et al.* (2017) ‘Suitability and characteristics of rocks for sensible heat storage in CSP plants’, *Solar Energy Materials and Solar Cells*, 169(December 2016), pp. 245–257. Available at: https://doi.org/10.1016/j.solmat.2017.05.033.

Ucar, A. and Inalli, M. (2008) ‘Thermal and economic comparisons of solar heating systems with seasonal storage used in building heating’, *Renewable Energy*, 33(12), pp. 2532–2539. Available at: https://doi.org/10.1016/j.renene.2008.02.019.

Umair, M.M. *et al.* (2019) ‘Novel strategies and supporting materials applied to shape-stabilize organic phase change materials for thermal energy storage–A review’, *Applied Energy*, 235(June 2018), pp. 846–873. Available at: https://doi.org/10.1016/j.apenergy.2018.11.017.

Vakiloroaya, V. *et al.* (2014) ‘A review of different strategies for HVAC energy saving’, *Energy Conversion and Management*, 77, pp. 738–754. Available at: https://doi.org/10.1016/j.enconman.2013.10.023.

Vali, A. *et al.* (2009) ‘Numerical model and effectiveness correlations for a run-around heat recovery system with combined counter and cross flow exchangers’, *International Journal of Heat and Mass Transfer* [Preprint]. Available at: https://doi.org/10.1016/j.ijheatmasstransfer.2009.07.020.

Villar-Ramos, M.M. *et al.* (2020) ‘Parametric analysis of the thermal behavior of a single-channel solar chimney’, *Solar Energy*, 209, pp. 602–617. Available at: https://doi.org/10.1016/j.solener.2020.08.072.

Volk, A., Ghia, U. and Stoltz, C. (2017) ‘Effect of grid type and refinement method on CFD-DEM solution trend with grid size’, *Powder Technology*, 311, pp. 137–146. Available at: https://doi.org/10.1016/j.powtec.2017.01.088.

Walker, I.S. and Wilson, D.J. (1993) ‘Evaluating models for superposition of wind and stack effect in air infiltration’, *Building and Environment*, 28(2), pp. 201–210. Available at: https://doi.org/10.1016/0360-1323(93)90053-6.

Wallin, J., Madani, H. and Claesson, J. (2009) ‘Ventilation heat recovery with run-around coil : System analysis and a study on efficiency improvement – Part I’, pp. 1–6.

Wallin, J., Madani, H. and Claesson, J. (2012) ‘Run-around coil ventilation heat recovery system: A comparative study between different system configurations’, *Applied Energy*, 90(1), pp. 258–265. Available at: https://doi.org/10.1016/j.apenergy.2011.05.012.

Walraven, D. (2014) *Optimization of the Energy Conversion Starting from Low-Temperature Heat: Application to Geothermal Binary Cycles*. Available at: https://www.researchgate.net/publication/271072901.

Wang, L. and Greenberg, S. (2015) ‘Window operation and impacts on building energy consumption’, *Energy and Buildings*, 92, pp. 313–321. Available at: https://doi.org/10.1016/j.enbuild.2015.01.060.

Wang, Z. *et al.* (2017) ‘Field test and numerical investigation on the heat transfer characteristics and optimal design of the heat exchangers of a deep borehole ground source heat pump system’, *Energy Conversion and Management*, 153(October), pp. 603–615. Available at: https://doi.org/10.1016/j.enconman.2017.10.038.

Wesselink, M. *et al.* (2018) ‘Conceptual market potential framework of high temperature aquifer thermal energy storage - A case study in the Netherlands’, *Energy*, 147, pp. 477–489. Available at: https://doi.org/10.1016/j.energy.2018.01.072.

Wołoszyn, J. (2020) ‘Global sensitivity analysis of borehole thermal energy storage efficiency for seventeen material, design and operating parameters’, *Renewable Energy*, 157, pp. 545–559. Available at: https://doi.org/10.1016/j.renene.2020.05.047.

Wong, B. and Mesquita, L. (2020) ‘Drake landing solar community: Financial summary and lessons learned’, *Proceedings of the ISES Solar World Congress 2019 and IEA SHC International Conference on Solar Heating and Cooling for Buildings and Industry 2019*, pp. 482–493. Available at: https://doi.org/10.18086/swc.2019.11.03.

Wu, Y. *et al.* (2021) ‘Numerical study on natural ventilation of the wind tower: Effects of combining with different window configurations in a low-rise house’, *Building and Environment*, 188. Available at: https://doi.org/10.1016/j.buildenv.2020.107450.

Xu, Q., Riffat, S. and Zhang, S. (2019) ‘Review of heat recovery technologies for building applications’, *Energies*. MDPI AG. Available at: https://doi.org/10.3390/en12071285.

Xu, Z.Y., Wang, R.Z. and Yang, C. (2019) ‘Perspectives for low-temperature waste heat recovery’, *Energy*, 176, pp. 1037–1043. Available at: https://doi.org/10.1016/j.energy.2019.04.001.

Yang, H. *et al.* (2019) ‘Experimental study on a pulsating heat pipe heat exchanger for energy saving in air-conditioning system in summer’, *Energy and Buildings*, 197, pp. 1–6. Available at: https://doi.org/10.1016/j.enbuild.2019.05.032.

Yang, H., Khandekar, S. and Groll, M. (2008) ‘Operational limit of closed loop pulsating heat pipes’, *Applied Thermal Engineering* [Preprint]. Available at: https://doi.org/10.1016/j.applthermaleng.2007.01.033.

Zeghici, R.M. *et al.* (2015) ‘Integrated assessment of variable density-viscosity groundwater flow for a high temperature mono-well aquifer thermal energy storage (HT-ATES) system in a geothermal reservoir’, *Geothermics*, 55, pp. 58–68. Available at: https://doi.org/10.1016/j.geothermics.2014.12.006.

Zhai, Z.J. and Helman, J.M. (2019) ‘Implications of climate changes to building energy and design’, *Sustainable Cities and Society*, 44(June 2018), pp. 511–519. Available at: https://doi.org/10.1016/j.scs.2018.10.043.

Zhang, L.Z. (2012) ‘Progress on heat and moisture recovery with membranes: From fundamentals to engineering applications’, *Energy Conversion and Management*, 63, pp. 173–195. Available at: https://doi.org/10.1016/j.enconman.2011.11.033.

Zhao, Y. *et al.* (2022) ‘High Temperature Sensible Storage—Industrial Applications’, *Encyclopedia of Energy Storage: Volume 1-4*, 1–4(1), pp. 424–432. Available at: https://doi.org/10.1016/B978-0-12-819723-3.00070-6.

Zhu, L. and Chen, S. (2019) ‘Sensitivity analysis on borehole thermal energy storage under intermittent operation mode’, *Energy Procedia*, 158(2018), pp. 4655–4663. Available at: https://doi.org/10.1016/j.egypro.2019.01.740.

Zmrhal, V. *et al.* (2023) ‘Determination of the sensible heat effectiveness and pressure loss of a rotary regenerative heat exchanger using CFD’, *Building Simulation* [Preprint]. Available at: https://doi.org/10.1007/s12273-022-0983-z.

Zubair, M., Abdullah, M.Z. and Ahmad, K.A. (2013) ‘Hybrid mesh for nasal airflow studies’, *Computational and Mathematical Methods in Medicine*, 2013. Available at: https://doi.org/10.1155/2013/727362.